Contribution de l'hydrogéochimie à la compréhension des écoulements d'eaux souterraines en Outaouais, Québec, Canada

Thèse

Nelly Montcoudiol

Doctorat interuniversitaire en sciences de la Terre

Philosophiae doctor (Ph.D.)

Québec, Canada

Résumé

En Outaouais, les eaux souterraines sont une ressource essentielle pour les besoins domestiques et agricoles (hors ville de Gatineau, qui utilise les eaux de surface). La région d'étude repose sur le Bouclier Canadien, fait de roches silicatées fracturées recouvertes par les sédiments résultants de la dernière glaciation-déglaciation. Dans ce contexte, améliorer les connaissances sur le fonctionnement des aquifères est vital pour une utilisation durable de la ressource. Pour atteindre cet objectif, un modèle conceptuel a été proposé résultant de l'interprétation des données géochimiques couplée à la modélisation numérique.

L'altération des silicates, l'intrusion d'eau saline de l'ancienne Mer de Champlain suivie de l'échange cationique dans les argiles marines affectant les aquifères confinés ainsi que les mélanges d'eaux sont les principaux processus identifiés par une analyse statistique multivariée. A échelle locale, une signature des isotopes stables similaire à celle de la pluie actuelle et la présence de tritium indiquent des temps de résidence relativement courts dans les 100 premiers mètres de profondeur, ce qui est confirmé par la modélisation des écoulements et des âges. La présence d'hélium 4 est attribuée à la diffusion depuis des eaux plus profondes et plus âgées, résultant de la diminution de la conductivité hydraulique avec la profondeur. Des mélanges résultent de l'échantillonnage dans des puits ouverts. Dans les aquifères non confinés, les activités en ^{14}C sont principalement le résultat de l'équilibre de l'eau de recharge avec le CO_2 du sol dans un système ouvert suivi de l'altération des silicates par du CO_2 fossile ou de la dissolution des carbonates en milieu fermé plutôt que de la décroissance radioactive. Finalement, la simulation des chlorures montre que les restes de la Mer de Champlain seraient présents dans les argiles marines et dans les zones moins perméables de l'aquifère confiné par rapport aux eaux caractérisés par l'échange cationique.

L'étude a permis de caractériser la qualité des eaux souterraines dans la partie fracturée du bouclier canadien dans les dépôts du Quaternaire à l'échelle régionale. Les systèmes locaux d'écoulement, avec des temps de résidence courts dans la partie supérieure du roc sont essentiels et doivent être pris en compte pour évaluer la vulnérabilité des ressources en eaux souterraines.

Abstract

Throughout most of the Outaouais Region, groundwater is an essential resource for both for domestic and agricultural use (except in the city of Gatineau which uses surface water). The study area lies in the Canadian Shield, and includes a fractured silicate bedrock aquifer which is covered by sediments from the last glacial-deglacial period. In this context, improving our understanding of aquifers is vital for a sustainable use of this resource. To fulfill this objective, a conceptual model was proposed based on the interpretation of geochemical data coupled to numerical modelling.

Silicate weathering, seawater intrusion by the former Champlain Sea and subsequent cation exchange in marine clays affecting groundwater quality in confined aquifers, and mixing between waters of different ages are identified by a multivariate statistical analysis as the principal geochemical processes. At the local scale, a stable isotope signature similar to current precipitation and the presence of tritium indicate relatively short residence times in the first 100 m below ground surface, which was confirmed by numerical flow and age modelling. The occurrence of helium 4 is attributed to diffusion from deeper older groundwater within lower hydraulic conductivity zones. Some mixing due to sampling in open boreholes may also have occurred. In the unconfined aquifer, ^{14}C activities appear to be the result of such as equilibration of recharge water with soil CO_2 in open conditions coupled to silicate weathering by fossil CO_2 or carbonate dissolution under closed conditions, rather than from radioactive decay. Finally, chloride transport simulations show that remnants of the Champlain Sea would still be found in marine clays and in the less permeable zones of the confined aquifer whereas groundwater characterised by cation exchange are found in more permeable zones.

The study has helped characterize regional groundwater quality in the upper fractured zone of the Canadian Shield and in the Quaternary sediments of the Outaouais region. It has shown the importance of local scale groundwater flow systems and relatively rapid flow in the upper part of the bedrock which need to be considered when assessing the vulnerability of these regional groundwater resources.

Table des matières

Liste des figures

Liste des tableaux

Liste des abréviations

CID : Carbone Inorganique Dissous

DIC : Dissolved Inorganic Carbon

D.L. : detection limit

EPM : Equivalent Porous Medium

FA : Factor Analysis

HCA : Hierarchical Cluster Analysis

IAEA ; international Atomic Energy Agency

m.a.s.l. : meter above sea level

MDT : Matières Dissoutes Totales

MRC : Municipalité Régionale de Comté

NGT : Noble Gas Temperature

OBV : Organisme de Bassin Versant

PACES : Programme d'Acquisition de Connaissances sur les Eaux Souterraines

PDB : Pee Dee Belemnite

pmC : percent modern Carbon

SIH : Système d'Information Hydrogéologique

STP : Standard Temperature and Pressure

TDS : Total Dissolved Solids

TU : Tritium Unit

V-SMOW : Vienna - Standard Mean Ocean Water

WMO : World Meteorological Organisation

Remerciements

Tout d'abord, je voudrais remercier mon directeur de thèse, John Molson, qui m'a fait confiance pour mener à son terme ce projet de recherche. Merci pour ces encouragements tout au long de ces quatre années, sa disponibilité ainsi que pour m'avoir fait profiter de sa large expérience en modélisation. Merci pour le support financier qui m'a permis de participer à de nombreuses conférences internationales et faire de nombreux contacts. Merci aussi pour les leçons de tennis.

Merci à Jean-Michel Lemieux, mon co-directeur de thèse et professeur à l'université Laval, pour ses précieux conseils dans l'interprétation des résultats. Je voudrais aussi le remercier pour m'avoir fait partager sa science du terrain en ce qui concerne l'utilisation des packers. Merci de m'avoir fait confiance pour leur bonne utilisation et j'espère avoir l'occasion de réutiliser cette technique dans le futur.

Sincères remerciements à quelques précieux collaborateurs scientifiques. Je pense notamment à Vincent Cloutier, professeur à l'UQAT et co-auteur du deuxième article, pour ses suggestions concernant l'interprétation des isotopes stables ainsi ses conseils sur les analyses statistiques multi-variées ; Daniele Pinti, professeur à l'UQAM, pour des discussions sur les isotopes et en particulier sur la datation tritium-hélium 3 ; Clara Castro, professeur à l'université du Michigan, pour toute son aide concernant l'échantillonnage des gaz rares et l'interprétation des résultats d'analyses, ainsi que son collègue, Chris Hall. Pour finir, je remercie Pierre Therrien, professionnel de recherche à l'université Laval, spécialiste des maillages, compagnon de raquette et blagueur invétéré, qui m'a fait gagner un temps précieux lors de la réalisation de mon maillage et qui a contribué à une amélioration significative de mon niveau en tennis.

Je remercie aussi l'ensemble du personnel du département, pour les discussions professionnelles ou autres, qui ont aussi contribué, à leur manière, à l'achèvement de cette thèse. Merci à tous les stagiaires qui nous ont donné un coup de main sur le terrain. Une mention spéciale pour mes collègues de bureau, Fabien, Guillaume, Jalil, Elham, Tobias… qui ont su créer une atmosphère de travail unique dans notre bureau.

Les dernières personnes, mais pas des moindres, que je souhaite remercier sont mes parents pour leur soutien infaillible tout au long de ces longues années d'études et Carlos, mi pareja, que agradezco por tener tanta confianza en mi y esperarme con mucha paciencia del otro lado del Atlantico.

Avant-propos

Cette thèse est écrite sous forme d'un manuscrit avec insertion d'articles. Elle comprend trois articles, chacun correspondant à un chapitre de la thèse. Les échantillons d'eau sur lesquels les travaux sont basés ont été collectés en partie par l'auteur, avec l'aide d'étudiants stagiaires. Tous les articles ont été rédigés par l'auteur, qui est à l'origine de l'interprétation des résultats d'analyses des échantillons d'eau ainsi que des travaux de modélisation. Chaque article a fait l'objet de plusieurs révisions par le directeur et co-directeur de thèse avant soumission (articles 1 et 2) ou insertion dans cette thèse (article 3).

Le premier article intitulé « Groundwater geochemistry of the Outaouais Region (Québec, Canada): a regional-scale study », est publié dans Hydrogeology Journal, DOI: 10.1007/s10040-014-1190-5. Quelques erreurs ont été repérées dans la version soumise et ont été corrigées dans la version incluse dans cette thèse. La présentation de l'article a été modifiée par rapport à la version publiée afin de correspondre au format de la thèse.

Le second article intitulé « A conceptual model for groundwater flow and geochemical evolution in the southern Outaouais Region, Québec, Canada » a été soumis à Applied Geochemistry. Il vient d'être accepté pour publication. Vincent Cloutier, co-auteur de l'article, a apporté son expertise concernant l'interprétation des données isotopiques, en particulier les isotopes stables.

Le troisième article intitulé « A numerical model of groundwater flow, tritium and chloride transport, and residence time in the southern Outaouais Region, Quebec, Canada » n'a pas encore été soumis. L'article est dans une version quasi définitive et fera probablement l'objet de quelques améliorations complémentaires en vue d'une soumission au journal Ground Water.

Introduction

1 Mise en contexte

Les travaux de recherche de cette thèse se sont déroulés dans le cadre du projet PACES (Programme d'Acquisition de Connaissances des Eaux Souterraines) en Outaouais, Québec, Canada. A ce jour, treize projets ont été mis en place dans le territoire municipalisé de la province du Québec (Fig. 1). Ils sont financés sur trois ans par le Ministère du Développement Durable, de l'Environnement et de la Lutte contre les Changements Climatiques (MDDELCC) et sont réalisés par les universités en collaboration avec les acteurs locaux tels que les MRC (Municipalités Régionales de Comté) et les OBV (Organismes de Bassins Versants).

Dans un contexte d'habitat assez dispersé, les eaux souterraines sont bien souvent la seule source d'eau potable dans les zones rurales, non desservies par un réseau d'aqueduc (90% du territoire pour 20% de la population). L'objectif de ces projets est donc de dresser un portrait régional des ressources en eaux souterraines ainsi que d'uniformiser les connaissances à l'échelle du territoire municipalisé du Québec (MDDEFP 2008). Chaque projet est découpé en trois étapes. La première étape consiste à rassembler l'ensemble des données disponibles sur la région d'étude. L'interprétation préliminaire des données disponibles a permis d'identifier les zones où des données sont manquantes ou insuffisantes. Grâce à deux campagnes de terrain réalisées pendant les étés 2011 et 2012, les données supplémentaires ont été acquises pour les zones identifiées précédemment. Finalement, l'ensemble des données a été interprété à l'échelle régionale, selon une approche multidisciplinaire, avec une emphase particulière sur les enjeux spécifiques à la région d'étude.

Ce doctorat se concentre sur le volet portant sur la caractérisation hydrogéochimique des aquifères. Cependant, l'hydrogéochimie des eaux souterraines ne pouvant être étudiée hors contexte, les données et résultats produits par le projet dans d'autres disciplines seront utilisés car nécessaires à la compréhension de l'évolution géochimique des eaux souterraines à l'échelle régionale.

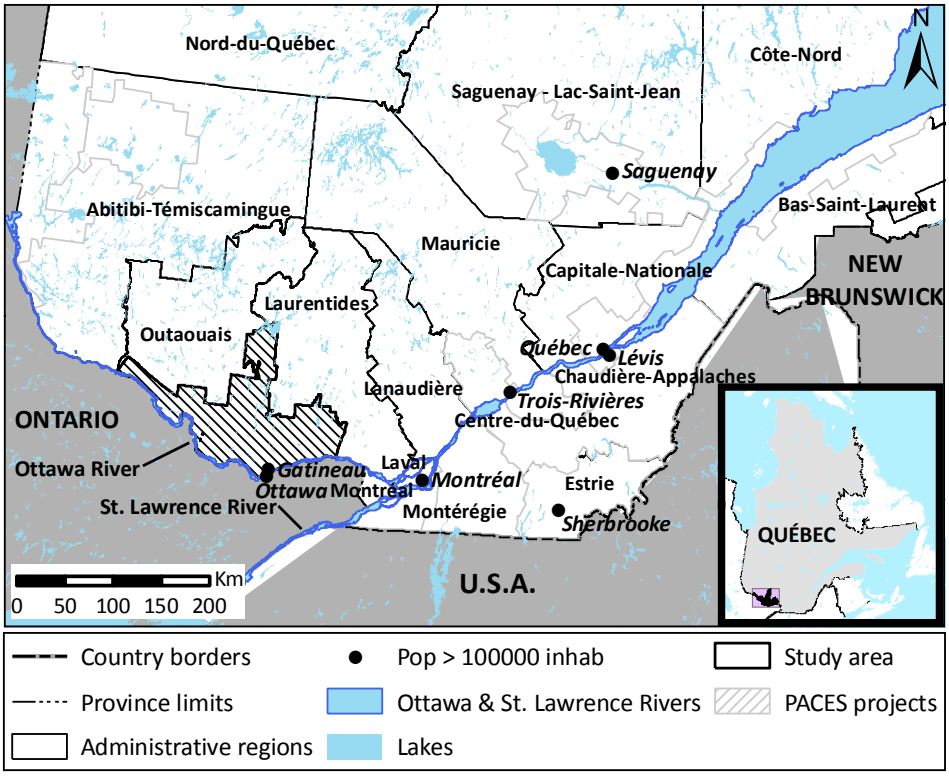

Fig. 1 Carte du sud du Québec, où sont localisées les zones d'études des projets PACES dont la région d'intérêt, l'Outaouais

2 Présentation de la zone d'étude

La région de l'Outaouais est localisée au sud-ouest de la province du Québec, séparée de l'Ontario par la rivière des Outaouais (Fig. 1). Dans le cadre du projet PACES, seul 40% du territoire municipalisé de l'Outaouais est à l'étude, soit une superficie de 13 762 km^2 et une population de 340 000 habitants, correspondant à la partie la plus densément peuplée (Comeau et al. 2013).

2.1 Contexte géologique

La région de l'Outaouais repose essentiellement sur le Bouclier Canadien (Province du Grenville, plus de 90% de la superficie de la zone d'étude) ainsi que sur les Basses Terres du St Laurent au sud de la région, le long de la rivière des Outaouais (Fig. 2). Le Bouclier Canadien est constitué majoritairement de roches silicatées datant du précambrien et de diverses origines : intrusives, migmatiques ou métasédimentaires (Bélanger

2014) tandis que les Basses Terres du St Laurent sont des roches sédimentaires datant d'environ 500 millions d'années. Gneiss, paragneiss, marbre et syénite sont les roches dominantes du Bouclier Canadien (Bear et al. 1971). Le Bouclier Canadien est caractérisé par une fracturation importante en surface telle que mise en évidence par Sterckx (2013), avec des conductivités hydrauliques variant entre 10^{-8} et 10^{-4} m.s^{-1} dans les 60 premiers mètres. En profondeur, le roc est nettement moins perméable (entre 10^{-12} et 10^{-8} m.s^{-1}).

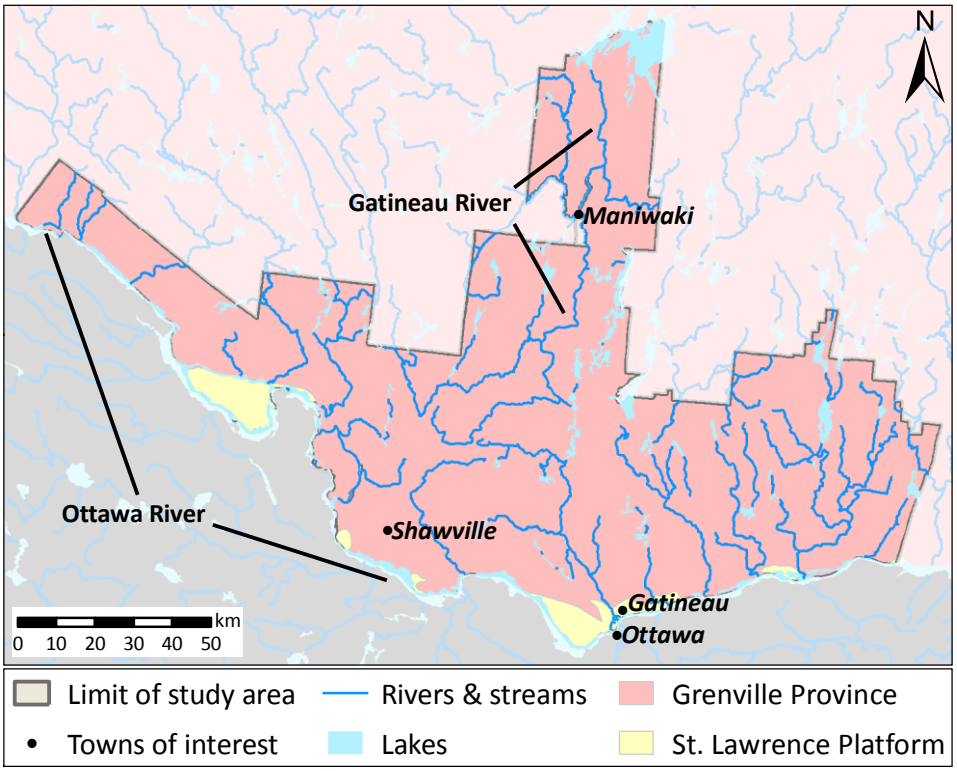

Fig. 2 Répartition des provinces géologiques dans la zone d'étude

Le socle rocheux est recouvert par des dépôts datant du Quaternaire, plus précisément de la dernière glaciation qui a pris fin il y a environ 10 000 ans. Les sédiments produits lors des cycles de glaciation-déglaciation précédents ont été érodés par les cycles suivants, c'est pourquoi seuls subsistent les dépôts résultant de la dernière glaciation. A la base de la séquence stratigraphique, le roc est recouvert par du till, produit par l'érosion exercée par le glacier sur le roc ainsi que par des sédiments fluvio-glaciaires, de granulométrie grossière, charriés par les eaux de fonte du glacier (Daigneault et al. 2012) et localisés dans les dépressions du roc. Le retrait de l'inlandsis a permis l'invasion par la Mer de Champlain des vallées fortement

abaissées par le poids de la glace, il y a 12 000 ans environ. Cette eau de mer est un mélange d'eau salée de l'océan Atlantique et d'eau douce en provenance de la fonte des glaciers (34 % d'eau marine et 66% d'eau douce selon Cloutier et al. (2010), proportions similaires par Desaulniers & Cherry (1989) et Quigley et al. (1983)). Cet environnement a été propice au dépôt d'argiles marines et de sédiments deltaïques et littoraux. La remontée isostatique a peu à peu chassé la Mer de Champlain il y a 10 000 ans environ (Parent & Occhietti 1988), conduisant progressivement à la configuration actuelle des vallées (à partir de 4 700 ans, d'après Fulton & Richard (1987)). Selon Parent & Occhietti (1988), la durée de l'invasion de la Mer de Champlain a varié entre 3 000 ans environ dans la région de Québec (il y a 12 400 à 9 300 ans) et seulement 800 ans dans les vallées des Hautes Terres laurentiennes (vallée de la Gatineau, de la Petite-Nation pour la région d'étude). Cette durée est aussi variable au sein même de la région d'étude : la vallée des Outaouais a généralement été envahie en premier il y a environ 12 000 ans, les vallées secondaires plus tardivement vers 10 800 ans, après l'épisode de la moraine de St Narcisse (Parent & Occhietti 1988). Dans les vallées des cours d'eau actuels, des alluvions anciennes et récentes complètent la séquence stratigraphique.

La Fig. 3 présente la carte de répartition des dépôts du Quaternaire ainsi que la limite maximale d'extension de la Mer de Champlain. Le socle rocheux affleure en peu d'endroits car il est majoritairement recouvert par du till présent à l'affleurement dans les hauts topographiques. Dans les vallées, la séquence est en générale complète : les dépôts fluvio-glaciaires affleurent dans les parties supérieures de ces vallées et ont été érodés ou recouverts dans les parties inférieures des vallées par les argiles ou autres sédiments déposés par la Mer de Champlain.

2.2 Contexte hydrogéologique

La couche de till recouvrant le roc dans cette région est discontinue et assez mince, d'épaisseur maximale 15 m. Sa nature est assez variable mais caractérisée par la présence d'une matrice sableuse (Daigneault et al. 2012). De par sa faible épaisseur, le till ne constitue pas un aquifère très intéressant bien que sa perméabilité puisse être relativement élevée. Dans ces zones, qui sont situées dans les hauts topographiques, la

population est généralement assez dispersée et s'alimente à partir de puits individuels creusés dans le roc, dont la présence de fractures assure un débit suffisant pour l'approvisionnement en eau potable. Les aquifères au roc surmontés par le till sont considérés comme libres ou semi-confinés selon l'épaisseur de la couche.

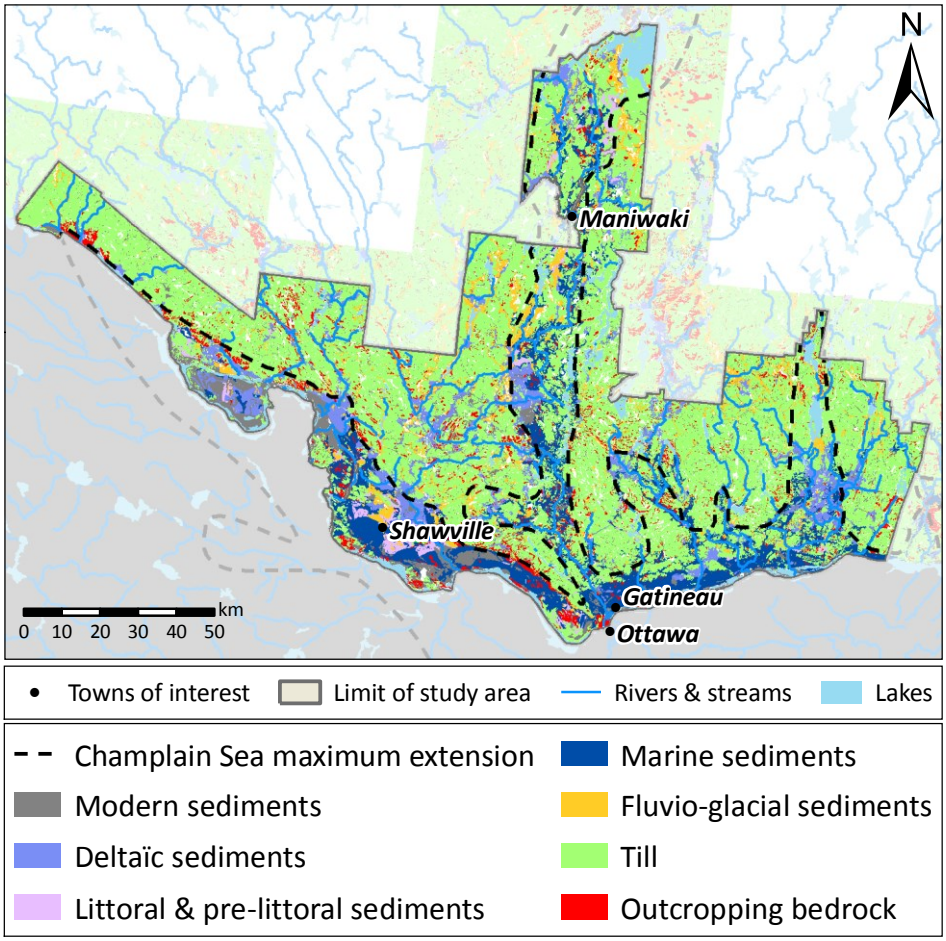

Fig. 3 Carte de répartition des dépôts du Quaternaire (d'après Comeau et al. (2013))

Dans les vallées, les sédiments fluvio-glaciaires, de granulométrie grossière et présentant des épaisseurs pouvant atteindre 50 m (Daigneault et al. 2012), constituent d'importants aquifères dans la région. Dans la partie supérieure des vallées, ce sont généralement des aquifères libres tandis que plus au sud, ils sont en général recouvert par d'épaisses couches d'argiles de la Mer de Champlain, qui sont responsables de leur confinement. En leur absence, la population s'alimente par des puits au roc confiné par les argiles. Les sédiments littoraux et deltaïques déposés par la Mer de Champlain sont principalement composés de sables et graviers (Daigneault et al. 2012) et peuvent être localement de bons aquifères libres (épaisseur maximale

de 6 m et 40 m respectivement). C'est aussi le cas des sédiments des plaines alluviales mais de façon moindre (épaisseur moyenne d'environ 5 m, Daigneault et al. (2012)).

L'écoulement régional suit la direction générale des rivières principales, soit une direction nord-sud depuis les Hautes-Terres (Bouclier Canadien, avec des altitudes en moyenne plus élevées) en direction de la vallée des Outaouais, exutoire de l'ensemble de la région (zone d'élévation la plus faible). Le niveau piézométrique suit la topographie (Comeau et al. 2013), en particulier dans les aquifères libres du Bouclier Canadien, et les eaux de surface en sont les zones de résurgence (Fig. A1 en Annexe 1). Des écoulements intermédiaires de direction est-ouest ont lieu en direction des rivières principales et des écoulements plus locaux en direction des cours d'eau de plus faible envergure. En l'absence de couches de dépôts peu perméables, les rivières sont supposées en lien hydraulique avec l'aquifère sous-jacent.

La recharge des aquifères (le premier rencontré depuis la surface) a été estimée à l'aide du logiciel HELP® (Hydrologic Evaluation of Landfill Performance, Schroeder & Ammon (1994)) dans le cadre du projet PACES (Comeau et al. 2013). Les composantes du bilan hydrologique ont été calées avec les débits de base estimés des cours d'eau de la région (trois stations). A l'échelle régionale, les valeurs de recharge moyennes calculées sont entre 30 et 34% des précipitations totales mais la distribution spatiale de la recharge est variable selon l'occupation des sols et la nature des dépôts (Fig. A2 en Annexe 1). La recharge est limitée (< 100 mm/an) dans la plaine argileuse de la rivière des Outaouais, qui correspond aussi aux zones urbanisées (sols imperméabilisés), et le long des rivières principales. Dans les Hautes Terres, où le roc affleure ou est recouvert par une couche de till de faible épaisseur, les taux de recharge sont importants (300 à 400 mm/an). Les valeurs les plus élevées (> 400 mm/an) sont typiques des aquifères localisés dans les dépôts fluvio-glaciaires. Les valeurs intermédiaires (entre 100 et 300 mm/an) caractérisent les aquifères recouverts par de plus faibles épaisseurs d'argiles.

La recharge est l'un des sept paramètres pris en compte dans le calcul de la vulnérabilité des aquifères (le premier rencontré depuis la surface) selon la méthode DRASTIC (Aller et al. 1987) appliquée dans le cadre

des projets PACES. La distribution spatiale de la vulnérabilité est assez similaire à celle de la recharge (Fig. A3 en Annexe 1) avec des zones peu vulnérables (indice < 100) où la recharge est faible et la couche argileuse assez épaisse et des zones plus vulnérables (indice > 160) où la recharge est importante (sédiments fluvio-glaciaires). Concernant les aquifères au roc recouverts par du till, les valeurs de vulnérabilité sont intermédiaires (entre 100 et 140).

3 Évolution géochimique des eaux souterraines

Grâce à la carte piézométrique établie dans le cadre du projet (Comeau et al. 2013), les systèmes d'écoulement ont pu être définis, selon la terminologie établie par Tóth (1963). Avec les seules données de piézométrie, la compréhension des écoulements d'eaux souterraines reste assez limitée et généralement représentative des conditions actuelles (Glynn & Plummer 2005; Sanford et al. 2011). La géochimie permet d'améliorer la compréhension des écoulements en intégrant les informations relatives aux conditions passées et actuelles d'écoulement.

Différents outils géochimiques ont été développés au cours des 60 dernières années (Glynn & Plummer 2005). Ceux utilisés dans le cadre de ce doctorat (ions majeurs et mineurs, isotopes stables de l'eau, tritium, isotopes du carbone, gaz rares et modélisation numérique) sont présentés dans ce qui suit.

3.1 Evolution des concentrations en ions majeurs et mineurs le long d'une ligne d'écoulement

Chebotarev (1955) a été un des premiers à proposer une séquence d'évolution de la composition géochimique des eaux basée sur l'identification de trois groupes d'eaux souterraines naturelles : passage d'une eau à dominance HCO_3^- à une eau Cl^- dominant en passant par une eau SO_4^{2-} dominant. Ces concepts ont été révisés par Tóth (1999) et sont illustrés par la Fig. 4. Une classification plus rigoureuse des eaux souterraines en faciès hydrochimique a été proposée par Back (1966). Chaque faciès ou groupe d'eau est interprété

comme étant la réponse chimique au passage de l'eau dans différentes formations géologiques, qui dépend de la direction et vitesse d'écoulement et de la nature des roches rencontrées.

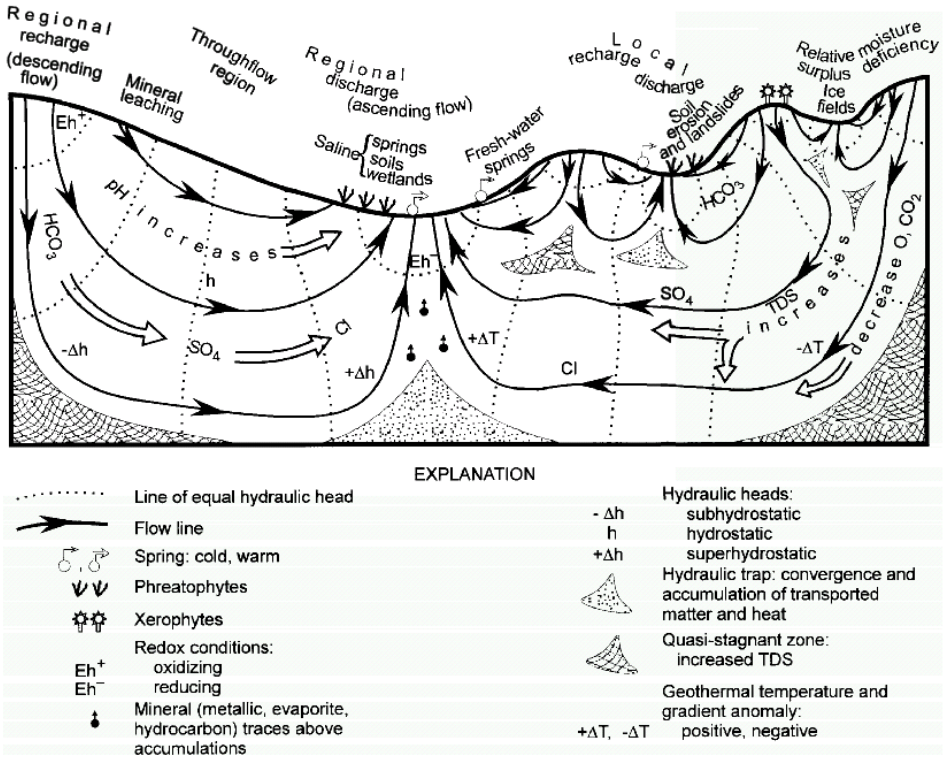

Fig. 4 Effets et manifestations de l'écoulement gravitaire dans un bassin régional non confiné (Tóth 1999)

De très nombreuses études, dans des contextes géologiques variés, reposent sur l'utilisation de la chimie des ions majeurs. Gascoyne (2004) a montré que les variations de chimie avec la profondeur dans le Bouclier Canadien suivent la séquence proposée par Chebotarev (1955) et ne dépendent pas du type de roche (Gascoyne & Kamineni 1994). Gascoyne & Kamineni (1994) et Gerla (1992) mettent aussi en évidence des variations longitudinales dans les systèmes d'écoulement superficiels (200 premiers mètres de profondeur). Au Québec, dans les aquifères de surface, Blanchette et al. (2010b) et Cloutier et al. (2006) ont montré l'importance du contrôle des conditions hydrogéologiques sur la géochimie de l'eau par rapport à la géologie, dans des aquifères sédimentaires des Basses Terres du Saint-Laurent. Les zones de recharge (conditions de nappe libre) sont caractérisées dans ces régions par des faciès de type Ca-Mg-HCO_3 tandis que dans les zones exutoires confinées par la présence d'argiles marines, les facies Na-HCO_3 et Na-Cl sont dominants. La

séquence de Chebotarev (1955) n'est pas toujours respectée. Ceci peut être synonyme d'une pollution anthropogénique : faciès Na-Cl dans les aquifères libres, dû à l'épandage de sels de déglaçage en grande quantité le long des axes routiers principaux (Cloutier et al. 2006), excès de sulfates (SO_4^{2-}) dû à l'irrigation avec les eaux usées en Chine (Guo & Wang 2004) par exemple. Dans le complexe morainique de Waterloo, les aquifères de surface et ceux en profondeur ont des signatures chimiques particulières (Ca-Mg-HCO_3 et Ca-SO_4 respectivement) et Stotler et al. (2011) ont pu mettre en évidence l'existence de « fenêtres hydrauliques » dans la couche imperméable séparant les deux aquifères, identifiées par la présence de zones dans les aquifères avec une signature intermédiaire ou celle de l'autre aquifère. Ces structures hydrogéologiques pourraient avoir l'effet d'induire des zones d'écoulement préférentiel et de modifier l'évolution géochimique 'typique'.

L'analyse des variations des concentrations en ions majeurs le long d'une ligne d'écoulement permet de déduire quels peuvent être les processus géochimiques qui en sont responsables. Parmi les mécanismes naturels responsables de la signature géochimique de l'eau, sont inclus les réactions entre l'eau et les roches, les mélanges entre différentes eaux, les réactions biologiques... Les principales réactions eau-roche sont celles de dissolution/précipitation de minéraux comme les carbonates (Cloutier et al. 2006) et les silicates (Rajmohan & Elango 2004), d'échange ionique (Cloutier et al. 2010; Walraevens et al. 2007) et d'oxydo-réduction (Smedley & Edmunds 2002). Les ions mineurs et traces sont aussi utiles pour mettre en évidence des réactions secondaires telles que la dissolution de minéraux riches en fer et manganèse ou en fluorures et strontium (Blanchette et al. 2010b; Cloutier et al. 2006) ou encore en uranium (Woo et al. 2002). Les nitrates-nitrites et les phosphates sont le plus souvent synonymes de pollution d'origine agricole (Smedley & Edmunds 2002). De fortes concentrations en bromures, associées à des valeurs élevées en chlorures et sodium, signifient une origine marine de l'eau, permettant ainsi de distinguer la source de NaCl (Alcalá & Custodio 2008; Vengosh & Pankratov 1998).

3.2 Isotopes et gaz rares

Depuis une trentaine d'années, les traceurs environnementaux (isotopes et gaz rares) se sont ajoutés à la panoplie d'outils géochimiques disponibles. Ils aident à identifier les sources de recharge (infiltration d'eau de surface par exemple), les échanges entre aquifères, à définir les directions d'écoulement et à connaître les temps de résidence (Clark & Fritz 1997; Glynn & Plummer 2005). L'utilisation combinée de plusieurs traceurs est souvent appliquée et permet, par exemple, l'identification des mélanges entre eaux récentes et eaux plus anciennes (Glynn & Plummer 2005). Les données d'âge des eaux sont souvent utilisées pour la calibration des modèles numériques (Sanford 2011; Zuber et al. 2011). Dans ce qui suit, seuls les traceurs environnementaux utilisés dans le cadre de ce projet de recherche seront décrits : les isotopes stables de l'eau ($\delta^{18}O$ et $\delta^{2}H$), le tritium (^{3}H), les isotopes du carbone ($\delta^{13}C$ et ^{14}C) et les gaz rares (He, Ne, Xe, Ar et Kr). Pour ceux non-décrits, l'article de Plummer et al. (2004) et le livre de Clark & Fritz (1997) proposent une revue de leurs applications et une liste de références pertinentes.

3.2.1 Les isotopes stables de l'eau

Les isotopes stables de l'eau ont de multiples applications en hydrogéologie. En conséquence du fractionnement isotopique, des eaux de pluie infiltrées sous des conditions climatiques différentes présenteront des rapports isotopiques différents. Durant les cycles de déglaciation, lorsque les températures sont plus chaudes, la signature isotopique est enrichie en isotopes lourds. Cette tendance s'observe aussi sur des données saisonnières d'isotopes stables dans les eaux de pluie où les précipitations hivernales sont appauvries en isotopes lourds par rapport aux précipitations estivales (Clark & Fritz 1997). C'est le contraire durant les cycles de glaciation avec une signature isotopique appauvrie en isotopes lourds. Ainsi, la différence de signature permet de faire la distinction entre les eaux modernes (postglaciaires) et les eaux du Pléistocène dans le Bouclier Canadien (Ophori 1999). En combinaison avec des mesures en tritium, les eaux très récentes (après le pic de 1963) peuvent être différenciées des eaux modernes postglaciaires antérieures à 1963 (Zuber et al. 2004). Les isotopes stables permettent aussi de préciser l'origine météorique des eaux souterraines (Edmunds et al. 2002). Dans les zones montagneuses, la signature isotopique varie avec l'altitude, avec un

enrichissement en isotopes lourds. En échantillonnant les eaux de pluie à différentes altitudes et en les comparant avec la signature des eaux souterraines, il est possible de déterminer l'altitude de recharge (Carreira et al. 2011). La signature isotopique permet aussi de mettre en évidence les phénomènes d'évaporation comme c'est le cas dans les aquifères en milieu aride (Herczeg & Leaney 2011; Zouari et al. 2011).

3.2.2 Les isotopes du carbone et la datation des eaux au ^{14}C

La datation au ^{14}C permet de préciser le sens d'écoulement des eaux souterraines (Chen et al. 2011), d'estimer les vitesses apparentes d'écoulement (Mayer et al. 2013; Zouari et al. 2011) et les temps de résidence des eaux souterraines (Sültenfuβ et al. 2011). Cependant, la datation est rendue plus compliquée par la présence de source de carbone le long d'une ligne d'écoulement. Les roches carbonatées ne possèdent plus de carbone 14 et leur dissolution entraîne une diminution de l'activité en ^{14}C de l'échantillon et donc un âge apparent plus élevé que l'âge réel (Clark & Fritz 1997). La mesure du $\delta^{13}C$ permet d'identifier les sources de carbone inorganique et de quantifier les interactions eau-roche (Clark & Fritz 1997; Zouari et al. 2011). Il existe de nombreux modèles pour prendre en compte ces interactions, dont certains basés sur la mesure de $\delta^{13}C$, pour corriger et interpréter les âges au carbone 14 (Fontes & Garnier 1979; Ingerson & Pearson 1964; Mook 1976; Tamers 1975; Vogel 1970).

3.2.3 Datation au tritium (^{3}H) et tritium-hélium (^{3}H-^{3}He)

La méthode de datation au tritium est utilisée pour les eaux récemment infiltrées (<60 ans). Le tritium est un isotope radioactif de l'hydrogène caractérisé par une demi-vie de 12.43 ans. Le tritium a été relâché dans l'atmosphère en grande quantité pendant les essais nucléaires des années 60. Par équilibre avec l'eau atmosphérique, le tritium s'est retrouvé dans les eaux de pluie comme le montre les mesures effectuées sur les eaux de pluie collectées à la station météorologique d'Ottawa (WMO code 7162800, IAEA/WMO (2011), Fig. 5). Les concentrations en tritium sont exprimées en TU (Tritium Unit) : 1 TU correspond à 1 atome de ^{3}H pour 10^{18} atomes d'hydrogène. En appliquant la loi de décroissance radioactive à partir de la concentration

mesurée dans un échantillon à une date connue, la droite obtenue (en échelle semi-log) recoupe la courbe de la Fig. 5. Pour une valeur mesurée, différentes dates d'infiltration sont possibles à cause des fluctuations de concentrations en tritium dans les eaux de pluie. De plus, les variations à partir de la fin des années 80 - début des années 90 sont beaucoup plus faibles et les concentrations mesurées sont similaires à celles actuelles (valeurs similaires à celles avant les essais nucléaires). Cette méthode de datation a donc fait ses preuves jusqu'au début des années 90 (Allison & Hughes 1975; Robertson & Cherry 1989) pour estimer les taux de recharge des aquifères par exemple.

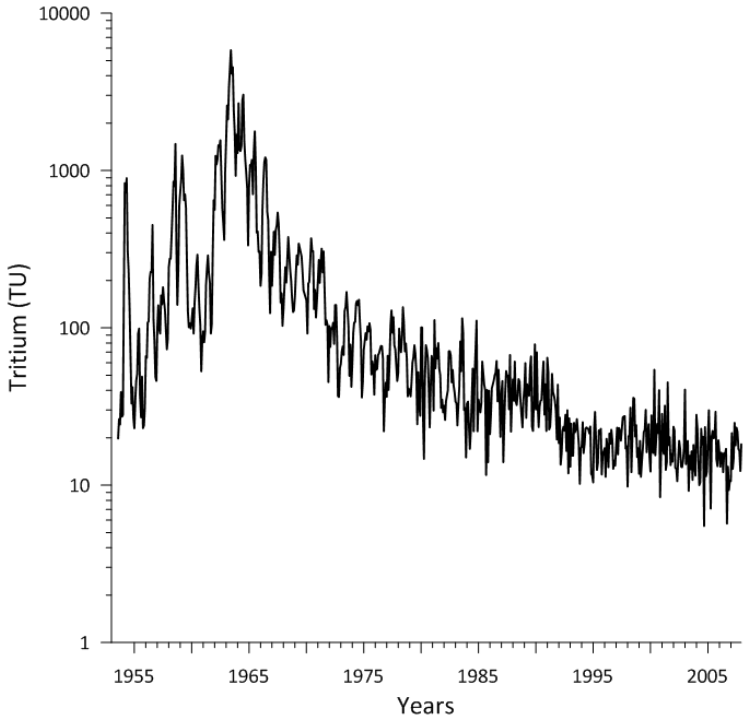

Fig. 5 Concentrations mensuelles en tritium dans les eaux de pluie de la station d'Ottawa (WMO code 7162800, IAEA/WMO (2011))

Pour pallier à ces inconvénients, Tolstikhin & Kamensky (1969) ont introduit la méthode tritium-hélium ($^3H/^3He$) qui repose sur la mesure du tritium et de l'hélium 3, produit de la dégradation radioactive du tritium (voir les détails dans le Chapitre 2). L'avantage de la méthode réside dans le fait qu'il n'ait pas nécessaire de connaitre l'historique des concentrations en tritium dans les précipitations. Parmi les études ayant appliqué cette méthode de datation, Solomon & Sudicky (1991) ont considéré que les sources d'hélium 3 en provenance de

la fission de ^{6}Li et du manteau sont négligeables dans les eaux souterraines peu profondes. Ainsi, ils ont pu estimer les vitesses d'écoulement vertical à partir des gradients d'âge $^{3}H/^{3}He$ et conclut que c'est une mesure robuste pour interpréter les écoulements complexes en milieu hétérogène ainsi que pour la calibration des modèles numériques d'écoulement. Les résultats de calcul de taux de recharge et de vitesses d'écoulement sont bien plus précis qu'à partir des charges hydrauliques (Cook & Solomon 1997). Cependant, les autres sources d'hélium 3 ne peuvent pas être considérées comme négligeables dans tous les cas. Pour séparer les différentes sources, les concentrations en hélium 4 (rapport $^{3}He/^{4}He$) et en néon sont utilisées. Dans l'étude de Aeschbach-Hertig et al. (1998), les incertitudes sur les âges ont été améliorées en tenant compte des différentes sources d'hélium 3, en particulier pour un des puits présentant une forte concentration en hélium radiogénique, synonyme d'un âge plus élevé. C'est aussi le cas d'une partie des échantillons de l'étude de Shapiro et al. (1998).

3.2.4 Les gaz rares

Les gaz rares mesurés comprennent les isotopes de l'hélium, du néon, de l'argon, du krypton et du xénon, qui sont présentés sous de forme de rapport de masses entre deux isotopes. L'intérêt des gaz rares réside dans leur inertie, c'est-à-dire qu'ils ne participent à aucune réaction chimique ou biologique. Dans les eaux souterraines, ils proviennent de la dissolution des gaz atmosphériques dans l'eau d'infiltration. Ils peuvent aussi être produits in-situ par dégradation radioactive ou diffuser depuis le manteau ou la croûte terrestre. Dans les eaux de pluie, les concentrations en gaz rares sont à l'équilibre : elles dépendent de la pression partielle et de la solubilité des gaz dans l'eau, cette dernière étant fonction de la température et de la salinité (Beyerle 1999).

De manière générale, chaque gaz rare peut avoir plusieurs sources : origine atmosphérique (concentrations résultant de l'équilibre eau-atmosphère et air en excès) et non-atmosphérique (radiogénique et terrigène). La concentration en gaz résultant de l'équilibre entre l'eau et l'atmosphère est une valeur connue dans la littérature (Kipfer et al. 2002; Peeters et al. 2002), en fonction de la température et de la salinité. Plusieurs

modèles existent pour expliquer et estimer la quantité d'air en excès (Aeschbach-Hertig et al. 2008; Aeschbach-Hertig & Solomon 2013; Kipfer et al. 2002; Sun et al. 2010) : cet excès d'air (ou déficit dans certains cas) est d'origine atmosphérique (composition isotopique similaire à celle de l'eau en équilibre avec l'atmosphère) et peut avoir subi du fractionnement. Pour les sources de gaz non atmosphériques, la terminologie diffère selon les auteurs (Kipfer et al. 2002). Les gaz d'origine radiogénique sont produits par la dégradation radioactive des éléments dans les roches. Leur accumulation dans les eaux souterraines permet d'estimer l'âge des eaux anciennes. Les gaz terrigènes ont des signatures (rapports isotopiques) variables selon le réservoir géochimique d'où ils proviennent. Les deux principaux réservoirs sont la croute et le manteau. En général, les gaz en provenance de la croute sont assimilés à du gaz d'origine radiogénique puisque c'est le processus de production dominant dans la croute (Kipfer et al. 2002).

Comme mentionné dans la partie précédente, la datation $^{3}H/^{3}He$ nécessite les isotopes de l'hélium (le ratio $^{3}He/^{4}He$) et du néon pour différencier les différentes sources d'hélium. En effet, les quantités de néon, krypton et xénon produites en sub-surface sont négligeables par rapport à celles d'origine atmosphérique (Lehmann et al. 1993). C'est pourquoi le néon est utilisé pour quantifier l'excès d'air par rapport à l'équilibre atmosphérique. Les gaz rares produits par dégradation radioactive ont tendance à s'accumuler dans les eaux avec des faibles vitesses d'écoulement et peuvent être utilisés pour dater les eaux souterraines, en estimant leur taux de production. C'est le cas de l'hélium 4, de l'argon 40 et du néon 21 (Clark & Fritz 1997).

L'application la plus courante pour l'ensemble des gaz rares est la reconstruction des paléo-températures (Aeschbach-Hertig & Solomon 2013). Une équation à cinq inconnues peut être donc écrite pour chaque gaz (Aeschbach-Hertig et al. 1999; Ballentine & Hall 1999; Beyerle 1999) : la concentration mesurée dépend de la concentration initiale à l'équilibre du gaz, qui est fonction de la température T, de la salinité S et de la pression P, de la quantité d'air en excès A et du paramètre de rééquilibration R qui tient compte du possible fractionnement de l'air en excès. Il y a autant de façon d'écrire l'équation que de modèles pour expliquer l'air en excès (Aeschbach-Hertig & Solomon 2013). Un système de cinq équations à cinq inconnues est donc obtenu. En général, l'équation pour l'hélium n'est pas utilisée à cause de la multitude de sources qui sont

difficiles à séparer. Certains des paramètres peuvent être estimés conduisant à un système surdéterminé et plus facile à résoudre (Aeschbach-Hertig et al. 1999). Les détails sur les méthodes de résolution de ce système par modélisation inverse peuvent être trouvés dans Aeschbach-Hertig et al. (1999) et Ballentine & Hall (1999). Les paléo-températures calculées par cette méthode couplée avec la datation au carbone 14 ont permis de mettre en évidence la transition entre le dernier maximum glaciaire et l'Holocène, avec des différences de températures entre les deux périodes d'au moins 10°C (Aeschbach-Hertig & Solomon 2013). Parmi les autres applications des gaz rares, l'excès d'air quantifié par ΔNe peut aussi être interprété comme un indicateur des conditions d'humidité et d'amplitude des variations de la nappe (Aeschbach-Hertig et al. 2002).

3.3 Modèle conceptuel et validation par modélisation numérique

L'interprétation simultanée de l'ensemble des données géochimiques présentées précédemment permet d'améliorer la compréhension des systèmes d'écoulement de manière bien plus approfondie qu'avec les seules données de piézométrie et de proposer un modèle conceptuel plus complet. L'interprétation des données n'étant pas toujours unique, un modèle numérique peut permettre de tester des hypothèses et de corriger et/ou valider le modèle conceptuel. De plus, l'utilisation des données géochimiques permet d'améliorer la calibration des modèles numériques (Hunter et al. 2008; Plummer et al. 2004; Sanford et al. 2004). De nombreux modèles sont disponibles, chacun avec ses propres spécificités (Cloutier 2004).

Il existe deux approches : la modélisation inverse et la modélisation prédictive (Glynn & Plummer 2005). La modélisation inverse sert à identifier les réactions responsables de l'évolution chimique et isotopique d'une eau. Elle requiert l'identification de la composition initiale de l'eau (par exemple, l'eau de recharge) et une composition finale (l'eau vers l'exutoire), représentatives de l'évolution géochimique de l'eau. Les résultats sont essentiellement qualitatifs. Ce type de modélisation nécessite une bonne connaissance de la composition minéralogique des formations présentes et des cinétiques de réactions (Glynn & Plummer 2005). PHREEQC (Parkhurst & Appelo 1999) et NETPATH (Plummer et al. 1991) sont parmi les programmes les plus connus

pour ce type de modélisation. Cependant, le programme est limité à une dimension le long d'une ligne d'écoulement mais il permet de se faire une première idée sur les processus responsables de l'évolution géochimique de l'eau souterraine le long d'une ligne d'écoulement typique. La modélisation prédictive est associée à la simulation des écoulements et le transport de solutés par advection-dispersion, couplée aux processus géochimiques. C'est un outil permettant aussi d'améliorer les modèles conceptuels et d'évaluer l'importance des différents processus dans l'évolution chimique des eaux souterraines.

A titre d'exemple, dans leur étude de l'aquifère du bassin aquitain, André et al. (2005) ont employé les données géochimiques et la modélisation pour une meilleure compréhension des écoulements. Ils ont utilisé PHREEQC afin de quantifier l'importance des réactions chimiques pour chacun des échantillons. Dans une première approche, ils ont considéré uniquement les ions majeurs pour lesquels ils ont calculé les indices de saturation. A partir de ces résultats, les phases minérales d'importance ont été identifiées. A partir de la composition initiale de l'eau de recharge, la composition de chaque échantillon d'eau a été reconstituée. La modélisation a été contrainte par le pH et les données isotopiques de $\delta^{13}C$, appelés variables de validation par les auteurs. De plus, les données de $\delta^{13}C$ permettent d'identifier des sources additionnelles de CO_2. La modélisation géochimique leur a permis d'estimer qualitativement les directions régionales d'écoulement, l'existence de barrières à l'écoulement, les mélanges d'eau dans l'aquifère et les interactions entre aquifère et aquitard. Pour une évaluation quantitative, les auteurs recommandent une modélisation 3D des écoulements, du transport et de la chimie. Toujours avec PHREEQC, Walraevens et al. (2007) ont simulé la dessalure de l'aquifère Tertiaire en Flandres (Belgique). Ils ont sélectionné une ligne d'écoulement qu'ils ont modélisée en 1D, en tenant compte des vitesses d'écoulement selon la couche géologique traversée et des processus géochimiques importants tels que l'échange cationique, l'équilibre avec la calcite, la dissolution du gypse dans les argiles et la réduction des sulfates dans l'aquifère.

Les exemples de modélisation de transport réactif en 2D ou 3D sont un peu plus rares et à des échelles plus restreintes, dus des durées de temps de calcul assez longues (Glynn & Plummer 2005) et les modèles ne prennent en compte qu'un nombre limité de processus. Ce type de modèles est souvent utilisé pour

l'évaluation des sites destinés au stockage des déchets radioactifs (Arcos et al. 2008; Molinero et al. 2008), les cas de drainage minier acide (Molson et al. 2007; Walter et al. 1994) ou les panaches de contamination (Mao et al. 2006; Mayer et al. 2002; Salas & Ayora 2004).

4 Problématique et objectifs du projet de recherche

4.1 Synthèse des connaissances actuelles dans la région et définition de la problématique

Les études sur la qualité des eaux souterraines du Bouclier Canadien pouvant être utilisées comme source d'eau potable (150 premiers mètres de profondeur) sont assez limitées. En excluant les actuels projets PACES, peu d'études de cette envergure (échelle régionale) existent. Seules deux études similaires, basées sur l'échantillonnage de puits de particulier (profondeur maximale supposée de 150 m), ont été recensés dans la littérature. Betcher et al. (1988) ont mis en évidence des concentrations naturelles anormalement élevées en uranium dans les eaux souterraines de la province supérieure du Bouclier Canadien (Lac du Bonnet, sud-est du Manitoba). Ils ont expliqué ces concentrations par le lessivage des argiles riches en uranium ainsi que par la dissolution de minéraux uranifères présents dans le roc. Couture (1997) s'est intéressé à la qualité des eaux souterraines en fonction de la nature des roches de la ceinture méta-sédimentaire centrale de la province du Grenville (région de Mont-Laurier, Québec). Les principaux dépassements concernent les fluorures, le fer, le manganèse, le pH (pH<6.5) ainsi que quelques éléments traces tels que le cuivre et le nickel. A part ces deux derniers, les autres dépassements sont similaires à ceux observés en Outaouais. Le tritium a été détecté dans tous les puits et témoigne donc d'une circulation rapide des eaux souterraines, comme c'est le cas dans la région de l'Outaouais.

A part ces deux études, la plupart des études faites dans le Bouclier Canadien vise à caractériser les eaux profondes de type saumâtre dans le cadre de programme de recherche pour l'enfouissement des déchets

radioactifs. Ces études reposent principalement sur la chimie des cations majeurs et quelques mesures isotopiques (isotopes stables, tritium). Quelques échantillons ont été pris dans les eaux souterraines peu profondes, considérées comme un des membres extrêmes (« end member » en anglais). Les résultats d'analyses ont montré que les eaux douces peu profondes (< 200 m) reflètent les conditions climatiques locales (Frape & Fritz 1987; Frape et al. 1984) et sont similaires aux eaux de surface (Farvolden et al. 1988). Fritz & Frape (1982) et Gascoyne et al. (1987) se sont intéressés seulement aux eaux salines à des profondeurs supérieures à 300-400 m, voire plus. Bottomley et al. (1984) ont aussi mesuré différents isotopes dans des échantillons d'eaux souterraines pour la plupart prélevés à des profondeurs supérieures à 200 m.

Quelques études utilisant la modélisation ont été réalisées dans le contexte géologique du Bouclier Canadien. Gleeson & Manning (2008) ont modélisé en 3D l'impact de la topographie et des paramètres hydrogéologiques sur les écoulements. A partir d'un modèle 2D avec des fractures calibré sur des observations de terrain, Ophori (2004) a calculé des temps de transport mais les résultats n'ont pas été comparés à des données de terrain. Sykes et al. (2009) se sont intéressés à la modélisation en 3D les concentrations en eaux saumâtres à grandes profondeurs. Seul Ophori (1999) a utilisé les données géochimiques pour caler son modèle d'écoulement. En effet, il a contraint ses valeurs de conductivités hydrauliques en calculant des profils verticaux en MDT, chlorures et $\delta^{18}O$ (modélisation en 1D).

Ainsi, les connaissances sur les eaux souterraines sont très fragmentaires dans la région de l'Outaouais. De plus, le territoire à l'étude est grand et les données collectées à l'échelle régionale sont en quantité limitée. A partir d'un faible nombre d'échantillons supposés représentatifs de la qualité des eaux souterraines et de données complémentaires disponibles dans le cadre du projet PACES (piézométrie, géophysique…), on se propose de combiner le domaine de l'hydraulique souterraine à celui de l'hydrogéochimie afin de développer et de valider un modèle conceptuel d'évolution géochimique des eaux souterraines en Outaouais. Pour répondre à cette problématique, différents objectifs ont été définis :

1. Evaluer la qualité de l'eau souterraine à l'échelle régionale grâce à une campagne d'échantillonnage d'envergure et interpréter les dépassements de normes selon les contextes hydrogéologiques. Seuls les 100 à 150 premiers mètres sous la surface du sol ont été étudiés et sont d'intérêt pour l'utilisation des eaux souterraines comme eau potable par des particuliers. Vérifier que l'impact de l'invasion par la Mer de Champlain est significatif sur la qualité de l'eau comme dans d'autres régions localisées dans la vallée du St Laurent, bien que l'épisode ait été plus court de quelques centaines d'années.

2. Identifier les principaux processus géochimiques responsables de la qualité de l'eau souterraine et proposer un modèle conceptuel d'évolution de la géochimie de l'eau souterraine à l'échelle régionale le long d'une ligne d'écoulement représentative de la région. Ce modèle sera amélioré en intégrant des données supplémentaires d'isotopie (isotopes stables $\delta^{18}O$ et $\delta^{2}H$, tritium ^{3}H, isotopes stables du carbone $\delta^{13}C$ et datation au ^{14}C sur le CID, gaz rares He, Ne, Ar, Kr, Xe) collectées le long de cette ligne d'écoulement (échelle locale).

3. Valider le modèle conceptuel par modélisation numérique des écoulements, de l'âge des eaux et des processus géochimiques. Cette étape permettra d'étayer les hypothèses développées lors des étapes précédentes.

4. Evaluation des ressources en eaux souterraines et de leur durabilité et proposer des recommandations pour une bonne gestion.

4.2 Choix de la zone dite « à l'échelle locale » et acquisition des données géochimiques et isotopiques

Dans l'objectif 2, l'échelle locale correspond à une ligne d'écoulement identifiée à partir d'une carte piézométrique du roc à l'échelle de la région (autre volet du projet PACES). Initialement, plusieurs lignes piézométriques avaient été identifiées et des coupes géologiques réalisées le long de chacune d'elles. Seule celle passant proche de la localité de Shawville a été retenue pour les raisons suivantes. A son endroit, la

géologie est relativement simple et représentative de la région : roc du Bouclier Canadien surmonté par quelques couches de dépôts du Quaternaire, absence de grandes failles tectoniques ou de linéaments dont le rôle est variable et dont la détermination nécessite souvent des données supplémentaires (Bense et al. 2013), absence de roches sédimentaires des Basses Terres du St Laurent. La population n'est pas trop concentrée en un seul endroit : elle est disséminée et possède probablement des puits individuels pour s'alimenter en eau potable (Shawville a son réseau d'aqueduc). Avant les travaux, c'était la partie de la région la moins bien connue (peu d'informations disponibles).

Le long de la ligne d'écoulement, le prélèvement d'échantillons en fonction de la profondeur est préférable à des échantillons composites en vue d'une modélisation 2D vertical des écoulements, des âges et de la chimie. Une des méthodes de prélèvement d'échantillons à différentes profondeurs repose sur l'utilisation de packers qui isolent une portion du puits. En plus de permettre l'échantillonnage, il est possible de faire quelques tests hydrauliques afin d'obtenir un profil des transmissivités en fonction de la profondeur. Cependant, l'échantillonnage repose essentiellement sur la permission du propriétaire à échantillonner son puits, dans lequel se trouve une pompe, qui rend le puits inutile pour l'utilisation des packers. Les travaux pouvant durer plusieurs jours, il est donc évidemment hors de question d'envisager un retrait temporaire de la pompe (à supposer que ce soit faisable par les équipes de terrain). Finalement, seuls deux puits (un creusé dans le cadre du projet PACES et un abandonné) ont pu être utilisés avec les packers. Le puits creusé dans le cadre du projet, d'une profondeur de 42 m, a fait l'objet d'essais hydrauliques sur trois intervalles dont un a été échantillonné tandis que le puits abandonné, d'une profondeur de 90 m, a été testé sur 9 intervalles dont deux ont été échantillonnés. Les essais hydrauliques ont été concluants et les résultats interprétés selon Illman (2004) ont été utilisés pour ce projet de recherche. En revanche, les résultats d'analyses chimiques et isotopiques sont peu pertinents, en particulier pour un des puits dont le taux de renouvellement de l'eau était très lent (conductivité hydraulique de l'ordre de 10^{-7} $m.s^{-1}$). En raison de contrainte de temps, les purges n'ont pas suivi exactement le protocole. Ces résultats ne seront donc peu ou pas mentionnés dans ce qui suit.

5 Organisation de la thèse

Cette thèse est une thèse par articles, qui se compose de trois chapitres précédés d'une partie introduction et d'une partie conclusion.

Le premier chapitre est un article intitulé « Groundwater geochemistry of the Outaouais Region (Québec, Canada): a regional-scale study », publié dans Hydrogeology Journal (Montcoudiol et al. 2015). Dans cet article, les groupes d'eau établis en utilisant une analyse statistique multi-variée sont interprétés en fonction des contextes hydrogéologiques de la région et aident à l'identification des processus dominants responsables de l'évolution géochimique de l'eau. Des processus secondaires permettent d'expliquer les dépassements des normes d'eau potable pour certains éléments mineurs. Un modèle conceptuel est construit à partir de l'interprétation de ces résultats.

Le second chapitre est un article intitulé « A conceptual model for groundwater flow and geochemical evolution in the southern Outaouais Region, Québec, Canada », accepté pour publication par Applied Geochemistry (Montcoudiol et al. accepted). Dans cet article, en plus d'analyses chimiques standards, des données supplémentaires d'isotopie sont disponibles le long d'une ligne d'écoulement, passant par Shawville. L'ensemble des données est interprétée afin d'améliorer le modèle conceptuel en termes de caractérisation de la recharge, de temps de résidence moyens et de mélange.

Le troisième chapitre intitulé « A numerical model of groundwater flow, tritium and chloride transport, and residence time in the southern Outaouais Region, Quebec, Canada » sera soumis au journal Ground Water (Montcoudiol et al. in prep.). Dans cet article, le modèle conceptuel développé dans le précédent article est testé à l'aide de modèles numériques en 2D vertical. Premièrement, un modèle d'écoulement a été réalisé et calibré à l'aide des données piézométriques et des résultats d'un modèle de transport du tritium. les conséquences de l'invasion de la région par la Mer de Champlain ont été évaluées avec un modèle en deux étapes du transport des chlorures. Pour finir, les temps de résidence moyens dans l'aquifère ont été calculés avec un modèle de transport d'âge advectif-dispersif de l'eau.

Pour finir, la partie « Conclusion » synthétise l'ensemble des résultats et des conclusions décrites dans chaque article. Cette discussion se poursuit par une liste de quelques recommandations pour la gestion de l'aquifère ainsi que par un bilan sur les contributions à la science et une ouverture sur les perspectives de futurs travaux.

Chapitre 1 – Géochimie des eaux souterraines de l'Outaouais (Québec, Canada) : une étude à l'échelle régionale

Groundwater geochemistry of the Outaouais Region (Québec, Canada): a regional-scale study

N. Montcoudiol, J. Molson et J.-M. Lemieux
Département de Géologie et de Génie Géologique
Université Laval, Québec City, QC, Canada, G1V 0A6

Référence : Montcoudiol N, Molson JW, Lemieux JM (2014) Groundwater geochemistry of the Outaouais Region (Québec, Canada) – A regional scale study. Hydrogeol J. 23(2): 377-396. DOI: 10.1007/s10040-014-1190-5.

1 Résumé

Dans le cadre d'un programme de caractérisation des eaux souterraines à l'échelle provinciale, une étude hydrogéochimique a été menée dans l'Outaouais (Québec, Canada) dans le but d'identifier les principaux processus responsables de la qualité des eaux souterraines et de développer un modèle conceptuel d'évolution géochimique. Pendant les étés 2011 et 2012, 139 échantillons ont été prélevés dans des puits municipaux et privés et ont été analysés pour les ions majeurs, les nutriments, les éléments traces et les sulfures. Environ 70% des échantillons proviennent de puits au roc, principalement dans le Bouclier Canadien, et le restant de puits localisés dans les dépôts du Quaternaire. La répartition des faciès hydrogéochimiques a été déterminée pour les 127 échantillons ayant une balance électronique entre ±10%. La classification par les facies est étayée par une analyse statistique multi-variée incluant une analyse factorielle et une analyse hiérarchique par groupement. L'invasion par la Mer de Champlain, l'échange cationique et la recharge par des eaux météoriques peu minéralisées sont les principaux processus géochimiques affectant la géochimie des eaux souterraines de la région. Les processus secondaires, liés à la nature géologique du roc, sont responsables des dépassements des normes d'eau potable canadiennes pour les fluorures, l'uranium, le fer et le manganèse.

Mots clés : hydrogéochimie régionale, qualité de l'eau souterraine, roches cristallines, Canada, modèle conceptuel

2 Abstract

As part of a province-wide groundwater characterization program, a detailed groundwater geochemistry survey was undertaken in the Outaouais Region (Québec, Canada) in order to identify the primary processes responsible for groundwater quality and to develop a conceptual model for groundwater flow and geochemical evolution. During the summers of 2011 and 2012, 139 samples were collected from municipal and private

wells which were analysed for major ions, nutrients, trace elements and sulphides. About 70 % of the samples were obtained from bedrock wells, mainly in the silicate rocks of the Canadian Shield and the remainder from wells screened in Quaternary deposit aquifers. Hydrogeochemical facies distributions were determined from 127 of these samples which had anion-cation charge balance errors within ±10 %. The classification by facies was also supported by a multivariate statistical analysis, namely factor analysis combined with hierarchical cluster analysis. The study identified Champlain Sea invasion, cation exchange and freshwater recharge as the main geochemical processes affecting groundwater chemistry in this region. Secondary processes, related to the bedrock geology, are responsible for exceedances of Canadian drinking-water standards, namely for fluoride, uranium, iron and manganese.

Keywords: regional hydrogeochemistry, groundwater quality, crystalline rocks, Canada, conceptual model

3 Introduction

In the province of Quebec, Canada, groundwater resources are increasingly being relied upon for drinking water, as well as for industrial and agricultural use. Groundwater supply and quality is also under threat from resource extraction industries, for example mining in the north, and possible shale gas extraction in the south. In response to growing demand for groundwater and increased risk of contamination, a better understanding of groundwater availability and quality is required. While groundwater availability is generally well understood in the St. Lawrence and Ottawa valleys due to municipal groundwater research studies, groundwater quality, and more specifically groundwater geochemical evolution, is poorly constrained. This is in part due to the complex geology of these areas that spans three geological provinces: the St. Lawrence Lowlands Platform (sedimentary clastic and carbonate rocks), the Appalachians (sedimentary clastic and metamorphic rocks) and the Canadian Shield (crystalline silicate rocks), which are covered with discontinuous and highly heterogeneous surficial deposits left during the last glacial period (Wisconsin glaciation). Moreover, following the last glaciation, salt water from the Champlain Sea invaded the region (Fig. 6).

According to Blanchette et al. (2010b), Beaudry (2013), Carrier et al. (2013) and Larocque et al. (2013) who studied shallow (<100m) groundwater geochemistry in the St. Lawrence Platform and Appalachians south of the St. Lawrence River (Fig. 6), the Champlain Sea invasion some 10,000 years ago is still having consequences on the groundwater quality of aquifers located in the flooded area. These authors also identified carbonate dissolution, Ca/Na cation exchange and mixing as the main processes controlling the geochemical evolution of groundwater. These processes were also recognized in the fractured clastic and carbonate rock aquifers of the St. Lawrence Platform north of the St. Lawrence River (Cloutier et al. 2008) covered by the Champlain Sea.

In the Canadian Shield, north of the St. Lawrence River, the impact of the Champlain Sea invasion is less documented. Leblanc et al. (2013) collected 243 groundwater samples from aquifers located in the south-western part of the Mauricie region but most were taken from superficial deposit aquifers. Moreover, they did not propose any geochemical processes explaining the observed groundwater composition. However, some samples located in confined aquifers were recognized as remnant water of the former Champlain Sea (Na-Cl water type). In the area of Québec City, Talbot Poulin et al. (2013) investigated groundwater quality in the Canadian Shield where some samples were of Na-Cl water type but they did not specifically investigate the influence of the Champlain Sea episode on geochemical evolution. Other studies (Frape et al. 1984; Fritz & Frape 1982) have focused on groundwater quality of bedrock aquifers in the Canadian Shield but at depths of more than 500 m where groundwater is characterised by high salinity brines. In addition, Couture (1997) investigated the influence on groundwater geochemistry of different lithologies from the central metasedimentary belt of the Canadian Shield. From samples taken in the surficial layer of the crystalline bedrock aquifers (maximum depth of 120 m), Couture (1997) identified different factors responsible for a relatively uniform groundwater quality despite different host rock composition and structure. These factors include limited water-rock interaction times, highly permeable fracture networks and possible adsorption or precipitation of many of the more discriminating elements.

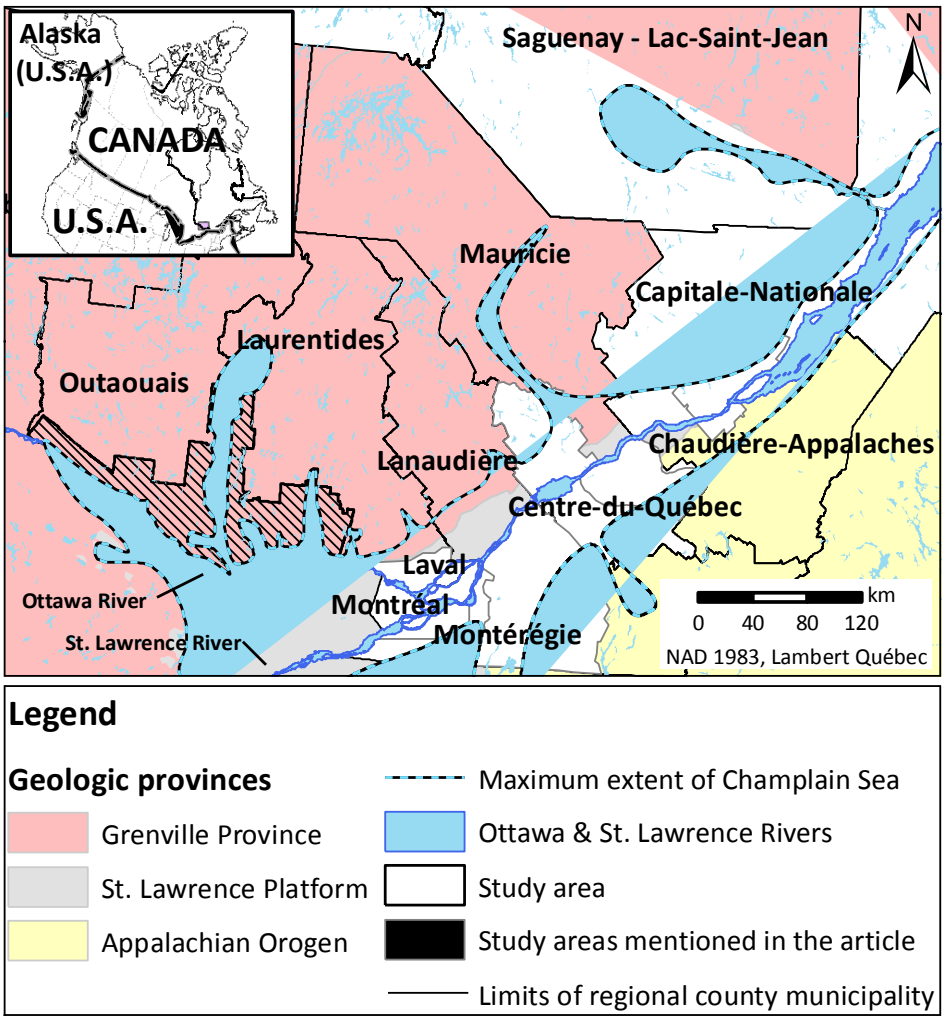

Fig. 6 Location of the Outaouais regional study area, showing the study areas mentioned in the article

The main objective of this study is to identify the primary processes responsible for groundwater chemistry and quality in the Outaouais Region (Quebec), and to develop a conceptual model for understanding geochemical evolution and groundwater flow in the study area. More specifically, this study will provide a conceptual model of geochemical evolution in crystalline fractured rock aquifers of the Canadian Shield, the St. Lawrence Lowlands and surficial deposits in an area where the Champlain Sea episode was shorter compared to other regions, especially in the valleys of the Ottawa River tributaries in which the marine invasion started later and the seawater left earlier.

To date, no comprehensive studies on groundwater quality in the Outaouais Region have been conducted. Only scattered results from local consulting reports as well as limited chemical analyses of groundwater

samples over the last few decades are available. The present study is part of a comprehensive project on groundwater characterisation of the Outaouais Region. While the complete project includes physical and chemical hydrogeological characterization, including pumping tests, surface geophysics and Quaternary mapping (Comeau et al. 2013), the current paper will focus on the regional hydrogeochemistry.

After a thorough description of the study area, the sampling and analysis methodology is presented, in particular how the data were handled for the statistical analysis. To address the objectives, water types are defined and interpreted along with the results from a multivariate statistical analysis (factor analysis combined with hierarchical cluster analysis) and incorporating the geologic and hydrogeological knowledge of the region. The separation of groundwater samples into clusters helped provide insight into the main processes responsible for groundwater chemical evolution in the region. Secondary processes were also identified to explain exceedances of drinking water standards for fluoride, uranium, iron and manganese. Finally, a regional conceptual model of groundwater geochemical evolution was developed based on the interpretation of these results.

4 Study area

The Outaouais Region is located in south-west Québec, close to the national capital of Ottawa, on the northern bank of the Ottawa River which forms its southern boundary (Fig. 6). The Ottawa River is a tributary of the St. Lawrence River, and is situated upstream from the regions investigated in the previously cited studies. The study area covers 13,762 km^2, which includes the most populated areas of the Outaouais Region, and in which 40% of the over 340,000 habitants rely on groundwater via municipal networks or individual wells (Comeau et al. 2013). Groundwater is used primarily for household use and as a drinking water supply (72%), while other uses include industrial, commercial and institutional (23%) with the remaining 5% used for agricultural purposes. Surface elevation varies from 37 meters along the Ottawa River, which is the discharge zone for the major southward-flowing rivers, to 555 m above sea level. The hydrographical network is well

branched with about 9,400 km of perennial streams and more than 16,000 lakes. The study area is characterized by a wet continental climate with four seasons. Mean annual precipitation varies between 862 and 1,193 mm with the higher values towards the east. Annual mean temperatures are between 3.7 and 5.7°C, with the colder temperature range towards the north.

4.1 Bedrock geology

Approximately 90% of the Outaouais study area is located in the Grenville Province of the Canadian Shield (Fig. 6), dating from the Proterozoic (Precambrian). Within the shield, three primary, mainly silicate rock types can be defined depending on their origins, whether intrusive (felsic, mafic and ultra-mafic), migmatic or metasedimentary (Bélanger 2014).

The bedrock underlying the remaining 10% of the area is composed of rocks from the St. Lawrence Platform along the Ottawa River (east of Gatineau and in the area of Île-aux-Allumettes, an island in the Ottawa River, in the western part of the region, Fig. 6). The St. Lawrence Platform, dating from Cambrian to Ordovician, forms a series of sedimentary rocks including sandstone, dolostone, shale and limestone (Globensky 1987).

The Canadian Shield and Paleozoic bedrock formations are extensively fractured and while the maximum pumping rates and aquifer storativities may be relatively low, they are important sources of groundwater for individual households. According to Sterckx (2013), fractures near the bedrock surface have preferred NE and ESE orientations, similar to the regional lineaments, with fracture density decreasing with depth. Bulk hydraulic conductivities vary from 10^{-8} to 10^{-4} m/s in the fractured bedrock and from 10^{-13} to 10^{-10} m/s in the less permeable (matrix) zones (Sterckx 2013).

4.2 Quaternary deposits

The bedrock in the Outaouais Region is covered by discontinuous layers of Quaternary till, fluvio-glacial sediments and marine clay. Following the most recent deglaciation of the area about 10,000 years ago, the long-term subsidence of the continent due to the weight of ice allowed invasion of the Champlain Sea into the

main valleys of the Outaouais Region, including the Ottawa and Gatineau River valleys (Fig. 6). Water from the Champlain Sea was a mixture of freshwater (66%) from melting ice and rainfall, and salt water (34%) from the Gulf of St. Lawrence (Cloutier et al. 2006). In addition to inducing saltwater recharge, the Champlain Sea also left a layer of sensitive marine clay up to 100 m in thickness in some areas. Due to glacial isostatic rebound over several thousand years following incursion, the Champlain Sea retreated from the area leaving various deltaic, littoral and pre-littoral sediments of mostly sand and gravel which are up to 70 m thick in the Gatineau valley. Along the main rivers, this sequence is buried by thin layers of ancient and more recent alluvium (up to 10 m).

4.3 Hydrogeology

The complex geological history of the Outaouais Region has created several unique hydrogeological flow systems which are controlled primarily by the distribution of the Quaternary sediments (Comeau et al. 2013). These flow systems can be divided into four hydrogeological contexts:

a) At higher elevations, in the Laurentian Highlands (northern part of the region), the bedrock is covered by a discontinuous layer of till. In some of these areas the till is absent, leaving exposed bedrock outcrops where groundwater recharge is relatively high and the bedrock serves as an unconfined or semi-confined aquifer. Much of the regional groundwater recharge occurs in these northern areas.

b) Fluvio-glacial sediments outcrop only in the higher parts of the major valleys, where the invading Champlain Sea did not reach. Where their thickness is sufficient, these sand and gravel deposits are generally good aquifers. They are even more productive in the lower parts of the valleys, if not washed out by the Champlain Sea, where the overlying marine clays act as aquifer confining layers, especially along the Ottawa River and the lower parts of the main valleys.

c) Glacio-lacustrine sediments, including deltaic plains and littoral sediments, are generally coarse-grained and are also good aquifers.

d) In some local areas, alluvial sediments are potentially good shallow aquifers.

The main groundwater flow paths through the bedrock aquifer can be identified from the piezometric map generated from about 15,000 water table levels (Comeau et al. 2013). The regional groundwater flow direction is from the higher elevation regions in the north towards the Ottawa River in the south. The main southward-flowing rivers (Fig. 6) also serve as sub-watershed-scale discharge areas towards which intermediate-scale groundwater flow paths, primarily east-west oriented, are directed.

5 Material and methods

Following sample collection in carefully selected wells, analysis quality was checked and water types were determined for samples with a charge balance error within ± 10%, before preparing the dataset for subsequent statistical analysis. The methodology is outlined below.

5.1 Selection of the sampled wells

During the summers of 2011 and 2012, 139 groundwater samples were collected from municipal and private wells and analyzed for major ions (total alkalinity, Ca^{2+}, Mg^{2+}, K^{+}, Na^{+}, Br^{-}, Cl^{-}, F^{-}, $NO_3^{-}NO_2^{-}$ and SO_4^{2-}), nutrients (NH_4 and total inorganic P), trace elements (Al, Sb, Ag, As, Ba, Be, Bi, B, Cd, Cr, Co, Cu, Sn, Fe, Li, Mn, Mo, Ni, Pb, Se, Si, Sr, Ti, U ,V and Zn) and sulphides (total S) (Annexe 2). A standard sampling protocol was adopted in which samples were taken after pumping three wellbore volumes (in abandoned wells) or after stabilization of the primary physico-chemical parameters (in wells used daily, which applied to most samples). The physico-chemical parameters (temperature, pH, electrical conductivity, specific conductivity, dissolved oxygen, salinity, TDS and oxidation-reduction potential, Annexe 2) were measured using a multi-parameter probe (model YSI Professional Plus). Nutrients and trace elements were filtered using a 0.45 µm nitrocellulose filter. Selected preservatives were used to stabilize the samples: sulphuric acid for nutrients, nitric acid for trace elements and zinc acetate and sodium hydroxide for sulphides. Samples were kept at 4°C before being

sent to the laboratory. All samples were analysed by the same accredited commercial laboratory in Montréal, Canada. Assurance quality was ensured by taking about 10% duplicates and 1% blanks.

Despite field constraints (sparse population, water supply networks, inaccessible protected areas, non-uniform well-owner cooperation), special care was taken in the choice of the wells to be sampled. As much as possible, the wells were selected to be uniformly distributed throughout the study area and to be representative of the different types of aquifers (bedrock vs Quaternary deposits) and of the various degrees of confinement (unconfined vs semi-confined vs confined, Fig. 7a).

Consistent with the distribution of water supply wells, about 70% of the groundwater samples were obtained from bedrock wells, mainly in the Canadian Shield (86 samples), and in carbonate rocks (13 samples) in the southern part, along the Ottawa River. The remainder was from wells screened in Quaternary deposit aquifers (40 samples). Bedrock wells have greater depths (maximum of 160 m and an averaged depth of 78 m, Fig. 7b) whereas Quaternary deposit wells are shallower with an averaged depth of 36 m (maximal depth of 90 m, Fig. 7c).

5.2 Analysis quality

Assessment of analysis quality is of prime importance before any interpretation of the groundwater samples. First, 16 transport and field blanks were analysed and were considered as contaminated if concentrations exceeded twice the detection limit, according to the lab recommendations. Aluminum exceeded this criteria most often (4/16). Other parameters presenting exceedances were boron, molybdenum and sodium (2 each) as well as chloride, chromium, nickel and lead (1 each). Care should be taken with these parameters but the concentrations in the sample blanks were generally many orders of magnitude less than the groundwater sample concentrations. Although all groundwater sample duplicates showed concentration differences over 5% for at least one parameter, all duplicate samples showed a maximum charge balance error of only 6%. The sample duplicate with the lower charge balance was chosen for further analysis.

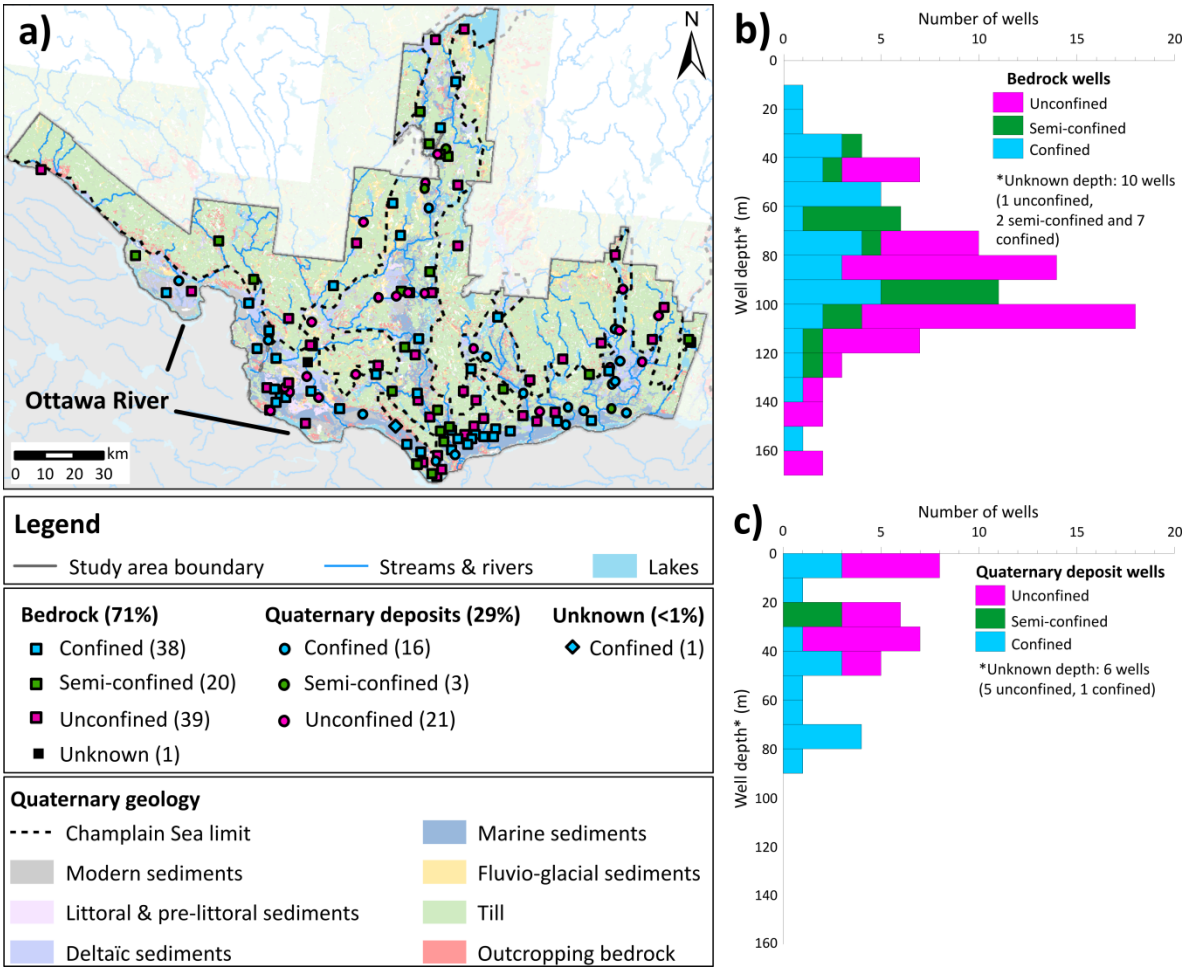

Fig. 7 Characteristics of the sampled wells: a) spatial distribution and hydrogeological context (number of wells shown in brackets), b) depth distribution for bedrock wells and c) depth distribution for Quaternary deposit wells

The second step involved calculating the charge balance (Hounslow 1995). Here, the model PHREEQC 2.18 (Parkhurst & Appelo 1999) was used to infer bicarbonate and carbonate concentrations from alkalinity and pH and other species in solution from total concentrations (Annexe 2). For one of the samples, in-situ parameters could not be measured thus the pH value was not available and was calculated by the program.

According to Hounslow (1995) and other authors, a charge balance error within ±10% is considered acceptable. Our study results showed that 127 samples had a cation-anion balance which respected this criterion. The remaining 12 samples with higher errors were rejected and not included for the determination of groundwater types and in the statistical analyses.

5.3 Data treatment for multivariate statistical analysis

Since a significant number of parameters were measured for each sample (8 parameters in the field and 39 species by a commercial laboratory, Annexe 2), multivariate statistical analysis was used to identify groups of parameters showing similar trends and to classify samples according to these trends. Processes controlling groundwater chemical trends were then inferred. The adopted procedure for preparing the chemical dataset for multivariate statistical analysis was based on the approach used by Cloutier et al. (2008).

To optimize the multivariate statistical analysis, some parameters were excluded based on the recommendations from Güler et al. (2002). For example, all elements for which more than 15% of samples were below the detection limit were not included. In addition, all redundant parameters (including hardness, total dissolved solids (TDS) and alkalinity) were not used. Except for the pH, all field-measured parameters were also discarded due to redundancy or to high uncertainty in their values resulting from the direct influence of surface conditions on the measurements. For example, Eh and O_2 were not measured directly in the well or using a flow cell, and sample temperature was likely influenced by exposure of the sampling hose to the sun. However, most of the field parameters were considered in the final discussion to support the analysis results. Fourteen parameters were finally retained: the major ions Ca^{2+}, Mg^{2+}, Na^{+}, K^{+}, HCO_3^{-}, Cl^{-} and SO_4^{2-} as well as the minor and trace elements B, Ba^{2+}, F^{-}, Mn^{2+}, Si and Sr^{2+}, as well as pH.

For the statistical analysis, concentrations below detection limits had to be replaced by a numerical value otherwise samples would be excluded during the analysis. Farnham et al. (2002) present several methods including the approach adopted in the present study in which such values are replaced by half the value of the detection limit.

Because of the wide range of concentrations, especially between major ions (mg/l) and minor ions (µg/l), standardization of the data is required for applying multivariate statistical techniques so that each concentration has an equivalent weight (Davis 1986). Descriptive statistics were determined for each retained parameter and histograms were generated to evaluate the concentration distributions. Special attention was

brought to the value of skewness, which is an indicator for the symmetry of a distribution and which complements the histograms. The results show that all concentration distributions are positively skewed except for pH (Table 1). Skewness values calculated for log-normal values show improvement and are close to zero except for Ca^{2+}, Mg^{2+}, Si and pH. Skewness values on log-normal values were only slightly lower for Ca^{2+} and Mg^{2+}. On the contrary, skewness was closer to zero on normal values for Si and pH. As a consequence, all parameters were assumed to follow a log-normal distribution except for pH and Si. Standardization was carried out according to the distribution of each parameter (Davis 1986; Güler et al. 2002). At this point, each distribution has a zero mean and the values for each parameter are measured in standard deviation units.

Once the standardized dataset was obtained, a multivariate statistical analysis was carried out. Two types of complementary statistical analysis were chosen using the statistical software SAS/STAT® 9.2 (SAS Institute Inc. 2009). First, factor analysis (FA) was used to infer interrelations between parameters (i.e. parameters showing the same trends). From the standardized dataset, a correlation matrix was computed, and eigenvalues (or factors) and eigenvectors were calculated. The eigenvalues represent the weight of each component in explaining the variance within the dataset whereas the eigenvectors are the weight of the parameters on each component (loadings). The eigenvalues which are less important in explaining the variance in the dataset are discarded. There is no consensus in the literature (Davis 1986) about the choice of the number of factors to be retained. Generally, factors with an eigenvalue greater than one (with a variance greater than the original standardized variables) are kept since these components explain most of the variance (Davis 1986). In our dataset, only the first three factors had eigenvalues greater than 1 which accounted for two-thirds of the explained variance. Since the eigenvectors were very similar for the different parameters, a varimax rotation was applied, changing the position of the axes in order to maximize the variance of the loadings on the three retained factors. This resulted in only a few significant high loadings for each factor, improving the interpretation of the results (Davis 1986).

Secondly, hierarchical cluster analysis (HCA) was applied to define groups that have the most similar chemical signature. From the standardized dataset, a distance matrix is first obtained by calculating the similarity

between samples. Groups of samples are then formed according to their similarities and are joined using a linkage rule. Several distance measure methods as well as different linkage rules are available. We adopted the approach of Güler et al. (2002) who tested different combinations of distance measures with linkage rules and concluded that Euclidian distance together with Ward's method for linkage produces the most distinctive groups. Results are displayed as a dendrogram, a type of tree graph which links the samples according to their similarities (Davis 1986).

Table 1 Descriptive statistics for the data matrix (concentrations in mg.l^{-1})

Parameter	Mean	Median	Minimum	Maximum	Std.[a]	Skewness
B	0.163	0.034	0.0025	6.9	0.631	9.9
Ba^{2+}	0.089	0.049	0.001	1	0.144	3.9
HCO_3^-	189	170	17.1	572	121	1.1
Ca^{2+}	47.3	37	1.9	290	39.0	2.7
Cl^-	76.7	14	0.39	1100	181	3.7
F^-	0.52	0.3	0.05	3.6	0.63	2.3
K^+	4.27	2.9	0.53	26	4.00	2.4
Mg^{2+}	12.3	7.2	0.71	57	12.3	1.9
Mn^{2+}	0.054	0.011	0.0002	0.63	0.103	3.0
Na^+	64.8	12	1.2	860	134	3.7
pH	7.93	7.93	5.98	9.66	0.75	-0.2
Si	6.79	6.7	0.05	22	2.44	1.9
SO_4^{2-}	43.6	22	0.25	970	97.3	7.8
Sr^{2+}	1.52	0.35	0.032	47	4.80	7.5

[a]Std. = standard deviation

6 Results

6.1 Water types

Water type (Back 1966) was defined for all samples having a charge balance error within ±10%. Basically, water type was determined from a combination of the principal cation and anion based on concentrations expressed in meq/l (see Cloutier (2004) for a complete description of the procedure). Using this method, ten water types were defined for the study area for which the spatial distribution is shown in Fig. 8.

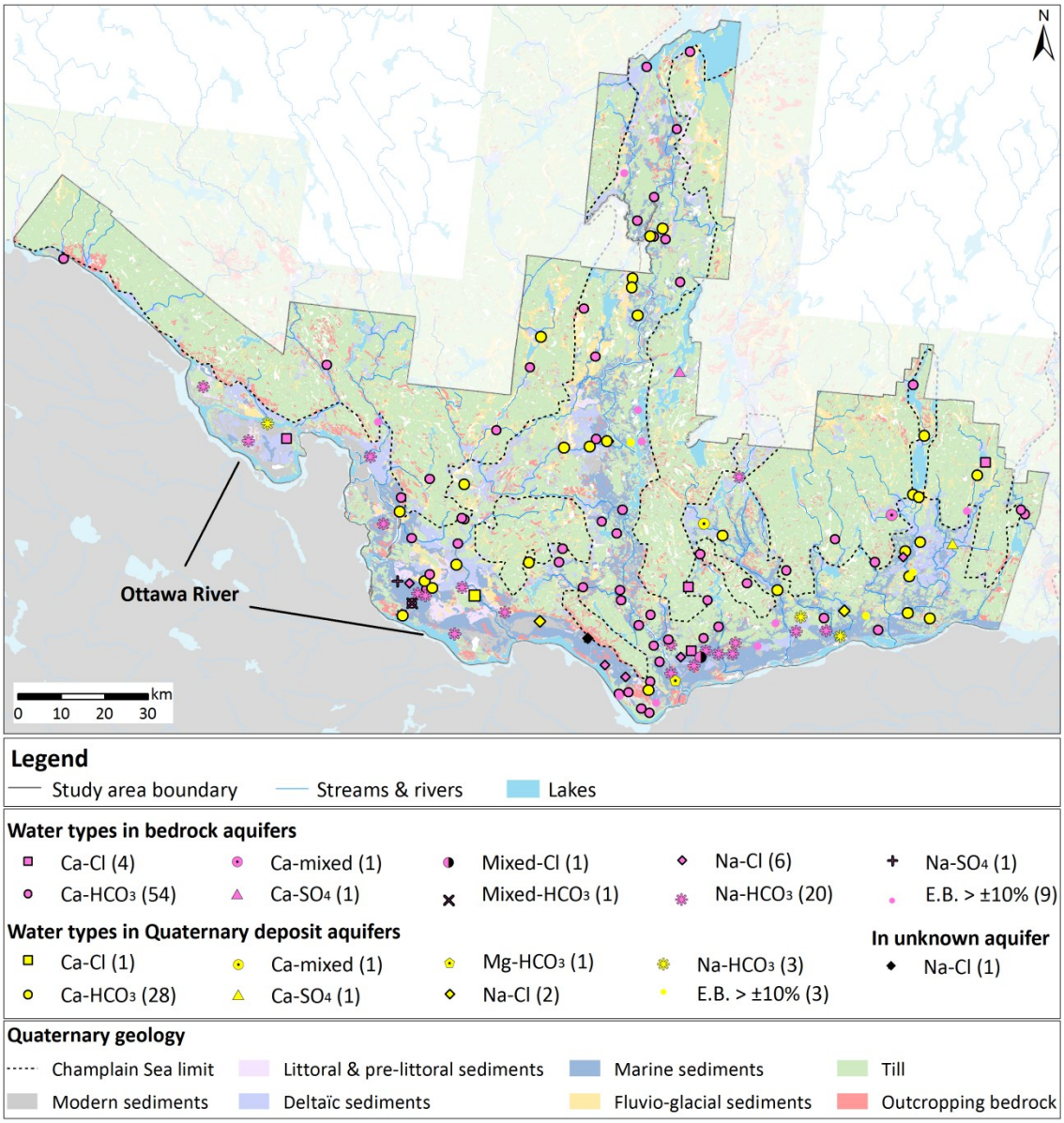

Fig. 8 Spatial distribution of water types based on geochemical signatures (number of samples for each type shown in brackets). E.B. stands for electronic balance

The analysis showed that calcium-bicarbonate ($Ca\text{-}HCO_3$) water type is dominant (65%), and is found throughout the study area. This water type characterized 76% of the Quaternary deposit aquifers, which is consistent with this water type being associated with shallow groundwater having a short residence time. These water types represent recently infiltrated water and their chemical signature is not very different from rain water. Sodium-dominant types ($Na\text{-}HCO_3$, Na-Cl and $Na\text{-}SO_4$) are also important water types in the area (26%) and are found mainly along the Ottawa River and the main tributaries, where the Champlain Sea had

invaded inland (leaving marine clays). Thus, these water types, especially Na-Cl, seem to be remnants of the former Champlain Sea. The remaining water types (9%) are intermediate water types between those previously mentioned.

6.2 Factor analysis (FA)

According to Table 2, the first factor is characterized by high loadings for SO_4^{2-}, Cl^-, Na^+ and Sr^{2+}, which are related to saline water and are consistent with the geological history of the region, invasion by the Champlain Sea in particular. The second factor presents high loadings for silica. This factor could be associated with silicate dissolution since the area is mainly underlain by silicate rocks. Although silicate weathering is a slow process, it seems to be more important than calcite or dolomite dissolution (although HCO_3^- and Mg^{2+} have higher loadings in Factor 1 and 2). The third factor seems to be associated with the dissolution of F bearing minerals at high pH such as fluorite which is currently being mined in the study area.

Using the same approach as for the parameters, scores for each water sample were also calculated during the FA procedure. These scores represent the influence of the component on the samples. Most samples from Quaternary deposit aquifers have negative scores on the three factors, indicating that they are characterized by a low salinity content, low concentrations in silica and fluoride, and relatively more acidic waters. These observations are also valid for most samples from unconfined aquifers and for Ca-CO_3 water types since most of the Ca-HCO_3 water-type samples are from unconfined aquifers, either located in bedrock or Quaternary deposit wells. Confined aquifers have high scores on factor 2 and 3, suggesting these samples are more chemically evolved with high silica content, high fluoride concentrations and high pH values. Na-HCO_3 and Na-Cl water types have high scores on factor 3 (mostly in confined aquifers). The Na-Cl water type also has high scores on factor 1, which is related to the sample salinity.

Table 2 Factor analysis loadings and explained variance after applying a varimax rotation

Parameter	Factor 1	Factor 2	Factor 3
B	0.623	0.156	0.569
Ba^{2+}	0.301	0.595	-0.051
HCO_3^-	0.544	0.580	0.177
Ca^{2+}	0.464	0.417	-0.646
Cl^-	*0.807*	0.135	0.084
F^-	0.334	0.261	*0.748*
K^+	0.522	0.520	0.458
Mg^{2+}	0.602	0.637	-0.139
Mn^{2+}	0.100	0.542	0.089
Na^+	*0.749*	0.169	0.500
pH	0.045	0.005	*0.745*
Si	-0.260	*0.763*	0.083
SO_4^{2-}	*0.848*	-0.081	0.058
Sr^{2+}	0.732	0.314	0.055
Explained variance	4.285	2.660	2.396
Explained variance (%)	30.6	19.0	17.1
Cumulative % of variance	30.6	49.6	66.7

Values in italic: dominant loadings (>±0.7)

6.3 Hierarchical cluster analysis (HCA)

The results of the HCA are displayed as a dendrogram, from which related chemical groups can be identified (Fig. 9a). To divide the samples into groups, a so-called phenon line was drawn for a value of 0.025. Seven clusters were identified with their own characteristics. Clusters 1 and 2 are quite different from the five other clusters, while clusters 3, 4 and 5 are more similar. Note that cluster 5 is composed of only one sample and was thus not included in the dendrogram.

In Fig. 9b, average Stiff diagrams, which display concentrations for major ions as milli-equivalents per litre, are represented for each cluster. The differences and similarities between each cluster can be easily identified. For example, Stiff diagrams for clusters 1 to 4 show similar shapes, with Ca^{2+} and HCO_3^- as the dominant ions. In these groups, the Ca-HCO_3 water type is dominant as seen in the Piper plot (Fig. 9c). As mentioned previously, these waters are only slightly mineralized and probably have short residence times. Most samples from Quaternary deposit wells (confined or unconfined) lie within these clusters, including most unconfined

bedrock wells. Cluster 1 represents very low mineralized waters which have infiltrated very recently. Gradually, these waters become increasingly mineralized as they dissolve the rock they are migrating through. Stiff diagrams from C1 to C4 show this trend as a widening at the level of Ca^{2+} and HCO_3^- concentrations (Fig. 9b) and also as increasing values of alkalinity, hardness, TDS and other major ions (Table 3).

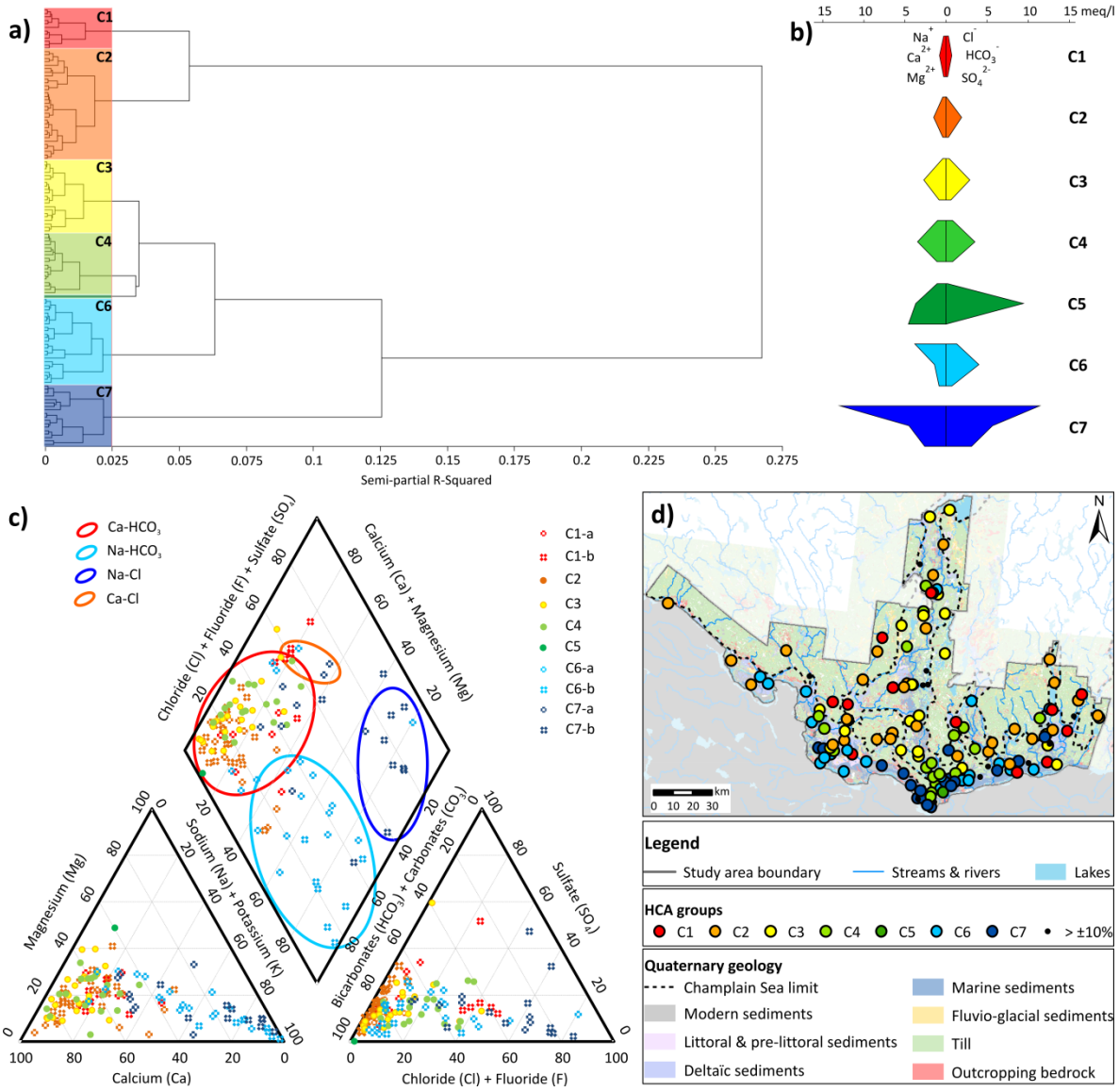

Fig. 9 Results from the HCA: a) Stiff diagrams showing the average composition of samples from each cluster; b) dendrogram (for clarity, sample names are not displayed) and identification of the clusters; c) Piper diagram according to HCA results and d) spatial distribution of the samples according to HCA results

Cluster 1 can be divided into two sub-groups of equal size (see the shape of C1 in Fig. 9a and the distinction between the two-sub-groups C1-a and C1-b on the Piper diagram in Fig. 9c). These two sub-groups are differentiated by their chloride concentrations. Samples from sub-group C1-a have low chloride concentrations of less than 4 mg/l (similar to cluster 2). This sub-group is also characterized by lower concentrations of major ions compared to the second sub-group (except HCO_3^-). In sub-group C1-b, chloride concentrations are quite high compared to cluster 2 (next in the chemical evolution). Many explanations for this trend could be invoked including contamination from de-icing salts for wells close to main roads, from animal or domestic sewage, or from fertilizer. The presence of anthropogenic chloride contamination in some samples would explain why the average chloride concentration for cluster 1 is greater than that for clusters 2 and 3 while samples from this cluster are also less chemically evolved.

Most minor elements have similar median values for these four clusters. However, clusters 1 and 3 have higher nitrate concentrations. At this level of characterization, it is difficult to provide a reasonable explanation since it cannot be explained by a higher proportion of unconfined/semi-confined aquifers compared to the two other clusters (C2 and C4). The trend is perhaps related to the location of the wells in relation to farming zones. Cluster 4 is characterized by higher concentrations of Ba^{2+}, Mn^{2+} and Sr^{2+} compared to the three other clusters, suggesting the dissolution of Ba-, Mn- and Sr-bearing minerals. Median pH values are acidic for cluster 1 and oxidation-reduction potential (ORP) values indicate oxidizing conditions. These characteristics are typical of groundwater in recharge zones.

Cluster 5 includes only one sample and has a quite atypical chemical composition. According to the shape of the Stiff diagram, this sample is of a Mg-HCO_3 water type. This sample also has the highest concentrations in the dataset for the following parameters: HCO_3, Mg, Si, Ag, NH_4 and exceedances for Fe, Mn and TDS. These high concentrations seem to indicate that the sample has a long residence time. The sample was taken in a sand-point well which was located in a sandy layer covered by a clayey silt layer of 18m thickness, which could be responsible for the chemical evolution of this sample. The chemistry of this sample is not yet fully understood.

On the anion side of the Stiff diagram, cluster 6 has the same shape as cluster 4 but on the cation side, a shift can be observed between the concentrations of Na^+ and Ca^{2+} (noticeable in Table 3 as well), indicating cation exchange. Due to Champlain Sea invasion, the shallow bedrock aquifers were invaded by salt water with Na^+ adsorbing onto minerals and retained by clays whose pores became filled with salt water. Since then, these aquifers have been recharged by infiltrating freshwater rich in Ca^{2+}, which replaces Na^+ on minerals and clays. Samples in this cluster present various degrees of cation exchange with exchange in samples on the upper branch less advanced than those on the lower branch (Fig. 9a). These samples were generally of Na-HCO_3 water type and were taken from confined aquifers under reducing conditions (Table 3).

Samples from cluster 7 are characterized by high concentrations in Na^+ and Cl^- and are mainly of a Na-Cl water type. Most of the Na^+ and Cl^- concentrations are above drinking water standards (200 and 250 mg/l, respectively) as are all the TDS values (500 mg/l). The median concentrations for the other major ions and for minor constituents are the highest among all clusters (except for Ba^{2+}, Mn^{2+} and NO_3-NO_2).

Similar to cluster 1, cluster 7 can be divided into two sub-groups. The first sub-group, C7-a, of 8 samples (the higher branch of C7 in Fig. 9a), has similar averaged equivalent concentrations for Na^+, Ca^{2+}, Cl^- and HCO_3^-. In samples taken in wells drilled in the St. Lawrence Lowlands Platform, the recharge signature is dominant (Ca-HCO_3 water type) because of the ease of carbonate dissolution compared to silicate dissolution. Samples from the Canadian Shield have different water types (Ca-Cl, Na-HCO_3 and Na-Cl) depending on the degree of mixing and the occurrence of cation exchange between recharge waters (Ca-HCO_3) and remnants of the Champlain Sea (Na-Cl). The second sub-group, C7-b, of 10 samples (lower branch of C7 on Fig. 9a), includes samples of Na-Cl water type and also Na-HCO_3, Na-SO_4 and mixed-Cl (one sample each). Most of these samples are from confined aquifers. Due to confinement by marine clays, they represent diluted sea water, with less dilution than in sub-group C7-a.

This study has also highlighted the importance of specific hydrogeological conditions, within the general background geology, on groundwater hydrogeochemistry. This can be illustrated using the 13 samples taken

from the St. Lawrence Lowlands bedrock which is composed mainly of limestone where the groundwater is expected to be of Ca-HCO_3 type. Most of these samples belong to clusters 6 and 7. Half of the samples were taken from unconfined/semi-confined aquifers and the other half from confined aquifers. Samples from unconfined or semi-confined aquifers are all Ca-HCO_3 water type whereas samples from the confined aquifers are Na-HCO_3 or Na-Cl water type (except one of Ca-HCO_3 type). The recent geological history of the region and associated hydrogeological context, i.e. Champlain Sea invasion and the associated deposition of marine clays, has thus played a major role on defining the hydrochemistry of these samples.

Table 3 Characteristics of the different clusters (C5 not included since it is only one sample, the description of which is provided in the text)

	C1 (12)	**C2 (32)**	**C3 (21)**	**C4 (18)**	**C6 (25)**	**C7 (19)**
Water type	Ca-HCO_3 (7); Ca-Cl (2); Ca-SO_4 (1); Na-HCO_3 (1); Ca-mixed (1)	Ca-HCO_3 (30); Na-HCO_3 (2)	Ca-HCO_3 (20); Ca-SO_4 (1)	Ca-HCO_3 (17); Ca-mixed (1)	Na-HCO_3 (18); Ca-HCO_3 (4); Ca-Cl (1); Mixed-HCO_3 (1); Na-Cl (1)	Na-Cl (8); Ca-HCO_3 (4); Ca-Cl (2); Na-HCO_3 (2); Mixed-Cl (1); Na-SO_4 (1)
Geology						
Q. sed.[a]	10	8	6	5	5	2
St L.L.[b]	-	1	-	1	4	6
Grenville	2	23	15	12	16	9
Unknown	-	-	-	-	-	1
Confinement						
Unconfined	10	18	9	6	5	7
Semi-conf.[c]	1	5	5	6	1	1
Confined	1	9	6	6	19	10
Unknown	-	-	1	-	-	-
Geographic location	Overall study area, a few samples along the Ottawa River (median elevation: 191, 187, 178 and 168 m.a.s.l. respectively)				Mainly along the Ottawa River, a few samples along main river valleys (median elevation: 138 and 100 m.a.s.l. respectively)	
Median conc.[d] (mg/l)						
Ca^{2+}	17	29.5	54	68	23	86.5
Mg^{2+}	3.05	4.65	6.6	13	9.4	33
Na^{+}	6.55	5	7.4	17.5	69	225
K^{+}	1.35	1.95	1.9	3	6.8	7.85
HCO_3^{-}	42.7	107	158	200	201	346
Cl^{-}	9.05	1.1	8.4	36.5	27	350
SO_4^{2-}	8.25	15.5	21	34	25	80.5

B	0.00925	0.017	0.02	0.02	0.14	0.335
Ba^{2+}	0.0145	0.033	0.028	0.18	0.055	0.061
Br^-	D.L.[e]	D.L.	0.05	D.L.	0.1	0.375
F^-	D.L.	0.25	0.1	0.2	0.8	0.7
Mn^{2+}	0.0016	0.0135	0.00083	0.051	0.019	0.016
NH_4^+	0.04	0.03	0.02	0.025	0.14	0.165
NO_3-NO_2	0.65	0.05	0.85	0.045	0.03	0.15
Si	5.5	6.4	7.3	6.55	6.6	7.1
Sr^{2+}	0.0905	0.22	0.21	0.435	0.64	1.9
Alkalinity	35	89	130	165	180	285
Hardness	59	90	176	224	104	333
TDS	111	184	304	404	452	1054
pH	6.69	8.3	7.72	7.54	8.6	8.01
ORP[f] (mV)	-1.5	-160	-24	-63	-275	-147
O_2 (%)	72	4.9	38	5	1.8	12.6

[a]Quaternary sediments
[b]St. Lawrence Lowland Platform
[c]Semi-confined
[d]Median concentrations
[e]D.L. = below detection limit
[f]Oxidation-reduction potential

As mentioned in Table 3, samples from clusters 1 to 4 are located throughout the study area, with many samples from cluster 4 in the lower part of the Gatineau valley, whereas samples from clusters 5 to 7 are located mainly along the Ottawa River (Fig. 9d).

The HCA results are consistent with the FA results, as illustrated in Fig. 10. The distinction between groups of samples is clearer when plotting scores for factor 1 vs factor 3 compared to factor 1 vs factor 2. In Fig. 10a, recharge waters (C1) or low-mineralized waters (C2 and C3) are on the left side of the vertical axis whereas more evolved waters are on the right side, towards higher salinity values. Except for the sample of cluster 5 with high loadings for silica and cluster 1 with low loadings, other clusters cannot be differentiated according to this factor. On the contrary, in Fig. 10b, clusters can be distinguished according to factor 3 as well as factor 1 (salinity), even at the level of the sub-groups for clusters 6 and 7.

Cluster 6 can be subdivided into two sub-groups which represent various degrees of cation exchange. The first sub-group (C6-a) shows Na^+ concentrations slightly higher than the Ca^{2+} concentrations whereas samples in the second sub-group (C6-b) have higher Na^+ concentrations compared to Ca^{2+} and have HCO_3^- concentrations higher than those of sub-group C6-a. As suggested by the FA results (Fig. 10b), samples in sub-group C6-b have higher fluoride concentrations (1.6 vs 0.7 mg/l as mean values) and higher pH values

(9.1 vs 8.4 as mean values) than samples from sub-group C6-a. From Fig. 10b, it can be deduced that samples from sub-group C7-a have lower concentrations in fluoride and lower pH values than samples from sub-group C7-b. Finally, exceedances of drinking water standards with respect to fluoride occurred mainly in samples from clusters 6 and 7.

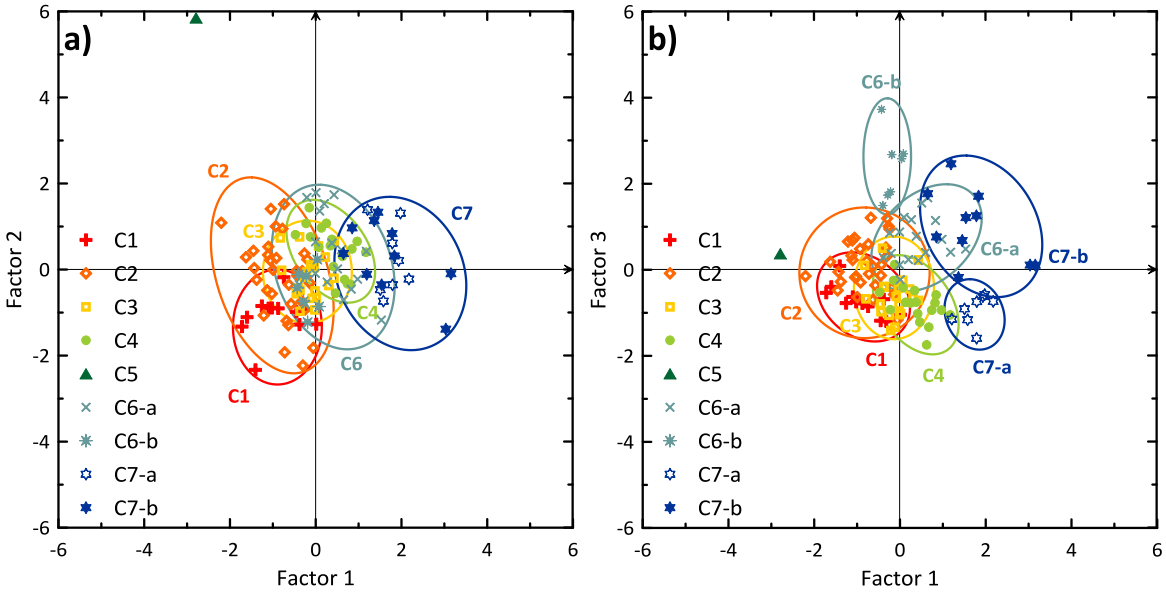

Fig. 10 FA scores according to HCA groups: a) factor 1 vs factor 2 and b) factor 1 vs factor 3

The conclusions presented from the multivariate statistical analysis can be illustrated with Gibbs diagrams (Fig. 11). In Fig. 11a, showing TDS concentrations as a function of the ratio between Na and Na+Ca, samples from clusters 1 to 4 fall in the domain influenced by geology. Samples from clusters 4 and 7 (especially sub-group C7-a) as well as the sample from cluster 5 show some mixing with the former Champlain Sea. Outside the limits, most samples are from cluster 6 and sub-group C7-b. Freshening has affected samples from cluster 6 and cluster 7, with samples from sub-group C7-b reflecting a mixture between seawater and water undergoing some freshening (Fig. 11a). Fig. 11b shows the TDS concentrations as a function of the ratio between Cl and Cl+HCO_3 and allows distinguishing between sub-groups C1-a and C1-b, supporting the idea of contamination by anthropogenic chloride. Chemical data for precipitation from five meteorological stations located in the study area (Environment Canada 2009) are also plotted on the diagrams.

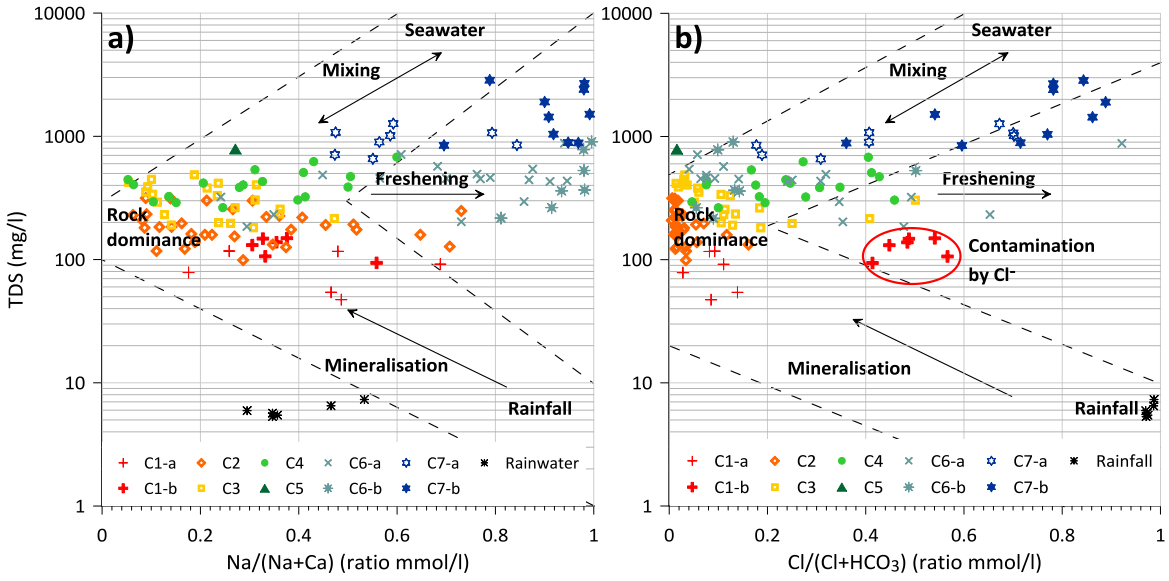

Fig. 11 Identification of the main processes on Gibbs diagrams (adapted from Gibbs (1970)), rainwater data from the meteorological stations distributed over the study area (Environment Canada 2009): a) according to Na and Ca ratio, and b) according to Cl and HCO_3 ratio.

7 Identification and interpretation of geochemical processes

7.1 Enrichment in majors ions (from C1 to C4)

As mentioned before, clusters 1 to 4 are characterized by enrichment in Ca^{2+} and HCO_3^- (Fig. 12a), which tends to imply Ca-rich mineral dissolution as the primary process responsible for this trend. Immediately, calcite comes to mind since it is quite common and easy to dissolve. However, the study area is covered primarily by the Canadian Shield bedrock, mainly composed of silicate rocks (for example granite and gneiss), along with some calc-silicate rocks (marble) and carbonate rocks (dolostone). Analysis of cuttings from drilling wells shows that the silicate rocks are rich in plagioclase minerals (Ca- and Na-feldspars) and the calc-silicate rocks are rich in calcite; these are two examples of Ca-rich minerals which release Ca^{2+} and HCO_3^- during dissolution. Where sufficiently thick, the till layer could also play a role in element enrichment, depending on the nature of the matrix (which was not characterized during this project).

According to Fig. 12a, samples from clusters 1 to 4 are located along the theoretical line for the dissolution of anorthite (Ca-feldspar) or calcite, expressed by the following reactions:

$$2CO_2 + 3H_2O + CaAl_2Si_2O_8 \rightarrow Ca^{2+} + 2HCO_3^- + Si_2Al_2O_5(OH)_4 \quad \text{Eq. 1}$$

$$CO_2 + H_2O + CaCO_3 \rightarrow Ca^{2+} + 2HCO_3^- \quad \text{Eq. 2}$$

in which the dissolution of 1 mole of anorthite ($CaAl_2Si_2O_8$) or 1 mole of calcite ($CaCO_3$) by waters rich in CO_2 typical of recharge areas (Appelo & Postma 2005) releases 1 mole of calcium (Ca^{2+}) and 2 moles of bicarbonate (HCO_3^-), respectively. In addition, 1 mole of kaolinite ($Si_2Al_2O_5(OH)_4$) is produced in the case of anorthite dissolution. Thus, the theoretical HCO_3:Ca line has a 2:1 slope.

Fitting a straight line to samples from clusters 1 to 4 yields almost the same equation with a slope of 0.42, similar to the theoretical line, which supports the hypothesis of anorthite and/or calcite dissolution.

With a silicate-rich bedrock geology throughout the study area, weathering of Ca-rich silicates (one of the easiest silicates to dissolve; Appelo & Postma (2005)) is probably the dominant weathering process (with some local carbonate dissolution) contributing to the enrichment in calcium and bicarbonate observed from clusters 1 to 4. This observation is also in agreement with the FA results, which show a high loading for silica on the second factor, further suggesting the importance of silicate weathering. As illustrated in Fig. 12b, most samples from clusters 1 to 4 plot above the $[Ca^{2+}] = 2\,[Mg^{2+}]$ line, indicating silicate weathering dominates over carbonate dissolution (Rajmohan & Elango 2004; Sonkamble et al. 2012).

For the above weathering reactions to occur, CO_2 must be present in the system. To verify the CO_2 content, the CO_2 partial pressure (Pco_2) was calculated using the PHREEQC geochemical speciation model (Parkhurst & Appelo 1999). Groundwater from cluster 1, with calculated Pco_2 values close to those found in soils and characteristic of recharge waters, has the capacity to dissolve silicates and carbonates. The CO_2 partial pressure is also relatively higher in soils than in the atmosphere due to root respiration (Appelo & Postma

2005). As recharge water infiltrates into the system, it will easily dissolve carbonate minerals first (at higher dissolution rates) followed by silicates.

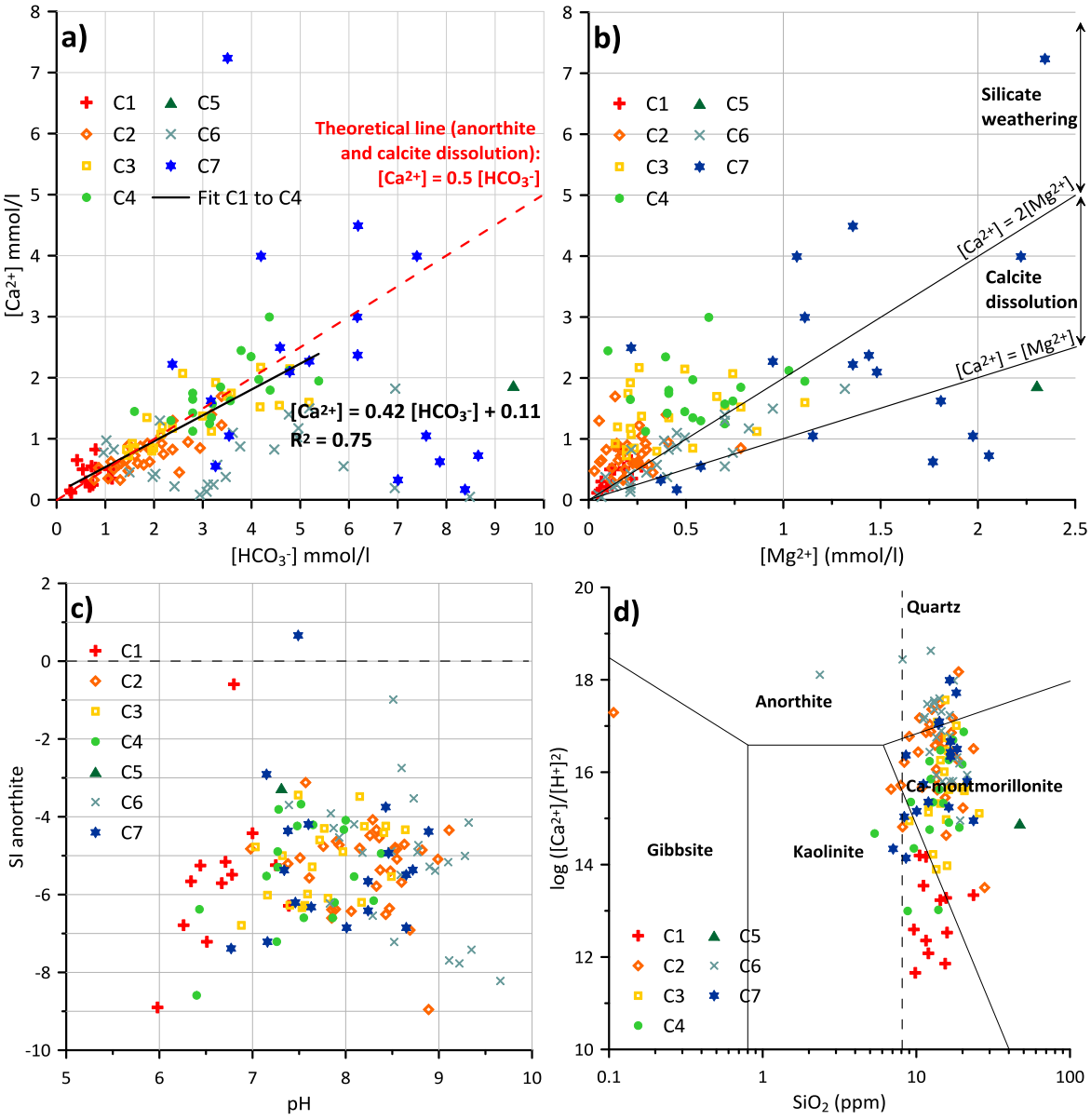

Fig. 12 Evidence for Ca-silicate weathering: a) linear relationship between Ca and HCO_3 for samples from clusters 1 to 4; b) comparison between Ca and Mg concentrations; c) anorthite saturation indexes and d) anorthite and weathering product stability fields

Using PHREEQC, saturation indexes were calculated for several minerals. Here, only results for anorthite are presented since this is the silicate mineral the most easily dissolved. Except for one, all samples are under-

saturated with respect to anorthite, suggesting anorthite is indeed very likely to be dissolving. Moreover, most samples plot in the Ca-montmorillonite or kaolinite stability fields (Fig. 12d), meaning that anorthite is unstable under the current aquifer conditions. Most samples are on the right side of the stability line for quartz (Fig. 12d) indicating they have reached saturation with respect to quartz (verified with saturation indexes) but are under-saturated with respect to amorphous silica.

7.2 Origin of groundwater salinity: remnants of the Champlain Sea (C7)

Although much of the study area had been invaded by the Champlain Sea after ice retreat, seawater intrusion was unevenly distributed. According to Parent & Occhietti (1988), glacial melt waters formed a major freshwater lake in the area, known as Lake Candona, which extended along the Ottawa River valley lowlands and was separated from the Champlain Sea by a glacial barrier. The barrier collapsed about twelve thousand years ago which allowed invasion of the Ottawa River valley by seawater, although ice was still present in the major valleys of the Laurentian Highlands, as proven by the presence of the St Narcisse moraine complex (Parent & Occhietti 1988). Ice retreat from the St Narcisse moraine is dated at 10.8 ka after which the major secondary river valleys (Gatineau, Le Lièvre and La Petite Nation) were invaded by the Champlain Sea to form brackish or freshwater bodies (with significant dilution caused by freshwater influx from the rivers). Due to isostatic rebound, the Champlain Sea left the area about ten thousand years ago, the Ottawa River valley having been flooded by seawater for 2,000 years and the major valleys in the Laurentian Highlands for only 800 years. Therefore, the marine signature is expected to be stronger in the samples taken in the Ottawa River valley compared to those from the other valleys.

The HCA (Fig. 9b) and the Piper diagram (Fig. 9c) allow distinguishing between two sub-groups in cluster 7. The first sub-group (C7-a) plots in the Ca-HCO_3 part of the upper diamond on the Piper diagram: calcium concentrations are slightly higher than sodium concentrations and chloride and bicarbonate concentrations are within the same range. Sub-group C7-b has a typical seawater signature (Na-Cl), with Na/Cl ratios close to 1. Samples from sub-group C7-a are concentrated in the south-east part of the study area where carbonate rocks

outcrop or in the southern parts of the main river valleys, whereas samples from sub-group C7-b are located near the Ottawa River where marine clays confine the aquifers.

The ratio between chloride and bromide is often used as an indicator for the origin of salinity. In their study area close to Montréal (150-200 km downstream on the Ottawa River), using Br/Cl ratios and assuming that their clay pore water samples were representative of the original Champlain Sea, Cloutier et al. (2010) demonstrated that the pore water was a mixture of 34% sea water with 66% fresh water from melting ice and rainfall. In Fig. 13, only samples from sub-group C7-b plot along the dilution line and are thus remnants of the former Champlain Sea. Samples from sub-group C7-a, with prevailing unconfined conditions, are too diluted by recharge waters and bromide concentrations are below the detection limit. Among the samples from sub-group C7-b, if we considered the sample with the highest concentrations in bromide and chloride (OUT022510 with concentrations of 5 mg/l and 1,100 mg/l, respectively), it appears that this most saline sample (least diluted) is a mixture of about 20% seawater from the Champlain Sea and 80% fresh water. Similar trends were noted by Blanchette et al. (2010b) in the Chateauguay area, south of Montreal, although their samples were more saline, due to a longer inundation period by the Champlain Sea.

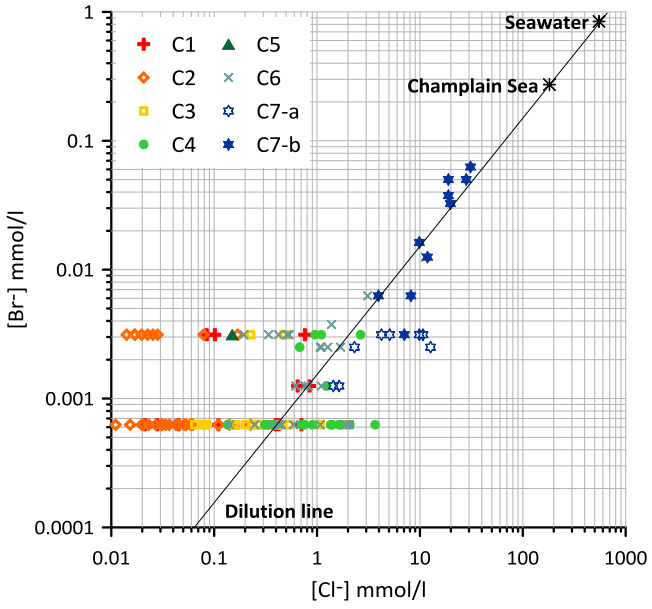

Fig. 13 Presence of diluted seawater in the study area, with seawater data from Hem (1985) and Champlain Sea seawater data from Cloutier et al. (2010)

7.3 Na-Ca exchange (C6)

Cation exchange of Na by Ca explains the shape of the Stiff diagram for samples in cluster 6, characterized by high sodium concentrations and depletion in calcium whereas bicarbonate concentrations are similar to those for samples in cluster 4 (Fig. 9a). This process was also inferred from the Gibbs diagram (Fig. 11a).

The cation exchange reaction, responsible for the freshening of the aquifer, is given by Eq. 3 (Appelo & Postma 2005):

$$\frac{1}{2}\,Ca^{2+} + Na - X \rightarrow \frac{1}{2}\,Ca - X_2 + Na^{+} \qquad \text{Eq. 3}$$

where X represents a mineral-surface exchange site. Before the Champlain Sea invasion, fresh groundwater rich in Ca^{2+} extended over the entire area (recharge by weakly mineralized melting ice water), including within the upper bedrock. Following invasion by the Champlain Sea, recharge water became rich in Na^{+} which infiltrated the bedrock with Na^{+} replacing Ca^{2+} on the exchange sites (inverse of Eq. 3). Also, marine clay deposits became loaded with pore water rich in Na^{+} (Cloutier et al. 2010). After the Champlain Sea retreat, the freshening process began with recharge by calcium-rich fresh water.

As seen in Fig. 14a, concentrations in calcium and sodium increase from cluster 1 to cluster 5, explained by silicate weathering (not only Ca-feldspar) and calcite dissolution. For cluster 6, calcium concentrations decrease whereas sodium concentrations increase, with more significant cation exchange for sub-group C6-b compared to C6-a. With regard to cluster 7, while samples from sub-group C7-b plot close to the seawater dilution line (Fig. 13), they show some evidence for Na-Ca exchange. Samples from sub-group C7-a have a similar trend to C1-C5 samples, with a slight increase in both Na and Ca concentrations. Cluster 6 appears as a mixture with cluster 7 (Fig. 14b). Moreover, the enrichment in sodium, due to sodium-silicate weathering, is obvious for clusters 1 to 3 as well as the chloride contamination for sub-group C1-b.

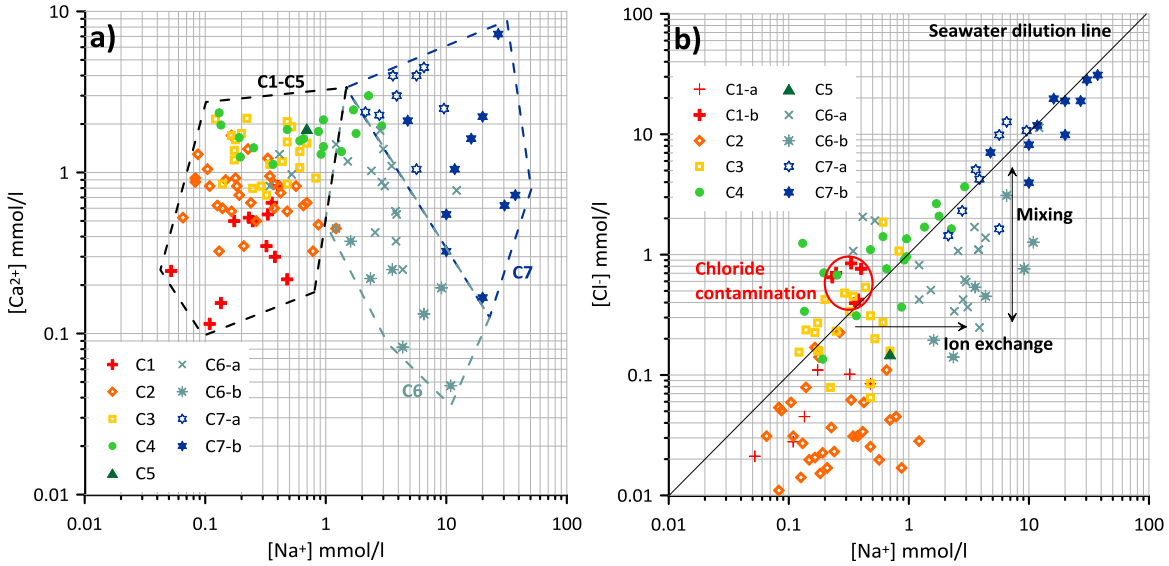

Fig. 14 Evidence in cluster C6 for cation exchange between Na and Ca, showing increases in Na coupled to: a) a decrease in Ca concentrations, and b) to constant Cl concentrations

7.4 Mixing/dilution

As introduced previously, mixing is another important process affecting the geochemical evolution of groundwater in the study area. For example, samples from sub-group C7-b, with a marine signature, are a mixture between seawater from the former Champlain Sea, and fresh water (Fig. 13). For the most saline sample, the freshwater/seawater ratio is 20/80%. Samples from sub-group C7-a, with Na/Cl ratios close to 1 (indicating halite dissolution), are too diluted to have detectible bromide concentrations because they are located in unconfined aquifers where the recharge rates are higher than in confined areas where samples from sub-group C7-b originate. Since marine clays are responsible for confinement of samples from sub-group C7-b, some cation exchange is likely to occur. For samples from cluster 6, cation exchange intensity is higher for sub-group C6-b than for C6-a (Fig. 14) which are from confined aquifers where dilution by recharge water is less likely to occur. Some samples from sub-group C6-a, located in unconfined aquifers, appear as a mixture of recharge and saline waters.

7.5 Secondary natural processes

Comparing the concentrations of the different elements with the maximum admissible concentrations (Gouvernement du Québec 2013a, b) and with aesthetic objectives (Health Canada 2014), several quality issues (in addition to salinity issues previously mentioned) can be identified which are likely to have a natural origin.

As seen in Table 4, significant exceedances for drinking-water standards were observed for fluoride and uranium (eight and seven samples, respectively) as well as for boron and nitrate (one sample each). Many parameters exceeded aesthetic objectives such as chloride, sodium and TDS (already mentioned), hardness (due to carbonate dissolution), iron, manganese, pH and sulphide.

Table 4 Exceedances for drinking water standards and aesthetic objectives (see Fig. 9d for cluster locations)

	Unit	MAC/AO[a]	C1 (12)	C2 (32)	C3 (21)	C4 (18)	C5 (1)	C6 (25)	C7 (18)	No. of exceedances
B	mg/l	5	-	-	-	-	-	-	1	1
F^-	mg/l	1.5	-	1	-	-	-	3	4	8
NO_2+NO_3	mgN/l	10	-	-	-	1	-	-	-	1
U	mg/l	0.02	-	1	1	3	-	2	-	7
Mo	mg/l	0.07	-	-	1	-	-	-	-	1
Al	mg/l	0.1	1	-	-	-	-	1	1	3
Cl^-	mg/l	250	-	-	-	-	-	1	11	12
Hardness[b]	mg$CaCO_3$/l	200/500[c]	-	-	8/0	11/0	1/0	3/0	11/4	34/4
Fe	mg/l	0.3	1	5	1	6	1	2	2	18
Mn	mg/l	0.05	1	6	1	9	1	7	3	28
pH		6.5-8.5	4/0	0/10	0/1	2/0	-	0/16	0/4	6/31
Ag	mg/l	0.1	-	-	-	-	-	-	1	1
Na	mg/l	200	-	-	-	-	-	3	10	13
SO_4	mg/l	500	-	-	-	-	-	-	1	1
Sulphide	mg/l	0.05	-	-	-	-	-	3	3	6
TDS[d]	mg/l	500	-	-	-	4	1	7	18	30

[a]The following species, with no exceedances, are not including in this table: Sb, As, Ba, Cd, Total Cr, Cu, Pb, Se, Ni and Zn with MAC/AO of 0.006, 0.01, 1, 0.005, 0.05, 1, 0.01, 0.01, 0.02 and 5 mg/l respectively

[b]Calculated by summing Ca^{2+} and Mg^{2+} concentrations according to the following formula: hardness (mg$CaCO_3$) = 2.5 [Ca^{2+}] (mg/l) + 4.1 [Mg^{2+}] (mg/l)

[c]Between 200 and 500 mg$CaCO_3$/l: water of poor quality but tolerated by consumers / > 500 mg$CaCO_3$/l: unacceptable for most domestic uses

[d]Calculated by summing major ion and SiO_2 concentrations

7.5.1 Fluoride exceedances: dissolution of F-bearing minerals and anion exchange

Except for fluoride exceedance from cluster 2, all other affected wells are located in confined aquifers, mostly from the bedrock, with Na-HCO_3 or Na-Cl water types and with pH between 8 and 9.3. The presence of fluoride in confined aquifers discredits the hypothesis of contamination from recent anthropogenic sources since the confining layer, characterised by low permeability, offers natural protection to the aquifer. Dissolution of fluoride-rich minerals such as fluorite, apatite or F-bearing micas and amphiboles is a common natural source for fluoride in groundwater (Hounslow 1995), and is a likely source in the Outaouais Region since apatite and fluorite deposits are common in the southern part of the study area. Chemical analyses carried out on rock and sediment samples from well cuttings in the area show fluoride concentrations ranging from 175 to 1020 ppm (with higher concentrations in Quaternary sediments than in bedrock), which is consistent with fluoride concentrations found in alkaline igneous rocks (Ozsvath 2009) and with studies where high-fluoride groundwaters are identified (Jacks et al. 2005). Fluoride can also be affected by anion exchange on clay minerals (with OH^-, according to Ozsvath (2009) and Rao (2009)). This anion exchange is pH-dependant, with adsorption between pH 4 and 7.5 and desorption outside this range (Hounslow 1995), which could explain why the highest fluoride concentrations are found in samples with basic pH.

According to Ozsvath (2009), fluoride concentrations are usually controlled by the dissolution of fluorite (CaF_2 with $K_{fluorite} = 10^{-10.6}$ according to Parkhurst & Appelo (1999)). Since fluorite dissolution is dependent on concentrations of calcium and fluoride, fluorite dissolution cannot occur if groundwater is over-saturated with respect to calcite (SI>0, Sracek & Hirata (2002)). An increase in fluoride concentrations is coupled with an increase in the fluorite saturation index as a result of fluorite dissolution. All samples are under-saturated with respect to fluorite. Meanwhile, most samples with exeedances for fluoride (6/8) are super-saturated with respect to calcite.

In order for fluorite dissolution to continue when super-saturation with respect to calcite is reached, calcium has to be removed, for which several mechanisms are possible. For example, samples with Na-HCO_3 water

types (4/8) are affected by Na-Ca cation exchange, which acts as a sink for calcium (Chae et al. 2007; Ozsvath 2009; Rao 2009; Sracek & Hirata 2002). Fig. 15 illustrates the enhancement of fluorite dissolution by removal of Ca during Na-Ca exchange. High fluoride concentrations are often associated with low Ca concentrations (<100 mg/l, Fig. 15a) and with high Na concentrations (>10 mg/l, Fig. 14b), as shown by Chae et al. (2007). Carbonate precipitation may also remove calcium from the solution (Rao 2009).

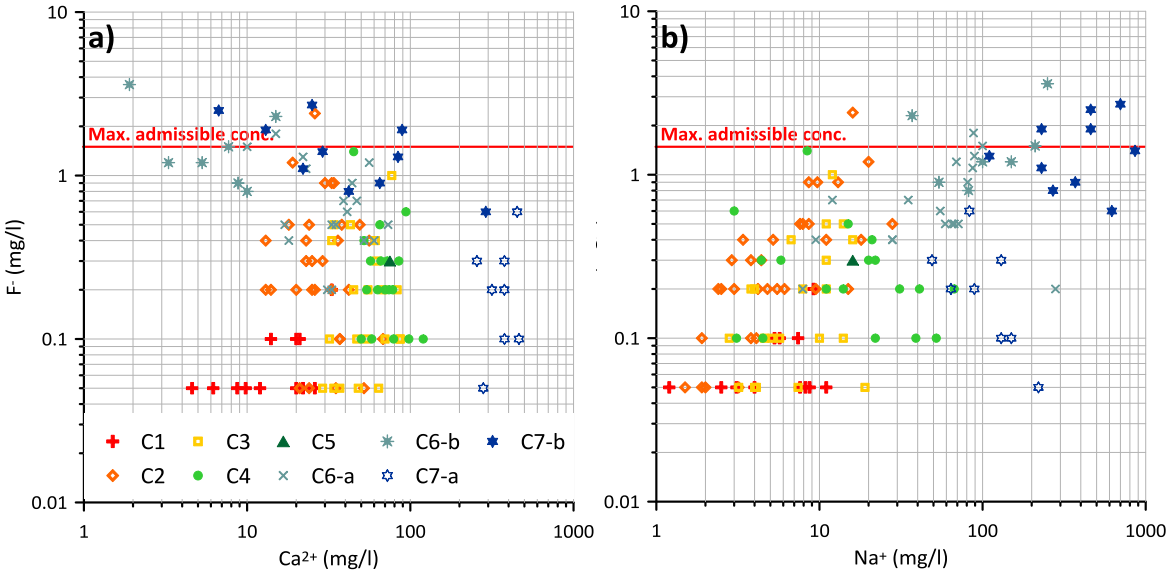

Fig. 15 Na-Ca exchange as a sink for Ca from fluorite dissolution: high fluoride concentrations associated with: a) low Ca concentrations, and b) high Na concentrations

To conclude on the mechanisms responsible for fluoride exceedances, the dissolution of F-bearing minerals such as fluorite and fluoro-apatite is probably the source of fluoride in groundwater from the Outaouais Region. As recharge water enters the aquifer, it starts dissolving fluorite since the water is under-saturated with respect to calcite and fluorite, and fluoride goes into solution since the pH is lower than 7.5. As groundwater migrates through the aquifer, it becomes saturated with respect to calcite and fluorite, and as CO_2 is consumed by silicate weathering and calcite dissolution, the pH increases which limits the adsorption of fluoride. When groundwater reaches the confined parts of the aquifers where cation exchange is occurring, the presence of a sink for calcium allows increased dissolution of fluoride which stays in solution since the pH is relatively basic.

As a consequence, higher fluoride concentrations are found in areas where cation exchange is occurring and where the pH is basic.

7.5.2 Uranium exceedances: dissolution of U-bearing minerals

Uranium exceedances occurred only in bedrock wells but were found in different groups (C2, C3, C4 and C6) and were either in Ca-HCO_3 or Na-HCO_3 water types. Uranium has a natural origin: uranium deposits have been identified in the study region (but are not mined), reflecting the natural abundance of uranium in the bedrock. Uranium concentrations measured in well cuttings are in the range 0.8-5.9 ppm. Several studies have suggested that these solid mineral concentrations are high enough to explain observed exceedances (Betcher et al. 1988; Brown et al. 2007; Moncur 2010).

The geochemical behaviour of uranium is mainly controlled by redox conditions, pH, presence of ligands (formation of complexes), ionic strength and mineralogy. Uranium can be found in four oxidation states in aqueous environments (from +3 to +6). Under natural environmental conditions, U(IV) and U(VI) are the most common oxidation states, U(III) being easily oxidised to U(IV) under the most reducing conditions and U(V) being unstable and degraded into U(IV) and U(VI). U(IV) and U(VI) have different behaviour depending on the redox and pH conditions (Krupka & Serne 2002).

U(IV) is stable, forming low-solubilty minerals such as uraninite (UO_2) under reducing conditions, which makes it relatively immobile (Krupka & Serne 2002; Langmuir 1997). However, hydrolysis of U(IV) species results in neutral or positively charged species which are more likely to be adsorbed under high pH conditions. Therefore, adsorption is low under acidic conditions and increases with increasing pH values, with maximal adsorption under basic pH conditions (Krupka & Serne 2002).

In comparison, U(VI) is found under oxidizing to mildly reducing environments, under a wide range of pH. In the presence of carbonates and pH values higher than 3, it forms complexes which increase the solubility of uranium: the carbonate complexes are negatively charged and poorly adsorbed at basic pH. Therefore, it is

more the adsorption rather than the solubility of uranium that controls the concentration of U(VI) under oxidizing conditions. Adsorption is greatest under neutral pH (5 to 7) and decreases when conditions are too acidic or too basic. In high ionic strength solutions, major cations are more likely to replace U(VI) on adsorbents, increasing the concentration of uranium in the aqueous solution. At neutral pH, CO_2 partial pressure could also have an impact on the adsorption of U(VI), with increasing pCO_2 resulting in less adsorption (Barnett et al. 2000; Krupka & Serne 2002; Langmuir 1997).

Most of the samples where U concentrations are high have high Eh values (>0 mV) representing oxidising conditions. Thus, U(VI) dominates, under the form of $UO_2(OH)_2^0(aq)$ in the absence of complexing ligands. However, groundwater samples are not pure water and contain dissolved ions such as carbonates. Considering the presence of ligands, most samples (especially those presenting exceedances) plot in the stability field of $UO_2(CO_3)_2^{2-}$ and $UO_2(CO_3)_3^{4-}$ (cf. Fig. A4 in Annexe 3). These complexes can be adsorbed at near-neutral pH, resulting in less uranium in solution and therefore increasing the solubility of uranium.

7.5.3 Iron and manganese exceedances: dissolution of Fe- and Mn-bearing minerals

Fe and Mn exceedances were found throughout the study area, also suggesting a natural origin. In addition to uranium, iron deposits are also present in the Outaouais Region and minerals rich in iron and manganese such as hornblende and biotite were identified in well cuttings. Iron exceedances are generally associated with manganese exceedances which is consistent with iron and manganese having a similar chemical behaviour (Hem 1972) subject to pH and redox conditions. These Eh-pH diagrams show that the redox conditions seem to be controlled mostly by the Fe^{2+}/Fe^{3+} iron couple, with conditions being slightly reductive (cf. Fig. A5 and Fig. A6 in Annexe 3).

As for uranium, stability diagrams are available for iron and manganese, under different environmental conditions. Most samples, especially those with exceedances, lie in the stability field of Fe^{2+} or $FeCO_3$ (siderite). The formation of low solubility solids ($FeCO_3$) or iron complexes can enhance the dissolution of Fe-bearing minerals and increases the total iron concentration (Hem 1972). As for iron, manganese exceedances

are located in the soluble manganese stability field (either $MnSO_4(aq)$ if sulphate concentrations are high or Mn^{2+}).

7.6 Contamination by chloride for cluster C1-b

Interpretation of the HCA led to cluster 1 being divided into two sub-groups, based on the chloride concentrations for these samples (mean concentrations are 2.3 and 22.3 mg/l, respectively). For comparison purposes, the mean rainwater chloride concentration is 0.23 mg/l (Environment Canada 2009), based on six meteorological stations located in the study area.

In Fig. 11, samples from sub-group C1-b plot outside of the domain, due to a high $Cl/(Cl+HCO_3)$ ratio. In Fig. 14b, these samples appear to have relatively low Na/Cl ratios (<1, ranging from 0.35 to 0.90) whereas samples from sub-group C1-a have ratios greater than 1 (between 1.58 and 5.65). These observations tend to indicate contamination as the source of chloride. Moreover, chloride concentrations for sub-group C1-b are quite high compared to other groups of less evolved groundwater (especially C1-a, C2 and C3; see Table 3). These samples originate from various types of aquifers, with different water types. Each was studied separately to deduce the origin of the higher chloride concentrations, using Cl/Br ratios as defined by Alcalá & Custodio (2008), Panno et al. (2006) and Vengosh & Pankratov (1998). All samples from this C1-b sub-group are from unconfined aquifers, meaning they are naturally vulnerable to contamination. Three probable origins were identified: use of de-icing salts for samples close to major roads, as well as domestic wastewater and agricultural runoff (for one sample taken on a stud farm, where the nitrogen concentration is also high).

8 Regional geochemical conceptual model

Based on the results of the multivariate statistical analysis and the identification of the main processes, a regional geochemical conceptual model was proposed along a representative flow line following the regional

hydraulic gradient, from north to south (Fig. 16). On the 2D cross-section, different hydrogeologic environments are represented with their typical clusters and associated main geochemical processes.

The bedrock is mainly composed of silicate rocks (Canadian Shield) which outcrop in high elevation areas (unconfined bedrock conditions) or are covered by a discontinuous layer of till (not represented at this scale, Fig. 16). Carbonate rocks are found along the Ottawa River (St. Lawrence Lowland Platform). In the unconfined part of the Canadian Shield, rainwater infiltrates and becomes mineralized by silicate weathering, especially Ca-feldspar which is easier to dissolve. Thus, groundwater is of Ca-HCO_3 water type and evolves from cluster C1 to C4, which are expected to be found in other parts of the Canadian Shield In the unconfined part of the St. Lawrence Lowland Platform, carbonate minerals (calcite for example) are quickly dissolved, resulting in groundwater characterised by a Ca-HCO_3 water type and a total dissolved solids content above the drinking water standard (and where mineralisation is much more extensive than for groundwater in silicate rock environments). Samples from this particular context belong to cluster C7-a.

In the upper valleys, the bedrock is covered by fluvio-glacial sediments. The aquifers remain generally unconfined and chemical evolution mechanisms are the same as those mentioned in the Canadian Shield. Samples from fluvio-glacial sediments, in this context, are generally less mineralized and their composition is close to rainwater (cluster C1).

In the lower main valleys, which were invaded by the Champlain Sea, fluvio-glacial sediments are covered by marine clays (producing confined Quaternary deposit or bedrock aquifers). Because of little infiltration of rainwater and greater residence time, they are more evolved (from clusters C3 and C4, possibly C5). In this part of the aquifer, some samples from the confined bedrock show signs of cation exchange (cluster C6).

In the Ottawa River valley, most of the fluvio-glacial sediments have been partly eroded and have been covered by a thick layer of Champlain Sea marine clays (confining the silicate and carbonate bedrock aquifers). Mechanisms are similar as in the lower valleys but much more intense. In low-flow zones, remnants of the former Champlain Sea can be still found, with a typical Na-Cl signature (samples from cluster C7-b).

Finally, alluvium from the current rivers has been deposited which has formed locally unconfined aquifers, with similar characteristics to aquifers in the fluvio-glacial sediments located in the upper valleys (cluster C1). Mixing between different waters also occurs in many parts of the aquifer.

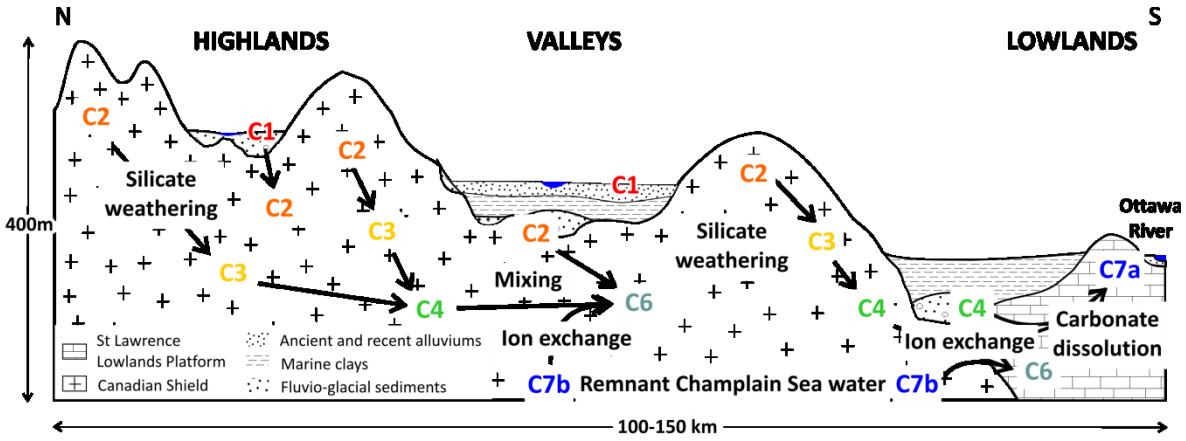

Fig. 16 Regional geochemical conceptual model (group C5 was not included since it contained only a single sample which might not be representative of the regional groundwater evolution)

9 Conclusions and perspectives

A groundwater quality assessment of the Outaouais Region based on 127 high-quality groundwater samples showed that Ca-HCO_3 is the dominant water type throughout the study area, which characterizes waters with low to medium mineralization, located in recharge areas at higher elevations. Other important water types are Na-HCO_3 and Na-Cl which have resulted from regional invasion by the Champlain Sea.

These observations were supported by a multivariate statistical analysis, including a FA analysis which allowed identifying parameters contributing to the variance between the samples, and grouping them together according to their behavior. The first component was found to be related to salinity parameters (SO_4^{2-}, Cl^-, Na^+ and Sr^{2+}), the second to the silica content (silicate dissolution) and the third to the dissolution of F^- bearing minerals under high pH conditions. Thus, FA gives a general idea of the processes involved in the chemical evolution of groundwater. Using HCA, samples were classified into groups according to their similarity. Seven

clusters were defined with cluster 1 and 7 divided into two sub-groups. The definition of the clusters closely follows the classification by water types. Samples from clusters 1 to 4 are mainly Ca-HCO_3 water type with increasing mineralization from C1 to C4. The division of cluster 1 into two sub-groups was justified by the higher concentrations in Cl^- for sub-group 2, indicating potential contamination by de-icing salts or mixing of young waters with residual marine water whereas sub-group 1 has a signature of recharge waters. Although geochemistry of the unique sample from cluster 5 is atypical, it looks like a more evolved sample from cluster 4. Cluster 6 helps in identifying cation exchange between Na^+ from the marine episode and Ca^{2+} from recharge waters (Na-HCO_3 water type). Finally, cluster 7 can be divided into two sub-groups showing various degrees of marine water dilution according to the degree of confinement, whether from unconfined/semi-confined (dominantly Ca-HCO_3) or confined aquifer conditions (dominantly Na-Cl).

From these results, the primary and secondary chemical processes were also better identified. The primary chemical processes include dissolution of carbonates and silicates by recharge waters, Na-Ca cation exchange accompanied by mixing, and recharge water induced dilution of remnant seawater from the Champlain Sea. Secondary processes are responsible for observed exceedances of several aesthetic objectives and are mainly correlated to the geology of the study area (those areas rich in F-, U-, Fe- and Mn-bearing minerals). The multivariate analysis also allowed the identification of some samples which appeared contaminated by chloride which likely originates from de-icing salts, animal and domestic waste.

These results, especially the impact of the Champlain Sea invasion on groundwater chemistry, are consistent with other studies carried out in the Québec region where the Champlain Sea was also present (Blanchette et al. 2010b; Carrier et al. 2013; Cloutier et al. 2006; Larocque et al. 2013; Leblanc et al. 2013; Talbot Poulin et al. 2013). Further studies within the context of the Outaouais PACES project are currently in progress, including numerical modelling to evaluate long-term geochemical evolution and implications for groundwater quality and sustainability.

Chapitre 2 – Un modèle conceptuel d'écoulement et d'évolution géochimique dans le sud de l'Outaouais, Québec, Canada

A conceptual model for groundwater flow and geochemical evolution in the southern Outaouais region, Québec, Canada

N. Montcoudiol, J. Molson et J.-M. Lemieux
Département de Géologie et de Génie Géologique
Université Laval, Québec City, QC, Canada, G1V 0A6

V. Cloutier
Research Institute on Mines and the Environment,
Université du Québec en Abitibi-Témiscamingue, Campus d'Amos, Amos, QC, Canada, J9T 2L8

Soumis à Applied Chemistry en août 2014, accepté le 11 mars 2015.

1 Résumé

Un modèle conceptuel a été développé pour un système d'écoulement d'eau souterraine dans le sud de l'Outaouais, Québec, Canada, où la population locale est fortement dépendante de l'eau souterraine qui provient aussi bien d'aquifères superficiels que plus profonds, dans le roc cristallin fracturé. Le modèle est basé sur l'interprétation d'analyses géochimiques pour 14 puits le long d'une ligne d'écoulement, parmi lesquels 9 le sont également pour les isotopes ($\delta^{18}O$, $\delta^{2}H$, ^{3}H, $\delta^{13}C$, ^{14}C) et 4 pour les gaz rares (He, Ne, Ar, Xe, Kr). Trois types d'eau dominants ont été identifiés : 1) Ca-HCO_3 dans l'aquifère non confiné, résultant de l'altération des silicates (feldspath calcique), 2) Na-Cl comme restes de la Mer de Champlain dans les zones stagnantes de l'aquifère confiné et 3) Na-HCO_3 résultant de l'adoucissement de l'aquifère confiné par échange cationique entre Ca et Na. Les données géochimiques ont aussi permis l'identification de zones de mélange. Les données isotopiques et les gaz rares confirment l'hypothèse concernant les restes de la Mer de Champlain et soutiennent l'hypothèse sur le mélange entre une composante récente (tritium détecté dans 8 des 9 puits) avec une composante plus ancienne (concentrations élevées en ^{4}He). Il n'est toujours pas clairement défini si les mélanges ont lieu dans les conditions normales d'écoulement ou s'ils sont induits par le pompage lors de l'échantillonnage, la plupart des puits étant ouverts dans le roc. Il est cependant clair que le système hydrogéochimique est dynamique et continue d'évoluer suite aux changements induits par la dernière glaciation. Lors de la prochaine étape, le modèle conceptuel servira de base pour la modélisation des écoulements, des âges et de la géochimie afin de valider les hypothèses développées dans cet article.

Mots clés : hydrogéochimie, isotopes, modèle conceptuel, roc fracturé, Canada

2 Abstract

A conceptual model was developed for a hydrogeological flow system in the southern Outaouais Region, Quebec, Canada, where the local population relies heavily on groundwater pumped from shallow overburden

aquifers and from deeper fractured crystalline bedrock. The model is based on the interpretation of aqueous inorganic geochemical data from 14 wells along a cross-section following the general flow direction, of which 9 were also analyzed for isotopes ($\delta^{18}O$, $\delta^{2}H$, ^{3}H, $\delta^{13}C$, ^{14}C) and 4 for noble gases (He, Ne, Ar, Xe, Kr). Three major water types were identified: 1) Ca-HCO_3 in the unconfined aquifer as a result of silicate (Ca-feldspar) weathering, 2) Na-Cl as a remnant of the post-glacial Champlain Sea in stagnant confined zones of the aquifer, and 3) Na-HCO_3, resulting from freshening of the confined aquifer due to Ca-Na cation exchange. Chemical data also allowed the identification of significant mixing zones. Isotopic and noble gas data confirm the hypothesis of remnant water from the Champlain Sea and also support the hypothesis of mixing processes between a young tritium-rich component with an older component containing high ^{4}He concentrations. It is still unclear if the mixing occurs under natural flow conditions or if it is induced by pumping during the sampling, most wells being open boreholes in the bedrock. It is clear, however, that the hydro-geochemical system is dynamic and still evolving from induced changes since the last glaciation. As a next step, the conceptual model will serve as a basis for groundwater flow, mass transport and geochemical modelling to validate the hypotheses developed in this paper.

Keywords: hydrogeochemistry, isotopes, conceptual model, fractured bedrock, Canada

3 Introduction

In response to increasing reliance on groundwater resources in the province of Quebec, Canada, the Quebec Ministry of Environment, Wildlife and Parks recently initiated a province-wide regional groundwater characterization program known as the PACES projects (MDDEFP 2008). The program covers the most populated areas of Quebec within 13 regions, including over 50 major drainage basins, and will be completed by 2015. The objective of the PACES program is to better characterize groundwater resources as a response to increasing pressure from growing residential, industrial and agricultural uses. The Outaouais PACES project in southwest Quebec (Fig. 17) began in 2010 in partnership with 5 regional county municipalities and 3

drainage basin organizations. It includes the Gatineau City region, one of the most rapidly growing urban areas in Quebec.

Groundwater quality in the Outaouais Region is of critical importance where 40% of the total 368,000 population uses groundwater as their drinking water supply. As part of the regional study, an extensive sampling survey was carried out, including the collection of 139 groundwater samples from municipal and private wells. In Chapitre 1, the regional-scale data were interpreted to identify the primary and secondary geochemical processes responsible for groundwater quality. Most samples were taken in the fractured bedrock of the Grenville geological province, which is mainly composed of silicate rocks. The primary geochemical processes were identified as seawater intrusion from the Champlain Sea which invaded the region for 1,000 to 2,000 years at the end of the last glaciation about 10,000 years ago, freshwater recharge and Ca-Na cation exchange, while natural silicate weathering was determined to be the cause of increased concentrations of fluoride, uranium, iron and manganese.

Similar processes were found in neighbouring hydrogeological systems in southern Quebec which had also been invaded by the Champlain Sea (Beaudry 2013; Blanchette et al. 2010b; Carrier et al. 2013; Cloutier et al. 2010; Larocque et al. 2013). In the Basses-Laurentides sedimentary rock aquifer system (Québec, Canada), Cloutier et al. (2006) applied stable isotopes and dating techniques for improving their conceptual hydrogeological model, showing evidence of recently infiltrated groundwater and older groundwater infiltrated during the invasion of the region by the Champlain Sea, with intermediate ages in the mixing zones. Carbon isotopes showed that rock-water interactions in the region play an important role in geochemical evolution, while isotopic data suggested the presence of preferential flow paths in the upper part of the fractured bedrock aquifer. Beaudry (2013) arrived at similar conclusions in the region of Montérégie Est, Québec, in a similar hydrogeological context.

These studies took place downstream from the Outaouais region, mostly south of the St. Lawrence River, in different geological provinces, and where seawater invasion had lasted longer than in the study area. Instead

of silicate weathering, carbonate dissolution was identified as one of the dominant processes, along with flushing of former Champlain Sea water and subsequent freshening by freshwater recharge.

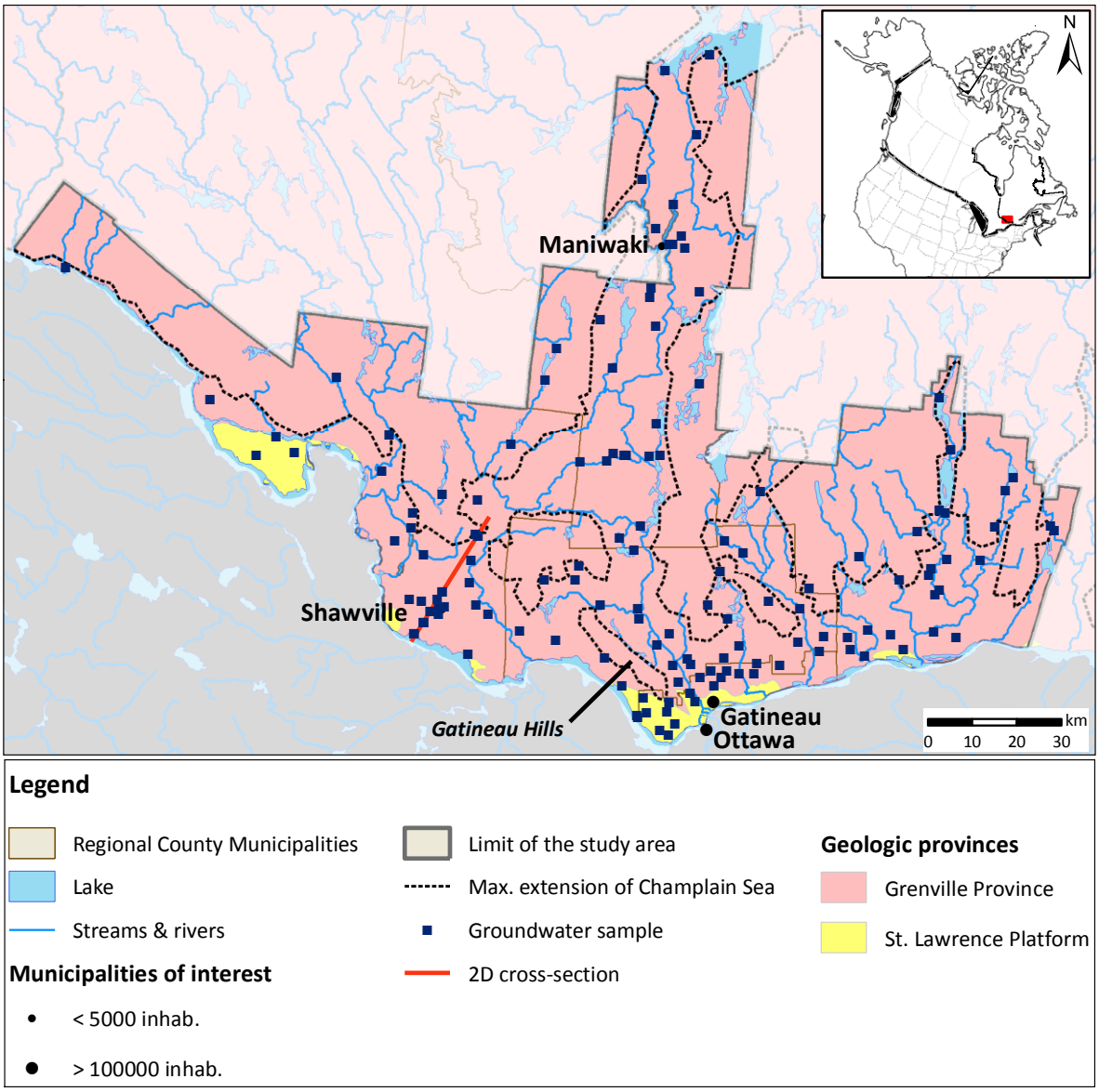

Fig. 17 Location of the 2D cross-section within the Outaouais PACES project and other main features of interest for this study

In this current study, selected data from the regional-scale study (Chapitre 1) are interpreted in a 2D vertical cross-section following the dominant groundwater flow direction, extending approximately 30 km from the Gatineau Hills in the northeast, to the Ottawa River in the southwest, passing through the town of Shawville (Fig. 17). In addition to the regional-scale hydrogeochemical data, the current study also includes water

isotope data ($\delta^{2}H$, ^{3}H (tritium) and $\delta^{18}O$), $\delta^{13}C$ and ^{14}C in dissolved inorganic carbon (DIC), and noble gases (He, Ne, Ar, Kr and Xe). These data are used to help develop an improved and refined hydrogeological conceptual model summarized at the end of this paper.

4 Geology and hydrogeology of the study area

The geological history of the region and the resulting distribution of Quaternary deposits within the Outaouais study area were presented in Chapitre 1. A brief review of the geological history is presented herein with a particular focus on the geology and hydrogeology along the selected cross-section and its immediate surroundings.

4.1 Regional geological history

Throughout the cross-section, the underlying bedrock is part of the Grenville Province of the Canadian Shield, dating from the Proterozoic (Precambrian). The cross-section passes through two types of rocks: non-carbonated metamorphic rocks (gneiss and paragneiss) in the northeast and calco-silicate rocks (marble) to the southwest (towards the Ottawa River). Minerals were identified from microscopic observations of thin sections made from cuttings collected during the drilling in the gneiss of one of the wells. Main minerals include quartz (50%), feldspars (between 30 and 40%, mainly of plagioclase type), hornblende (10% as a maximum) and biotite (5-6%). Traces of garnet, magnetite, pyrite, muscovite and chlorite (1% each) as well as calcite and apatite were also found. The bedrock is characterised by a high degree of fracturing in the upper 50-60 m (Sterckx 2013), which could be responsible for preferential flow paths. In the upper part of the bedrock, the hydraulic conductivities vary from 10^{-8} to 10^{-4} $m.s^{-1}$ according to the interpretation of results from borehole tests made by Sterckx (2013) at regional scale. A similar range is obtained for tested wells located on the 2D cross-section. One higher conductive zone ($K = 10^{-3}$ $m.s^{-1}$), differing by about two orders of magnitude from the surroundings, was found during hydraulic testing using packers in well CONV-PON. Locally,

horizontal fractures, were identified in bedrock using seismic reflection in the vicinity of well SANDBAY (Fabien-Ouellet 2014). At depth, hydraulic conductivities are decreasing as it has been widely documented in this type of crystalline bedrock (Maréchal 1998).

Unconsolidated deposits prior to the last glaciation no longer exist in the study area due to erosion by the many glacial-deglacial cycles during the Quaternary period. However, during the last glaciation, abrasion of the bedrock and ice movement deposited a discontinuous layer of till directly overlying the bedrock, while during the last deglaciation, freshwater fluvio-glacial sediments were deposited in the lower valleys. The Ottawa River valley (including lower reaches of secondary river valleys) was then invaded by the Champlain Sea about 12,000 years ago (Parent & Occhietti 1988) which left marine clays on top of the fluvio-glacial sediments which had not previously been eroded. Due to isostatic rebound, the Champlain Sea progressively left the region about 10,000 years ago, leaving behind deltaic, littoral and pre-littoral sediments. Along the main rivers, this sequence is buried by ancient and more recent alluvium (Comeau et al. 2013). The permeability of Quaternary deposits is extremely variable, from 10^{-11} m.s^{-1} in the marine clays (Catto et al. 1981) to 3×10^{-4} m.s^{-1} in the fluvio-glacial sediments, deltaic sediments and alluvium (Comeau et al. 2013).

4.2 Conceptual 2D stratigraphic cross-section

A simplified stratigraphic cross-section was built by combining stratigraphic information from well logs with the Quaternary deposit map and geophysical surveys. In the Shawville area, along the transect identified in Fig. 28, deposits from the different geological episodes are shown in Fig. 18.

In some high-elevation areas, the bedrock is covered by a discontinuous layer of till (green in Fig. 18). In other areas, the till has been eroded and the bedrock outcrops. In some valleys and areas of lower elevation, the till has either been eroded or covered by fluvio-glacial deposits, which are up to 50 meters thick and form important aquifers for domestic water supply. Following glacial retreat, marine clays as well as littoral and deltaic sediments were deposit by the Champlain Sea. Close to the Ottawa River, an important layer of marine clay (turquoise blue), about 20-30 meters thick, acts as a confining layer for the underlying bedrock aquifer.

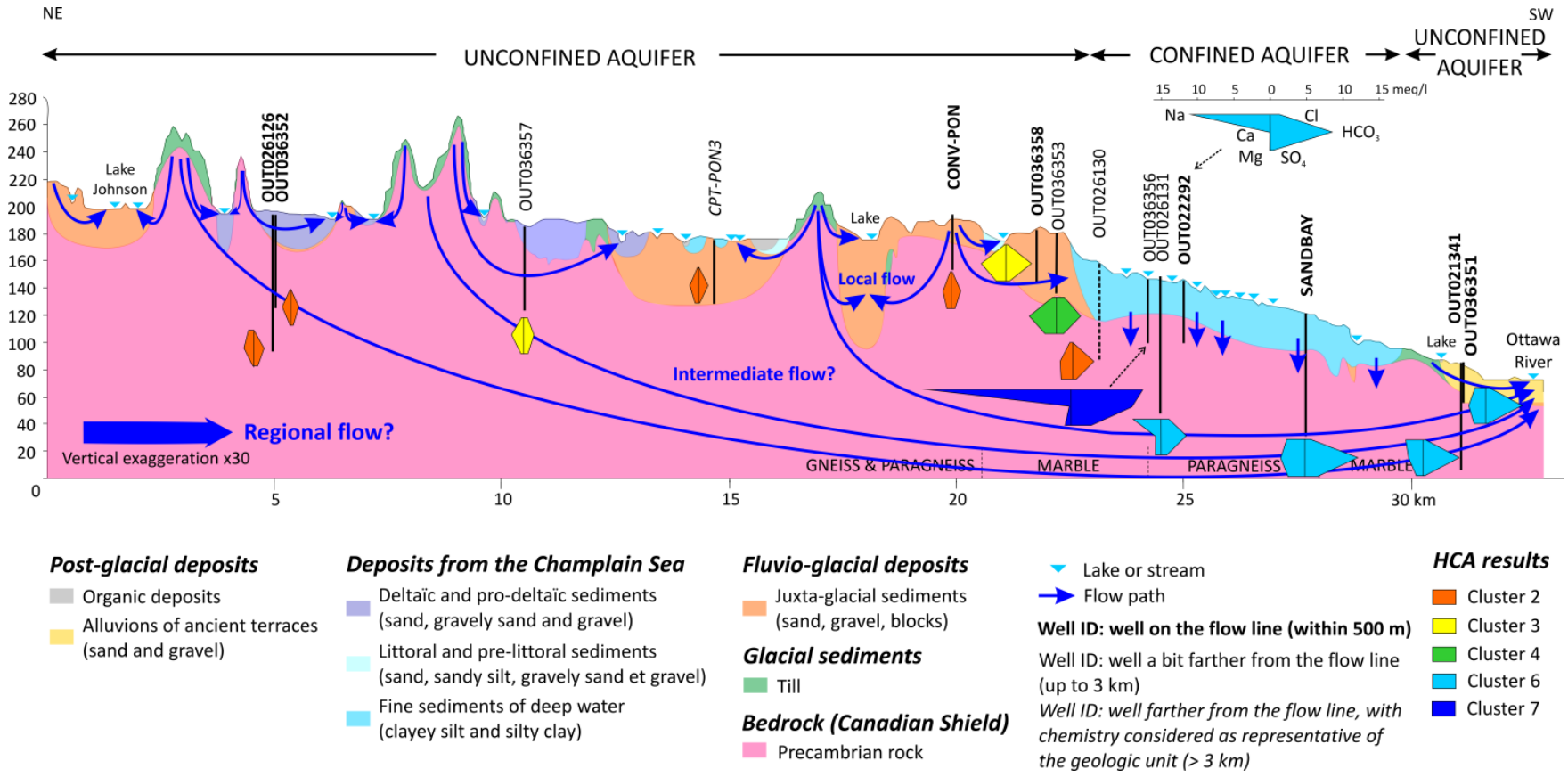

Fig. 18 Conceptual 2D stratigraphic cross-section along the selected flow path showing chemical results for major ions (cluster colours refer to Hierarchical Clustering Analysis (HCA) results from Chapitre 1 section 6.3)

Some fluvio-glacial deposits are found as lenses in the bedrock depressions. Further from the river, mainly deltaic sediments (purple) remain from the Champlain Sea invasion, with thicknesses up to 15 meters. After the Champlain Sea retreat, the Ottawa River partly or entirely eroded some clay deposits and left generally coarse and permeable alluvial deposits (light yellow).

Information about the water table depth is sparse, especially towards the north-east, but available data suggest that it is less than 10 m below ground surface in the south-west (down-gradient) part of the cross-section. As shown by Tóth (1963) for these types of flow systems, water generally infiltrates in the topographic highs and discharges in the topographic lows. Along the cross-section of this study area, recharge occurs mainly in the northeast upland areas while the Ottawa River appears as the main discharge zone for the regional and intermediate flow components. In the unconfined part, connectivity between aquifers and surface water bodies is assumed, the latter acting as local discharge zones. In the confined part, the clay layer hydraulically separates the aquifer and streams while an intermediate flow system allows groundwater flow from the upstream to the downstream aquifer which then discharges in the Ottawa River. To date, the identification at the regional scale of freshening in the confined aquifer suggests that replacement of marine waters by upstream fresh water is continuing, either within the intermediate zone or even within the regional flow components.

5 Methodology

5.1 Groundwater sampling

As explained in the regional study (Chapitre 1), groundwater sample collection was carried out throughout the Outaouais Region over the summer field campaigns of 2011 and 2012. The second campaign in 2012 focused on wells near the selected flow line where well density was higher. Samples came from a variety of hydrogeological contexts including bedrock and Quaternary deposits under confined and unconfined

conditions. A total of 14 wells were sampled: 4 in 2011 and 10 in 2012. Wells drilled in the bedrock are open boreholes (20 to 100 m long) whereas generally no information is available on the well screens in the Quaternary sediments (Table 5). Selected physico-chemical parameters, including pH, electrical conductivity, redox potential, dissolved oxygen and temperature, were measured using a multi-parameter probe for all samples. Domestic wells, which are daily used, were purged until the stabilization of physico-chemical parameters whereas for others wells (abandoned or recently drilled wells), samples were taken after pumping 3 wellbore volumes. Groundwater levels were monitored during the purge and for some wells, drawdowns were interpreted as hydraulic tests and transmissivities were calculated. Samples were analysed for major ions, nutrients, metals and sulphides by an accredited laboratory in Montreal, Canada. In 2012, inflated packers were used to take some samples, for which the open interval is specified in Table 5. All samples (except one) were analysed for isotopic content: the stable isotopes $\delta^{2}H$ and $\delta^{18}O$ with a precision of ±1‰ at 1σ and ±0.05‰ at 1σ respectively, as well as tritium ^{3}H (with a detection limit of 0.8 TU and an average precision of ±8% of the ^{3}H value at 1σ, 1 tritium unit is equivalent to 0.118 disintegration per second per kg water), and the carbon isotopes $\delta^{13}C$ (error of ±0.2‰) and ^{14}C in DIC (average precision about 0.3-0.6% at 1σ), which were all collected in HDPE bottles filled to the top according to the protocol established by Blanchette et al. (2010a). When field conditions allowed (sufficient flow rate and pressure), wells were also sampled for noble gases (4 wells), using clamped copper tubes (as first described by Weiss (1968)). Errors on noble gas concentrations vary from one gas to the other, between 1.3% for Ne and Ar, 1.5% for He and Kr and 2.2% for Xe. Avoiding presence of atmospheric air is essential and was prevented by having enough pressure in the sampling hoses and the use of transparent hoses allows checking for the presence of air bubbles. Samples were sent to three different laboratories: stable isotopes were analysed by equilibration at the GEOTOP laboratory, University of Québec in Montréal (UQAM), Canada, tritium by electrolytic enrichment and carbon isotopes by AMS (Accelerator Mass Spectrometry) at the Environmental Isotope Laboratory, University of Waterloo, Canada, and noble gases by mass spectrometer at the Noble Gas Laboratory, University of Michigan, USA.

Analysis reliability was estimated from electro-neutrality balances and all samples out of range (>±10%, Hounslow (1995)) were excluded from the data interpretation phase. None of the samples located along the 2D cross-section were excluded. Their charge balance errors, calculated using PHREEQC (Parkhurst & Appelo 1999), were all within ±6%. More details on the data treatment can be found in Chapitre 1.

Table 5 Characteristics of the sampled wells

Sample ID	Distance from NE limit (m)	Distance from cross-section (m)	Depth (m)	Aquifer type[a]	Confinement[b]	Quaternary geology	Analysis type[c]
OUT026126	5000	140	99	F	UC	Deltaic deposits (20 m)	C
OUT036352	5000	500	69	F	UC	Deltaic deposits (20 m)	C + I
CONV-PON	19000	0	42	F	UC	Fluvio-glacial deposits (18 m)	C + I + NG
OUT036358	21800	140	38	Q	UC	Fluvio-glacial deposits (38 m)	C + I
OUT022292	25100	0	55	F	C	Marine clays (30 m)	C
SANDBAY	27800	0	90	F	C	Marine clays (30 m)	C + I
OUT021341	31200	420	78	F	UC	Alluviums (20 m)	C + I + NG
OUT036351	31200	260	22	Q	UC	Alluviums (22 m)	C + I
OUT036357	10500	1700	54	F	UC	Deltaic deposits (10 m)	C + I + NG
OUT036353	22400	2000	50	Q	UC	Fluvio-glacial deposits (50 m)	C + I
OUT026130	23400	1100	?	F	C	Marine clays (40 m)	C
OUT036356	23800	2900	41	F	C	Marine clays (25 m)	C + I + NG
OUT026131	24500	1800	101	F	C	Marine clays (25 m)	C
CPT-PON3	15500	4000	9	Q	UC	Deltaic deposits (9 m)	C

[a]Aquifer type: fractured bedrock (F) or Quaternary deposits (Q)
[b]Confinement: unconfined (UC) or confined (C)
[c]Analysis type: chemistry (C) including major ions, minor and trace elements; isotopes (I) including δ^2H, $\delta^{18}O$, ^3H, $\delta^{13}C$ and ^{14}C; and noble gases (NG) including He, Ne, Ar, Kr and Xe isotopes

5.2 Cutting and sediment analyses

Drill cuttings were analysed to support the interpretation of groundwater analysis results. At regional scale, 5 boreholes have been drilled and some cone penetration tests (CPT) were carried out, for which cuttings from the different lithologies were collected. The cuttings were sent to AcmeLabs, Vancouver, BC, Canada. Before analysis, sediments were dried at 60°C and sieved to 180 µm (80 mesh) whereas bedrock cuttings were crushed to pass a 10 mesh and 250 g was pulverized to 80% passing 200 mesh. All samples were then analysed for major oxides by ICP-ES (Inductively Coupled Plasma – Emission Spectrometry) and trace elements by ICP-MS (Mass Spectrometry) after lithium borate fusion. In addition to this whole rock

characterisation, the cuttings were also transformed into thin-sections for which minerals were identified using a petrographic microscope under natural and polarized light.

6 Results

Groundwater chemical data were extensively discussed in our previous work in the context of regional-scale processes (Chapitre 1) and mentioned in the introduction. Here, using the findings of the regional-scale study, the interpretation focuses on the chemical processes occurring within a 2D cross-section which follows a selected regional flow direction.

6.1 Water types

Water types were defined in the regional-scale study (Chapitre 1) and are reported in Fig. 18 as Stiff diagrams, in which the color refers to the results of the Hierarchical Clustering Analysis (HCA).

From northeast to southwest, the Stiff diagrams show that groundwater in the bedrock becomes increasingly mineralized as it approaches the discharge area at the Ottawa River (Chapitre 1). In the unconfined part of the bedrock aquifer toward the northeast, all samples have TDS values less than 200 mg/l and are Ca-HCO_3 water type from cluster 2 and 3. TDS increases up to 900 mg/l in the confined part of the bedrock towards the southwest where the dominant water type is Na-HCO_3 from cluster 6.

Four samples within the section were taken in Quaternary deposits: CPT-PON3 was sampled in deltaic sediments from the Champlain Sea invasion (although the well appears to lie in fluvio-glacial sediments in Fig. 18 because it is offset from the 2D cross-section), OUT036358 and OUT036353 originate from fluvio-glacial sediments and OUT036351 was taken in recent alluvial sediments deposited by the Ottawa River. All these samples are Ca-HCO_3 water type, with increasing TDS values towards the Ottawa River.

6.2 Hydrogeochemical processes

6.2.1 Upstream unconfined, unconsolidated and bedrock aquifers

In the unconfined (up-gradient) part of the bedrock aquifer, the major ion chemical composition of groundwater is quite uniform (Fig. 19), which made it difficult to infer the relevant chemical processes based on major ion concentrations alone. The first two wells, OUT026126 and OUT036352, present some differences, with the deeper one (OUT026126) showing more evidence of water-rock interactions (concentrations for major ions systematically higher than those of the shallower one). Similar variations in calcium and bicarbonate concentrations, as well as saturation indexes for calcite, anorthite and chlorite, suggest silicate and/or calcite dissolution (Chapitre 1). Mineral characterisation of bedrock cuttings from this area shows the predominance of feldspars over calcite which was found only in trace amounts. The controlling process is more likely to be anorthite weathering, which is responsible for the geochemical evolution of groundwater in the unconfined part of the bedrock aquifer (Eq. 4).

$$CaAl_2Si_2O_8 + 2CO_2 + 3H_2O \rightarrow Ca^{2+} + Si_2Al_2O_5(OH)_4 + 2HCO_3^- \quad \textbf{Eq. 4}$$

Contrary to samples taken in the bedrock, samples from the Quaternary deposits are all over-saturated with respect to calcite and dolomite. As for samples from bedrock, they are under-saturated with respect to anorthite and close to equilibrium with respect to chlorite. Fluvio-glacial sediments have a similar mineralogy to the bedrock, from which they originate from. At km 21-24, the underlying bedrock is made of marble and higher calcite content is expected in the sediments. Some calcite dissolution would explain the higher mineralisation of samples OUT036358 and OUT036353 although this trend was not observed at regional scale. In areas where the underlying bedrock is predominantly made of silicate rock, some calcite is found that could have precipitated as a secondary mineral.

6.2.2 Confined bedrock aquifer

In the confined aquifers in the southern part of the section, the TDS values increase along the flow path (>300 mg/l) and reach a maximum in sample OUT036356 from the confined aquifer below the fine-grained deep-water sediments at about km 24. Bicarbonate and sodium concentrations follow the same trend (Fig. 19). However, calcium and magnesium concentrations show the opposite trend, with decreasing concentrations in this part of the aquifer (Fig. 19a). These observations, as well as the Na-HCO_3 water type determined in most of the samples, are indicative of cation exchange between Ca^{2+} and Na^{+}, as explained in Chapitre 1. Sample OUT036356, of Na-Cl water type, is considered in more detail below due to the availability of isotopic and groundwater age data. This sample is interpreted as a remnant of the former Champlain Sea since it has a Br/Cl ratio close to that of seawater. This sample was taken at depth just below the clay-bedrock interface thus its chemistry might be influenced by diffusion from the marine clay layer as well as by its location in a stagnant or low-flow zone.

6.2.3 Downstream unconfined aquifers

Within the cross-section, cation and anion concentrations are similar in the two down-gradient wells, although OUT021314 is drilled in the bedrock and OUT036351 in Quaternary sediments (Fig. 19). However, as a consequence of its higher Na concentrations, the bedrock sample is a Na-HCO_3 water type whereas the Quaternary deposit sample is Ca-HCO_3 type (see Stiff diagrams in Fig. 18).

During invasion by the Champlain Sea, this area of the Outaouais Region was flooded and probably covered by a continuous clay layer, which has since been completely or partly eroded by the Ottawa River and replaced/covered by alluvial sediments. It is difficult to confirm if a continuous marine clay unit still remains since the number of borehole logs is limited and they are often difficult to interpret (e.g. one mentions a clay layer, others a mixed layer of sand and clay and some mention only sand above the bedrock). The presence of a discontinuous marine clay layer thus cannot be excluded.

Sample OUT021341 (km 31) is a Na-HCO_3 water type, likely a result of cation exchange (as mentioned above). This process does not appear as clear as for samples OUT022292 and OUT026131 (see Stiff diagrams in Fig. 18), which have probably been diluted by upstream groundwater including local recharge (rich in Ca-HCO_3) through the till outcrop zone just upstream of the alluvial sediments. Sample OUT036351, located in the alluvial sediments, has a recharge signature suggested from its Ca-HCO_3 water type. Na concentrations are relatively significant compared to the regional dataset, thus this sample could be a result of a mixture of discharging water with recharge water (Blanchette et al. 2010b).

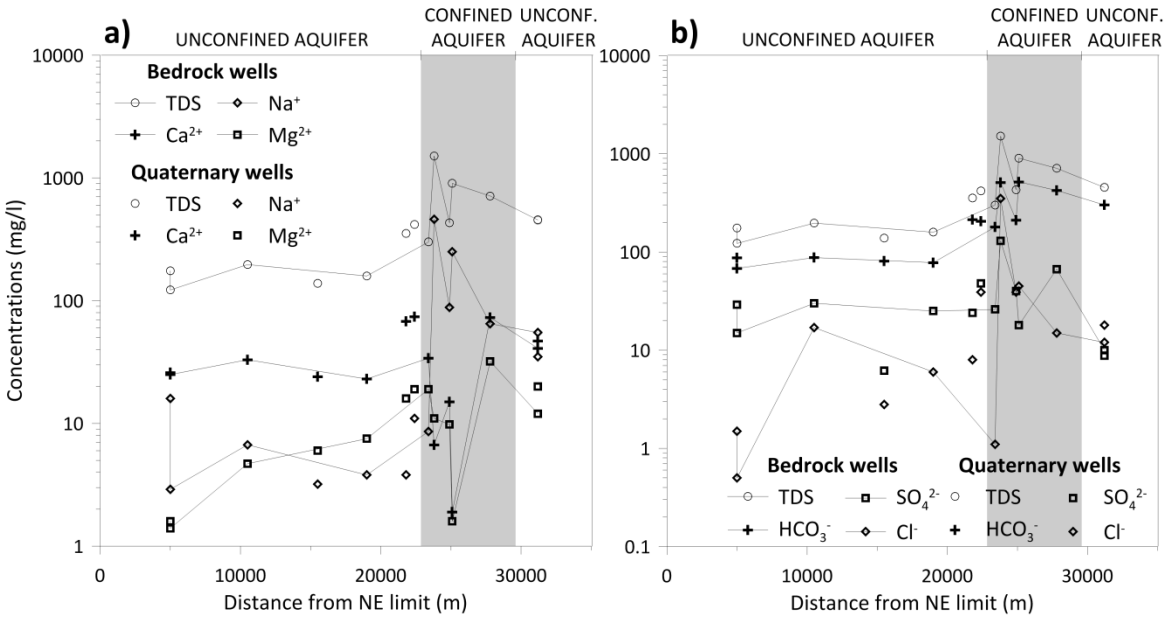

Fig. 19 Profiles for a) cation and b) anion concentrations along the selected cross-sectional flow path

6.3 Interpretation of isotopic data

Isotopic data, which were not available at the regional scale, were a significant addition to this local-scale study which included 9 wells sampled for $\delta^{18}O$, $\delta^{2}H$, ^{3}H, $\delta^{13}C$ and ^{14}C (Table 6). When integrated together, isotope measurements provide insight into the source and characteristics of recharge, groundwater residence time, flow directions and mixing processes, and they help constrain groundwater flow models.

Table 6 Results of isotopic measurements

Sample ID[a]	Distance from NE limit (m)	$\delta^{18}O$ (±0.05‰)	$\delta^{2}H$ (±1‰)	^{3}H (TU) (±1σ)	$\delta^{13}C$ (±0.2‰)	Normalized ^{14}C (pmC) (±1σ)
OUT036352	5000	-11.56	-77.9	16.9±1.3	-8.72	59.46±0.24
OUT036357	10500	-11.35	-82.8	14.9±1.2	-16.31	72.02±0.22
CONV-PON	19000	-12.36	-87.5	18.8±1.4	-10.58	47.13±0.20
CONV-PON / 27-31.5 m	19000	-12.28	-86.0	15.6±1.2	-10.31	47.71±0.21
OUT036358	*21800*	*-12.38*	*-84.3*	*20.7±1.5*	*-11.55*	*77.90±0.28*
OUT036353	*22400*	*-12.14*	*-84.8*	*15.1±1.2*	*-13.91*	*71.84±0.30*
OUT036356	**23800**	**-12.22**	**-85.1**	**<0.8±0.3**	**-12.58**	**15.94±0.10**
SANDBAY	**27800**	**-11.05**	**-75.9**	**10.9±0.9**	**-15.96**	**83.21±0.30**
SANDBAY / 42.5-47 m	**27800**	**-11.06**	**-77.9**	**13.2±1.1**	**-17.8**	**87.57±0.28**
SANDBAY / 67.5-72 m	**27800**	**-11.12**	**-75.6**	**13.1±1.0**	**-17.23**	**88.09±0.31**
OUT021341	31200	-10.75	-79.8	9.8±0.8	-13.32	75.32±0.24
OUT036351	*31200*	*-10.55*	*-76.5*	*17.5±1.3*	*-9.57*	*73.82±0.39*

Bold: wells in confined bedrock; *italic*: wells in Quaternary deposits; plain: wells in unconfined bedrock.
[a]Wells are ordered along the flow path, from the furthest to the closest to the Ottawa River.

6.3.1 Groundwater stable isotopes ($\delta^{2}H$ and $\delta^{18}O$)

Site-specific regional or local meteoric water lines (MWLs; $\delta^{2}H$ vs. $\delta^{18}O$) are usually defined for studies at regional or local scales (Clark & Fritz 1997) and compared to those inferred by groundwater stable isotope measurements. To define the local meteoric line at this site, a meteorological station which collected monthly rain samples for stable isotope analyses was installed at the Maniwaki airport (located 100 km northeast of Shawville, at an elevation of 201 m.a.s.l., Fig. 28) during the summer of 2012. Due to technical and logistical constraints during winter, data were collected only from the beginning of June to the end of November 2012. This series being too short for interpretation, monthly data were obtained from the closest GNIP (Global Network of Isotopes in Precipitation) station (WMO code 7162800, IAEA/WMO (2011)), located in Ottawa, Ontario (70 km southeast of Shawville, at an elevation of 114 m.a.s.l.; this station being even closer than the Maniwaki airport). Stable isotope and tritium concentrations were recorded from 1973 to 2007, making it one of the longest continuous time-series records of precipitation (Gibson et al. 2005).

All meteorological stable isotope data are shown in Fig. 20. Data from the Ottawa station span a relatively wide range of $\delta^{18}O$ and $\delta^{2}H$ values due to strong seasonal temperature variations (Clark & Fritz 1997). Maniwaki

airport data plot within the range of the values from the Ottawa station, specifically in the upper right side where rainwater is richer in heavy isotopes. Considering the few available points, the Ottawa MWL is considered a good approximation of the local MWL in the Shawville area.

Twelve groundwater samples were analysed for stable isotopes, of which three were multi-level samples and did not show significant differences (wells CONV-PON and SANDBAY). Their distribution falls in the range of values from the Ottawa meteorological station in which the weighted mean for $\delta^{18}O$ is -11‰ and for $\delta^{2}H$ is -75.7‰ (Fig. 20). This trend supports a meteoric origin of groundwater which is not affected by evaporation (Cloutier et al. 2006; Mook 2000).

Samples with the heaviest signature, close to the actual weighted averaged isotopic signature of rain, originated from wells close to the recharge area (along the first 10 km of the section) and close to the Ottawa River. Samples with lighter signatures were taken in wells between 15 and 25 km on the 2D cross-section. The pattern appeared similar in both Quaternary deposits and bedrock wells. Close to the Ottawa River, the isotopic signature is heavier, especially for $\delta^{18}O$. Based on a groundwater mixing model, Cloutier et al. (2010) estimated the $\delta^{18}O$ isotopic signature of the Champlain Sea water for the Basses-Laurentides to be -10.6‰ (seawater diluted by melted water from the ice sheet), which cannot be differentiated from the modern precipitation isotopic signature. None of the Outaouais samples showed a $\delta^{18}O$ isotopic signature as light as -16‰, which is the isotopic signature of glacial meltwater and Pleistocene meteoric water (Cloutier et al. 2010), which confirms that groundwater is recently infiltrated rainwater (less than 10,000 years old). Sample OUT036356, which is diluted Champlain Sea water (5.5% Champlain Sea and 94.5% fresh water) and has a $\delta^{18}O$ of -12.2‰, has been diluted by depleted fresh water. The small variations in isotopic signatures could be explained by the altitude effect, with $\delta^{18}O$ values decreasing with increasing altitude. An attempt was made to evaluate the altitude effect considering the elevation of the top well casing as recharge elevation for wells in the unconfined parts of the aquifer. In absence of rain collecting stations at different elevations, it is a first approximation considering the presence of tritium in the samples and the short residence times i.e. recharge areas are not too distant (within 10 km). Gradients of -0.017 $‰.m^{-1}$ for $\delta^{18}O$ and -0.13 $‰.m^{-1}$ for $\delta^{2}H$ were

found (with R^2 = 0.83 and 0.42, respectively), which are five to ten times higher than those usually reported in the literature (Parisi et al. 2011; Poage & Chamberlain 2001). These gradients are not very well constrained because of the little variation of well elevations (between 180 and 200 m in the up-gradient unconfined part) but it could explain partly the difference in the isotopic signature between the up-gradient and down-gradient unconfined part. It should be noticed that values from well SANDBAY in the confined aquifer lie on the line and tend to confirm the hypothesis of badly sealed casing. Recharge patterns could also play a role in creating the observed differences between the two groups of samples, should the flow conditions not promote efficient mixing.

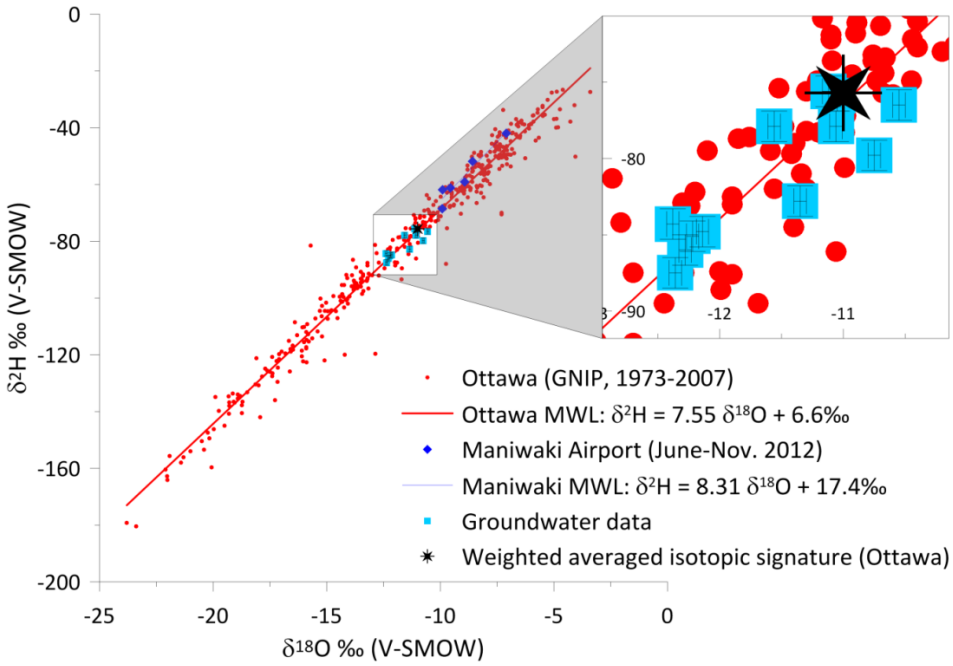

Fig. 20 Stable isotopes in groundwater and in regional precipitation compared to global meteoric water lines

6.3.2 Groundwater dating by ^3H

Qualitative dating was done by comparing the tritium content in groundwater with the current atmospheric tritium content. The precipitation tritium content was also monitored on a monthly basis at the Ottawa station from 1953 to 2007 (WMO code 7162800, IAEA/WMO (2011); Fig. A7 in Annexe 4) and the averaged tritium content is about 15 TU. Samples from the up-gradient unconfined part of the bedrock aquifer had tritium

concentrations between 14 and 20 TU whereas the single sample from the confined down-gradient aquifer with tritium above the detection limit had a lower tritium content of around 11 TU (sample SANDBAY). Sample OUT036356, also in the confined aquifer but slightly offset from the cross-section, had a tritium content below the detection limit (Table 6). With tritium contents above the current atmospheric tritium level, the unconfined aquifer therefore shows evidence of bomb test tritium, which suggests relatively younger groundwater based on the expected tritium concentrations identified by Clark & Fritz (1997). According to the same authors, the sample from the confined part of the section (SANDBAY), however, would be interpreted as being much younger (modern), as would samples from the down-gradient unconfined aquifer, near the Ottawa River. Samples taken in the unconfined Quaternary deposit aquifers have tritium concentrations above 15 TU, similar to those in the up-gradient unconfined bedrock aquifer.

This qualitative interpretation of these analyses does not fit with the characteristics of the aquifer (unconfined vs confined conditions and bedrock vs Quaternary deposits). However, it can be concluded that, with the exception of sample OUT036356, all samples include a modern recharge component (of less than 60 years) since tritium was detected in all of them. Groundwater represented by sample OUT036356, with a tritium concentration below the detection limit, likely infiltrated prior to the bomb peak in 1962.

Quantitative dating would also be possible in our case since the tritium input is known. However, this method has proven to be not so meaningful and greater improvement can be achieved by including the daughter product ^{3}He from the tritium disintegration ($^{3}H/^{3}He$ dating described first by Tolstikhin & Kamensky (1969)).

6.3.3 The use of noble gases for $^{3}H/^{3}He$ dating

With the $^{3}H/^{3}He$ method, the tritium input concentration is no longer required. The total concentration in helium (in cm^{3} STP / gram of water) as well as the ratio between its two isotopes, namely ^{3}He and ^{4}He (R in Table 7), were measured in four samples, allowing the calculation of the concentration in ^{3}He. However, as noted by other authors (Aeschbach-Hertig et al. 1998; Kipfer et al. 2002), ^{3}He has other sources in addition to tritium decay ($^{3}He_{tri}$), which have to be accounted for. The different components can be separated using noble gas

analyses. The atmospheric component, resulting from equilibrium with the atmosphere can be easily calculated knowing the pressure and temperature conditions during the recharge. The excess air component can be assessed by comparing the neon concentration of the sample with the neon concentration at atmospheric equilibrium recharge conditions, usually expressed by ΔNe (%) = (Ne_{meas} / Ne_{eq} - 1)*100 (Aeschbach-Hertig et al. 2001). If there is no excess air, these two neon concentrations should be similar. Table 7 presents ΔNe which was calculated assuming a recharge temperature of 5°C, based on records from the Ottawa station (mean temperature for the 1953-2007 period was about 6°C, WMO code 7162800, IAEA/WMO (2011)) and from the historical climate data of Environment Canada (2013) at Shawville (station ID 7038040, 5°C for a measurement period from 1966 to 2012). Under such conditions and for pure water, the equilibrium concentration of neon is 2.123×10^{-7} cm^3 $STP.g^{-1}$ (Table 7). For comparison, at 10°C, this concentration is 2.017×10^{-7} cm^3 $STP.g^{-1}$ (Kipfer et al. 2002; Peeters et al. 2002), decreasing with increases in temperature and salinity. Therefore, it is difficult to know the precise value under the recharge conditions. Samples OUT021341 and OUT036356 clearly show neon enrichment of about 10% compared to the atmospheric equilibrium value. However, samples OUT036357 and CON-PON/27-31.5m plot slightly below the zero line, suggesting no excess air or even some degassing due to microbial activity (Hall, 2013, personal communication).

The ratio $^3He/^4He$ of the terrigenic component (R_{ter}) can be assessed either from tritium–free samples or using typical values from the literature (e.g. 2×10^{-8}, Mamyrin & Tolstikhin (1984)). Sample OUT036356 has a tritium concentration below the detection limit and could be used to assess the terrigenic ratio, using the method presented by Aeschbach-Hertig et al. (1998). Excess air-corrected He isotope was plotted versus the inverse of the normalized excess air-corrected He concentration. The mixing line passing by ASW (air saturated water) and well OUT036356 (with no tritium) intersects the y-axis for a $^3He/^4He$ ratio of about 2.05×10^{-7}, ten times the value from Mamyrin & Tolstikhin (1984). In Fig. 21, $^3He/^4He$ is plotted against Ne/He. If He becomes very important compared to Ne (i.e. Ne/He is very small) due to terrigenic production, then the $^3He/^4He$ ratio should be close to the terrigenic ratio $(^3He/^4He)_{ter}$ (Peeters et al. 2002). Using this method, the estimated value is half

the previous value (1.09×10^{-7}). However, the first value calculated according to Aeschbach-Hertig et al. (1998) is too high for one of the samples, leading to a negative value for $^3He_{tri}$, whereas a tritium concentration of 14.9 TU was measured. The ratio $(^3He/^4He)_{ter}$ should probably be between this value and the value from Mamyrin & Tolstikhin (1984). Acknowledging this uncertainty in the $(^3He/^4He)_{ter}$ ratio, ages presented in Table 7 were calculated using the value from Mamyrin & Tolstikhin (1984).

Table 7 Noble gas data relevant for calculating $^3H/^3He$ ages (see Table A1 to Table A4 in Annexe 4 for the measurement errors and additional data)

Sample ID[a]	^3H TU (±1σ)	R/R_a[b] (±1σ)	Total He cm^3 STP g^{-1}	Total Ne cm^3 STP g^{-1}	$^{20}Ne_{tot}$ cm^3 STP g^{-1}	ΔNe %	$^3He_{trit}$ TU	$^3H/^3He$ ages Years ±2σ
OUT036357a	14.9±1.2	0.155±0.005	$1.151*10^{-6}$	$2.049*10^{-7}$	$1.885*10^{-7}$	-3.5	65.4	30 (±2.3)
OUT036357b	14.9±1.2	0.196±0.012	$1.982*10^{-6}$	$1.963*10^{-7}$	$1.778*10^{-7}$	-7.5	177	46 (±2.7)
CONV-PON / 27-31.5 m	15.6±1.2	0.917±0.017	$1.624*10^{-7}$	$2.055*10^{-7}$	$1.861*10^{-7}$	-3.2	56.9	28 (±2.2)
OUT036356	**<0.8±0.3**	**0.180±0.006**	**$1.352*10^{-6}$**	**$2.302*10^{-7}$**	**$2.085*10^{-7}$**	**8.4**	**-**	**>60**
OUT021341a	9.8±0.8	0.207±0.005	$1.971*10^{-6}$	$2.336*10^{-7}$	$2.114*10^{-7}$	10	183	53 (±2.8)
OUT021341b	9.8±0.8	0.258±0.012	$3.577*10^{-6}$	$2.317*10^{-7}$	$2.099*10^{-7}$	9.1	456	69 (±2.9)
Equilibrium with atmosphere		[c]0.9824	[d]$4.760*10^{-8}$	[d]$2.123*10^{-7}$	[d]$1.921*10^{-7}$	0.0		

Bold: wells in confined bedrock; plain: wells in unconfined bedrock.
a and b differenciate the two duplicates.
[a]Wells are listed from the furthest to the closest to the Ottawa River.
[b]$R_a = 1.384*10^{-6}$ in the atmosphere (Clarke et al. 1976)
[c]$R_{eq} = 1.3596*10^{-6}$ at 5°C (Peeters et al. 2002)
[d]At 5°C (Peeters et al. 2002)
[e]Beyerle (1999)

The results of the $^3H/^3He$ dating method against the Ottawa station data are shown in Fig. 22. The calculated age for sample OUT021341a is consistent with the tritium input whereas its duplicate is out of range (before the tritium peak in 1963 although tritium is detected). For samples OUT036357, the age difference between the two duplicates is about 15 years, with OUT036357b closer to the tritium input. Sample CONV-PON/27-31.5m lies above the tritium curve by about 30 TU.

Changing the R_{ter} value from 2×10^{-8} to 2×10^{-7} in order to get a better fit on the ^3H input curve does not significantly improve the results and a better estimate of the R_{ter} value could not be obtained. Due to its relatively high tritium content, sample CONV-PON/27-31.5m is not very sensitive to R_{ter} and according to our calculations, the sample was about 27 years old in 2012 (Table 7). The other samples are quite sensitive. Moreover, as explained by Aeschbach-Hertig et al. (1998), several hypotheses can lead to these observations,

including significant degassing of tritiogenic ^{3}He (without fractionation as suggested by $^{22}Ne/^{20}Ne$ ratio according to the methodology of Visser et al. (2007)). In such cases, ^{3}He produced by radioactive decay is underestimated as are the ages. Finally, this method is not very helpful for the determination of groundwater ages, not only due to the poor constrain on R_{ter} but also due to the variability within the replicates. The method suggests other processes affecting groundwater ages rather than mixing with tritium-free water. At least, except for sample OUT036356, the presence of tritium confirms the hypothesis of modern recharge for the aquifer.

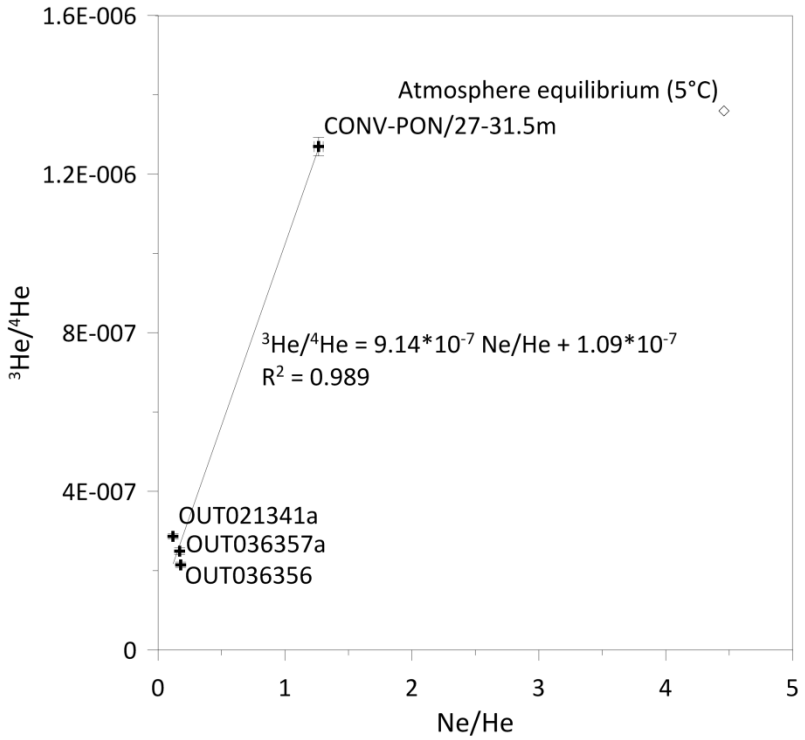

Fig. 21 Estimation for R_{ter} according to Peeters et al. (2002). R_{ter} corresponds to the value of $^{3}He/^{4}He$ where the regression line intersects the vertical axis (Y-intercept value)

6.3.4 Understanding subsurface processes with ^{14}C and $\delta^{13}C_{DIC}$

Due to nuclear weapon testing, current ^{14}C concentrations in precipitation are above 100 pmC and can be used as an indicator of very young groundwater (Clark & Fritz 1997). In this study, none of the samples had ^{14}C contents higher than 100 pmC (Table 6), indicating a lack of very recently infiltrated rainwater (which can

be excluded based on the detection of tritium) or that the ^{14}C activity has dropped below 100 pmC by reactions taking place during infiltration in the recharge areas. As soon as ^{14}C becomes trapped in groundwater in closed system conditions, it undergoes decay following the radioactive decay law with a half-life of 5,730 years (Appelo & Postma 2005; Clark & Fritz 1997). As for tritium, determining the true age is not straightforward since sources of depleted ^{14}C can change the signal. For example, the dissolution of carbonate rocks can dilute the signal by "dead carbon" (carbonate rocks are old enough to be ^{14}C-free).

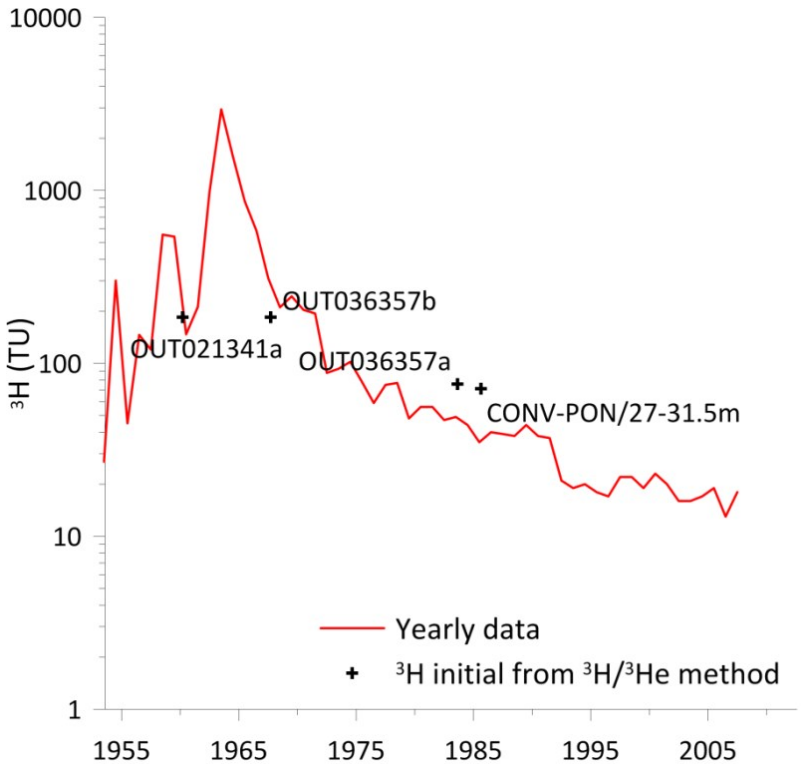

Fig. 22 Comparison of calculated initial tritium ($^3H+^3He_{tri}$) with the historical ^3H input at Ottawa (IAEA/WMO 2011)

The geochemistry of the samples shows that DIC concentrations vary between 1 and 10 mM.l^{-1} (Table 8). There is not a clear linear relationship between DIC concentrations and pH due to varying P_{CO2}. However, for a similar P_{CO2}, DIC concentrations increase with pH following a linear trend for most samples (except sample SANDBAY with higher DIC and OUT036357 with lower than expected). It suggests infiltrated groundwater equilibrates with soil CO_2. In addition, most samples have calculated CO_2 pressures (using PHREEQC by Parkhurst & Appelo (1999)) generally higher than atmospheric pressure by about one order of magnitude (10$^-$

$^{2.5}$ atm). The elevated CO_2 pressures implied that some processes occur under open system conditions i.e. mainly in the unsaturated zone (Clark & Fritz 1997). In Fig. 23a, $\delta^{13}C_{DIC}$ values are plotted against pH. Fig. 23a also shows the $\delta^{13}C_{DIC}$ signature resulting from DIC equilibrium with soil CO_2 (Jin et al. 2009). A few samples are close to the equilibrium line such as OUT036357, OUT036353, OUT021341 and OUT036356. However, all these samples do not have ^{14}C signature similar to the soil (about 100 pmC before nuclear tests, above after). When isotope equilibrium is not obtained (in kinetically controlled system) and in presence of carbonates, the isotopic signature is close to the mixing line between soil CO_2 and carbonates ($\delta^{13}C_{DIC}$ around -12 and -11‰). ^{14}C activities vary upon the system conditions: in open systems, ^{14}C is similar to the soil signature (around 100 pmC) whereas it will decrease to half of it (around 50 pmC) under closed conditions.

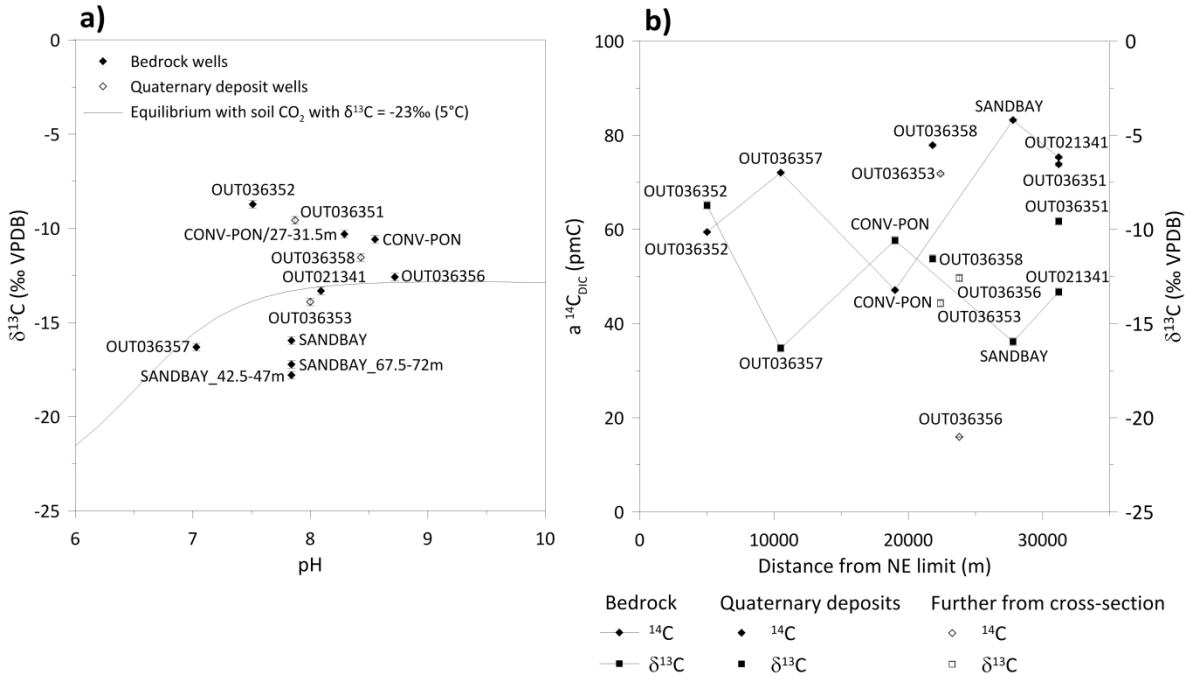

Fig. 23 Carbon isotopic data: a) identification of samples with DIC in equilibrium with soil CO_2 at 5°C in an open system and b) profiles along the 2D cross-section for ^{14}C and $\delta^{13}C$

Plotting ^{14}C values against $\delta^{13}C$ along the Outaouais flow path shows an inverse relation, especially in the bedrock, where high ^{14}C values are associated with low $\delta^{13}C$ values (Fig. 23b). In such settings dominated by silicate weathering, the absence of a linear relationship between ^{14}C and $\delta^{13}C$ indicates the occurrence of

various processes in the subsurface in addition to possible calcite dissolution (e.g. oxidation of organic matter, isotopic exchange between water and soil CO_2, loss of CO_2 gas…).

Han et al. (2012) developed a method based on graphics representing $\delta^{13}C$, ^{14}C and DIC as a function of each other, which gives an idea of the processes affecting the samples, depending on the area where they plot on each graph (Fig. 24). To construct the graphics, the initial soil $\delta^{13}C$ signature is considered to be -23‰ and 100 pmC for ^{14}C. Based on the above observations, these signatures were further refined considering that samples OUT036358 and OUT036353 have undergone some calcite dissolution (Chapitre 2 section 6.2.1) under closed conditions after equilibration with soil CO_2 in the unsaturated zone (plotting near point O in each graph of Fig. 24). Silicate weathering by fossil CO_2 under closed conditions would have similar effects on DIC, $\delta^{13}C$ and ^{14}C variations. The signature to the infiltrated recharge water was estimated to be about 25‰ for $\delta^{13}C$ and 150-160 pmC for ^{14}C. The ^{14}C value is compatible with a recharge occurring during the 60's and 70's for samples with detected tritium and may vary among the samples. Although the bedrock is dominated by silicate rocks, sample OUT021341, plotting near point O, may have undergone the same reactions. Samples OUT036351 and OUT036357 have similar ^{14}C signatures but with differences in DIC concentrations and $\delta^{13}C$. Other processes such as silicate weathering and precipitation of secondary calcite for example might explain this evolution. Sample SANDBAY is interpreted as a mixture of different waters and the dominant process seems to be silicate weathering. Samples CONV-PON and OUT036352 seems to have undergone similar processes leading to lower values in ^{14}C and DIC whereas $\delta^{13}C$ are higher. The interpretation is not straightforward for these two samples but their high $\delta^{13}C$ suggests either they were in equilibrium with CO_2 from the atmosphere and/or they have undergone multiple reactions in closed system conditions involving depleted sources in ^{14}C (radioactive decay is ruled out due to detection of tritium in these samples). Given its low activity in ^{14}C and the absence of tritium, sample OUT036356 is the only one which has undergone some significant radioactive decay (no detected tritium) and at time of recharge, the ^{14}C value of the atmosphere was about 100 pmC (atmospheric value before bomb testing).

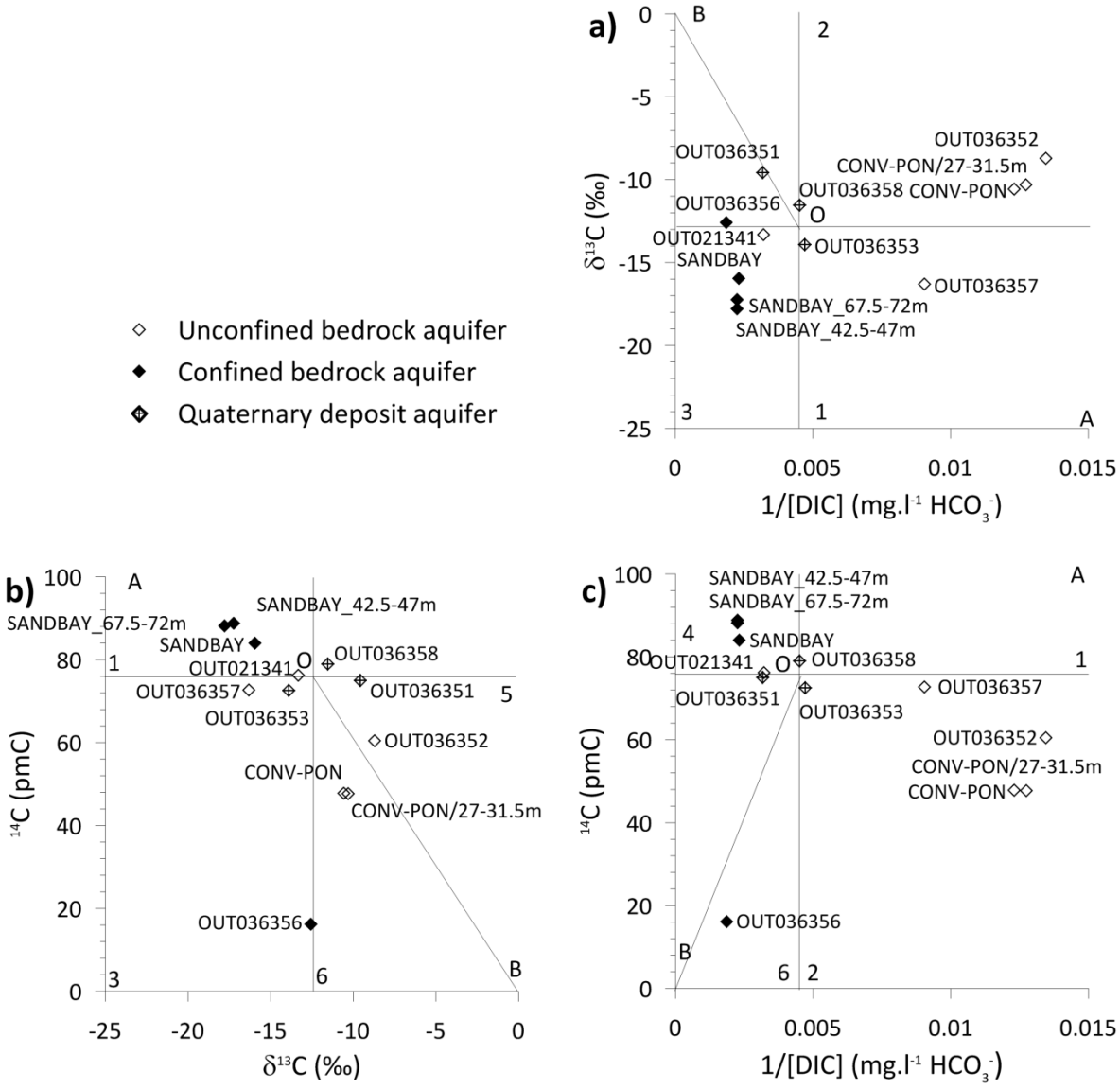

Fig. 24 Carbon data interpretation adapted from to Han et al. (2012): a) $\delta^{13}C$ vs 1/[DIC], b) ^{14}C vs $\delta^{13}C$ and c) ^{14}C vs 1/[DIC]. Zones 1 to 6 are numbered according to Han et al. (2012). Points A, O and B are end members with A representing $CO_{2(aq)}$ in equilibrium with soil CO_2 in an open system, O for water having completely reacting with soil CO_2 and carbonates in a closed system and B for water enriched in $\delta^{13}C$ and/or with low ^{14}C

The low ^{14}C contents measured in groundwater compared to atmospheric or soil CO_2 imply dilution by ^{14}C-free carbon, either by dilution of carbonates or silicate weathering by fossil CO_2. Several methods can be used to correct the data and take into account additional ^{14}C-free carbon from processes occurring in the subsurface (Clark & Fritz 1997). By including a dilution factor q, the radioactive decay equation becomes (Eq. 5):

$$a_t{}^{14}C = q * a_0{}^{14}C * e^{-\lambda t} \quad \text{Eq. 5}$$

With $a_t{}^{14}C$, measured activity in ^{14}C of the sample at time t; $a_0{}^{14}C$, activity in ^{14}C of the rain at time $t = 0$ and λ, radioactive decay constant for ^{14}C ($\lambda = \ln 2/t_{1/2}$ where $t_{1/2}$, the ^{14}C half-life is 5730 years).

Corrected radiocarbon ages were calculated using traditional methods found in the literature to verify if they are consistent with tritium ages (Table 8). The Chemical Mass Balance (CMB) method, based on the mass balance of inorganic carbon in the closed system of CO_2, soil $CaCO_3$ and water, is clearly inappropriate in regard to the previous observations (mostly equilibration with soil CO_2 under open conditions). This observation is also applicable to the $\delta^{13}C$ method (Ingerson & Pearson 1964; Pearson & White 1967) at the 2D local scale and to the Fontes-Garnier (F-G) model (Fontes & Garnier 1979). Finally, the methods which seem most appropriate and consistent with tritium contents are the statistical method (Vogel 1970), the alkalinity method (Tamers 1975) and the $\delta^{13}C$ method (Ingerson & Pearson 1964; Pearson & White 1967) at the regional scale (considering regional scale provide better constraints on recharge conditions). With these methods, most obtained ages are modern (negative values). The F-G model has been recently revised by Han & Plummer (2013) in the way of calculating the initial ^{14}C content, taking into account the isotopic exchange dominated either by gaseous CO_2 in the unsaturated zone or by solid carbonate mineral in the saturated zone. With this method, considering the dominance of isotopic exchange in the unsaturated zone, only samples SANDBAY and OUT036356 present old ages, between 1,000 and 2,500 years for the different samples from SANDBAY and 10,400 years for OUT036356. If considering the saturated zone, only OUT036356 has an old age of 9,635 years. The $\delta^{13}C$ method and the revised version of the F-G model appear to be the more adequate methods since they consider both open and closed conditions (Chowdhury et al. 2004; Han & Plummer 2013).

Table 8 Comparison of radiocarbon ages obtained by applying different correction methods

Sample ID	log P_{CO2} atm	DIC mmol.l^{-1}	pH	$\delta^{13}C$ ‰	Normalized ^{14}C pmC (±1σ)	Uncorrected age[a] yr. B.P. (±1σ)	STAT[b] age yr. B.P.	ALK age yr. B.P.	CMB[c] age yr. B.P.	CMB[d] age yr. B.P.	$\delta^{13}C^{c}$ age yr. B.P.	$\delta^{13}C^{d}$ age yr. B.P.	F-G age yr. B.P.	Revised F-G age Yr. B.P.
OUT036352	-2.52	1.22	7.51	-8.72	59.46±0.24	4175±32	1496	M	15214	7072	M	M	M	M
OUT036357	-1.93	1.81	7.03	-16.31	72.02±0.22	2631±25	M	M	10343	2201	787	3505	750	M
CONV-PON	-3.51	1.33	8.63	-10.58	47.13±0.20	6042±35	3417	591	16401	8259	719	3437	M	M
CONV-PON / 27-31.5 m	-3.34	1.29	8.29	-10.31	47.71±0.21	5945±36	3317	522	16584	8442	405	3123	M	M
OUT036358	-2.96	3.63	8.43	-11.55	77.90±0.28	2007±29	M	M	3953	M	M	9	M	M
OUT036353	-2.56	3.48	8.00	-13.91	71.84±0.30	2657±33	M	M	4968	M	M	2216	890	M
OUT036356	-2.92	8.83	8.72	-12.58	15.94±0.10	14752±51	12381	9530	9727	1585	11114	13832	11291	10411
SANDBAY	-2.55	7.08	7.84	-15.96	83.21±0.30	1476±29	M	M	M	M	M	2137	1672	1027
SANDBAY / 42.5-47 m	-2.55	7.28	7.84	-17.8	87.57±0.28	1066±25	M	M	M	M	M	2617	2157	2440
SANDBAY / 67.5-72 m	-2.55	7.28	7.84	-17.23	88.09±0.31	1018±28	M	M	M	M	M	2299	1629	1848
OUT021341	-2.47	5.10	8.09	-13.32	75.32±0.24	2277±26	M	M	1422	M	M	1466	M	M
OUT036151	-2.26	5.17	7.87	-9.57	73.82±0.39	2439±43	M	M	1485	M	M	M	M	M

[a]Age calculated by the lab using a half time of 5568 years for ^{14}C

[b]Dilution factor q=0.71

[c]Using lower pH and P_{CO2} values at the regional scale (consistent with values from available samples taken along the 2D cross-section in 1989), $\delta^{13}C$=-23‰ for soil and $\delta^{13}C$=0‰ for carbonate rocks

[d]Using lower pH and P_{CO2} values at the local scale i.e. among the samples mentioned throughout this article, $\delta^{13}C$=-23‰ for soil and $\delta^{13}C$=0‰ for carbonate rocks

6.3.5 Accumulation of ^4He

There are three sources of radiogenic ^4He: *in situ* production within the aquifer matrix, a flux from adjacent layers or underlying crust and released of stored He from sediments by weathering which are difficult to distinguish from each other (Kipfer et al. 2002). Heaton (1984) proposed a method to assess the different contributing He sources and concluded that an external flux from rocks below the considered aquifer was responsible for the observed He concentrations. As a consequence, helium could not be used to infer groundwater residence times but provide relative ages and flow directions (Heaton 1984; Kipfer et al. 2002). In our case, we are lacking of data to assess which source is the main contributor to the observed helium concentrations, following the methodology from Heaton (1984). Nonetheless, He resulting from the decay of U and Th is the easier source to assess. Assuming that the accumulation of radiogenic ^4He in groundwater is due only to its production from host rocks, quantitative dating is possible and can be compared to ^{14}C dating. Although all Outaouais samples have much higher He concentrations than the atmospheric equilibrium concentration which suggests the presence of radiogenic helium, only sample OUT036356 was used since it did not have any tritium and its corrected ^{14}C age is around 11,000 years.

Assuming that ^4He is produced at a constant rate predominantly by crustal minerals containing uranium and thorium (Andrews & Lee 1979), the accumulation rate J_{He} is written as (Eq. 6):

$$J_{He} = \Lambda_{He} \frac{\rho_r}{\rho_w} (C_U P_U + C_{Th} P_{Th}) \left(\frac{1-\theta}{\theta} \right) \qquad \textbf{Eq. 6}$$

where Λ_{He} is the fraction of produced ^4He which is released from minerals into the water and is usually taken to be 1, ρ_r and ρ_w are the rock and water densities, respectively, with ρ_r = 2650 kg.m^{-3} (a typical value from the literature, e.g. Fetter (2001)) and ρ_w = 1000 kg.m^{-3}, C_U and C_{Th} are the concentrations of uranium and thorium (µg.g^{-1}), P_U and P_{Th} are the production rates from U and Th decay ($P_U = 1.19 \times 10^{-13}$ and $P_{Th} = 2.88 \times 10^{-14}$ cm^3 STP.µg$_{U/P}^{-1}$.yr^{-1}), and θ is the porosity of the aquifer matrix (typically ~2% for plutonic rocks, (Fetter 2001)). The concentrations C_U and C_{Th} are available from chemical analyses on two cuttings samples from well CONV-

PON: C_U = 2.0 ppm between depths of 19.2 and 20.7 m, and 5.9 ppm between depths of 29.9 and 42.1 m, and C_{Th} = 3.8 and 8.9 ppm for the same depths, respectively. These values were used to calculate a minimum and a maximum accumulation rate of 9.1×10^{-11} and 2.5×10^{-10} cm^3 $STP.g^{-1}.yr^{-1}$, respectively. These rates are significantly higher than in the Aquia Aquifer (1.6×10^{-12} cm^3 $STP.g^{-1}.yr^{-1}$, Aeschbach-Hertig et al. (2002)) due to differences in the geology of the two regions, the Canadian Shield having higher concentrations in U and Th than the Aquia sandy aquifer.

The water residence time is calculated using the following relationship (Eq. 7, Kipfer et al. (2002)):

$$\tau = \frac{^4He_{ter}}{J_{He}} \qquad \textbf{Eq. 7}$$

where $^4He_{ter}$ is the concentration calculated for sample OUT036356. With these data, we found a residence time range between 5,180 and 14,250 years, including the ^{14}C age. Although this age span is reasonable, many assumptions were made for the two methods (^{14}C and ^4He), and it cannot be concluded, based on this only sample, that the α-decay of U and Th is the only process responsible for the measured He concentrations in the sample.

As seen from Table 7 and Fig. 25a, although sample OUT03656 is the oldest, it does not have the highest concentration in helium. When the helium concentration is plotted as a function of the well depth (Fig. 25b) or as a function of the well bottom elevation (R^2 = 0.72 and 0.63 respectively), a good correlation is obtained and suggests the existence of an external helium flux from deeper in the bedrock rather than the production of helium from α-decay of U and Th. Thus, it would better explain the occurrence of helium even in the samples containing tritium.

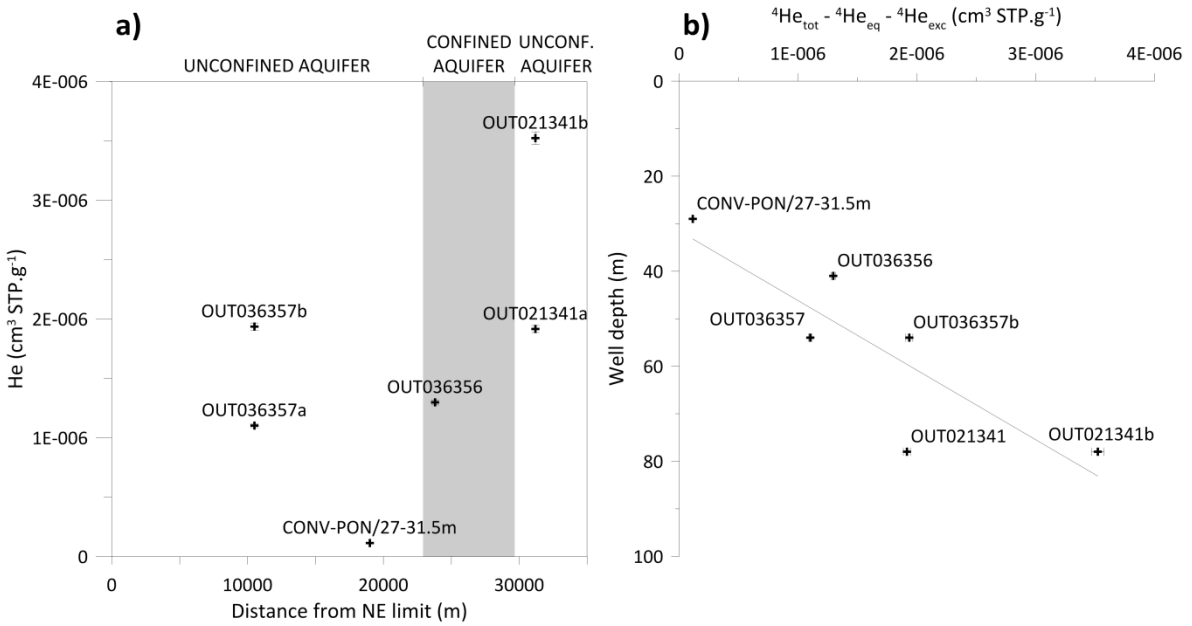

Fig. 25 Total helium (similar if $^4He_{eq}$ and $^4He_{exc}$ are subtracted from $^4He_{tot}$): a) variations along the 2D cross-section and b) depth profile showing increasing He concentrations with well depth

6.3.6 Noble gases and recharge temperature

Samples were analysed for helium, neon, argon, krypton and xenon total concentrations as well as 15 isotopic ratios (results in Table A1 to Table A4 in Annexe 4). Different models are available to calculate the noble gas temperatures (NGTs) and the calculations were made using the error-weighted, nonlinear inverse technique described by Ballentine & Hall (1999). Usually, resulting noble gas temperatures are compared to mean atmospheric recharge temperature, and it is generally assumed that mean air temperature and mean ground temperature are similar (Aeschbach-Hertig et al. 1999; Stute et al. 1992). Depending on the model used (Sun et al. 2010), the noble gas temperatures from this study (Table 9) are either above or below the mean air temperature at Shawville over the last fifty years (station ID 7038040, Environment Canada (2013)). The duplicate samples (OUT036357 and OUT021341) had different NGT values (about 1°C difference) with overlapping confidence intervals.

NGTs were first calculated using the Unfractionated Air (UA) model which is based on the complete dissolution of entrapped air bubbles (Heaton & Vogel 1981). Assuming a recharge elevation of 200 m (Table 9), a

difference of about 4.2°C exists between the lowest and highest values (which was similar for the UA model assuming a recharge elevation of 300 m.a.s.l.). When assuming a recharge elevation of 300 m.a.s.l., the calculated recharge temperatures are between 0.33 and 0.35°C lower. The NGTs appear lower in the sample from the confined aquifer (sample OUT036356) but it cannot be generalized based on a single measurement. However, this sample also had a tritium concentration below the detection limit as well as a low ^{14}C activity, which is consistent with recharge under cooler climate conditions, i.e. melting at the glacier base during the last deglaciation.

NGTs were calculated using models other than the UA model to optimize the results obtained for each sample (Table 9, a description of these models can be found in Sun et al. (2010)). Sample OUT036357 has a deficit in neon (Table 7), which evidence for some degassing (probably due to microbial activity) and CE model was found to be more appropriated, with a fractionation factor greater than 1 (Hall, 2013, personal communication). Sample CONV-PON_27-31.5m is best modelled using the UA model (Hall, 2013, personal communication). For samples OUT036356 and OUT021341, the OD model was the most appropriated with excess air near zero and the air saturated component equilibrated at high pressure (Hall, 2013, personal communication). The maximum temperature difference is smaller (3.4°C) and the variation along the flow path is more difficult to explain. However, to compare actual temperature variations for the entire dataset without bias, it is better to compare temperatures obtained with the same model because significant offsets between models may introduce apparent temperature variations (Sun et al. 2010). If we consider only the results produced by the UA model, NGTs for samples OUT036357 and OUT021341 with their confidence intervals are close to the actual mean air temperature; sample CON-PON/27-31.5m is slightly above whereas sample OUT036356 is below. The first three of these samples have tritium levels which suggest young water, thus it makes sense that their noble gas temperatures are close to the actual mean temperature. For the latter (sample OUT036356), the lower NGT suggests that recharge occurred during a cooler period, e.g. during the last glaciation, which is corroborated by the absence of tritium, the low content in ^{14}C, as well as the sample geochemistry.

Table 9 Noble gas temperature (NGT) results according to different methods and assuming different recharge elevations

	UA[a] model		Other models
Recharge elevation	200 m.a.s.l.	300 m.a.s.l.	200 m.a.s.l.
OUT036357a	4.37±1.11	4.03±1.13	4.37±1.11 (CE[b])
OUT036357b	5.39±1.18	5.04±1.20	5.39±1.20 (CE[b])
CONV-PON / 27-31.5 m	6.65±1.04	6.30±1.06	6.65±1.04 (UA[a])
OUT036356	2.49±0.92	2.15±0.94	5.99±0.64 (OD[c])
OUT021341a	3.22±1.03	2.89±1.05	7.80±0.67 (OD[c])
OUT021341b	4.29±1.21	3.95±1.23	8.92±1.01 (OD[c])
Shawville mean temperature (1966-2012): 5°C			

[a]UA: Unfractionated Air

[b]CE: Continuous Equilibration

[c]OD: Oxygen Depletion

7 Discussion and conceptual model

The addition of isotope data to the major ion geochemistry provides some important new insights on the recharge conditions as well as the groundwater residence time in the aquifer. However, its interpretation is not straightforward and some of the data appear contradictory, possibly indicating that a variety of groundwater processes is affecting the data.

7.1 Groundwater mean residence times

Undoubtedly, the presence of tritium at the relatively high observed concentrations (higher than the actual atmospheric level) is a sign of recently infiltrated water. Moreover, the stable isotope concentrations lie along the Ottawa meteoric water line (IAEA/WMO 2011) and have an averaged signature of recently infiltrated water (at least as attested by the 54-year record). Although the samples can be divided into two subplots, this may not necessarily indicate infiltration under different climate conditions but may instead reflect altitude or seasonal effects.

Only sample OUT036356 had tritium concentrations below the detection limit suggesting older water. The age of this sample was also confirmed by the low ^{14}C activity and a corrected age of about 11,000 years. With such

a chemical composition (Na-Cl water type and presence of bromide), this sample is likely to have infiltrated during the invasion by diluted seawater of the Champlain Sea about 10,000 years ago. Although samples shown in Fig. 26 have tritium concentrations well above the detection limit, meaning recently infiltrated groundwater, they display carbon activity well below the standard soil concentrations (100.5 pmC, Clark & Fritz (1997)), with uncorrected ages ranging from about 1,000 to 6,000 years old. .

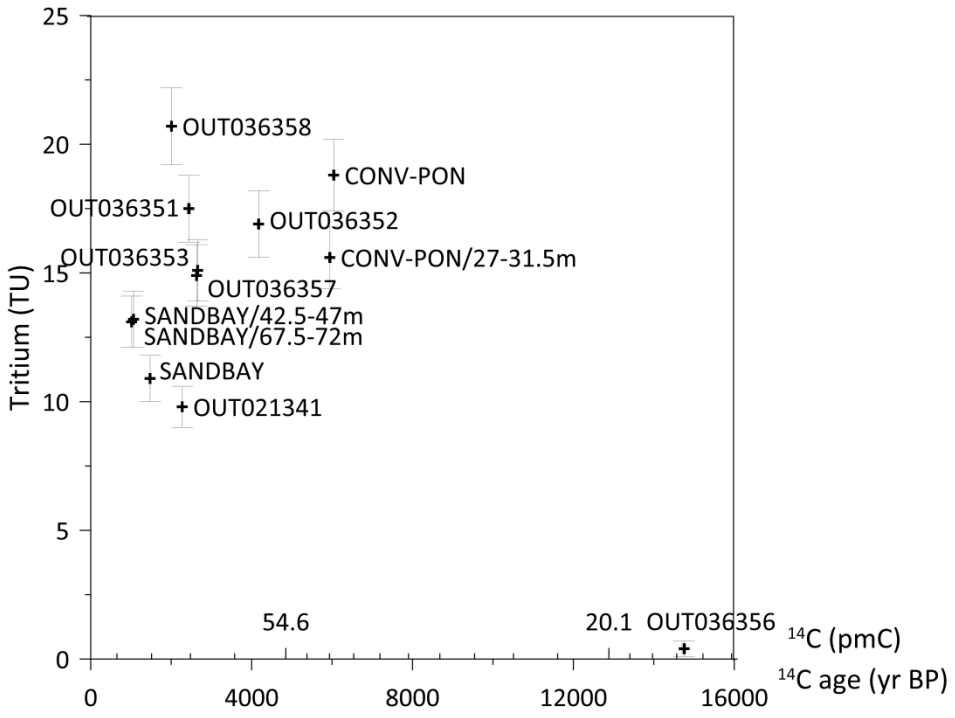

Fig. 26 Comparison between tritium content and uncorrected ^{14}C ages (with error bars on the measurements)

Four explanations can be proposed for possible over-estimated tritium contents (Lehmann et al. 1993). First, fluid containing tritium was likely introduced into groundwater during the drilling process. Although the drilling dates are unknown for most of the sampled wells, this explanation seems unlikely since the wells are used daily by their owners and were purged before sampling. Secondly, highly permeable zones through the bedrock fractures may extend deep into the subsurface and transport ^{3}H deeper than expected. It could explain some mixing between younger and older groundwater. The third possible source is *in-situ* ^{3}H production, mainly by $^{6}Li(n,\alpha)^{3}H$ reactions. However, *in-situ* ^{3}H production cannot be responsible for more than 4 TU in the water matrix (in case of rocks with high concentrations of Li, U and Th, 1500, 40 and 30 ppm,

respectively (Andrews & Kay 1982)). Unfortunately, due to the analytical method used for rock sample analyses, Li concentrations are not available but uranium and thorium concentrations are around a few ppm each (see Chapitre 2 section 6.3.5). Even if all samples contain some ^{3}H produced *in-situ*, the measured concentrations are too high to be explained by this source alone. Finally, these measurements could include some sampling or analytical errors but it would be quite unlikely for all samples to be affected. Except for the possible presence of fractures connecting young to old groundwater (mixing) and considering the carbon isotope behaviour (Fig. 23), the difference between ^{3}H and ^{14}C ages is better explained by processes occurring in the unsaturated and saturated zones, leading to an underestimation of the ^{14}C activity and higher ages (Chapitre 2 section 6.3.4). Main processes affecting the ^{14}C activities have been identified to be soil CO_2 equilibration in the unsaturated zone followed by silicate weathering by fossil CO_2 or calcite dissolution under closed system conditions. Other processes such as dissolution of calcite in samples taken in marble rocks or precipitation of secondary calcite following silicate weathering (presence of calcite traces in the well cuttings) was also suggested by the graphical method of Han et al. (2012). Diffusion of old porewater from confining clay layers into the flowing bedrock groundwater (Sudicky & Frind 1981) can also release ^{14}C-free carbon or carbon with low ^{14}C content and affects sample OUT036356.

Results of the noble gas analyses are difficult to interpret due to the lack of measurements, and appear in apparent contradiction with other data. Looking at the helium concentrations, the ratio $R = {}^{3}He/{}^{4}He$ is much lower than in the atmosphere and the ^{4}He concentrations are one to two orders of magnitude higher than the atmospheric equilibrium concentrations, whereas Ne concentrations are close to equilibrium (±10% depletion or enrichment). Therefore, the high He concentrations are not due to excess air but suggest an accumulation of helium in groundwater due to longer residence times, which seems inconsistent with the tritium measurements and the ^{14}C activities (no inverse-correlation relationship, as observed by Mayer et al. (2013)).

The residence time calculated from ^{4}He for sample OUT036356, the only sample with tritium below the detection limit, is more or less the same order of magnitude as the ^{14}C age. This might, however, be a coincidence: the helium might not have been intrinsically produced but may have originated from the deeper

bedrock via diffusion (Clark & Fritz 1997) since samples with tritium above detection limits are also affected by high concentrations in ^{4}He. In their study, Aeschbach-Hertig et al. (1998) concluded that their samples with detected tritium and helium concentrations well above atmospheric equilibrium concentration were a mixture of younger water with old water in an approximate 50-50% ratio. But, in their case, their helium concentrations are one order of magnitude less than ours which are in the range of those from Mahara (1995), who investigated the possible sources for ^{4}He to explain these values and was able to divide his samples into different groups according to the suspected source of helium, depending on their ^{3}He/^{4}He and $^4He_{eq}$/^{4}He ratios. Our samples have ^{3}He/^{4}He ratios which are between the radiogenic ratio of Mamyrin & Tolstikhin (1984) and the atmospheric equilibrium ratio. Since it is unlikely that the mantle is the source of ^{4}He (otherwise ^{3}He/^{4}He ratios would be higher), the ^{4}He source is probably radiogenic.

Reasoning the other way around (i.e. assuming correct ^{3}H/^{3}He ages), concentrations of U and Th were back-calculated using Eq. 6 and Eq. 7 and were about 2 orders of magnitude higher than those measured in our rock cuttings samples or compiled in the SIGEOM database (Geoscience and Mine database of Québec). Thus, the *in-situ* production of ^{4}He over ^{3}H/^{3}He residence time could not be responsible for the measured ^{4}He concentrations. In addition, travel times for each well were roughly assessed assuming a hydraulic gradient of 1% (deduced from the regional piezometric map produced by Comeau et al. (2013) and from field measurements made during the summer of 2012) and considering the hydraulic conductivity and porosity of the layers as well as the presumed shorter flow path to the well. For wells in the unconfined bedrock aquifer, infiltrated rainwater can reach the wells within 60 years, which is consistent with the occurrence of tritium.

These data suggest that our samples are a mixture of modern (<50 years) and older (>1000 years) groundwater. The mixing hypothesis is further supported considering the sampling procedure and well construction. Except for wells sampled using inflated packers, most samples were obtained from open unscreened bedrock wells which would allow significant mixing.

However, in the confined bedrock aquifer, the presence of tritium is more difficult to explain: the sample from well SANDBAY was taken from below 30 meters of clay and the nearest unconfined recharge zone is located about 5 km away. The presence of bedrock fractures in the vicinity of this well, as evidenced by geophysics (Fabien-Ouellet 2014), could be responsible for preferential flow paths from recharge zones to the open borehole. Another possibility is the presence of a leaky casing which connects the bedrock groundwater with the surface.

7.2 Noble gas temperatures

Different models were applied to the noble gas data, again the lack of sampling points made interpretation difficult. According to some authors (Sun et al. 2010), the use of different models within a dataset is not recommended since artefacts may be introduced in the temperature variations. Considering the results obtained for the four samples using the UA model, it appears that the older sample, OUT036356, has the colder NGT, about 2.5°C below the current local mean temperature. Along with the other available data for this sample, this NGT value is consistent with the ^{14}C age and with recharge occurring during the Champlain Sea episode, during which temperatures were less than today (up to 7°C less (Terasmae 1961)). The other samples show NGTs close to the current mean temperature, within the confidence intervals, which is consistent with the occurrence of tritium.

7.3 Conceptual hydrogeological model

The conceptual model deduced from the available data is summarized in Fig. 27. The important features to be considered from the geology are the presence of permeable fractures in the superficial layer of the bedrock.

Three levels of nested flow systems, as described by Tóth (1999), are probably present along the 2D cross-section. Local groundwater flow systems are near the surface, from high-elevation zones to local rivers. Intermediate systems extend from the higher elevation areas towards the lowest discharge zone (i.e. the Ottawa River). Finally, a regional system, at even greater depth, is inferred to include water from further north (Comeau et al. 2013). In addition, marine clays impede horizontal flow due to their low permeability but vertical

diffusive transport towards the bedrock as well as preferential flow paths through the fracture network could remain important. The extent of each system is currently being refined using a numerical model which will be presented in a future paper.

In the unconfined part of the aquifer (NE part of the 2D cross-section), the hydrogeochemistry was investigated for elevations ranging from 100 to 200 m.a.s.l. The dominant water type is Ca-HCO_3 (in the bedrock as well as in the few samples from Quaternary deposits) due to rock-water interactions and silicate dissolution, especially Ca-feldspars (anorthite $CaAl_2Si_2O_8$). In the confined part, the investigated zone is located at elevations between 30 and 120 m.a.s.l. where all samples were obtained from bedrock wells. Some water samples are of Na-Cl type (such as sample OUT036356), but were further diluted compared to the original Champlain Sea. Otherwise, the other samples from this part of the aquifer are Na-HCO_3 water type, suggesting the occurrence of cation exchange between sodium and calcium ions, with the sodium sorbed on the clay minerals after the Champlain Sea invasion being replaced by calcium from upstream Ca-HCO_3 type groundwater. In the unconfined part located down-gradient, the bedrock sample is also affected by cation exchange whereas the sample from the alluvium is a Ca-HCO_3 water type which has a quite different chemical signature than samples located in the up-gradient unconfined aquifer. The alluvium water sample, being located close to the discharge zone, seems to be a mixture of recharge water (Ca-HCO_3 water type) and up-gradient and deeper groundwater (Na-HCO_3 water type).

Stable isotope contents for samples OUT036352, SANDBAY and OUT036351 are close to the weighted mean signature for modern meteoric water as measured at the Ottawa station (IAEA/WMO 2011) which is consistent for sample OUT036352, being close to the recharge zone, and for sample OUT036351 in the Quaternary deposits. These two samples also have tritium contents greater than 15 TU, indicating the presence of a modern component. The SANDBAY sample, with a stable isotopic signature close to modern recharge and with detected tritium, seems to have undergone some mixing between modern and older groundwater components. As this sample was taken in a bedrock well below 30m of clay, the possible presence of a hydraulic window or a leaky casing may explain the mixing (although the well was drilled in 2004 and has been

abandoned since 2006) or preferential flow paths may exist in the fractured bedrock. Otherwise, the data showed evidence for older water such as sample OUT036356 which has a slightly depleted stable isotopic signature, no detected tritium, a low ^{14}C content and a ratio R/R_a = 0.180. This more depleted stable isotopic signature is also shared by samples taken in fluvio-glacial deposits (such as OUT036358 and OUT036353) or in superficial bedrock below such deposits (CONV-PON) but these samples have more tritium (>15TU) and a higher ^{14}C content. It is then difficult to conclude if the variations in the isotope values are significant and if the variations are simply due to altitude or seasonal effects. Even if samples OUT036358 and OUT036353 were taken in Quaternary deposits with an assumed higher conductivity and shorter residence time, the chemistry data, with higher concentrations for all ions compared to samples taken in the unconfined bedrock aquifer, tends to show that residence times might be higher than expected or mixing between younger and older groundwater may be significant. For sample CONV-PON, the ratio R/R_a = 0.917 is close to the atmospheric ratio and the existence of a higher conductive zone also supports an important younger groundwater component. Finally, sample OUT021341 has similar isotopic characteristics to OUT036351 but is of Na-HCO_3 water type, supporting a mixture between younger and older groundwater. Although noble gas data were too few to fully gained clarification for them, they allow identifying the presence of high concentrations in ^{4}He which are probably due to diffusion of helium from greater depths.

Similar features can be seen in the conceptual model of Cloutier et al. (2010) for the nearby Basses-Laurentides region since the two regions share the same recent geological history, notably invasion by the Champlain Sea following the last deglaciation.

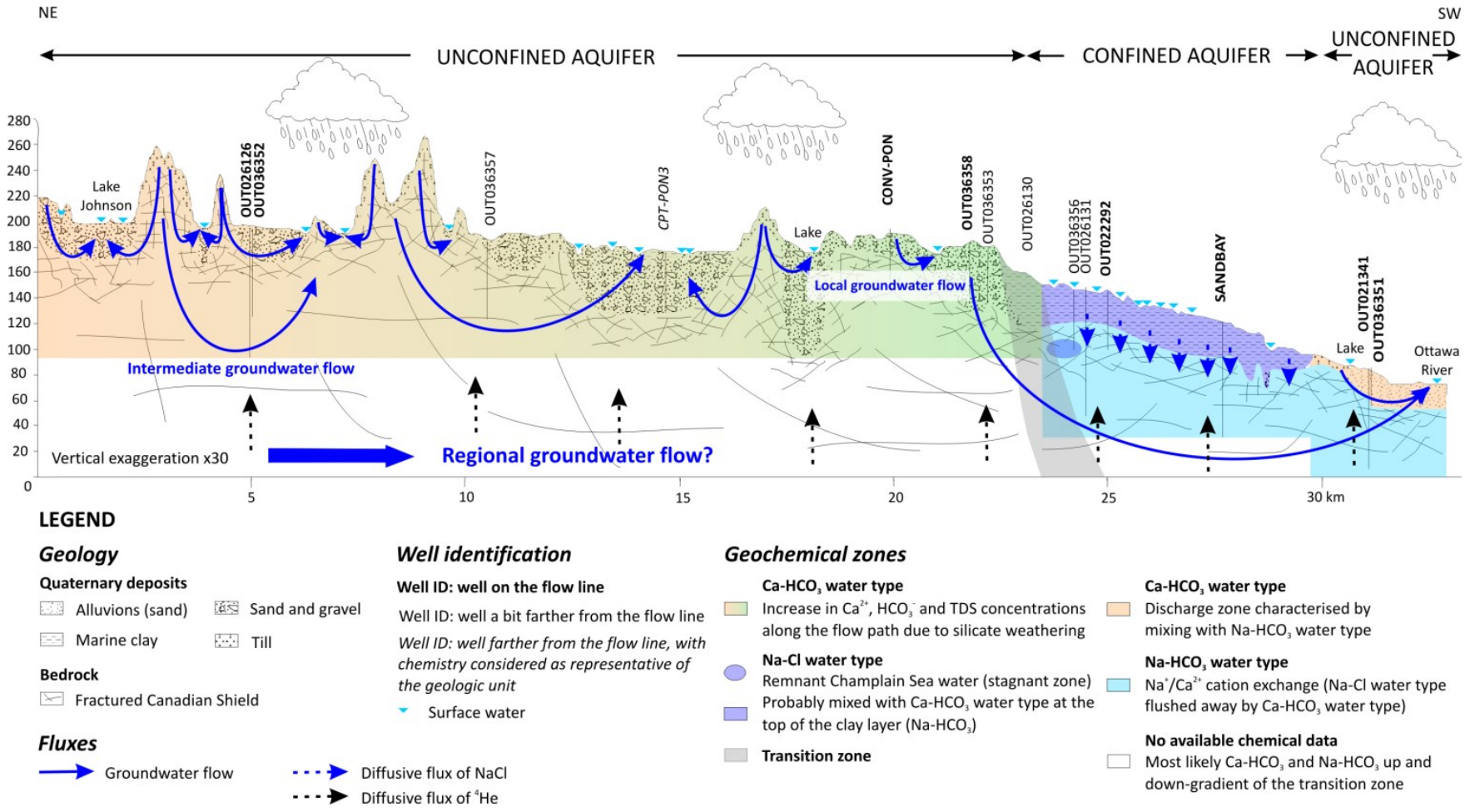

Fig. 27 Conceptual hydrogeological model along the selected 2D cross-section perpendicular to the Ottawa River

8 Conclusions and perspectives

A detailed local-scale evaluation of the geochemical evolution of groundwater has been carried out in the southern Outaouais Region, Quebec, Canada. Chemical signatures were analysed within a representative cross-section along a generalized flow path perpendicular to the Ottawa River. In addition to major ion concentrations and the definition of water-types, isotopic and noble gas data were used to confirm and improve our understanding of this important groundwater system. The depth of investigation extended to about 100 m which includes the most active groundwater flow zones in the unconsolidated aquifers as well as the upper zone of fractured crystalline and sedimentary bedrock.

Three major water types were identified. A Ca-HCO_3 water type was found in the unconfined aquifers and is a result mainly of silicate (especially Ca-feldspar) weathering. A Na-Cl water type was identified in one sample from the confined bedrock aquifer as some remnant of the former Champlain Sea. Since the end of the Champlain Sea episode, Na-Cl water has undergone flushing by Ca-HCO_3 type water from up-gradient areas, resulting in Na-HCO_3 water type with cation exchange between Na adsorbed on clay minerals and Ca in the flushing groundwater (freshening process).

The isotopic data are somewhat contradictory, but on more careful analysis, important mixing processes can be identified between older and younger groundwater. The presence of a younger component is mainly supported by the presence of tritium in almost all samples and the stable isotopic signature whereas the presence of an older component is shown by noble gas data with high ^{4}He concentrations. Except for one sample which undergoes some significant decay, ^{14}C activities in the samples results mainly from recharge water equilibrium with the soil CO_2 under open conditions and silicate weathering by fossil CO_2 or carbonate dissolution in the saturated zone. Some mixing zones have been identified under natural flow conditions (associated with discharge zones, presence of fractures, or diffusion) but other mixing processes might be better explained by the sampling procedure, most wells being open bedrock boreholes. It is unfortunate that borehole packers could not be used in all wells due to field constraints but ideally, they should be

systematically used in this type of settings, to give more insights on the chemical and age stratification in the bedrock and removed some uncertainties related to sampling in open boreholes. Assessing the residence time in the different parts of the aquifer can therefore be difficult but data tend to indicate a rapid turnover and short mean residence times in the unconfined part. Due to the scarcity of the noble gas data, it is difficult to draw definite conclusions about the temperature of recharge waters.

In terms of regional water supply, these results are important since little information was known about average residence times at shallow depths, at which the population gets its supply for drinking water, and in this type of settings, namely the Canadian Shield. The conceptual model elaborated here will be used as a basis for future modelling work, which will help address the remaining questions as well as test the different hypotheses developed in this paper.

Chapitre 3 – Un modèle numérique d'écoulement des eaux souterraines, de transport de tritium et de chlorures, et des temps de résidence dans le sud de la région de l'Outaouais, Québec, Canada

A numerical model of groundwater flow, tritium and chloride transport, and residence time in the southern Outaouais Region, Quebec, Canada

N. Montcoudiol, J. Molson et J.-M. Lemieux
Département de Géologie et de Génie Géologique
Université Laval, Québec City, QC, Canada, G1V 0A6

Pour soumission à Ground Water

1 Résumé

Un modèle numérique en 2D vertical d'écoulement et de transport a été utilisé afin de valider un modèle conceptuel d'évolution géochimique des eaux souterraines le long d'une ligne d'écoulement régional représentative de la région de l'Outaouais, Québec, Canada. Le système d'écoulement inclut jusqu'à 30 m de sédiments du Quaternaire et d'argiles marines déposés sur le socle rocheux silicaté et fracturé du Bouclier Canadien. La calibration du modèle d'écoulement régional est essentiellement basée sur les teneurs en tritium en complément de données de piézométrie incomplètes. Une conductivité hydraulique élevée dans les 40 premiers mètres de roc, due à la présence d'un système de fracturation, a permis d'expliquer les concentrations en tritium observées. Les systèmes d'écoulement sont contrôlés par la topographie et les eaux de surface, avec les systèmes locaux limités aux 30-40 premiers mètres de profondeur et avec des âges de l'eau de 10 à 50 ans. Les systèmes intermédiaires sont moins étendus qu'initialement pensé et sont caractérisés par des écoulements sub-horizontaux, avec des âges de 200 à 6000 ans. La zone active d'écoulement a une profondeur d'environ 100-200 m et il n'y a pas de preuve d'écoulement au-delà de cette profondeur. Les différences entre le tritium et les temps de résidences moyens modélisés et ceux des échantillons sont dues au mélange dans des puits ouverts aggravés par l'échantillonnage. Les concentrations en ^{4}He sont dues à la diffusion à partir d'eaux souterraines plus âgées. Les résultats appuient le modèle conceptuel d'écoulement et d'évolution géochimique existant (Chapitre 2), bien que l'importance de la composante régionale d'écoulement ait été réduite et l'importance des écoulements préférentiels dans les systèmes intermédiaires de la partie supérieure fracturée du roc ait été renforcée.

Mots clés : modèle conceptuel, modèle numérique, transport du tritium, âge de l'eau, hydrogéologie de la région de l'Outaouais, bouclier canadien

2 Abstract

A 2D vertical-section numerical model for groundwater flow and transport of age, tritium and chloride was used to validate a conceptual model of geochemical evolution along a representative regional-scale flow line in the Outaouais Region, Quebec, Canada. The flow system includes up to 30 m of Quaternary sediments and marine clays overlying fractured silicate rock of the Canadian Shield. Calibration of the regional flow model was based primarily on tritium concentrations which supplemented the incomplete hydraulic head data. A high hydraulic conductivity due to fracturing in the upper 40 m of the silicate bedrock was required to explain the observed tritium concentrations. Shallow groundwater flow is controlled by the topography and surface water bodies, with depths of local flow systems limited to 30-40 m and groundwater ages of 10-50 years. Intermediate systems are less extensive than initially thought and are characterized by sub-horizontal flow with ages from 200-6000 years. The active flow zone was inferred to be about 100-200 m deep, with any deeper regional flow essentially negligible. Differences between tritium-based ages and simulated mean residence times were attributed to mixing of groundwater in open boreholes exacerbated by sampling. ^{4}He concentrations could be explained by diffusive transport from deeper and older groundwater. The results support the existing conceptual models for flow and geochemical evolution presented in Chapitre 2, although the importance of the regional flow component has been reduced, and preferential flow through intermediate-scale flow systems within the upper fractured bedrock has been strengthened.

Keywords: conceptual model, numerical modelling, tritium transport, groundwater age, Outaouais Region hydrogeology, Canadian Shield

3 Introduction

As in most fractured bedrock environments, the Canadian Shield is characterized by a complex geological structure including fractures and mineralogical variations, making it difficult to understand groundwater flow

patterns and geochemical evolution. With increasing stresses on shallow groundwater sources, water supplies are becoming more reliant on fractured bedrock including areas of the Canadian Shield within the Outaouais Region, southern Quebec, Canada. Excluding the city of Gatineau, which contains 2/3 of the regional population and relies mainly on surface water, 91% of the remaining population uses groundwater as their main drinking water supply. A better understanding of these resources is important for future development, protection and sustainability, for which numerical modelling can provide useful insights.

Regional groundwater flow in Canadian Shield environments has been numerically simulated by several authors. Sykes et al. (2009), for example, present a comprehensive study on the 3D-modelling of regional-scale groundwater flow in the Canadian Shield (within the province of Manitoba). They take into account topography, surface water drainage, groundwater salinity and permeability variations. They divided the 1500 m deep bedrock into three zones: a fractured zone above a moderately fractured rock, and a sparsely fractured zone. Contrary to Tóth (1963) and his theory of nested flow systems (local, intermediate and regional), Sykes et al. (2009) did not find evidence of any regional groundwater flow i.e. from the highest to the lowest point (a difference of 140 m) of their 5,734 km^2 study area. They applied a recharge rate as the top boundary condition and prescribed heads for representing wetlands, lakes and rivers. The flow system thus appeared as a smooth reproduction of the topography, even at depths of 1000 m.b.s.l., regardless of the hydraulic conductivity field. Their system was therefore characterised by short local-scale flow paths with most of the flow occurring at shallow depths. Flow below 600 m accounted for only a small fraction of the total flow. High matrix pore pressures in the fractured zone were interpreted in their study as a remnant consequence of the ice load which has not yet dissipated, showing that the system is dynamic and still recovering from the last glaciation. In the same area, Gascoyne (2004) undertook a hydrogeochemical investigation which showed a zone of active circulation of groundwater at depths less than 200 m in the bedrock. Low or no-flow conditions characterised depths greater than 300-400 m. Farvolden et al. (1988) identified three flow regimes near Atikokan (Ontario), at similar depths as those from Sykes et al. (2009): a local system within about the first 150 m of bedrock and controlled by the surface topography, an intermediate zone between 150 and 600 m, and a zone below 600 m

with higher hydraulic heads. In this same area, Ophori (1999) identified a no-flow zone for depths greater than 800 m. Farvolden et al. (1988) also showed the importance of sub-horizontal and vertical fractures which act as major controls on the flow patterns (especially near the surface, as also shown by Gleeson (2009)).

Each of the two or three flow zones in these studies had a distinctive hydrogeochemistry. In the Sykes et al. (2009) model, for example, brines were considered at depths greater than 700 m (corresponding to the sparsely fractured zone). Their simulations produced more saline groundwater in discharge zones compared to similar depths in recharge zones after 100,000 years, even with diffusive-dominant transport at such depths. Other studies (Farvolden et al. 1988; Frape & Fritz 1987) have shown that shallow groundwater in the upper fractured zone is typically characterized by a low mineralization which increases with depth. Brackish water is often found at intermediate depths and brines at depths greater than 800 m (Farvolden et al. 1988; Frape & Fritz 1987). With data from four sites investigated under the Canadian Nuclear Fuel Waste Program, Gascoyne et al. (1987) identified the interface between fresh water and brackish and saline groundwater at a depth of about 300 m. In a more recent study in the Lac du Bonnet granitic batholith (southeastern Manitoba, Canada), Gascoyne (2004) found that saline waters lay at depths of more than 500 m.

In the above-mentioned studies, the focus had been either on characterisation of hydraulic properties of the bedrock or on the groundwater chemistry. Sykes et al. (2009) included 3D modelling to assess the different flow systems along with salt transport modelling. They concluded that higher density fluid at depth increases heads compared to the freshwater case but does not significantly change the flow pattern. Steady-state conditions were almost reached after 100,000 years of simulation. Ophori (2004) completed a similar study in the Atikokan research area (northwestern Ontario). In some scenarios, variable-density fluid was accounted for and similar conclusions as those of Sykes et al. (2009) were drawn about the limited impact of density on the shallow flow pattern. Chloride transport was simulated using a 1D advection-dispersion model under steady-state flow conditions to represent the concentration profiles as a function of depth. Apart from these two studies, no others on modelling flow patterns and geochemistry in the Canadian Shield seem to have been published.

Most studies of groundwater flow systems in the Canadian Shield environment were completed in the context of radioactive waste storage to assess the feasibility of the Canadian Shield as a long-term repository. For the same purpose and in a similar bedrock context of the Fenno-Scandinavian Shield, Laaksoharju et al. (2008a) used a multivariate mixing and mass-balance model (M3) to calculate the proportions of each end member and to assess water-rock interactions in a fractured aquifer under current conditions. The model was also used to calculate concentrations of several tracers (tritium, chloride and 18-oxygen). In this same context and based on the Laaksoharju (2008a) results, Molinero et al. (2008) proposed a two-step approach including the simulation of density-dependent groundwater flow and reactive transport under current conditions assuming a pseudo steady-state flow system while Laaksoharju et al. (2008b) simulated the major previous events that affected the region since the last glaciation. Although Molinero et al. (2008) commented on the possible importance of accounting for fluid density, they focused on the geochemical system and did not present results from the flow model.

In southeastern Canada, in areas invaded by the post-glacial Champlain Sea, several conceptual models have been proposed for explaining the evolution of groundwater geochemistry in different hydrogeological settings (Beaudry 2013; Blanchette et al. 2010b; Carrier et al. 2013; Cloutier et al. 2010; Larocque et al. 2013). However, none have been located within the Outaouais Region, and none were supported by flow and transport modelling. Here, the objective is to help validate the conceptual model proposed in Chapitre 2 for interpreting and explaining geochemical evolution of groundwater within the bedrock of the Grenville geologic province (Outaouais Region, Quebec). After presenting the relevant characteristics of the study area and summarizing the key geochemical processes from the conceptual model, the focus will be on the numerical modelling, which has been divided into four different steps.

The first step was to reproduce the current flow conditions, calibrating the model with available hydraulic head data. Since the hydraulic conductivities could not be uniquely calibrated based on observed hydraulic head data alone (due in part to the sparse available data which were not fully representative of the aquifer conditions), the calibration was improved in Step 2 by simulating the recent tritium distribution in the aquifer.

Using the tritium concentrations in precipitation from the nearby Ottawa station as a transient surface boundary condition, the theoretical tritium distribution at the sampling date (2012) was compared to the tritium concentrations measured in the groundwater samples and final adjustments were made to the hydraulic conductivity field. Step 3 involved simulating the transport and evolution of chloride (as an ideal tracer) following intrusion of water from the Champlain Sea into the aquifer system, followed by groundwater freshening after retreat of the sea, and continuing up to present-day conditions. The aim of this simulation was to explain the current chloride distribution in the aquifer and was also used to predict future chloride evolution. In Step 4, the steady-state mean groundwater age distribution was simulated under current flow conditions and checked against the tritium and ^{14}C isotope data. Simulation results from each of these four steps contributed towards a better understanding of aquifer system behaviour.

4 Study area

The study area is located in the southwestern part of the Outaouais region, in southern Québec, Canada (Fig. 28). The modelling is applied to the conceptual model proposed in Chapitre 2 which was developed based on interpreting groundwater chemical data along the 2D cross-section identified in Fig. 28. The cross-section is located along the dominant groundwater flow direction, extending approximately 30 km from the Gatineau Hills in the northeast to the Ottawa River in the southwest, passing through the township of Shawville.

4.1 Geological history of the region

The geological history of the region and the resulting distribution of Quaternary deposits within the Outaouais study area were presented in Chapitre 1. A brief review of the geological history is presented herein with a particular focus on the site geology and hydrogeology, and its immediate surroundings.

Along the cross-section, the underlying bedrock is part of the Grenville Province of the Canadian Shield, dating from the Proterozoic (Precambrian). The cross-section passes through two principal types of rocks: non-

carbonated metamorphic rocks (gneiss and paragneiss) in the northeast and calco-silicate rocks (marble) to the southwest (towards the Ottawa River). The bedrock is characterised by a high degree of fracturing in the upper 50-60 m (Sterckx 2013), which has likely produced extensive preferential flow paths.

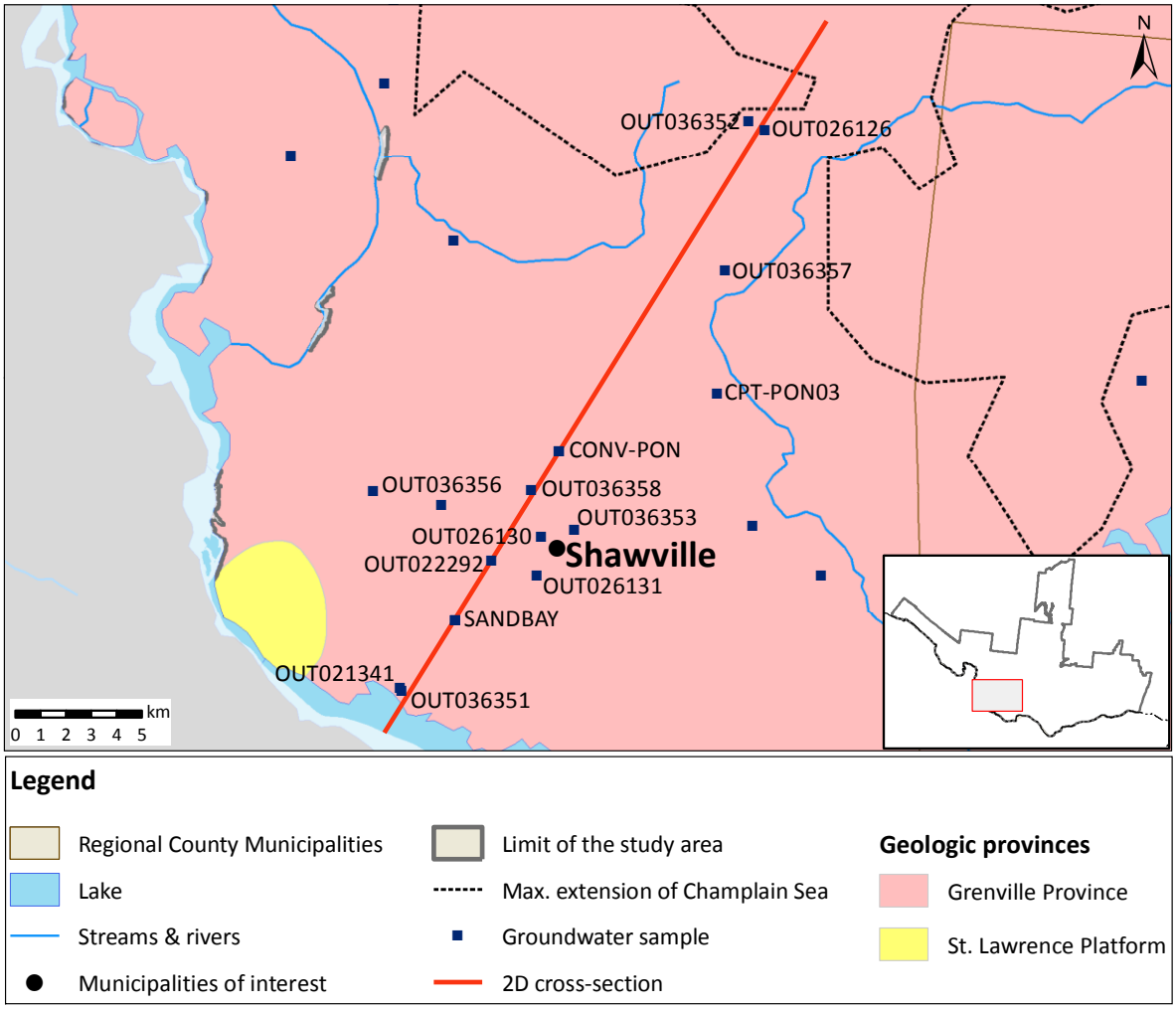

Fig. 28 Location of the 2D cross-section and nearby sampling wells

Unconsolidated deposits prior to the last glaciation no longer exist in the study area due to erosion by the many glacial-deglacial cycles during the Quaternary period. During the last glaciation, abrasion of the bedrock and ice movement deposited a discontinuous layer of till directly overlying the bedrock, while during the last deglaciation, freshwater fluvio-glacial sediments were deposited in the lower valleys. The Ottawa River valley (including lower reaches of secondary river valleys) was then invaded by the Champlain Sea about 12,000 years ago (Parent & Occhietti 1988) which left marine clays on top of the fluvio-glacial sediments if they had

not already been eroded. Due to isostatic rebound, the Champlain Sea progressively left the region about 10,000 years ago, leaving behind deltaic, littoral and pre-littoral sediments. Along the main rivers, this sequence is buried by ancient and more recent alluvium (Comeau et al. 2013).

4.2 Conceptual model and validation strategy

The conceptual model we propose to validate (and modify if necessary) with support from numerical modelling (Fig. 30) has been thoroughly detailed in Chapitre 2. Although the existing conceptual model was developed from quite detailed field data, several questions remain that will be addressed using different modelling approaches (Fig. 29).

One question regards the context of local, intermediate and regional flow systems (Tóth 1999) in the case of this specific Outaouais flow system. It is still unclear, for example, if a regional component exists at the Outaouais site. Based on the simulation results of Sykes et al. (2009), it is very unlikely that any regional flow system was intercepted by the Outaouais-sampled wells since their maximum depth was only about 100 m. The flow model presented here was designed in part to help provide insight into the local and intermediate flow systems and to determine their relative importance with respect to groundwater geochemical evolution (Fig. 29a). Any deeper regional flow component would also become apparent from the modelling. Transport of tritium was used to better constrain the flow model (Fig. 29b).

In Chapitre 2, the chemical zonation of groundwater along the 2D Outaouais section was identified using major ion concentrations. The main geochemical processes inferred responsible for this zonation were the dissolution of silicates (mainly anorthite $CaAl_2Si_2O_8$) in the unconfined (up-gradient) part of the aquifer, mixing with fossil waters from Champlain Sea and cation exchange in the confined part, as well as mixing between recently infiltrated and older water in the down-gradient unconfined part. The impact of the Champlain Sea invasion will be assessed in this paper by simulating chloride intrusion into the confined aquifer (Fig. 29c). Mean groundwater age (residence time) will also be simulated to provide further insight into the aquifer flow systems, including the effect of mixing and dispersion (Fig. 29d). The simulated ages will be compared to ages

inferred from the observed tritium and ^{14}C data. Helium fluxes as depicted in the conceptual model have not been included in this validation.

5 Numerical modelling

5.1 Simulation approach

A four-step modelling approach will be adopted in this study, including groundwater flow, tritium and chloride transport, and mean groundwater age (Fig. 29). The same 2D vertical domain, which follows the conceptual model of Fig. 30, and same discretization, will be used for all simulations; only the governing equations and boundary conditions are changed. Considering the regional scale of the model domain (about 32 km) and the absence of data pertaining to the distribution and characteristics of the fractures, an equivalent porous medium (EPM) approach was applied in all cases. Details on the numerical implementation of the flow and transport equations defined below can be found in Molson & Frind (2014).

5.1.1 Groundwater flow

The flow system representing the conceptual model was simulated using the FLONET/TR2 model (Molson & Frind 2014) which uses the dual formulation in terms of hydraulic potentials Φ [L] and stream functions ψ [$L^2.T^{-1}$], assuming 2D steady-state, isothermal and uniform density conditions, as defined by Eq. 8 and Eq. 9 respectively:

$$\frac{\partial}{\partial x}\left(K_{xx}\frac{\partial \phi}{\partial x}\right)+\frac{\partial}{\partial y}\left(K_{yy}\frac{\partial \phi}{\partial y}\right)=0 \qquad \textbf{Eq. 8}$$

$$\frac{\partial}{\partial x}\left(\frac{1}{K_{yy}}\frac{\partial \psi}{\partial x}\right)+\frac{\partial}{\partial y}\left(\frac{1}{K_{xx}}\frac{\partial \psi}{\partial y}\right)=0 \qquad \textbf{Eq. 9}$$

where x and y are the horizontal and vertical coordinate directions, respectively [L], and K_{xx} and K_{yy} are the principal components of the hydraulic conductivity tensor [$L.T^{-1}$].

The FLONET/TR2 model allows the grid to deform to accommodate the final equilibrium position of the free water table. During grid deformation element-based, hydraulic conductivities (K) initially assigned from the geological model are reattributed to grid elements depending on their final elevation in order to retain correct K values at corresponding elevations, for example as the water table drops below the initial topographic elevation. In this study, convergence to a water table elevation tolerance of 10^{-4} m was usually attained within 100 iterations.

Element-based groundwater velocities for the transport simulations are calculated in FLONET/TR2 based on the simulated streamfunctions. These velocities are also used to calculate advective groundwater ages based on particle tracking using a 4th-order Runge-Kutta integration scheme within Tecplot (©Tecplot Inc. (2014)). The flow field is assumed at steady state for all transport simulations.

5.1.2 Tritium and chloride

Tritium and chloride transport is simulated using the TR2 module within FLONET/TR2 which solves the 2D advective-dispersive mass transport equation (Eq. 10):

$$\frac{\partial}{\partial x_i}\left(\frac{D_{ij}}{R}\frac{\partial c}{\partial x_j}\right) - \frac{v_i}{R}\frac{\partial c}{\partial x_i} - \lambda c = \frac{\partial c}{\partial t} \qquad \textbf{Eq. 10}$$

where D_{ij} is the hydrodynamic dispersion tensor [$L^2.T^{-1}$], R is the retardation factor [-], c is the tritium or chloride concentration [$M.L^{-3}$], x_i are the spatial coordinates [L], v_i is the average linear flow velocity [$L.T^{-1}$], λ is the first-order decay rate [T^{-1}] and t is the time [T].

For tritium, a retardation of R=1 and a linear decay rate of $\lambda = 1.53\times10^{-4}$ d^{-1} was assumed, which corresponds to a half-life of 12.43 years (Clark & Fritz 1997). For chloride, which is non-reactive, λ=0 and R=1. The effective molecular diffusion coefficient for tritium was 1×10^{-10} $m^2.s^{-1}$ (i.e. identical to water), and 2×10^{-10} $m^2.s^{-1}$ for chloride (Desaulniers & Cherry 1989; Quigley et al. 1983).

The dispersion tensor D_{ij} in Eq. 10 and Eq. 11 is defined using the 4-component dispersivity formulation of Lichtner et al. (2002), which uses two principal longitudinal dispersivities (α_{LH}, α_{LV}) and two principal transverse dispersivities (α_{TH}, α_{TV}), for the horizontal and vertical directions, respectively. The dispersion terms are then calculated based on the angle of the velocity vector with respect to the vertical axis. In all transport simulations, the longitudinal horizontal dispersivity for the domain (α_{LH} = 20 m) was estimated using the relationships developed by Gelhar et al. (1992). The longitudinal vertical dispersivity (α_{LV}) was set at 2 m, (10× less than the longitudinal horizontal) while the two transverse dispersivities were set at 0.01 m (same order of magnitude as applied at similar scales by Bester et al. (2006)).

The tritium and chloride transport simulations assume steady-state flow conditions and dilute water. Density effects are not considered. The time step was 10 days which meets the Courant stability criterion.

5.1.3 Groundwater mean age

Advective-dispersive groundwater ages were computed to complement the advective ages as they include full mixing between different age groundwaters, and are therefore more realistic.

A similar equation to Eq. 10 is solved for mean groundwater age (Eq. 11):

$$\frac{\partial}{\partial x_i}\left(D_{ij}\frac{\partial A}{\partial x_j}\right) - v_i\frac{\partial A}{\partial x_i} + 1 = 0 \qquad \textbf{Eq. 11}$$

where A is groundwater age (T) relative to a recharge age of 0 day, and where the +1 term represents a growth of age at a rate of 1 day.day^{-1}. The dispersion tensor and dispersivities are defined identically as for tritium and chloride. A molecular diffusion coefficient of 1×10^{-10} m^2.s^{-1} was assumed. The approach accounts for advective-dispersive age mixing along flowlines.

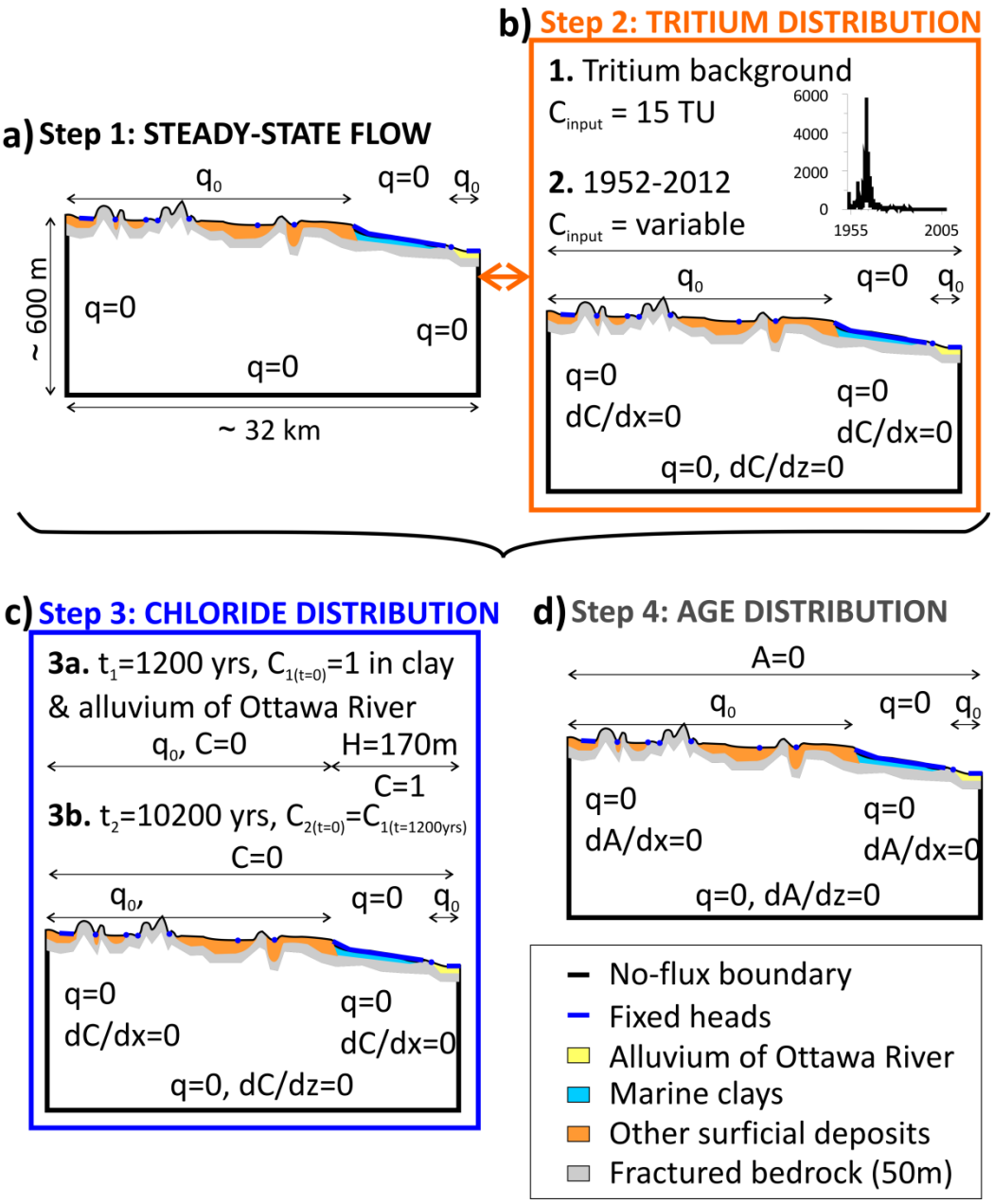

Fig. 29 Sequential modelling strategy: a) step 1: steady-state model of current flow conditions, b) step 2: calibration of the flow model using tritium, c) step 3: simulation of chloride transport from the Champlain Sea invasion, and d) step 4: groundwater age model under steady-state (current) flow conditions. For simplicity, the slope of the bottom was not represented.

5.2 Set-up for flow modeling

5.2.1 Model domain and flow boundary conditions

The model domain is 32.5 km long and varies in depth between 550 and 600 m from the ground surface to the bottom boundary. The up-gradient left boundary is located in the Gatineau Hills and corresponds to a surface water divide. The right (down-gradient) boundary is located at the centre of the Ottawa River, which acts as the major discharge zone for the entire Outaouais region. These two boundaries are both set as symmetry (no-flow) boundaries.

The bottom boundary was assigned a slope similar to the average topographic gradient, varying from -354 to -505 m.a.s.l. To set the bottom boundary limit, a 10 km deep model was first run assuming a uniform hydraulic conductivity of 1×10^{-9} m.s^{-1} below the base of the 100 m deep fractured zone. Although this model produced a weak regional flow component at depths below about 6 km, the low hydraulic conductivity in the deeper less fractured bedrock forced essentially all recharge water to flow within the uppermost layers (Quaternary sediments and upper fractured bedrock zone). Indeed, in this deep model, only 0.01% of the flow circulated at depths below -350 m.a.s.l. Moreover, at these depths, higher density saline groundwater would further inhibit deeper flow systems (Normani et al. 2009; Sykes et al. 2009). The bottom model boundary was therefore set at a mean elevation of -400 m.a.s.l., and assigned as a no-flow boundary condition (Fig. 29a).

The top boundary of the flow model corresponds to the water table which was initially positioned to correspond with the surface topography, then was allowed to deform during the simulation to its equilibrium position. The maximum elevation is 268 m.a.s.l, with the lowest elevation represented by the Ottawa River (72 m.a.s.l.) at the right down-gradient boundary. Topographic elevations were extracted from a Digital Elevation Model (DEM) with a resolution of 10 m (Comeau et al. 2013). To allow deformation of the water table, a recharge (type 2) condition was applied to most surface nodes while surface water bodies and water table elevations at the surface of the confining clay layer were represented using fixed heads (type 1) (Fig. 29a). Indeed, groundwater and surface water were assumed to be connected here which is generally the case under

temperate climates and relatively high recharge rates (Goderniaux et al. 2013). The applied recharge flux was equivalent to 30% of the total annual precipitation. Indeed, Comeau et al. (2013), using the model HELP® (Hydrologic Evaluation of Landfill Performance; Schroeder & Ammon (1994)), evaluated the recharge conditions throughout the Outaouais region. They calibrated their model for three sub-drainage basins and compared the results with those obtained using hydrograph separation. They found that an average of 30% of the precipitation infiltrates to recharge the aquifers. Observed data from the Shawville station (station ID 7038040, Environment Canada (2013)) from 1948 to 2012 showed an average annual precipitation rate of about 839 mm/year, thus a constant recharge rate of 8×10^{-9} m.s^{-1} was then assigned in the model.

5.2.2 Model discretization

The 2D vertical section (32.58 km, from the topographic highs to the middle of the Ottawa River) was discretized every 10 m in the horizontal direction, and vertically into 9 hydrostratigraphic layers. The bottom two layers represent the bedrock while the seven upper layers represent the Quaternary deposits, which were in total vertically discretized into 67 elements for the complete model (Table 10). Although the deepest elements are on the order of 15 m thick, most thicknesses range between 10 m and 0.5 m. The topmost layer is used as a *recharge-spreading layer* that redistributes recharge away from low conductivity zones and avoids the development of ponding conditions (Beckers & Frind 2000). The global mesh is composed of 3258×68 (=221,544) nodes in the horizontal and vertical dimensions, respectively, and 436,438 triangular elements. To accommodate the moving water table, the five top rows of elements are allowed to deform. Pinch-outs of the hydrostratigraphic layers in the deformed mesh were accommodated by reassigning hydraulic K's to those of the local host material (Fig. 30a).

5.2.3 Hydraulic properties

Comeau et al. (2013) compiled and validated more than 2,000 hydraulic tests in the Outaouais regional study area (Table 10, Fig. 30b and Fig. 30c). Since the hydraulic conductivity of the clay proposed by Comeau et al. (2013) appeared to be too high (2×10^{-7} m.s^{-1}) compared to published values for the Champlain Sea clays

(Since measured porosities were not available, values compiled by Fetter (2001) were applied (Table 10). The clay porosity was later adjusted during calibration to 0.65 which is similar to the mean porosity of similar clays measured by Desaulniers & Cherry (1989).

Table 11), a conductivity of 1×10^{-11} m.s^{-1} was applied (based in part on the chloride simulations). Bedrock hydraulic conductivities were assigned based on hydraulic tests performed on wells within the 2D cross-section. Hydraulic tests performed in four bedrock wells yielded hydraulic conductivities between 3×10^{-8} and 1×10^{-5} m.s^{-1} (tested wells identified on Fig. 30), which correspond well to the range of values for Canadian Shield fractured bedrock at the regional scale (Sterckx 2013). This range was applied for the top 150 m of bedrock with exponentially decreasing hydraulic conductivities with depth (Fig. 30d), as is commonly observed in crystalline bedrock (Maréchal 1998). Below this depth, the bedrock is considered to be much less permeable with hydraulic conductivities decreasing exponentially with depth from 10^{-10} to 10^{-12} m.s^{-1} (Table 10) (Farvolden et al. 1988; Maréchal 1998).

Table 10 Description of the geologic layers and their hydraulic properties

Geology type	Number of grid layers	Hydraulic conductivity (m.s^{-1})	Porosity (-)
RSL (Recharge Spreading Layer)	1	$1x10^{-5}$	0.30
Alluvium	2	$1x10^{-4}$ [$5x10^{-4}$]	0.35
Deltaic sediments	4	$1x10^{-4}$ [$2x10^{-4}$]	0.30
Littoral sediments	1	$3x10^{-4}$	0.35
Marine clays	4	$1x10^{-11}$	0.50 [0.65]
Fluvio-glacial sediments	4	$3x10^{-4}$ [$1x10^{-4}$]	0.25
Till	1	$8x10^{-5}$	0.15
Shallow bedrock	8	$1x10^{-6}$ [$1x10^{-5}$] (top 40 m)	0.03
Deep bedrock	42	$1x10^{-7}$ (40-50 m thick)	0.02
		$1x10^{-8}$ (50-60 m thick)	0.01
		$1x10^{-10}$ (60-70 m thick)	0.01
		$1x10^{-12}$ (to bottom)	0.01
Transport parameters: α_{LH} = 20 m; α_{LV} = 2 m and α_{TH} = α_{TV} = 0.01 m			

[-]: calibrated values of hydraulic conductivities and porosity

As pointed out by several authors (Farvolden et al. 1988; Gleeson 2009), fractured silicate rock is generally anisotropic, characterised by sub-horizontal fractures with ratios of horizontal to vertical hydraulic

conductivities of K_x/K_z from 1 to 10. Without any further data on anisotropy at the Outaouais site, an anisotropy factor of 5 (K_x/K_z=5) was applied for the entire bedrock unit. Quaternary deposits were considered isotropic.

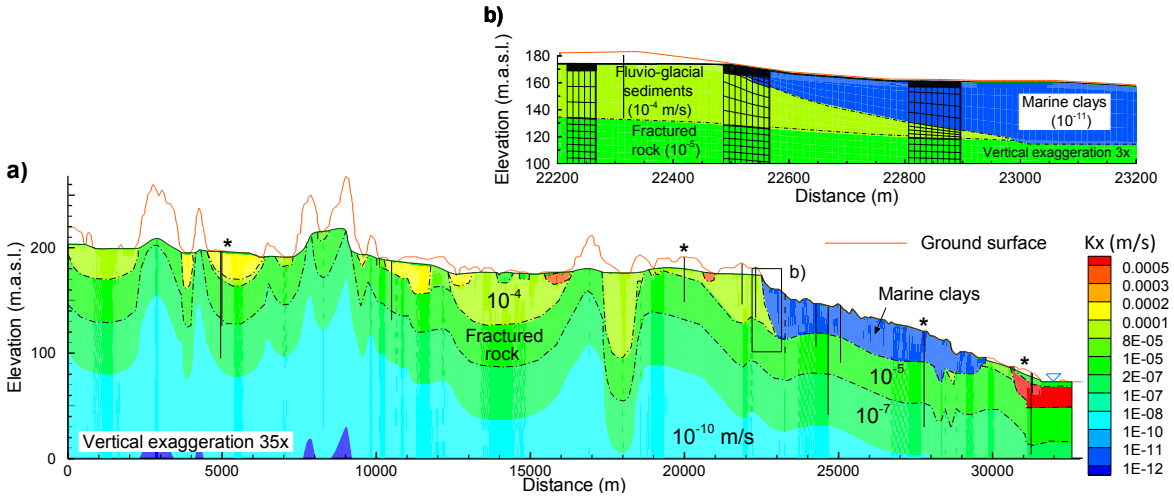

Fig. 30 Simulation domain showing: a) Distribution of hydraulic conductivities along the 2D cross-section; b) Selected mesh detail near the fluvio-glacial sediment and clay interface. The vertical bars represent the wells of Fig. 27. Wells where hydraulic conductivities were calculated from hydraulic testing are identified by an asterisk.

Since measured porosities were not available, values compiled by Fetter (2001) were applied (Table 10). The clay porosity was later adjusted during calibration to 0.65 which is similar to the mean porosity of similar clays measured by Desaulniers & Cherry (1989).

Table 11 Literature review of measured hydraulic conductivities of Champlain Sea clay deposits

Reference	Hydraulic conductivity ($m.s^{-1}$)	Porosity [-]
Tavenas et al. (1983)	$1x10^{-11}$ – $1x10^{-10}$	-
Leroueil et al. (1988)	$1x10^{-9}$ – $5x10^{-9}$	
Desaulniers & Cherry (1989)	$7.5x10^{-11}$ – $4.9x10^{-10}$	0.64
Lapierre et al. (1990)	~ $1x10^{-9}$	
O'Shaughnessy & Garga (1994) and Garga & O'Shaughnessy (1994)	$8x10^{-10}$ – $2x10^{-9}$	0.5
Leroueil et al. (2003)	~ $1x10^{-9}$	
Marques et al. (2004)	~ $1x10^{-9}$	

5.3 Calibration of the flow model: hydraulic heads and tritium

The first modelling step consisted of reproducing the current flow conditions based on available information on current water levels. The primary adjustments made during calibration were to the hydraulic conductivities in the bedrock and in sediment layers where shallow wells were sampled. The recharge was calibrated by Comeau et al. (2013) using the model HELP (Schroeder & Ammon 1994) and was considered a good approximation.

Calibration of the hydraulic conductivity was first completed using only the hydraulic head data (Fig. 31a). The observed head dataset includes 27 wells within 1 km from the 2D cross-section which were validated at the regional scale (for errors, anomalous data etc.) by Comeau et al. (2013). Most measurements were taken in wells located in the confined aquifer. The few measurements taken from the unconfined aquifer are located in the valleys of the higher topographic regions. During the calibration procedure, only hydraulic heads in the up-gradient unconfined bedrock aquifer reacted significantly to changes in hydraulic conductivity and recharge, especially in the local topographic highs where no water level measurements are available for comparison. Generally, too few observation points were available in the unconfined aquifer to obtain a unique response.

Since calibration to hydraulic heads alone was non-unique based on uncertain combinations of recharge and hydraulic conductivity (Ophori 1999), the flow model was further constrained by using the observed distribution of tritium.

The initial calibration based on heads showed a relatively poor fit for tritium concentrations with essentially no tritium predicted for the bedrock. A subsequent final re-calibration of K was therefore performed with more weight placed on the fit to tritium, whose concentrations are much more sensitive to changes in the hydraulic parameters, especially the hydraulic conductivity of the shallow bedrock. Tritium concentrations were available for 9 wells along the 2D cross-section (Fig. 27) and although the decrease in tritium activity in the unsaturated zone is not taken into account in the model, this is considered acceptable as the water table is relatively shallow in most parts of the aquifer (except in the topographic highs).

A first simulation was completed to obtain the background concentrations of tritium in the aquifer before the nuclear bomb testing peak in the 60's assuming current flow conditions (Fig. 29b). The initial tritium concentration for this simulation was set at 0 throughout the domain. A constant first-type boundary concentration of 15 TU was applied along the top recharge boundary, which is the estimated atmospheric background concentration of tritium in the Ottawa region prior to 1953 (Clark & Fritz 1997). This simulated steady-state distribution of tritium (not shown) is used as the initial condition for the transient simulation from 1953 until 2012 (Fig. 29b).

For the transient tritium simulation, the tritium concentrations measured on a monthly basis at the Ottawa station (WMO code 7162800, IAEA/WMO (2011)) were used as the top boundary condition from 1953 to 2012 (i.e. from the first measurement to the sampling date, Fig. 29b). A few missing data points were replaced by the average value between the closest measurement times. The series ends in 2007. From this last measurement to the sampling date, an average value of 15 TU was applied; similar to the background value (which also corresponds to the average value of the two final years of measurements).

Irrespective of the distance of the observation wells from the 2D cross-section, the deviation from the 1:1 best-fit line was similar which confirms that the 2D cross-section indeed closely follows a regional flow line and thus a 2D vertical model is an acceptable simplification. The root mean squared error (RMSE) is about 9 m, with calculated heads mainly greater than those measured, 7.6 m higher on average (Fig. 31a). In the unconfined aquifer, the water table is below ground surface (up to 60 m deep) whereas the confined aquifer is partly under artesian conditions (up to 10 m). In comparison, for their piezometric map of the entire Outaouais Region, Comeau et al. (2013) determined the average water table to be 6 m below ground surface throughout the study area. This value might be underestimated since most available water table levels were measured in areas of limited topographic variations. Some artesian wells were also identified in the area during field work.

Test simulations showed that when the shallow bedrock K was too low, the simulated tritium would remain only in the Quaternary sediments. In the final calibrated model, with a hydraulic conductivity of 1×10^{-5} $m.s^{-1}$ in the

shallow bedrock, a reasonable RMSE value of 5.3 TU was obtained (Fig. 31b). However, the simulated concentrations are still almost systematically under-estimated compared to tritium contents measured in the field.

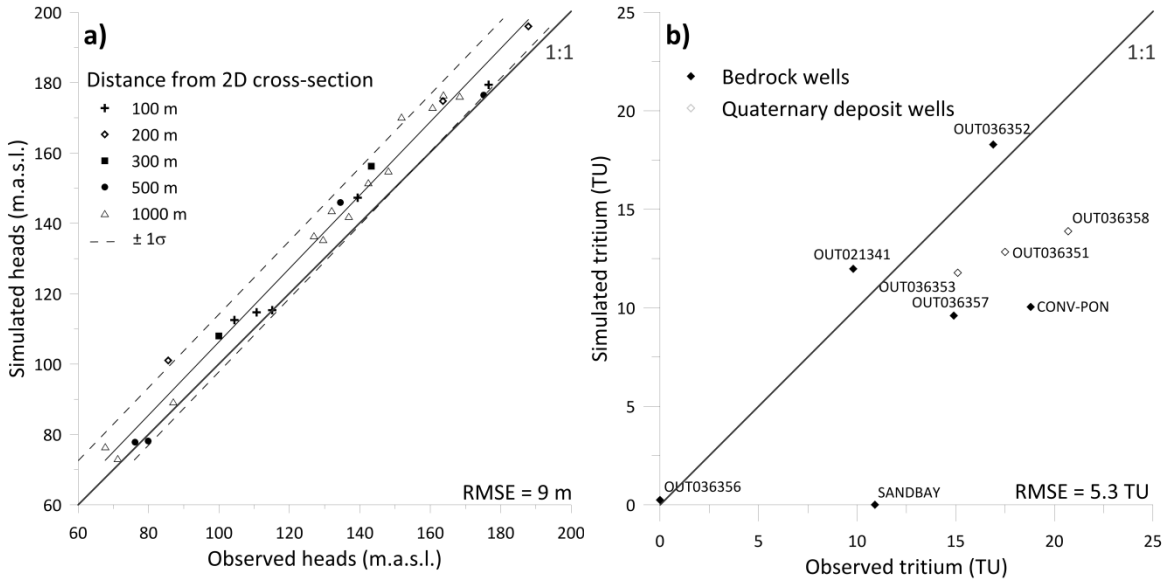

Fig. 31 Calibration results: a) simulated vs observed heads, b) simulated vs observed tritium concentrations

Since the model did not simulate the loss of tritium in the unsaturated zone, over-estimated tritium concentrations are expected. Different hypotheses can be made to explain these discrepancies. It is likely that a greater proportion of water at the depth of the pump would be collected in the sample. Also, even in bedrock wells cased through the overlying Quaternary deposits, leakage from shallow (younger) groundwater might be expected since the shallow bedrock is fractured. For wells in the Quaternary deposits, information on the location of the screen was not available and the well was considered screened over the entire thickness of the layer. Near the surface, tritium values are close to today‘s atmospheric concentration (15 TU) whereas values are even higher below the surface. Accounting for a screen length from the surface to the bottom of the well would likely lower the simulated tritium value by including lower tritium concentrations near the surface e.g. the first 5 m.

5.4 Simulated flow systems

The simulated steady-state groundwater flow system and advective (particle-track) travel times along selected streamlines are shown in Fig. 32. Flow system depths and the extent of intermediate flow systems are controlled by the topography and by surface water bodies, which act as discharge zones (Fig. 32a). Local systems are located in the first 50 meters below ground surface. Intermediate systems reach the base of the model but flow rates are essentially negligible at these depths (evident from the exponential decrease in streamfunction contour levels with depth). No evidence of regional groundwater flow was seen, consistent with simulation results in similar terrain by Sykes et al. (2009) and Ophori et al. (1996).

Due to the decrease of hydraulic conductivity in the bedrock at depths greater than 200 m, particle-tracking based advective ages are on the order of hundreds of thousands years. Detail shown in Fig. 32b reveals short travel times (< 100 years) in the first tens of meters of depth, within the Quaternary sediments. In rock outcrop areas, ages increase rapidly with depth and flow paths become controlled by the layer geometry. Water discharging to surface water bodies follows deeper flow paths and have longer mean residence times especially below Lake Johnson, a large surface water body (at km 1-2). In the confined aquifer (Fig. 32c), groundwater flows most rapidly in the upper fractured part of the bedrock, with groundwater ages since recharge on the order of 100-200 years.

In recharge and discharge zones, the decreasing hydraulic conductivity with depth has induced significant variations in the hydraulic heads. Below discharge areas, hydraulic heads increase by about 1 to 2 m over the model depth (Fig. A8 in Annexe 5) whereas they decrease by 7 m in recharge zones (Fig. A8b). In the clay layer overlying the up-gradient part of the confined aquifer (Fig. A8c), hydraulic heads increase with depth (-0.059 m/m) but slightly decrease with depth into the bedrock (4.6×10^{-4} m/m). The vertical gradient in the fractured confined bedrock aquifer is negligible where the flow is nearly horizontal. In the down-gradient part of the confining clay layer, hydraulic heads are higher (Fig. A8d) than in the underlying bedrock (where again, the

vertical hydraulic gradient is negligible). Therefore, conditions are artesian in the up-gradient part of the confined aquifer while fluxes are downward in the down-gradient part.

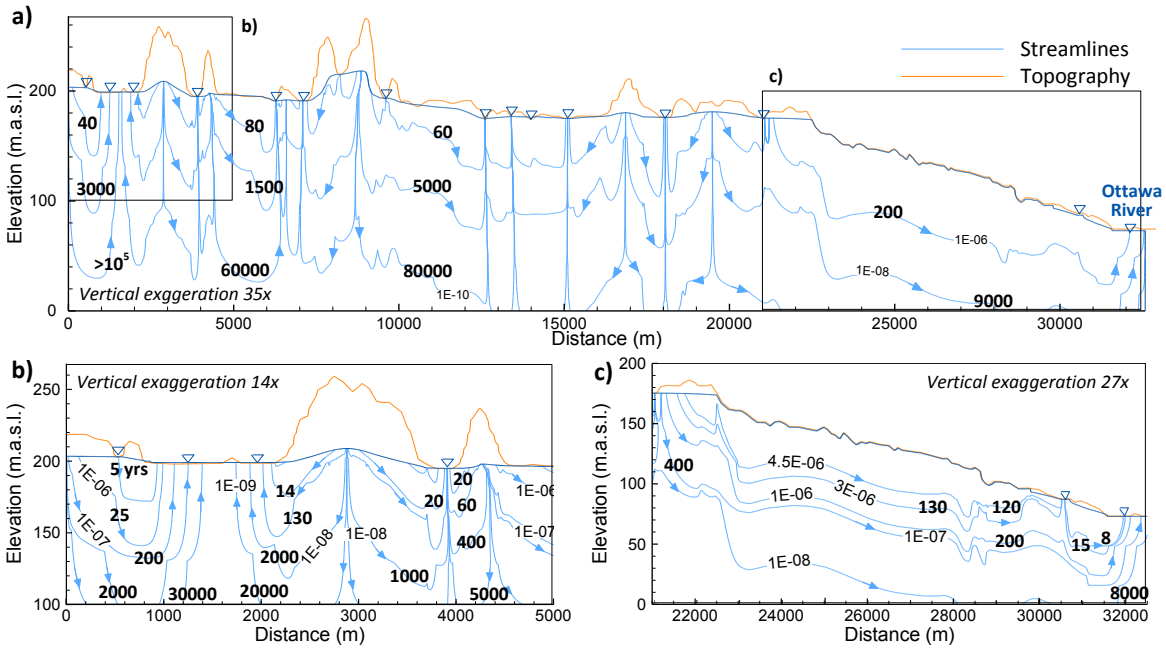

Fig. 32 Simulated flow system showing: a) steady-state flow lines, and detail of flow systems in b) the unconfined aquifer and c) in the confined aquifer below the clay, including total advective age from the recharge to discharge zones shown on corresponding streamlines (streamlines are identified by streamfunction contours in $m^2.s^{-1}$, e.g. 1E-06; ages are shown in years, e.g. 20, 60, 400 yrs in bold)

Analysis of vertical flux variations with depth (not shown) reveals that 99% of the total influx remains within the first 100-200 m of the watertable (depending on the position along the cross-section), which corresponds to the Quaternary deposits and the shallow fractured bedrock ($K=1\times10^{-5}$ m.s^{-1}, Table 10). In recharge areas where hydraulic gradients are high but hydraulic conductivities are low (ex. thin layers of Quaternary deposits or outcropping bedrock), fluxes are also low. Maximum fluxes are found in the fluvio-glacial sediments. Although the depth of the active flow zone is conditioned by the thickness of the most permeable layer of bedrock, these results are in agreement with observations made in similar settings of the Canadian Shield (Farvolden et al. 1988; Gascoyne 2004; Manning & Caine 2007).

Simulated fluxes across fixed-head nodes representing surface water (small streams) were checked against available stream flow data, assuming uniform fluxes in the direction transverse to the 2D section. Although observed gauging data were only available from a small stream well beyond the 2D cross-section, the simulated range in discharge rates (expressed as $m^3.s^{-1}$ per m wide and m long), varying from 2×10^{-9} to 2×10^{-6} $m.s^{-1}$ is consistent with the observed stream data where fluxes were on the order of 4×10^{-5} $m.s^{-1}$ with maximal groundwater contribution of 5% (assuming an average conservative width of 10 m for the stream). Simulated total discharge to the Ottawa River was on the order of 1×10^{-7} $m.s^{-1}$ (assuming equal contributions from both sides), compared to observed river discharges of 4×10^{-5} $m.s^{-1}$ 30 km downstream.

6 Chloride transport model

Simulation of chloride evolution in the 2D section (Fig. 29c) was divided into two sub-steps, accounting for the change of boundary conditions during flooding by saltwater of the Champlain Sea (Step 3a) and then following its retreat (Step 3b). Only the hydraulic conductivity distribution and boundary conditions were changed between sub-steps, while the simulated chloride concentrations from Step 3a were used as the initial condition for Step 3b.

6.1 Two-step modelling strategy

6.1.1 Step 3a: Champlain Sea invasion

Step 3a was simulated to represent the approximately 1200-year period of saltwater invasion from the Champlain Sea. Because accounting for gradual changes in material deposition and boundary conditions over this relatively short period would be difficult (and unnecessary), the clay layer deposited by the Champlain Sea in Step 3a was assumed to have been rapidly deposited. As the initial condition, the clay pore water was also assumed completely saturated with seawater (Desaulniers & Cherry (1989), Fig. 29c). During the Champlain Sea invasion (Step 3a), alluvium from the Ottawa River was not yet present, thus the hydraulic conductivity in this area (which was needed for Step 3b) was assigned the hydraulic conductivity of clay, which is considered

justified as marine clay lenses have been discovered in boreholes drilled along the Ottawa River (MDDEFP 2012). An initial normalized chloride concentration of $C/C_0 = 1$ was imposed as the initial condition in all clay units. The rest of the domain had an initial concentration of 0 (Fig. 29c).

The transport model in this study assumed effects of density-driven flow were negligible. This condition is considered justified since water from the Champlain Sea, being far from the ocean and at this late stage of inundation, was considered to be diluted marine water with a significant proportion of ice-melt water. Analyses of clay pore water by Catto et al. (1981) in the area (Chalk River, about 100 km upstream of Shawville on the Ottawa River) revealed Champlain Sea salinity between 12 and 16 $g.l^{-1}$, similar to the maximum concentration measured by Cloutier et al. (2010) in marine clays from the region of Montreal, about 200 km downstream. Others have found similar salinities, including Desaulniers & Cherry (1989) in marine clays near Montreal, and Quigley et al. (1983) in clays between Ottawa and Montréal. It is likely that the salinity was higher in the deep water-body of the central Champlain Sea but became more diluted during latter stages of the invasion and along its long arms which extended inland (Torrance 1988).

Deep brackish water was also not included in the model. The depth of the interface between fresh water and brackish groundwater in Canadian Shield areas has been observed to vary from 200 m (Frape & Fritz 1987) to 650 m (Frape et al. 1984). Salinity in the Canadian Shield generally does not exceed 1,000 $mg.l^{-1}$ at depths less than 500 m (Farvolden et al. 1988; Gascoyne & Kamineni 1994). Furthermore, at the Chalk River nuclear facility, which is the closest area where extensive investigations have been carried out for sighting nuclear fuel repositories, groundwater TDS content does not exceed 700 $mg.l^{-1}$ at a depth of 400 m. An initial concentration of 0 was therefore assigned throughout the bedrock where the average TDS content would only be about 5% of the Champlain Sea concentration.

The extent of the seawater boundary condition along the top surface of the model during the seawater invasion period was based on Barnett (1988) who found evidence for Champlain Sea elevations of 170 m.a.s.l. in the area of Renfrew, which faces Shawville on the opposite bank of the Ottawa River. This elevation also

corresponds to the maximum elevation of the clay layer on the 2D cross-section, along which a fixed head boundary condition was applied. Along the same boundary surface, a Cauchy transport boundary condition (Molson & Frind 2014) was set with a normalized chloride concentration of $C/C_0 = 1$ (Fig. 29d). In the valleys within the northern (up-gradient) part of the cross-section, some clay deposits were also found, suggesting that the Champlain Sea probably reached even higher elevations. It is likely, however, that the flooding here lasted a shorter time and thus would have had less impact on the hydrochemistry. We also assumed that the transitional period from one hydraulic regime to another was short and the aquifer responded immediately to these changes.

The duration of marine transgression varied within the basin, depending on the distance from the mouth of the St. Lawrence River. Our study area is located in an extreme north-western arm of the Champlain Sea, where the ice cover lasted longer, and where seawater invasion occurred relatively later (Catto et al. 1981). According to Catto et al. (1981), two events of marine transgression occurred in the nearby region of Renfrew. The first event lasted less than 200 years, between 12,150 and 12,000 years BP after which the Champlain Sea retreated in step with a new advance of the ice sheet for about 1,000 years. The second phase of the Champlain Sea lasted about 1,200 years, from the ice retreat 11,400 years BP to the withdrawal of the sea at about 10,200 years BP due to isostatic rebound. For modelling purposes, the first phase is considered negligible and only the second phase is simulated, representing 1,200 years of seawater intrusion (Fig. 29d).

6.1.2 Step 3b: Champlain Sea retreat

Similar to the assumption of rapid marine transgression, seawater retreat and aquifer response is also assumed to be rapid. After the retreat of the Champlain Sea about 10,200 years ago (Catto et al. 1982), the flow systems (including boundary conditions) were assumed to be similar to those of today, even though the Ottawa River valley has had its current shape for only about the last 8,000 years (Catto et al. 1982; Teller 1990). Isostatic rebound is not taken into account by the model although groundwater systems are dynamic and are still evolving as a result of the Laurentide Ice Sheet melting (Lemieux et al. 2008; Sykes et al. 2009).

In Step 3b, a Cauchy (type 3) condition is applied at the top boundary with a chloride concentration set to 0 representing low chloride content in rainwater. The initial condition in the domain corresponds to the final chloride distribution from the previous (Step 3a) model. The Step 3b chloride transport model is run for 10,200 years (Fig. 29d).

6.2 Simulated chloride distribution

The simulated chloride distribution at the end of the Champlain Sea invasion 10,200 years ago (end of Step 3a) as well as its current expected distribution (end of Step 3b), is shown in Fig. 33a and Fig. 33b, respectively. Due to the applied flow boundary conditions in Step 3a representing a constant sea level up to 170 m elevation, velocities in the upper fractured part of the bedrock are 100 times less than under the current conditions (Section 5.4). As a consequence, mean residence times are longer. The flow patterns are also different from the current flow situation. Most water which has infiltrated up-gradient of the clay layer discharges just before the aquifer becomes confined. Groundwater flowing within the confined fractured bedrock aquifer recharges from deeper and further up-gradient. Two distinctive discharge areas can be identified: one where the till currently outcrops (ca. km 30) and one at the far down-gradient end of the 2D cross-section. At the end of the Champlain Sea invasion (Fig. 33a), chloride from the marine clay begins diffusing downwards into the shallow fractured bedrock zone due to strong vertical concentration gradients from the clay into the aquifer which is recharged by chloride-free rainwater. Once in the bedrock, chloride is transported rapidly down-gradient by advection and dispersion. A gap in the simulated chloride plume is seen at km 30, where a preferential discharge zone has formed due to more conductive overburden.

The chloride distribution 10,200 years following seawater retreat (Fig. 33b) shows that most of the initial chloride in the bedrock aquifer has been flushed away (where concentrations are less than 1000 $mg.l^{-1}$), with most of the residual chloride found in the marine clay layer. In some parts of the clay layer, maximum chloride concentrations remain about 15,000 $mg.l^{-1}$, similar to the original assumed seawater concentrations. This behaviour corresponds to the theoretical case described by Atteia et al. (2005) and characterised areas with

very small concentration gradients. The results are generally consistent with the observed chloride concentrations in most of the sampled wells and with investigations in similar marine clays presented, for example, by Cloutier et al. (2010) and Desaulniers & Cherry (1989). Some differences were observed, however, in concentrations below 1 $g.l^{-1}$ (Table 12). Sample OUT036356 in the confined aquifer, for example, had a Na-Cl water type (Fig. 27) and the highest chloride concentration (around 350 $mg.l^{-1}$), whereas the corresponding simulated concentration was lower (150 $mg.l^{-1}$). Conversely, the simulated concentrations at the remaining sample locations (which varied from 69 to 210 $mg.l^{-1}$) were somewhat higher than the observed values (which were all less than 45 $mg.l^{-1}$). For most wells, the differences could be attributed to assuming a too saline Champlain Sea, where the true seawater Cl concentration would have been less than the assumed value of 15,000 $mg.l^{-1}$. Differences could also be simply due to heterogeneities in the fractured bedrock, which would also explain why the observed concentration in sample OUT036356 was higher compared to the others, if this sample was located in a less conductive zone.

Table 12 Comparison between calculated and measured chloride concentrations in the confined aquifer

Sample ID	Measured chloride concentration ($mg.l^{-1}$)	Calculated chloride concentration ($mg.l^{-1}$)
OUT026130	1.1	9.9
OUT036356	350	150
OUT026131	39	69
OUT022292	45	140
SANDBAY	15	210

Simulated chloride concentrations over time are shown in Fig. 33c and Fig. 33d at three different sites in the overburden (points 1 and 3 in the clay and 5 in the alluvium) and three in the confined fractured bedrock aquifer (points 2, 4 and 6). Within the clay, the breakthrough curve at point 1 shows a quasi-stagnant concentration over 10,200 years following seawater retreat, whereas at point 3, the simulated chloride concentrations follow a steady but slow diffusion-controlled decline. Additional simulations (not shown) suggested it would take over 50,000 years to reduce chloride concentrations in the clay to about 100 $mg.l^{-1}$.

In the bedrock aquifer at point 2, concentrations rise progressively during the Champlain Sea invasion while at point 4 further down-gradient, the increase is later and much faster. At both locations in the bedrock, concentrations decrease rapidly after retreat due to flushing of chloride-free water from up-gradient. Below the Ottawa River, the initial chloride in the alluvium is also quickly removed (Fig. 33e, point 5). However, after the Champlain Sea retreat, the simulation shows that the chloride plume migrating through the upper fractured bedrock (now under a new hydraulic regime with higher flow gradients) had also penetrated into the deeper unfractured bedrock, reaching a depth of 100 m at km 31, about 700 years after the Champlain Sea retreat. Thus, a low concentration chloride signal is seen at the base of the bedrock aquifer at point 6 (Fig. 33e), taking about 3000 years to be completely flushed in part because of low velocities below the Ottawa River bed).

Over the 10,200 year simulation time after seawater retreat, chloride has also diffused upwards at the surface of the clay over a thickness of about 10 m (Fig. 33f), due to high concentration gradients, resulting in similar profiles to those described by O'Shaughnessy & Garga (1994). Diffusion towards the bottom of the clay layer is also observed (Fig. 33f), similar to observations by Torrance (1979) for other sites in the Ottawa region. Diffusion is not the only process that can explain these profiles. Artesian conditions can also play a role in the leaching of marine clays (Rankka et al. 2004; Torrance 1979).

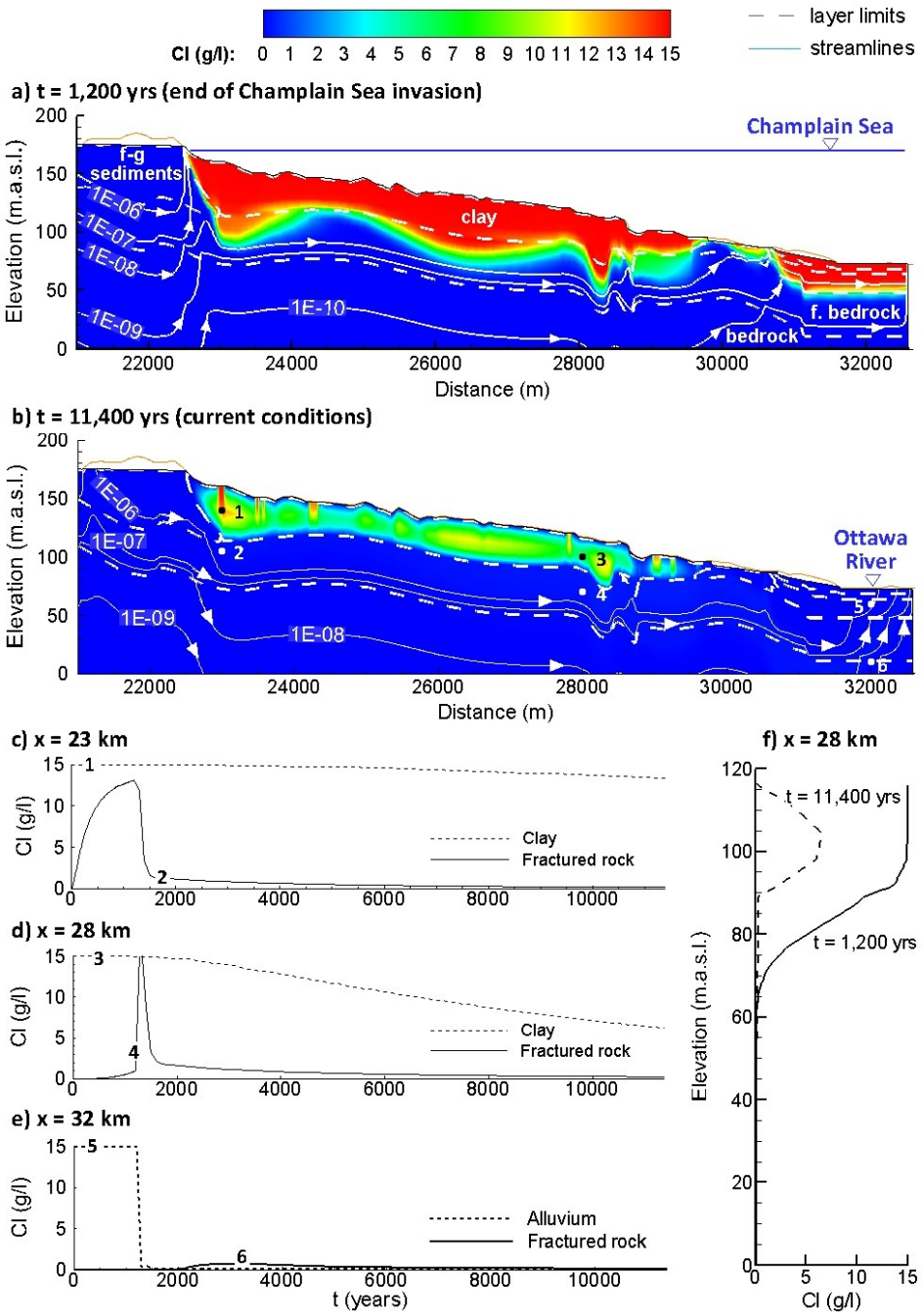

Fig. 33 Simulated chloride distribution from t=0 which represents the start of the Champlain Sea invasion, showing: a) step 3a: simulated Cl after 1,200 years of seawater invasion (about 10,200 years ago) and b) step 3b: current conditions 11,400 years after the start of sea invasion (10,200 years since seawater retreat). Selected streamlines are also shown in units of $m^2.s^{-1}$ (note exponential decrease with depth). c) d) and e) Chloride breakthrough curves at selected points shown as black dots in the clay layer and in the shallow bedrock and f) chloride profiles in the confined aquifer at the end of the invasion (1,200 yrs) and today (11,400 yrs). Concentrations are based on a maximum seawater concentration of 15 $g.l^{-1}$ (Catto et al. 1981).

7 Groundwater age simulation

7.1 Initial and boundary conditions

The TR2 module was subsequently applied to simulate mean steady-state groundwater residence times (advective-dispersive ages), according to Eq. 11. In the age simulation, all nodes corresponding to recharge at the top surface are assigned as type 1 fixed age boundaries (A=0) while all other boundaries are assigned zero age-gradient conditions with the initial age set at 0 throughout the domain (Fig. 29d). All other parameters (dispersivities, diffusion coefficient, retardation factor and radioactive decay constant) remain the same as for the transport of chloride.

7.2 Age distribution

The age model was run for 100,000 years which was sufficient to reach steady state (Fig. 34a). Mean residence times in the Quaternary deposits were less than 100 years with very short residence times in the alluvium of the Ottawa River (less than 10 years). The age contours are controlled by the flow system and by dispersion, with generally increasing ages with depth (except in the confined aquifer where mixing occurs between younger fresh groundwater and older pore clay marine water). At depths greater than about 150 m, groundwater is more than 50,000 years old due to very low flow conditions and limited mixing. Typical age profiles at different locations in the aquifer can be found in Annexe 5 (Fig. A9). Under large surface water bodies such as lakes (e.g. under Lake Johnson, at km 2, Fig. A9a and Fig. 34b) or the Ottawa River (Fig. A9d and Fig. 34c), ages rapidly increase with depth due to the low hydraulic gradient and the slow motion of groundwater. Residence times greater than 1,000 years are evident in the unfractured bedrock with low hydraulic conductivities (equal to or less than 1×10^{-7} m.s^{-1}). Marine clays are characterised by ages greater than 20,000 years whereas groundwater in the fractured bedrock layer is younger (Fig. A9c and Fig. 34c), due to the elevated hydraulic conductivity of the fractured bedrock layers which allows a rapid displacement of groundwater from the nearest recharge zone. In the unconfined part of the aquifer, the advective-dispersive

ages are similar to the advective ages obtained from the flow system alone (Fig. 32) whereas in the confined aquifer, mixing occurs between younger and older waters, resulting in much higher advective-dispersive ages.

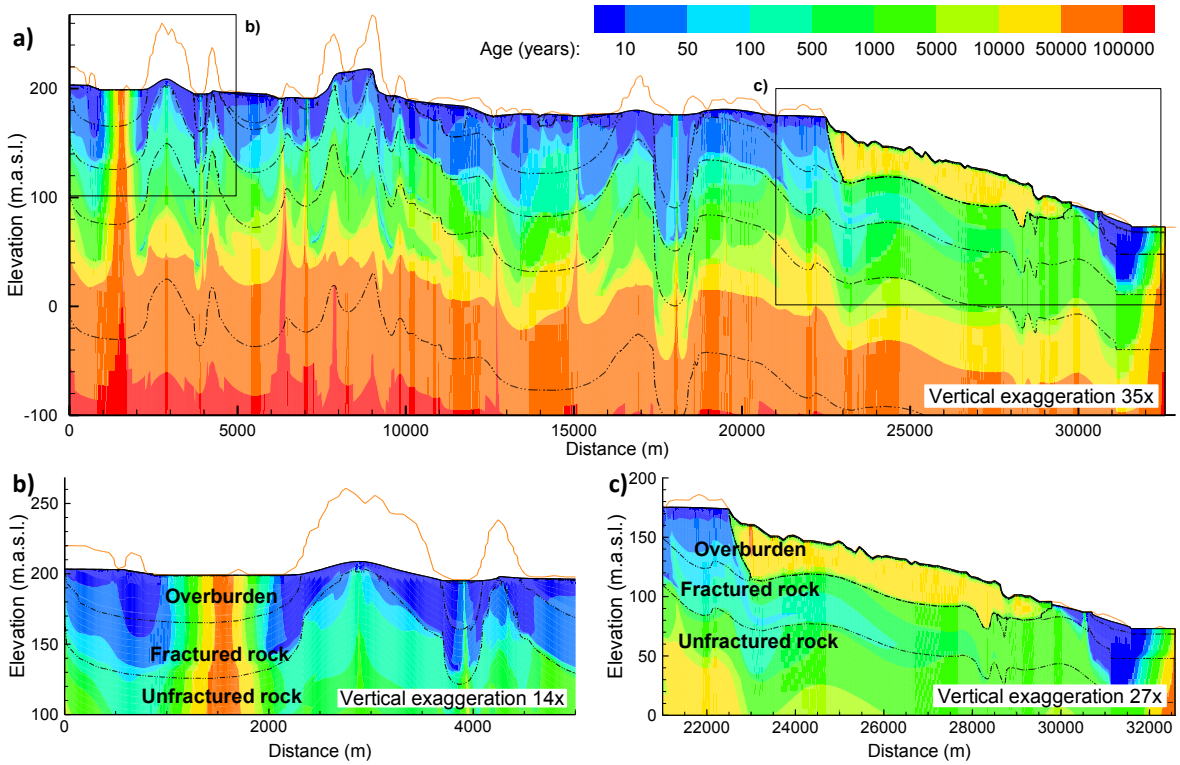

Fig. 34 Simulated steady-state mean groundwater ages, showing a) the full 2D cross-section to a depth of -100 m.a.s.l., b) age detail in the unconfined aquifer, and c) age detail in the confined aquifer with overburden and rock interfaces shown for reference (dashed lines).

8 Discussion and validation of the conceptual model

8.1 Model Sensitivity

8.1.1 Hydraulic and transport properties

As discussed in Section 5.3 (Chapitre 3), a unique flow model calibration was difficult to obtain due to a lack of data in critical topographically high elevations. To further support validation of the Outaouais Region model, the simulated maximum depth to the water table (60 m) was compared to water table depths measured over

the entire Outaouais Region, which were on average, about 30 m. The depth to water table calculated by our model appears reasonable regarding measured depths to water table at the regional scale.

The simulated tritium distribution was much more sensitive to the hydraulic conductivity of the bedrock than to the Quaternary deposits. The Quaternary deposits are on average only about 20 m thick with relatively high hydraulic conductivities, allowing rapid migration of tritium toward the bottom of these layers. Transport through the fractured bedrock controlled tritium behaviour, both because of its relatively lower K, and because of the much greater horizontal scales for the local flow systems which were on the order of 1 to 10 km. This behaviour also reflects the hydraulic link between the Quaternary sediments and the fractured bedrock.

Sensitivity of tritium transport to changes in recharge rates was assessed by testing different values (10, 20 and 35% of total precipitation, compared to 30% in the calibrated model). Simulated tritium concentrations showed only minor changes within the range of uncertainty in recharge compared to changes in the bedrock hydraulic conductivities. The model was also tested assuming a lower longitudinal dispersivity of α_{LH} = 10 m. Comparison with the base case (α_{LH} = 20 m) showed a slightly less extended but more concentrated tritium plume with the lower dispersivity (especially in zones of high velocities). The goodness of fit between observed and measured tritium concentrations was also less. Excessively high dispersivities will tend to homogenise the tritium concentrations, resulting in low simulated tritium concentrations, which do not reflect the observations.

8.1.2 Chloride transport scenarios

The chloride transport simulation assumed a 1,200-year fixed duration of the Champlain Sea invasion, and neglected an inferred initial 200-year invasion. Within a reasonable uncertainty of +/- 200 years, errors in assuming a shorter 1,200-year duration would appear to have a limited effect on the final results since the simulated chloride plume had almost reached steady state within 1,200 years following seawater invasion while most chloride had been flushed away within 2,600 years after its retreat. Thus, a possible 200-year invasion episode followed by 1,000 years of ice advance before the major invasion of 1,200 years most likely would not have changed the final result.

The impact of the assumed maximum elevation reached by the Champlain Sea (170 m.a.s.l.), which corresponded to the maximum elevation of the clay layer, was also of interest. The 170 m elevation was only an estimate, as within the 2D cross-section (Fig. 27), some marine clay had indeed been found at higher elevations of around 180 m.a.s.l., particularly in the unconfined part of the aquifer (at km 14-15). In a subsequent simulation (not shown), a higher fixed head of 180 m was applied in all areas less than 180 m in elevation, again with a fixed concentration of $C/C_0 = 1$ allowing intrusion of salt water. However, assuming the same invasion duration of 1200 years, chloride was again rapidly flushed away after the Champlain Sea retreat. These conclusions on sensitivity are further justified since we assume the same duration of seawater invasion in this 2D section as in the Ottawa River valley, even if it is likely to have been less.

The progressive sedimentation of marine clays and rise of the seawater level have not been tested in this study but they would have an impact on the flow patterns and on the chloride plume development. It would be of interest to model more realistic scenarios to justify the simplifications and compare simulated current chloride plumes.

8.2 Modelling approach and heterogeneities

The models developed here are relatively simple with respect to the complexity of the real system and the chronology of past events. For example, groundwater ages were simulated over a 100,000 year period assuming no changes in flow conditions. Model sensitivity tests showed that the simplifications applied to represent the Champlain Sea invasion (exact seawater levels) did not have a significant impact on the final results representing current conditions. The system response time to these major system changes (sea level rise, rate of clay sedimentation and uplift) was not tested. However, regarding groundwater ages in the system, especially in the Quaternary sediements where residence times are short, it is likely that uplift, which is a slow process occurring over 10,000 years, has a limited impact on transport in the Quaternary sediments as well as in the fractured bedrock. It is likely that the rate of clay sedimentation and the sea level rise have some impact on the chloride and age distribution when it occurred some 10,000 years ago since the magnitude of the

velocities is important between these two extreme situations. But the speed at which the confined aquifer recovered from the retreat of the Champlain Sea, going from one extreme to another one, is probably the main factor controlling the current chloride plume extension.

As expected, the distribution of the hydraulic conductivities at depth exerts an important control on the flow systems, affecting both the extent and depth of the tritium and chloride plumes as well as on the age distribution. Transport modelling thus appears to be a good means to improve the model calibration. The results of the tritium transport simulation showed that the hydraulic conductivities had to be high in the upper part of the bedrock to allow sufficient penetration of the tritium and to explain the occurrence of tritium concentrations well-above the detection limits in the unconfined bedrock wells. The estimated horizontal hydraulic conductivity in the fractured bedrock is only a bulk value as flow would be faster in fractures while negligible in the matrix. Also, the simplified modelling approach could explain why calculated tritium concentrations were generally less than measured in the field. Evidence of such highly-conductive zones were demonstrated by Sterckx (2013) in his analysis of aquifer transmissivities calculated from hydraulic tests as a function of well depth. The calibrated hydraulic conductivities in the current study are consistent with those determined by Sterckx (2013). Furthermore, hydraulic packer tests carried out in two wells along the cross-section (wells CONV-PON and SANDBAY) responded completely differently, with the SANDBAY well being tight all along the open borehole whereas well CONV-PON was characterised by a highly-conductive zone at depths between 20 and 25 m. A hydraulic conductivity on the order of 10^{-5} $m.s^{-1}$ was calculated at this location which was similar to the model-calibrated value.

Most of the wells are located in areas where the flow is sub-horizontal and mixing occurs as a result of sampling in open boreholes. Areas of natural flow mixing also occur near the discharge zones, as in bedrock well OUT021341 close to the Ottawa River. Generally, vertical profiles show from ground surface to the bottom of the wells, first a tritium concentration close to present atmospheric levels near the surface. Since atmospheric tritium has been almost constant over the last 10 years or so, tritium which has infiltrated into the first few metres during this period has already been partly degraded and concentrations are less than the

current atmospheric tritium levels. Concentrations then increase with depth, corresponding to what is left of the historic tritium peak, and are still higher than the current levels. At deeper depths, tritium is absent and is representative of levels which had recharged before the bomb testing peak and which have been decaying for several decades.

8.3 Comparison of ages obtained by different techniques

Most of the boreholes located in the bedrock pass through different groundwater age layers (Fig. 35). As mentioned in Chapitre 2, the groundwater samples show evidence of both low mean residence times (where tritium was detected) and higher mean residence times (accumulation of ^{4}He). For the four boreholes sampled for noble gases, it appears that the average (relatively young) age is not consistent with the high concentrations in helium 4 but rather reflects the maximum age of the groundwater component flowing through the open borehole, which seems to be a better indicator. For example, CONV-PON has the lowest concentration in helium 4 and has the smallest simulated age range (from 11 to 23 years along the open borehole, Fig. 35c). On the other hand, OUT036356 does not show evidence of tritium and has simulated ages varying from 580 to 900 years (Fig. 35f). Finally, wells OUT036357 and OUT021341 present the highest ^{4}He concentrations as well as the largest simulated age range, from 6 to 1,430 and from 1 to 1,530 years, respectively (Fig. 35b and Fig. 35i), with detected concentrations in tritium.

In the unconfined aquifer (bedrock and Quaternary sediments), simulated tritium concentrations display from surface to bottom of wells first a decrease in tritium concentrations then an increase followed by another decrease (Fig. 35. At the surface, tritium concentrations are similar to atmospheric levels and show traces of decay with depth (first decrease) since the tritium levels have been constant or almost constant since 1992 (<30 TU for a period of almost two half-lives, meaning initial tritium concentrations were divided by up to 4, which is consistent with minimal simulated tritium concentrations in most unconfined wells around 8 TU). The increase corresponds to the tritium peak in the 60's during which the atmospheric tritium contents were very high, up to 5817 TU in June 1963. Even with radioactive decay and mixing due to advection-dispersion, tritium

concentrations are still higher to the current atmospheric levels. Tritium concentrations progressively decrease again with depth and are representative of levels before the bomb testing peak undergoing decay for a long period a time.

^{14}C measurements for each well are also given in Fig. 35. In the light of the modelling results, the ^{14}C concentrations cannot be used for assessing groundwater mean residence times but rather reflect processes occurring in the unsaturated and saturated zones. Only the ^{14}C age calculated for sample OUT036356 (the only sample to have undergone some decay, see Chapitre 2) can be compared with modelling results. Simulated ages are lower than estimated ^{14}C ages and lower than ages suggested by chemical data. As mentioned before, chloride simulations suggested that sample OUT036356 comes from a well which is probably located within a less conductive zone where ages are higher than those calculated by the model.

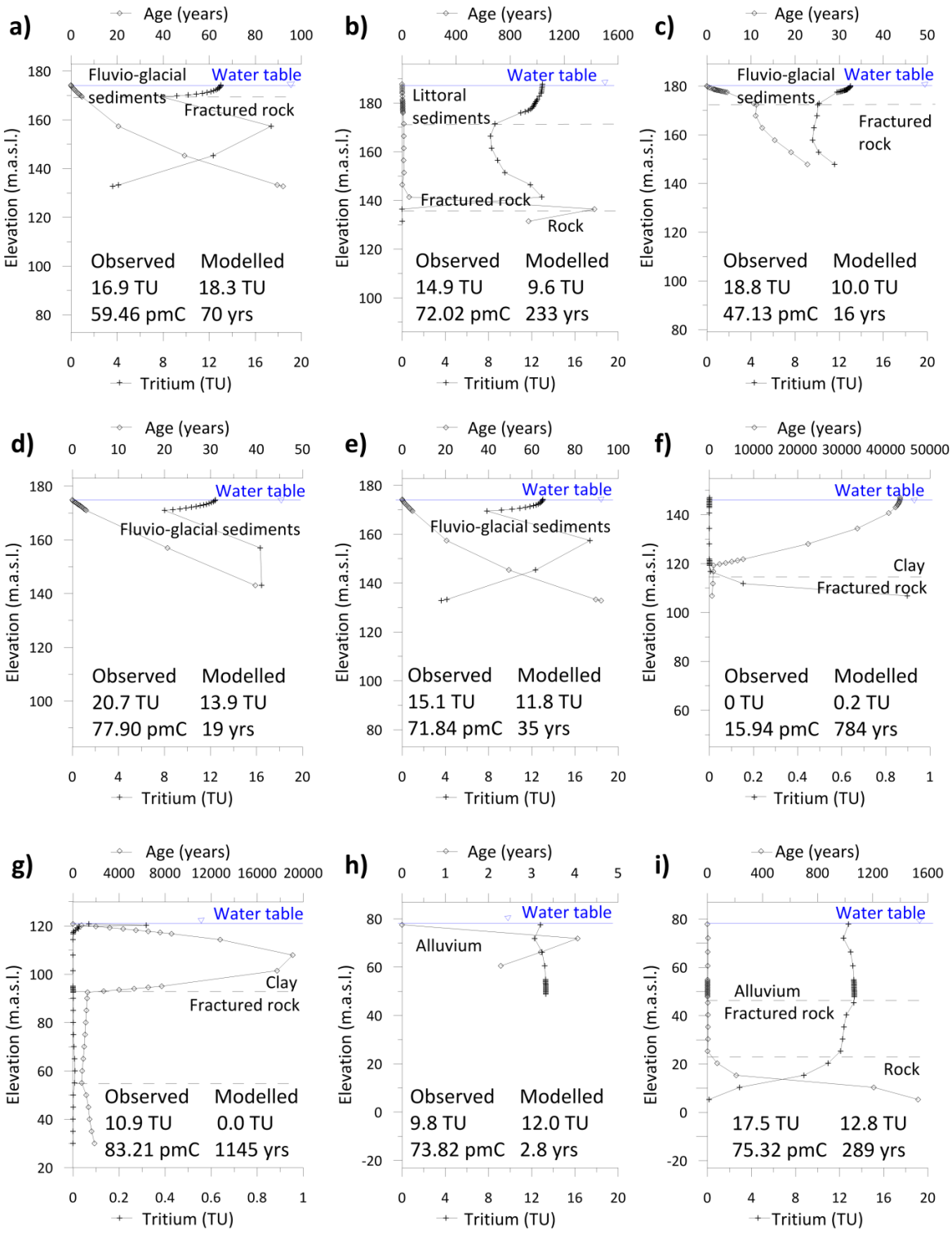

Fig. 35 Simulated advective-dispersive age and simulated tritium profiles for selected wells: a) OUT036352, b) OUT036357, c) CONV-PON, d) OUT036358, e) OUT036353, f) OUT036356, g) SANDBAY, h) OUT036351 and i) OUT021341. The modelled values for age and tritium are an averaged value considering the open borehole for wells in the bedrock and the whole well length for wells in Quaternary sediments for which the location of the screen is unknown.

8.4 Validation of the conceptual model

The updated conceptual model with the interpreted flow systems and groundwater ages is shown in Fig. 36. A major change to the original conceptual model was the elimination of a regional flow component. In general, local flow systems had already been well identified, but intermediate flow systems are now thought to be less extensive and shallower. Topography and surface water bodies also exercise a more important control than initially thought. Vertical flow gradients in the confined aquifer have now been clarified. The confined aquifer is now divided into two parts, with the up-gradient area characterized by upward vertical flow gradients (referred to previously as flowing artesian) whereas the down-gradient part has downward vertical flow gradients. These findings need to be verified against more detailed and reliable data. However, groundwater flow is very slow in the clay where chloride transport is dominated by downward diffusion into the fractured bedrock, where it becomes diluted due to rapidly flowing freshwater. Some diffusion towards surface fresh water occurs as well.

The reduced extent of intermediate flow systems has an impact on how the chemistry data should be interpreted. All samples were originally believed to have been taken along a flow line from an intermediate flow system extending along most of the 2D cross-section and were assumed to represent the geochemical evolution of groundwater. Although this is true in the confined part, all samples taken in the up-gradient unconfined bedrock are now presumed to belong to different flow systems, reflecting their own geochemical evolution depending on their mean residence times. Samples OUT036358 and OUT036353, taken in highly conductive fluvio-glacial sediments, show significant rock-water interactions compared to samples from the unconfined bedrock. While these sediments result from glacial erosion and have similar mineral chemistry to the bedrock, the higher mineralization of the samples could be explained by their proximity to the underlying marble bedrock. Local flow systems are characterized by very short residence times of less than 50 years, which explains the occurrence of tritium in most samples from the unconfined aquifer (except sample SANDBAY). Fast simulated flow conditions in the unconfined bedrock aquifer are consistent with the observed chemical composition of groundwater, which shows limited interaction between groundwater and rock. For sample SANDBAY, the presence of tritium is still not understood (possibly representing a preferential flow path

from the nearest recharge area, a leaky casing, or a hydraulic window in the clay which was missed in the field data) whereas the absence of tritium in sample OUT036356 can be explained. The high concentration in chloride in sample OUT036356 cannot be accurately simulated and likely reflects unresolved heterogeneities and less conductive zones, also suggested by the low ^{14}C activity. Except for this sample, ^{14}C contents cannot be interpreted because they largely result from mixing processes occurring in the unsaturated and saturated zones which are not taken into account in the model. Finally, old groundwater is found at intermediate depths (about 200 m) from which diffusion of ^{4}He could explain the high concentrations measured in some samples (Andrews 1987).

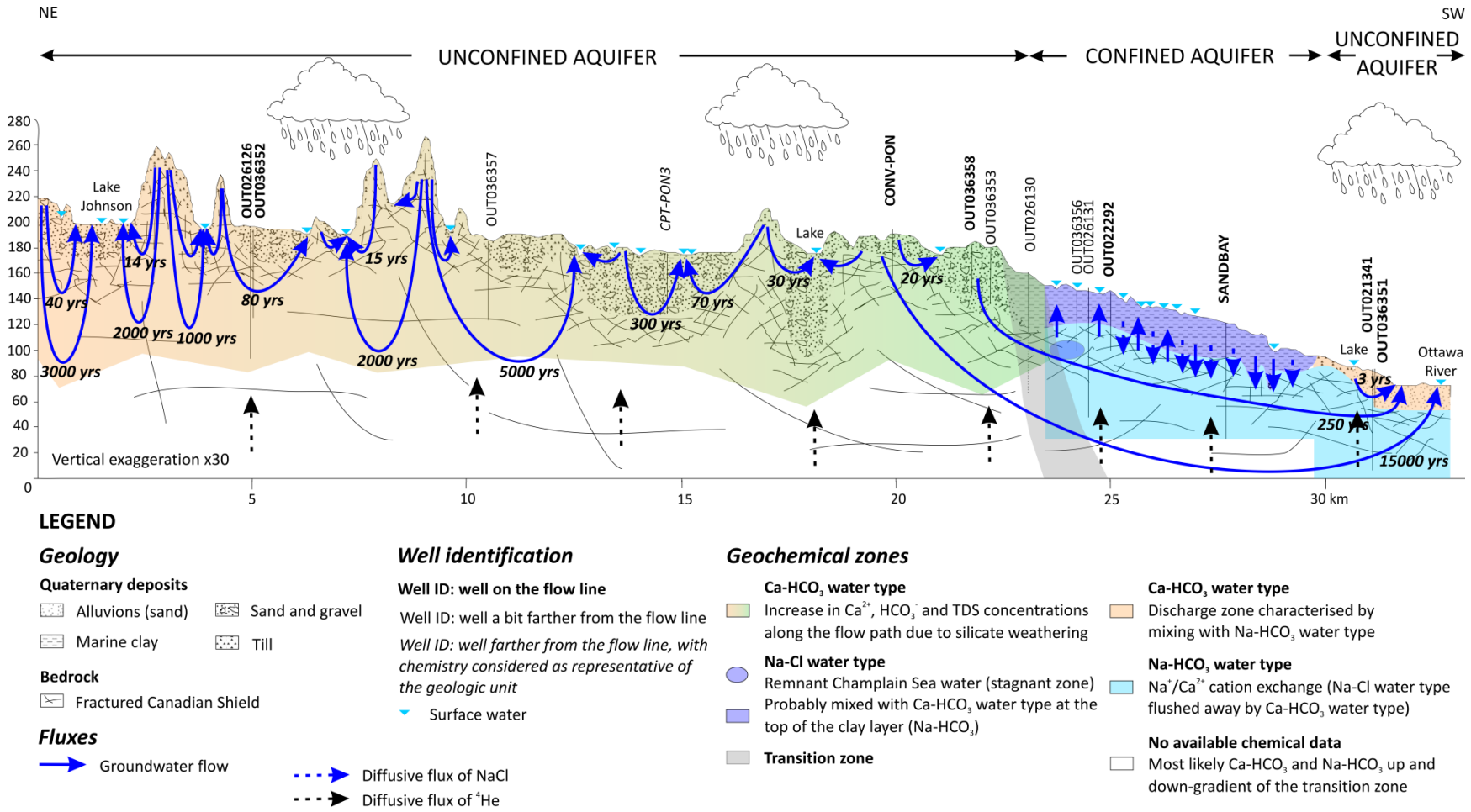

Fig. 36 Final revised conceptual model, showing flow directions and total travel times from recharge to discharge zones along selected conceptual flow lines

9 Conclusions and perspectives

Different numerical modelling approaches were successfully developed to support a 2D vertical plane conceptual hydrogeochemical model along a flow path representative of the western Outaouais area. Due to a lack of hydraulic head measurements along the 2D cross-section, especially at higher elevations, calibration was augmented using tritium transport modelling. Through this fitting procedure, tritium distribution appeared to be most sensitive to the hydraulic conductivities of the upper fractured bedrock compared to other parameters in the model. Although the simulated tritium concentrations were generally below those observed, the model seems to be well calibrated using the equilibrium porous media approach at this scale. The tritium concentration could not be well reproduced in one sample of the confined aquifer. Hydraulic testing in this well showed that it is relatively tight but all three samples taken in this well contain tritium, essentially ruling out sampling errors. Differences might be explained by nearby fractures which are possibly connected to recharge zones, by poorly sealed casings with preferential flow paths or by hydraulic windows in the clay layer, although these have not been documented in the field work. These hypotheses need to be independently tested. The final calibrated value of hydraulic conductivity in the upper bedrock is 1×10^{-5} m.s^{-1}, which is quite high but consistent with discrete hydraulic conductivities measured using packer tests and specific capacity tests in other regional wells. This average value would suggest that the upper part of the bedrock is densely fractured.

The results show no evidence of substantial regional flow (at scales > 20-30 km).The resulting flow systems are controlled by the topography and the presence of surface water bodies which define the horizontal extent of the intermediate systems which are likely less extensive than proposed in the original conceptual model. Therefore, only those water samples taken just up-gradient of the confined aquifer and those from the confined aquifer likely lie along the same flow path. Samples from the unconfined bedrock aquifer likely belong to different intermediate flow systems. Their relatively similar chemistry is the result of similar mean residence times within the different intermediate flow systems. Local flow system depths are limited to the first 40 meters, which mainly lie within the Quaternary sediment layers and the first tens of meters of bedrock in outcropping areas. These local flow systems are characterised by short residence times (a few tens of years), explaining

the occurrence of tritium. The active flow zone extends only into the first 100-150 m with low-flow or no-flow conditions below this depth. Old groundwater is also found at relatively shallow depths from which diffusion of ^{4}He can explain the high concentrations found in the samples.

The simulations support the conceptual model that the Champlain Sea invasion caused diluted seawater to reach the upper bedrock, but due to short mean residence times of less than 1,000 years, all chloride has since been flushed from the active flow system. Current residual chloride concentrations result from diffusion out of the clay layer and mixing with up-gradient groundwater. High chloride concentrations in sample OUT036356 are likely indicative of heterogeneities and less conductive areas as commonly found in fractured bedrock but which are not resolved in the current model. In terms of groundwater management, the groundwater is vulnerable to contamination due to rapid transit times but can be considered as a sustainable resource for drinking water purposes, especially for wells drilled in fractured areas.

The model was able to reproduce the general behaviour of the flow system, although some improvements could be made through the collection of additional data in the clays or within the fractured bedrock. A more complete validation of the model would require geochemical modelling which at this scale would need additional simplifications. For example, one approach could focus on silicate weathering along a flow line or on cation exchange in the confined aquifer. Changing the modelling approach by adding discrete fractures to assess their impact on the organization of the flow systems and the age distribution would also be of great interest in this type of geological setting. These approaches will be considered in future work.

Conclusion

1 Conclusion générale

Ce doctorat s'inscrit dans le contexte des projets PACES du Ministère du Développement Durable, de l'Environnement et de la Lutte contre les Changements Climatiques, dont l'objectif est de caractériser les aquifères du sud du Québec, où se situe la majorité de la population. Parmi les nombreux volets de ces projets, ce doctorat porte uniquement sur la caractérisation géochimique des eaux souterraines de la région de l'Outaouais (partie municipalisée seulement).

Les principaux objectifs de ce doctorat étaient d'évaluer la qualité des eaux souterraines et vérifier l'impact de l'épisode de la Mer de Champlain, de proposer un modèle conceptuel d'évolution géochimique des eaux souterraines basé sur l'identification des principaux processus géochimiques grâce à la classification des échantillons en groupes d'eaux et l'interprétation de données isotopiques et de valider ce modèle conceptuel par modélisation des écoulements, du transport du tritium et des chlorures et de l'âge de l'eau. Ces résultats permettent de préciser quelle est la durabilité des ressources en eaux souterraines grâce à une estimation de la vulnérabilité, dans le but de présenter des recommandations pour la gestion durable de la ressource.

1.1 Classification des eaux souterraines

La classification des eaux souterraines repose sur les résultats d'analyses de 139 échantillons prélevés dans les différents contextes hydrogéologiques rencontrés dans la région, c'est-à-dire aquifères libres ou confinés par les argiles de la Mer de Champlain, soit dans le roc (Bouclier Canadien ou roches sédimentaires des Basses Terres du St Laurent) ou dans les dépôts du Quaternaire (sédiments fluvio-glaciaires, sédiments deltaïques ou alluvions). Parmi ces 139 échantillons, 127 échantillons ont été retenus, les 12 rejetés ne remplissant pas les exigences d'électro-neutralité (balance supérieure à 10%). Plusieurs méthodes de classification ont été utilisées.

La première méthode a consisté à séparer les échantillons en groupes d'eau (faciès) selon le cation et l'anion dominant. Au total, 10 groupes d'eau ont été identifiés. La majorité des échantillons (65%) appartient au faciès Ca-HCO_3 (calco-bicarbonate) que l'on retrouve dans les différents contextes hydrogéologiques sur l'ensemble du territoire à l'étude. A noter que 76% des échantillons prélevés dans les dépôts du Quaternaire sont caractérisés par ce faciès, synonyme d'eau récemment infiltrée avec des temps de résidence assez courts, de l'ordre de quelques dizaines d'années. Les eaux de types Na-dominant (Na-HCO_3, Na-Cl et Na-SO_4) concernent 26% des échantillons et leur répartition est plus restreinte. Ils se concentrent principalement le long de la rivière des Outaouais et de ses principaux affluents, dans les zones envahies par l'ancienne Mer de Champlain. Les autres échantillons (9%) présentent des faciès intermédiaires d'évolution géochimique ou sont représentatifs de conditions locales. Cette méthode ne prend en compte que l'abondance relative des ions majeurs les uns par rapport aux autres mais ne permet pas de différencier les échantillons selon les valeurs absolues en concentrations, qui peuvent avoir des ordres de magnitude différents au sein d'un même faciès. C'est pourquoi une analyse factorielle couplée à une analyse de regroupement hiérarchique a été effectuée.

L'analyse factorielle a permis d'identifier les paramètres responsables de la variabilité de la chimie des échantillons. Ainsi, il a été montré que l'invasion de la région par la Mer de Champlain il y a environ 10 000 ans a encore un impact sur la géochimie de l'eau de la région (premier facteur lié aux paramètres de salinité SO_4^{2-}, Cl^-, Na^+ et Sr^{2+}). L'altération des silicates est aussi un processus géochimique important pour expliquer les variations de chimie des échantillons (deuxième facteur associé à la silice) puisque 79 échantillons (62%) proviennent de puits forés dans le Bouclier Canadien. Cette analyse factorielle a permis d'identifier un troisième processus lié à l'altération de minéraux riches en fluor en conditions de pH basiques.

L'analyse de regroupement hiérarchique a permis de classer les échantillons en 7 groupes. Les 4 premiers groupes incluent la majorité des échantillons de type Ca-HCO_3 et résultent de la dissolution des silicates, avec une augmentation des concentrations en ions majeurs, et tout particulièrement celles du calcium et du magnésium. La majorité des échantillons prélevés dans les dépôts du Quaternaire se trouvent dans ces groupes. Les échantillons avec les concentrations les plus faibles sont localisés dans les zones de recharge et

ceux avec les concentrations les plus élevées dans les zones exutoires intermédiaires (les principales rivières de direction nord-sud). Les échantillons des groupes 6 et 7 sont de faciès Na-dominant et proviennent essentiellement d'aquifères confinés localisés principalement le long de la rivière des Outaouais. Le groupe 6, majoritairement Na-HCO_3, est représentatif de l'échange cationique entre Na et Ca tandis que le groupe 7, à dominance Na-Cl, regroupe les échantillons reliques de l'ancienne Mer de Champlain. Le groupe 7 présente les teneurs les plus élevées en matières dissoutes totales : c'est pourquoi il comprend aussi les échantillons prélevés dans les Basses Terres du St Laurent, qui en aquifères non-confinés, sont de type Ca-HCO_3 (dissolution de roches carbonatées).

L'interprétation de ces résultats démontre l'importance des conditions passées sur la géochimie actuelle des eaux souterraines de l'Outaouais puisqu'on retrouve la signature marine sous forme diluée de la Mer de Champlain. Contrairement à d'autres régions en aval le long du fleuve St Laurent (Blanchette et al. 2010b; Cloutier et al. 2010), l'invasion par la Mer de Champlain a été beaucoup plus courte dans la région d'étude, du fait de l'éloignement à l'océan et des phases d'avancée et de recul du glacier. L'échantillon analysé le plus salin a des concentrations proches de celles de Blanchette et al. (2010b) mais beaucoup plus faibles que celles de Cloutier et al. (2010). Bien que la région ait été envahie plus tardivement, la signature marine est encore présente sous forme un peu plus diluée. Ceci peut être dû soit à des conditions locales (mélange avec de l'eau douce) ou soit à une salinité plus faible de la Mer de Champlain à cette localisation et à ce stade-ci de l'inondation (pourcentage d'eau de fonte des glaciers plus importante vers la fin de la période de déglaciation).

1.2 Qualité de l'eau souterraine

En plus de l'identification des processus responsables de l'évolution géochimique de l'eau, les échantillons ont permis de dresser un portrait de la qualité des eaux souterraines de l'Outaouais. Du point de vue de la santé, les principaux dépassements des normes d'eau potable du Québec concernent les fluorures et l'uranium (8 et 7 dépassements respectivement). Bore, nitrates + nitrites et molybdène présentent chacun un dépassement. Les fluorures avaient été identifiés comme un des paramètres expliquant la variabilité chimique, en association

avec des valeurs de pH élevées. Ces dépassements sont essentiellement localisés dans les aquifères au roc confinés. Les concentrations en uranium varient selon les conditions d'oxydo-réduction et de pH. Des minéraux riches en fluor et uranium sont naturellement présents dans le sous-sol de la région (Bouclier Canadien) où plusieurs gisements de minéraux riches en ces éléments ont été identifiés. Leur altération est responsable des concentrations élevées dans certains échantillons.

Concernant les paramètres esthétiques, les problèmes de salinité ont été évoqués plus haut avec le groupe 7 (12 dépassements pour les chlorures, 13 pour le sodium et 30 pour les MDT). Les fortes teneurs en MDT sont souvent associées à des duretés élevées (> 200 mg/l) et concernent surtout les groupes d'eau chimiquement évolués (groupes 3 à 7). C'est le cas de la plupart des échantillons prélevés dans les Basses Terres du St Laurent. Les dépassements en pH concernent 37 échantillons : les pH acides ont été principalement mesurés dans les eaux faiblement évoluées du groupe 1 tandis que les groupes 2 et 6 présentent de nombreux dépassements en pH basique. Ces dépassements résultent de l'évolution géochimique naturelle des eaux souterraines (consommation de CO_2 pour les réactions d'altération des minéraux). Finalement, le fer et le manganèse présentent de nombreux dépassements (18 et 28 respectivement) sur l'ensemble de la zone d'étude, en conséquence de leur relative abondance dans les minéraux des roches du Bouclier Canadien.

1.3 Représentativité de l'échantillonnage

La classification des eaux et l'évaluation de la qualité de l'eau repose sur une centaine d'échantillons prélevés sur un territoire d'environ 14 000 km^2. À cette échelle, l'échantillonnage est supposé représentatif dans la mesure où les échantillons ont été prélevés dans les différents contextes hydrogéologiques, proportionnellement à leur importance sur le territoire. Ces différents contextes géologiques ont été identifiés à partir de la carte du Quaternaire établie par le projet PACES (Fig. 3) et des informations disponibles dans la base de données de SIH. Bien que la qualité de la base de données puisse être questionnable, l'identification de l'interface entre roc fracturé et dépôts du Quaternaire est facile et la distinction entre puits dans le roc et puits dans les dépôts du Quaternaire est donc considérée fiable. En revanche, l'identification des différents

types de dépôts meubles est plus difficile. Cependant, les argiles sont plus facilement reconnaissables et les conditions de confinement sont assez bien identifiées. Des erreurs sont possibles, pour lesquels les données devraient être vérifiées au cas par cas. Dans certains cas, les données géochimiques peuvent être utilisées pour corriger les erreurs d'interprétation des conditions hydrogéologiques. En revanche, l'information sur l'emplacement des crépines est généralement manquante pour les puits dans les dépôts du Quaternaire. Les puits au roc sont ouverts sur toute leur longueur dans le roc. Les échantillons prélevés sont donc représentatifs de toute la longueur ouverte et ne permettent pas de mettre en évidence de stratification.

Les échantillons en provenance de la base de données du projet PACES auraient pu être pris en compte afin d'augmenter le jeu de données pour l'interprétation par analyse statistique multi-variée. Ils n'ont pas été pris en compte pour plusieurs raisons. Les résultats d'analyses de la base de données concernent des échantillons prélevés sur une longue période de temps (des décennies), dont les protocoles de prélèvements sont en général inconnus et variables dans le temps et selon les préleveurs. De plus, les techniques de laboratoire ont évoluées et les limites de détection abaissées en particulier pour les éléments traces. La plupart de ces analyses sont incomplètes par rapport aux paramètres mesurés dans le cadre du projet PACES et les inclure dans l'analyse statistique multi-variée aurait impliqué d'utiliser seulement les ions majeurs mesurés pour chacune des analyses (l'analyse étant retenue si sa balance électronique est correcte). Les analyses de la base de données présentent des biais par rapport à leur représentativité de la qualité naturelle de l'eau souterraine dans la mesure où la majorité des analyses compilées ont été réalisées sur des échantillons prélevés sur des sites contaminés. La plupart de ces sites sont localisés dans la partie sud de la région qui est la plus industrielle et cette partie de la région serait surreprésentée. Ainsi, les échantillons issus des deux campagnes de prélèvements des étés 2011 et 2012 permettent de s'affranchir de ces biais puisque l'ensemble des échantillons a été prélevé selon le même protocole. La plupart des puits étant en fonctionnement et ayant été purgés, l'échantillon est considéré comme représentatif de la qualité intrinsèque de l'eau de l'aquifère. La purge permet aussi de minimiser la variabilité temporelle de la qualité de l'eau, en particulier pour les puits peu profonds dans les sédiments du Quaternaire.

1.4 Interprétation des données isotopiques

Les données isotopiques ont permis de préciser les conditions de recharge ainsi que d'avoir une meilleure idée sur les temps de résidence des eaux souterraines dans les dépôts du Quaternaire et dans la partie supérieure du roc. Les teneurs en isotopes stables sont assez similaires à celles mesurées dans les eaux de pluie actuelles. De plus, du tritium a été détecté dans tous les échantillons excepté OUT036356 (localisé dans l'aquifère au roc confiné, au km 24). Ces résultats suggèrent des temps de résidence assez courts, de l'ordre de quelques dizaines d'années. Les résultats de datation au carbone 14 sont difficiles à interpréter car plusieurs processus semblent affecter les teneurs en carbone 14, en plus de la désintégration radioactive. Parmi ces processus, la mise à l'équilibre entre l'eau de recharge et le CO_2 du sol en milieu ouvert ainsi que l'altération des silicates par du CO_2 fossile ou la dissolution des carbonates en milieu fermé en sont les principaux. Cependant, l'échantillon OUT036356, avec des teneurs en tritium en dessous de la limite de détection, est le seul à avoir de faibles activités en carbone 14 (environ16 pmC) résultant essentiellement de la désintégration radioactive. L'âge corrigé est de l'ordre de 11 000 ans, correspondant à la période de présence de la Mer de Champlain dans la région. Ce résultat suggère la présence d'une zone à faible écoulement, où l'eau souterraine a conservé en grande partie la signature géochimique de l'eau de la Mer de Champlain. En l'absence d'un plus grand nombre d'échantillons (seulement 4 échantillons), les données sur les gaz rares sont difficiles à interpréter. Cependant, la température de recharge (NGT) calculée pour l'échantillon OUT036356 est la plus faible et tous les échantillons ont de fortes teneurs en ^4He. Cette accumulation d'hélium, qui suggère des temps de résidence assez longs, serait principalement le résultat de la diffusion d'hélium depuis des zones plus profondes où les eaux sont plus anciennes, et affecte l'ensemble des puits échantillonnés (même ceux avec du tritium). En plus du faible nombre de données, la reconstruction des paléo-températures est rendue plus difficile dans ce contexte-ci, due à la variabilité climatique des températures avec des eaux de fonte des neiges de l'ordre de 0°C et des eaux de pluie en été entre 10 et 20°C. Pour l'interprétation de ces résultats, bien connaître le mode de recharge de l'aquifère prend toute son importance.

Toutes les mesures effectuées dans l'échantillon OUT035356 semblent concordantes avec l'hypothèse sur les restes de la Mer de Champlain. En effet, cet échantillon présente une chimie de type eau de mer diluée (faciès Na-Cl et concentration en bromures élevée), avec absence de tritium, une faible activité en ^{14}C (âge estimé à environ 11 000 ans), une concentration élevée en ^{4}He et la température NGT la plus basse. Cet échantillon n'étant pas le plus concentré de la région, il a été dilué par de l'eau douce pas très récente (pas de tritium) et a subi aussi de l'échange ionique (concentration en Na bien plus élevée que celle en Cl et très faible concentration en Ca).

1.5 Modélisation numérique

Le calage du modèle d'écoulement a rapidement mis en évidence le manque de données piézométriques pour contraindre le modèle. Le modèle a donc été calé sur les concentrations en tritium et a permis de montrer l'importance de la conductivité hydraulique du roc dans le contrôle des écoulements et du transport (après la topographie qui contrôle l'organisation des systèmes d'écoulement). Seule une conductivité importante dans le roc de 1×10^{-5} m.s^{-1} permet d'expliquer les teneurs en tritium observées dans le roc. Les données géochimiques indiquent que cette valeur de conductivité hydraulique, néanmoins cohérente avec les essais sur le terrain et ceux compilés par Sterckx (2013) n'est pas homogène le long de la section 2D et devrait être un peu plus faible à proximité du puits OUT036356 où sodium et chlorures dominent, bien que l'échantillon montre tout de même des signes d'échange cationique (concentrations en calcium très faibles).

La modélisation des écoulements a permis de mettre en évidence l'organisation des systèmes d'écoulements. L'essentiel de l'écoulement a lieu dans les 200 premiers mètres sous la surface. Les systèmes locaux sont localisés dans les 50 premiers mètres de profondeur, essentiellement dans les dépôts meubles du Quaternaire ou dans les premiers mètres ou dizaines de mètres dans les zones de roc affleurant. Ils sont caractérisés par des âges de l'ordre de quelques dizaines d'années. L'extension des systèmes intermédiaires actifs est limitée en longueur par les rivières (simulées par des charges imposées) et par la conductivité hydraulique du roc en profondeur (200 m maximum). Dans ces systèmes intermédiaires, les âges varient entre

50 et 50 000 ans. Au-delà de cette profondeur, les écoulements sont très lents, avec des âges calculés supérieurs à 50 000 ans. Aucun écoulement régional n'a été vu dans le modèle à cette échelle.

Le modèle de transport des chlorures a permis de caler la conductivité hydraulique des argiles et a montré qu'à la fin de l'épisode de la Mer de Champlain, les concentrations en chlorures étaient élevées dans les premiers 40 m de roc. Ceci s'explique par un changement des conditions d'écoulement par rapport aux conditions actuelles : les vitesses d'écoulement étaient environ 100 fois plus faibles en présence de la Mer de Champlain. La distribution des âges est aussi très dépendante de la conductivité du roc. Les résultats de la modélisation montrent que les temps de résidence dans les dépôts du Quaternaire et dans la partie supérieure du roc de l'aquifère non confiné sont généralement de moins de 50 ans, ce qui explique la présence de tritium dans les échantillons prélevés dans ces formations. En revanche, les âges sont plus élevés dans les argiles qui ont une faible perméabilité et dans le roc sous les argiles (de 50 à 5000 ans). Pour finir, dans les zones où les écoulements sont faibles telles que les grandes étendues d'eau de surface (lac Johnson au km 2 et sous la rivière des Outaouais, au centre), les âges sont beaucoup plus élevés (supérieur à 50 000 ans sous Lac Johnson et jusqu'à 50 000 ans sous la rivière des Outaouais).

La sensibilité de certains paramètres ainsi que différents scénarios d'inondation par la Mer de Champlain ont été testés. A part les conductivités hydrauliques, le modèle est assez peu sensible aux autres paramètres, de même qu'aux différents scénarios envisagés. En ce qui concerne les scénarios, ceux-ci restent assez simplistes et des scénarios plus réalistes demanderaient l'utilisation de modèles plus sophistiqués. Sans reproduire parfaitement la réalité, le modèle développé simule le comportement moyen de l'aquifère compte tenu des hypothèses sous-jacentes.

1.6 Validation du modèle conceptuel

Le modèle conceptuel découle de l'interprétation de l'ensemble des analyses chimiques faites à l'échelle régionale ainsi que de l'interprétation des données isotopiques le long de la ligne d'écoulement. En plus, les résultats de la modélisation numérique ont été utilisés pour développer et valider le modèle conceptuel à partir

des systèmes d'écoulement basés sur les charges et les concentrations en tritium, le transport des chlorures et le calcul des âges.

Dans les aquifères non confinés, des dépôts du Quaternaire ou du roc, les eaux sont de type Ca-HCO_3 et sont faiblement minéralisées. Elles se sont récemment infiltrées (tritium au-dessus des limites de détection) mais présentent des concentrations importantes en ^4He, qui témoignent d'un mélange avec des eaux un peu plus anciennes. Ces résultats sont en accord avec l'organisation des systèmes d'écoulement tels que modélisés, avec des systèmes d'écoulement intermédiaires moins étendus qu'initialement pensés et l'absence de systèmes régionaux (Fig. 36) et où les interactions eau-roche sont plus limitées dans le temps (les échantillons proviennent de systèmes d'écoulement indépendants). La présence de tritium dans le roc est une indication de la connectivité entre les aquifères de dépôts du Quaternaire et l'aquifère au roc. De plus, les écoulements sont subhorizontaux, avec une stratification des âges. La présence d'hélium n'a pas fait l'objet d'une modélisation mais s'explique par la présence d'eaux anciennes à des profondeurs peu élevées, depuis lesquelles il diffuse vers la surface suivant les gradients de concentrations. Les conditions d'échantillonnage dans des puits ouverts dans le roc jouent également un rôle en permettant le mélange d'eaux d'âges différents. Les analyses des isotopes du carbone (^{14}C et $\delta^{13}C$) montrent que la mise à l'équilibre de l'eau avec le CO_2 du sol en milieu ouvert (zone non saturée) ainsi que la dissolution des silicates par du CO_2 fossile ou la dissolution des carbonates en milieu fermé sont les principaux mécanismes responsables de la diminution de l'activité en carbone 14. Il n'est pas à exclure que la présence de quelques traces de calcite modifie aussi les teneurs en carbone 14 (dissolution ou précipitation de calcite secondaire).

En allant en direction des zones d'exutoire, soit les vallées principales de direction nord-sud ou soit la rivière des Outaouais, les eaux deviennent de plus en plus minéralisées, en conséquence de la dissolution des silicates, l'anorthite en particulier, et possiblement de la calcite, qui est localement trouvée en faibles traces dans les dépôts du Quaternaire. Le long de la coupe, les échantillons les plus minéralisés se trouvent dans les sédiments fluvio-glaciaires quelques kilomètres en amont des argiles, et dont la minéralogie est similaire à celle du roc. La géochimie de ces échantillons devrait être semblable à celles des autres échantillons de

l'aquifère non confiné. La modélisation n'a pas permis de démontrer l'existence de temps de résidence plus longs dans cette partie de l'aquifère bien que les argiles pourraient constituer un obstacle à l'écoulement. Dans les zones d'exutoire localisées dans l'ancienne Mer de Champlain et où subsistent encore les argiles marines déposées à cette époque, l'impact de cet épisode est encore visible dans les échantillons présentant une signature marine diluée (eau de type Na-Cl), dans des zones où les conditions d'écoulement sont faibles, tels que l'ont montré les résultats de simulation des chlorures. Ces eaux ne contiennent pas de tritium et les activités en carbone 14 sont faibles, due en partie à la décroissance radioactive et aux processus mentionnés plus haut (échantillon OUT036356).

Dans les zones où les conductivités hydrauliques sont un peu plus importantes, l'échange cationique entre les ions sodium adsorbés sur les argiles de la Mer de Champlain et les ions calcium contenus dans l'eau douce enrichie en calcium suite à la dissolution des silicates, résulte en une eau de type Na-HCO_3. Dans les zones de conductivité hydraulique plus faible, l'échange cationique a lieu mais avec une intensité bien moindre (ou est masqué) et l'eau dans le roc est fortement influencée par la diffusion des ions depuis la couche d'argile et apparait donc avec une signature d'eau de mer diluée. Sur la section d'étude, dans le roc confiné, aucun échantillon de type Na-HCO_3 n'a pu être analysé pour les isotopes. Le seul autre échantillon en provenance de cet aquifère, excepté l'échantillon OUT035356 mentionné ci-dessus, est l'échantillon SANDBAY qui présente une géochimie atypique. L'eau est de type mixte-HCO_3 (avec Ca dominant), avec des concentrations en tritium au-dessus des limites de détection, ce qui était plutôt inattendu. Plusieurs hypothèses ont été soulevées dont la présence de chemins d'écoulement préférentiels au voisinage du puits (les essais hydrauliques ayant démontré que le puits est dans une zone peu perméable) ou la présence d'une fenêtre hydraulique dans l'argile à proximité du puits (non mise en évidence par la géophysique).

2 Contributions à la science

2.1 Qualité de l'eau dans le Bouclier Canadien

Parmi les projets PACES terminés, seuls quatre ont toute ou une partie de leur zone d'étude dans le Bouclier Canadien dont trois dans la Province du Grenville : Mauricie (Leblanc et al. 2013), Saguenay-Lac-St-Jean (CERM-PACES 2013) et Communauté Métropolitaine de Québec (Talbot Poulin et al. 2013). Comme en Outaouais, la présence d'eau salée a été mise en évidence le long du fleuve St Laurent ou de la rivière Saguenay, dans les aquifères confinés par les argiles marines de la Mer de Champlain ou de Laflamme respectivement. Outre les chlorures et le sodium, les autres paramètres concernés par des dépassements incluent les fluorures, les MDT, le fer couplé au manganèse, le pH, et dans une moindre mesure, le baryum. La problématique des dépassements en uranium parait donc être restreinte à l'Outaouais. Les puits présentant des dépassements sont tous localisés dans le roc du Bouclier Canadien (partie sud de la zone d'étude) mais dans des types de roches différentes (gneiss, syénite et paragneiss). Ils sont aussi bien situés en milieu confiné que non confiné et sont majoritairement de type Ca-HCO_3 (si non, Na-HCO_3). Concomitant à cette étude, le projet H2O des Collines, restreint géographiquement à la MRC des Collines de l'Outaouais (en centre de la zone d'étude), a mis en évidence des dépassements de normes d'eau potable en uranium (11.4%) et en fluorures (5.1%) (Lemieux et al. 2014). Les proportions sont similaires à celles observées à l'échelle de la région de l'Outaouais. Il serait donc intéressant de faire des recherches complémentaires afin les environnements où les concentrations en uranium dans les eaux souterraines de l'Outaouais sont élevées, et de spécifier les conditions d'oxydo-réduction afin de comprendre pourquoi des concentrations élevées sont limitées à cette région du Bouclier Canadien. Répondre à ces questions pourrait permettre de délimiter des zones aux eaux souterraines potentiellement riches en uranium. Ainsi, l'uranium n'étant pas un paramètre mesuré lors d'une analyse d'eau standard, tout usager propriétaire d'un puits dans ces zones devrait être averti quant aux risques et être fortement encouragé à analyser son eau pour ce paramètre-ci.

En Outaouais, les données compilées à l'échelle de la région (étape 1 des projets PACES) avaient mis en évidence la mauvaise répartition spatiale des données. La prise en compte de campagnes d'échantillonnage réalisées dans le cadre d'études de caractérisation des sites contaminés introduit des biais concernant la qualité de l'eau car les échantillons ne sont pas représentatifs de la qualité naturelle de l'eau. A cette échelle, tous les dépassements majeurs identifiés sont liés à la nature du sous-sol et aux évènements relatifs à la dernière déglaciation. L'étude a donc permis d'évaluer la qualité naturelle de l'eau grâce à un échantillonnage aléatoire et uniformément distribué (dans la mesure de la disponibilité en puits). Pour l'identification de problématiques plus locales de pollution, une plus grande densité d'échantillonnage serait nécessaire, ce qui n'était pas l'objectif de cette étude, ni des projets PACES.

2.2 Impact de la Mer de Champlain

L'un des objectifs était de quantifier l'impact de l'invasion par la Mer de Champlain dans la région de l'Outaouais. Le long de la rivière des Outaouais, où l'invasion a duré le plus longtemps dans la région d'étude, de nombreux échantillons présentent une signature marine. En revanche, dans les vallées secondaires envahies plus tardivement, très peu d'échantillons ont ces caractéristiques-ci, ce qui tendrait à soutenir l'hypothèse selon laquelle l'eau de la Mer de Champlain était plus diluée vers la fin de l'épisode.

Tous les projets PACES ont mis en évidence la présence d'eau saline le long du St Laurent (et de la rivière des Outaouais dans le cas de la présente étude), en milieu confiné, aussi bien dans le roc du Bouclier Canadien que dans les roches sédimentaires des Basses Terres du St Laurent, indiquant que le temps de contact entre l'eau et la roche n'a pas été suffisamment long pour modifier la signature marine. En revanche, en milieu non confiné, cette signature n'est plus lisible du fait des courts temps de résidence (faciès Ca-HCO_3) et les eaux souterraines apparaissent comme un mélange entre les deux types d'eaux (eau de recharge Ca-HCO_3 et eau marine Na-Cl), avec des concentrations en sodium et chlorures un peu plus élevées par rapport aux autres échantillons en aquifère libre.

2.3 Apport de de la modélisation

Lors de cette étude, l'importance des données géochimiques par rapport aux données hydrauliques a été démontrée lors de la phase de calibration du modèle. Le modèle a aussi démontré qu'à cette échelle, l'approche « milieu poreux équivalent » (EPM en anglais pour Equivalent Porous Medium) est satisfaisante pour modéliser le comportement moyen de l'aquifère sur 10 000 ans. Ceci indique que la partie supérieure du roc est très fracturée et peut donc être considérée comme un milieu poreux équivalent.

Assez peu d'études ont modélisé en 2D ou 3D l'intrusion d'eau salée puis la désalinisation des aquifères suite à la dernière déglaciation. L'Europe a aussi été concernée par des épisodes d'intrusion d'eau saline. Dans un aquifère côtier des Pays Bas, Delsman et al. (2014) ont modélisé en 2D vertical la distribution des chlorures pour lesquels ils disposent de mesures de concentrations (profils verticaux dans les puits) et ont pu identifier l'origine des eaux souterraines.

La partie modélisation de ce projet est donc originale dans le sens où différents indicateurs géochimiques ont été modélisés et chacun a permis de caler certains paramètres ou de confirmer le calage : calage de la conductivité de la partie supérieure du roc grâce au tritium, calage de la conductivité hydraulique des argiles avec les chlorures, sensibilité des paramètres et des différents scénarios d'invasion par l'eau marine. L'originalité réside aussi dans le peu de données de terrain à disposition mais qui, combinées à la modélisation, prennent toute leur importance. Cette approche peut être utilisée dans d'autres contextes de roches cristallines et ne se limite donc pas au Bouclier Canadien. Cette approche est aussi valable pour d'autres contextes d'invasion marine suite à la dernière déglaciation ou pourrait être appliquée aux aquifères côtiers (biseau salin). Dans ce dernier cas, il faudrait considérer la densité de l'eau saline qui serait moins diluée que dans le cas de la Mer de Champlain. Pour finir, une étude basée sur les données géochimiques n'aura de sens que lorsque le contexte géologique est bien défini et les aquifères hydrauliquement bien caractérisés.

3 Perspectives

3.1 Questions en suspens et travaux futurs

L'étude a permis de répondre à bon nombre de questions mais en a soulevé de nouvelles. Il conviendrait de refaire un échantillonnage du puits SANDBAY afin de confirmer ou non la présence de tritium. L'échantillonnage pourrait soit être un échantillonnage conventionnel ou réutiliser les packers afin de mettre en évidence ou non une stratification chimique verticale. Pour cela, il serait souhaitable de prévoir du temps pour permettre une bonne purge du puits qui est très peu perméable et/ou envisager une autre méthode d'échantillonnage (matériel adapté, échantillonnage low flow ou échantillonneurs passifs par exemple). Bien évidemment, quelques échantillons supplémentaires analysés pour les isotopes et les gaz rares dans l'aquifère confiné permettraient de confirmer le modèle conceptuel et les résultats de modélisation. Quelques profils d'ions majeurs dans les argiles pourraient aussi apporter un éclairage nouveau sur le comportement des ions dans les argiles et préciser la localisation du front d'échange cationique.

En ce qui concerne les concentrations en hélium, qui sont élevées, il serait intéressant de faire des modélisations complémentaires afin de confirmer l'hypothèse de la diffusion de l'hélium depuis des couches plus profondes où l'eau souterraine est considérée comme quasi stagnante avec des âges de l'ordre de dizaines de milliers d'années.

Une modélisation de l'échange cationique en 2D (pour estimer l'impact sur la géochimie de l'aquifère confiné) serait assez novatrice dans la mesure où la plupart des études ont été réalisées avec succès en 1D et à petite échelle. En Belgique, l'aquifère Ledo-Paniselien ne résulte pas de la dernière glaciation mais il est aussi un modèle d'adoucissement d'un aquifère confiné initialement rempli d'eau salée et qui est progressivement remplacée par de l'eau douce en provenance de la zone de recharge qui passe au travers des argiles (Walraevens et al. 2007; Walraevens et al. 2001). L'échange cationique a été modélisé mais seulement en 1D. Seule l'étude de Atteia et al. (2005) considère l'échange cationique dans un aquifère confiné entre une couche d'argile peu perméable et dominée par la diffusion et une couche sédimentaire plus perméable dominée par le

transport advectif-dispersif. Avec leur modèle 2D, ils ont simulé différents cas de diffusion associée ou non à l'échange cationique. Cependant, leurs résultats sont théoriques et n'ont pas été vérifiés avec des données de terrain. Une modélisation simplifiée de l'échange cationique constituerait une première étape (domaine simplifié à deux couches considérant uniquement l'échange cationique). Des simulations plus poussées devraient inclure les minéraux présents dans l'aquifère et un plus grand nombre de réactions telle que la précipitation de la calcite, et la dissolution des minéraux riches en fluorures. En effet, les résultats ont montré que les eaux de type Na-HCO_3 ou Na-Cl sont riches en F^- dans la région. Une fois le modèle satisfaisant, il pourrait être utilisé pour faire des prédictions quant au temps nécessaire pour la désalinisation totale de l'aquifère et comparer ces résultats avec ceux théoriques de Atteia et al. (2005). L'impact de la présence de puits dans l'aquifère sur le processus de désalinisation pourrait aussi être évalué.

Pour ce qui est de l'altération des silicates, de simples modélisations en 1D le long d'une ligne d'écoulement pourraient être effectuées (avec PHREEQC par exemple) en tenant compte des cinétiques de réactions afin de voir quel serait le temps nécessaire pour passer d'une eau de type « eau de recharge » (groupe 1) à une eau plus évoluée telle que dans le groupe 4. Pour cela, une meilleure caractérisation des phases minérales serait nécessaire. Les résultats pourraient ensuite être comparés avec ceux de la modélisation des âges en 2D afin de voir si la minéralisation observée est compatible avec les vitesses d'écoulement de la partie supérieure du roc.

Pour finir, si les ressources informatiques le permettent, la validation du modèle pourrait être complétée en tenant compte de tous les processus géochimiques importants en 2D (dissolution des carbonates et altération des silicates, échange cationique en régime permanant. Les résultats pourraient être aussi comparés avec ceux d'un modèle prenant en compte quelques fractures discrètes. Dans ce cas-ci, des travaux complémentaires seraient nécessaires à la caractérisation du roc fracturé. Les résultats pourraient être comparés avec le modèle simplifié en 2D vertical afin de discuter de la validité des simplifications.

Dans une perspective plus large, la méthodologie pourrait être appliquée dans les aquifères côtiers dont la surexploitation est responsable de l'intrusion d'eau saline. Des travaux de modélisation du transport des chlorures permettraient d'évaluer l'efficacité des méthodes de lutte contre l'intrusion saline et d'estimer le temps nécessaire pour un rétablissement total de l'aquifère.

3.2 Transfert de connaissances aux aménagistes du territoire

Outre les perspectives purement scientifiques, il est important de rappeler le contexte général du projet, qui s'inscrit dans une logique de développement durable et d'utilisation raisonnable des ressources en eaux souterraines. L'un des défis concernant les résultats de la recherche scientifique est de les transmettre sous forme vulgarisée aux responsables des régions, des organismes de bassins versants ainsi qu'aux municipalités afin qu'ils les prennent en compte dans la gestion et l'aménagement de leur territoire.

En tout état de cause, l'aquifère confiné est salin (au moins pour les concentrations en Na) dans sa quasi-totalité et les concentrations en fluorures y sont généralement élevées. L'utilisation pour l'eau potable ou l'irrigation de l'eau de puits localisés dans cet aquifère requiert un traitement. Au vu des temps de résidence, il conviendra aussi d'être prudent dans l'utilisation de cet aquifère, en plus de l'aspect qualitatif. En revanche, les aquifères dans les dépôts du Quaternaire, bien que limités en extension, sont des bons aquifères, avec des temps de résidence moyens de l'ordre de quelques dizaines d'années. C'est aussi le cas de l'aquifère au roc avec des temps de résidence à des profondeurs de puits domestiques de quelques centaines d'années.

Dans le cadre du projet PACES, la vulnérabilité de la ressource a été estimée avec l'outil DRASTIC. Cette méthode un peu simpliste donne une première idée mais ne considère que le premier aquifère à partir de la surface (Comeau et al. 2013), donnant ainsi une représentation un peu erronée dans certains contextes hydrogéologiques. L'approche par caractérisation hydrogéochimique et modélisation permet d'estimer la vulnérabilité de l'aquifère au roc même lorsque recouverts par des dépôts du Quaternaire (ce qui n'est pas le cas avec la méthode DRASTIC (Aller et al. 1987) telle qu'appliquée dans le cadre du projet PACES). Deux exemples peuvent être pris pour démontrer l'intérêt de l'approche développée dans cette thèse. Mesurer des

concentrations en tritium au-dessus des limites de détection dans l'aquifère au roc non confiné mais recouvert par des dépôts meubles perméables indique la connectivité entre l'aquifère fracturé et les dépôts meubles perméables. Les aquifères non confinés sont donc assez vulnérables en termes de pollution (courts temps de séjour) contrairement aux aquifères confinés. Il convient donc de bien délimiter les zones de protection des captages. En revanche, ils sont bien approvisionés par la recharge et constitues des ressources en eau potable durable. Les données géochimiques dont la signature diffère de celle attendue (échantillon SANDBAY) peuvent permettre la mise en évidence de fenêtres hydrauliques dans les argiles marines (Stotler et al. 2011), qui augmente la vulnérabilité de l'aquifère confiné. De plus, bien que la couche d'argile offre une protection naturelle, la présence d'eau marine dans les pores ainsi que les réactions d'échange cationique sont responsables des fortes concentrations en sodium et en chlorures.

Bibliographie

Aeschbach-Hertig W, Beyerle U, Holocher J et al. (2001) Excess air in groundwater as a potential indicator of past environmental changes, Study of environmental change using isotope techniques, International Atomic Energy Agency, Vienna, Austria.

Aeschbach-Hertig W, El-Gamal H, Wieser M et al. (2008) Modeling excess air and degassing in groundwater by equilibrium partitioning with a gas phase. Water Resour. Res. 44(8): W08449. DOI: 10.1029/2007wr006454.

Aeschbach-Hertig W, Peeters F, Beyerle U et al. (1999) Interpretation of dissolved atmospheric noble gases in natural waters. Water Resour. Res. 35(9): 2779-2792. DOI: 10.1029/1999wr900130.

Aeschbach-Hertig W, Schlosser P, Stute M et al. (1998) A $^{3}H/^{3}He$ study of ground water flow in a fractured bedrock aquifer. Ground Water. 36(4): 661-670. DOI: 10.1111/j.1745-6584.1998.tb02841.x.

Aeschbach-Hertig W, Solomon DK (2013) Noble gas thermometry in groundwater hydrology. In: P. Burnard, Ed. The Noble Gases as Geochemical Tracers. Springer Berlin Heidelberg: 81-122. DOI: 10.1007/978-3-642-28836-4_5.

Aeschbach-Hertig W, Stute M, Clark JF et al. (2002) A paleotemperature record derived from dissolved noble gases in groundwater of the Aquia Aquifer (Maryland, USA). Geochim et Cosmochim Acta. 66(5): 797-817. DOI: http://dx.doi.org/10.1016/S0016-7037(01)00804-3.

Alcalá FJ, Custodio E (2008) Using the Cl/Br ratio as a tracer to identify the origin of salinity in aquifers in Spain and Portugal. J Hydrol. 359(1–2): 189-207. DOI: 10.1016/j.jhydrol.2008.06.028.

Aller L, Bennett T, Lehr J et al. (1987) DRASTIC: A standardized system for evaluating ground water pollution potential using hydrogeologic settings. US Environmental Protection Agency. Ada. Oklahoma. USA.

Allison GB, Hughes MW (1975) The use of environmental tritium to estimate recharge to a South-Australian aquifer. J Hydrol. 26(3–4): 245-254. DOI: http://dx.doi.org/10.1016/0022-1694(75)90006-2.

André L, Franceschi M, Pouchan P et al. (2005) Using geochemical data and modelling to enhance the understanding of groundwater flow in a regional deep aquifer, Aquitaine Basin, south-west of France. J Hydrol. 305(1-4): 40-62.

Andrews J (1987) Noble gases in groundwaters from crystalline rocks. In: P. Fritz and S. K. Frape, Eds. Saline Water and Gases in Crystalline Rocks. Geological Association of Canada, St John's, Newfoundland, Canada. 33.

Andrews JN, Kay RLF (1982) Natural production of tritium in permeable rocks. Nat. 298(5872): 361-363.

Andrews JN, Lee DJ (1979) Inert gases in groundwater from the Bunter Sandstone of England as indicators of age and palaeoclimatic trends. J Hydrol. 41(3–4): 233-252. DOI: http://dx.doi.org/10.1016/0022-1694(79)90064-7.

Appelo CAJ, Postma D (2005) Geochemistry, Groundwater and Pollution. 2nd edn. A. A. Balkema Publishers. Leiden, The Netherlands.

Arcos D, Grandia F, Domènech C et al. (2008) Long-term geochemical evolution of the near field repository: Insights from reactive transport modelling and experimental evidences. J of Contam Hydrol. 102(3–4): 196-209. DOI: http://dx.doi.org/10.1016/j.jconhyd.2008.09.021.

Atteia O, Andre L, Dupuy A et al. (2005) Contributions of diffusion, dissolution, ion exchange, and leakage from low-permeability layers to confined aquifers. Water Resour. Res. 41(9): W09412.

Back W (1966) Hydrochemical facies and ground-water flow patterns in Northern Atlantic Coastal Plain. AAPG Bull. 44. DOI: 10.1306/0BDA6107-16BD-11D7-8645000102C1865D.

Ballentine CJ, Hall CM (1999) Determining paleotemperature and other variables by using an error-weighted, nonlinear inversion of noble gas concentrations in water. Geochim et Cosmochim Acta. 63(16): 2315-2336. DOI: http://dx.doi.org/10.1016/S0016-7037(99)00131-3.

Barnett MO, Jardine PM, Brooks SC et al. (2000) Adsorption and transport of uranium(VI) in subsurface media. Soil Sci Soc Am J. 64(3): 908-917. DOI: 10.2136/sssaj2000.643908x.

Barnett P (1988) History of the northwestern arm of the Champlain Sea. In: N. R. Gadd, Ed. The Late Quaternary Development of the Champlain Sea Basin. Geological Association of Canada, St John's, Newfoundland, Canada. 35: 25-36.

Bear AJ, Poole WH, Sanford BV et al. (1971). Map 1334A, Rivière Gatineau, Québec-Ontario, 1:1000,000 Geological Atlas, Sheet 31. Geological Survey of Canada, Ottawa, Canada.

Beaudry C (2013) Hydrogéochimie régionale de l'eau souterraine en Montérégie Est, Québec, Canada [Groundwater regional hydrogeochemistry in Montérégie Est, Québec, Canada]. Master thesis. INRS-Eau, Terre et Environnement, Québec, Canada.

Beckers J, Frind EO (2000) Simulating groundwater flow and runoff for the Oro Moraine aquifer system. Part I. Model formulation and conceptual analysis. J Hydrol. 229(3–4): 265-280. DOI: http://dx.doi.org/10.1016/S0022-1694(00)00167-0.

Bélanger R (2014) Urban geology of the National Capital Area. Available from http://geoscan.nrcan.gc.ca/starweb/geoscan/servlet.starweb?path=geoscan/fulle.web&search1=R%3D226165. Last access on 10/02/2014.

Bense VF, Gleeson T, Loveless SE et al. (2013) Fault zone hydrogeology. Earth-Sci Rev. 127(0): 171-192. DOI: http://dx.doi.org/10.1016/j.earscirev.2013.09.008.

Bester ML, Frind EO, Molson JW et al. (2006) Numerical Investigation of Road Salt Impact on an Urban Wellfield. Ground Water. 44(2): 165-175. DOI: 10.1111/j.1745-6584.2005.00126.x.

Betcher R, Gascoyne M, Brown D (1988) Uranium in groundwaters of Southeastern Manitoba, Canada. Can J Earth Sci. 25(12): 2089-2103.

Beyerle U (1999) Groundwater, paleoclimate and noble gases. PhD thesis. Swiss Federal Institute of Technology, Zürich, Switzerland.

Blanchette D, Cloutier V, Roy M et al. (2010a) Protocole officiel de prélèvement d'échantillons d'eau souterraine - Programme d'acquisition de connaissances sur les eaux souterraines au Québec *[Official protocol for groundwater sampling - Québec regional groundwater characterization program]*. 41 pp.

Blanchette D, Lefebvre R, Nastev M et al. (2010b) Groundwater quality, geochemical processes and groundwater evolution in the Chateauguay River watershed, Quebec, Canada. Can Water Resour J. 35(4): 503-526. DOI: 10.4296/cwrj3504503.

Bottomley DJ, Ross JD, Clarke WB (1984) Helium and neon isotope geochemistry of some ground waters from the Canadian Precambrian Shield. Geochim et Cosmochim Acta. 48(10): 1973-1985. DOI: http://dx.doi.org/10.1016/0016-7037(84)90379-X.

Brown CJ, Jurgens BC, Katz BG et al. (2007) Arsenic and uranium in four aquifer settings: occurrence, distribution, and mechanisms for transport to supply wells, Proceedings of the 2007 National Groundwater Association Naturally Occurring Contaminants Conference: Arsenic, Radium, Radon, and Uranium, Charleston, South Carolina.

Carreira PM, Marques JM, Marques JE et al. (2011) Defining the dynamics of groundwater in Serra da Estrela Mountain area, central Portugal: an isotopic and hydrogeochemical approach. Hydrogeol J. 19(1): 117-131. DOI: 10.1007/s10040-010-0675-0.

Carrier M-A, Lefebvre R, Rivard C et al. (2013) Portrait des ressources en eaux souterraines en Montérégie Est, Québec, Canada [Groundwater resource portrait in Montérégie Est, Québec, Canada]. Joint project between INRS, GSC-Québec, OBV Yamaska and IRDA within the Québec groundwater characterization program. Final report INRS R-1433.

Catto NR, Patterson RJ, Gorman WA (1981) Late Quaternary marine sediments at Chalk River, Ontario. Can J Earth Sci. 18(8): 1261-1267. DOI: 10.1139/e81-117.

Catto NR, Patterson RJ, Gorman WA (1982) The late Quaternary geology of the Chalk River region, Ontario and Quebec. Can J Earth Sci. 19(6): 1218-1231. DOI: 10.1139/e82-103.

CERM-PACES (2013) Résultats du programme d'acquisition de connaissances sur les eaux souterraines de la région du Saguenay-Lac-St-Jean [Results of the groundwater resources project for the Region Saguenay-Lac-St-Jean]. Centre d'Études sur les Ressources Minérales, Université du Québec à Chicoutimi. 330 pp.

Chae G-T, Yun S-T, Mayer B et al. (2007) Fluorine geochemistry in bedrock groundwater of South Korea. Sci Total Environ. 385(1–3): 272-283. DOI: http://dx.doi.org/10.1016/j.scitotenv.2007.06.038.

Chebotarev II (1955) Metamorphism of natural waters in the crust of weathering--1. Geochim et Cosmochim Acta. 8(1-2): 22-32, IN21-IN22, 33-48. DOI: 10.1016/0016-7037(55)90015-6.

Chen ZY, Wei W, Liu J et al. (2011) Identifying the recharge sources and age of groundwater in the Songnen Plain (Northeast China) using environmental isotopes. Hydrogeol J. 19(1): 163-176. DOI: 10.1007/s10040-010-0650-9.

Chowdhury AH, Ridgeway C, Mace RE (2004) Origin of the waters in the San Solomon spring system, Trans-Pecos Texas. Aquifers of the Edwards Plateau: Texas Water Development Board Report. 315-344 pp.

Clark I, Fritz P (1997) Environmental Isotopes in Hydrogeology. CRC-Press/Lewis Publishers. Boca Raton, Florida, USA.

Clarke WB, Jenkins WJ, Top Z (1976) Determination of tritium by mass spectrometric measurement of ^{3}He. Int J Appl Radiat & Isot. 27(9): 515-522. DOI: http://dx.doi.org/10.1016/0020-708X(76)90082-X.

Cloutier V (2004) Origin and geochemical evolution of groundwater in the Paleozoic Basses-Laurentides sedimentary rock aquifer system, Québec, Canada. PhD thesis. INRS-Eau, Terre et Environnement, Québec, Canada.

Cloutier V, Lefebvre R, Savard M et al. (2006) Hydrogeochemistry and groundwater origin of the Basses-Laurentides sedimentary rock aquifer system, St. Lawrence Lowlands, Québec, Canada. Hydrogeol J. 14(4): 573-590.

Cloutier V, Lefebvre R, Savard MM et al. (2010) Desalination of a sedimentary rock aquifer system invaded by Pleistocene Champlain Sea water and processes controlling groundwater geochemistry. Environ Earth Sci. 59(5): 977-994. DOI: 10.1007/s12665-009-0091-8.

Cloutier V, Lefebvre R, Therrien R et al. (2008) Multivariate statistical analysis of geochemical data as indicative of the hydrogeochemical evolution of groundwater in a sedimentary rock aquifer system. J Hydrol. 353(3-4): 294-313. DOI: 10.1016/j.jhydrol.2008.02.015.

Comeau G, Talbot Poulin M-C, Tremblay Y et al. (2013) Projet d'acquistion de connaissances sur les eaux souterraines en Outaouais - Rapport final [Groundwater characterisation program in Outaouais - Final report]. Département de géologie et de génie géologique, Université Laval. 148 pp.

Cook PG, Solomon DK (1997) Recent advances in dating young groundwater: chlorofluorocarbons, $^{3}H/^{3}He$ and ^{85}Kr. J Hydrol. 191(1-4): 245-265. DOI: 10.1016/s0022-1694(96)03051-x.

Couture G (1997) Hydrogéochimie d'eaux souterraines dans la ceinture métasédimentaire centrale de la province géologique du Grenville, Québec [Groundwater hydrogeochemistry in the central metasedimentary

belt of Grenville geologic province, Québec]. Master thesis. INRS-Eau, Terre et Environnement, Québec, Canada.

Daigneault R-A, Roy M, Lamothe M et al. (2012) Rapport sur les travaux de cartographie des formations superficielles réalisés dans la portion est du territoire municipalisé de l'Outaouais en 2011-2012 [Report on the mapping of superficial formations in the eastern portion of the Outaouais Region in 2011-2012]. Département des sciences de la Terre et de l'Atmosphère et Département de géographie, Université du Québec à Montréal.

Davis JC (1986) Statistics and Data Analysis in Geology. 2nd edn. John Wiley & Sons Inc. New York, NY, USA.

Delsman JR, Hu-a-ng KRM, Vos PC et al. (2014) Paleo-modeling of coastal saltwater intrusion during the Holocene: an application to the Netherlands. Hydrol. Earth Syst. Sci. 18(10): 3891-3905. DOI: 10.5194/hess-18-3891-2014.

Desaulniers DE, Cherry JA (1989) Origin and movement of groundwater and major ions in a thick deposit of Champlain Sea clay near Montréal. Can Geotech J. 26(1): 80-89. DOI: doi:10.1139/t89-009.

Edmunds WM, Carrillo-Rivera JJ, Cardona A (2002) Geochemical evolution of groundwater beneath Mexico City. J Hydrol. 258(1-4): 1-24.

Environment Canada (2009) Canadian National Atmospheric Chemistry Precipitation Database. Available from www.ec.gc.ca/natchem/default.asp?lang=En&n=90EDB4BC-1. Last access on 26/09/2013.

Environment Canada (2013) Historical climate data. Available from www.climate.weatheroffice.gc.ca. Last access on 09/10/2013.

Fabien-Ouellet G (2014) Mesures sismiques à faible profondeur: Une approche intégrée [Shallow seismic investigations: An integrated approach]. Master thesis. Département de Géologie et de Génie Géologique, Université Laval, Québec, Canada. 172 pp.

Farnham IM, Singh AK, Stetzenbach KJ et al. (2002) Treatment of nondetects in multivariate analysis of groundwater geochemistry data. Chemom and Intell Lab Syst. 60(1–2): 265-281. DOI: 10.1016/s0169-7439(01)00201-5.

Farvolden R, Pfannkuch O, Pearson R et al. (1988) Region 12, Precambrian Shield. In: The Geology of North America. The Geological Society of America. 2: 101-114.

Fetter CW (2001) Applied Hydrogeology. 4th edition. Prentice Hall. Upper Saddle River, New Jersey, USA.

Fontes J-C, Garnier J-M (1979) Determination of the initial 14C activity of the total dissolved carbon: A review of the existing models and a new approach. Water Resour Res. 15(2): 399-413. DOI: 10.1029/WR015i002p00399.

Frape S, Fritz P (1987) Geochemical trends for groundwaters from the Canadian Shield. In: P. Fritz and S. K. Frape, Eds. Saline Water and Gases in Crystalline Rocks. Geological Association of Canada, St John's, Newfoundland, Canada. 33: 19-38.

Frape SK, Fritz P, McNutt RH (1984) Water-rock interaction and chemistry of groundwaters from the Canadian Shield. Geochim et Cosmochim Acta. 48(8): 1617-1627.

Fritz P, Frape SK (1982) Saline groundwaters in the Canadian Shield -- A first overview. Chem Geol. 36(1-2): 179-190.

Fulton RJ, Richard SH (1987) Chronology of late Quaternary events in the Ottawa Region. In: R. J. Fulton, Ed. Quaternary Geology of the Ottawa Region, Ontario and Québec. Geological Survey of Canada. Paper 86-23.

Garga VK, O'Shaughnessy V (1994) The hydrogeological and contaminant-transport properties of fractured Champlain Sea clay in Eastern Ontario. Part 2. Contaminant transport. Can Geotech J. 31(6): 902-915. DOI: 10.1139/t94-105.

Gascoyne M (2004) Hydrogeochemistry, groundwater ages and sources of salts in a granitic batholith on the Canadian Shield, southeastern Manitoba. Appl Geochem. 19(4): 519-560. DOI: http://dx.doi.org/10.1016/S0883-2927(03)00155-0.

Gascoyne M, Davison CC, Ross J et al. (1987) Saline groundwaters and brines in plutons in the Canadian Shield. In: P. Fritz and S. K. Frape, Eds. Saline Water and Gases in Crystalline Rocks. Geological Association of Canada, St John's, Newfoundland, Canada. 33: 53-68.

Gascoyne M, Kamineni DC (1994) The hydrogeochemistry of fractured plutonic rocks in the Canadian Shield. Appl Hydrogeol. 2(2): 43-49. DOI: 10.1007/s100400050044.

Gerla PJ (1992) Pathline and geochemical evolution of ground water in a regional discharge area, Red River Valley, North Dakota. Ground Water. 30(5): 743-754.

Gibbs RJ (1970) Mechanisms controlling world water chemistry. Sci. 170(3962): 1088-1090.

Gibson JJ, Edwards TWD, Birks SJ et al. (2005) Progress in isotope tracer hydrology in Canada. Hydrol Process. 19(1): 303-327. DOI: 10.1002/hyp.5766.

Gleeson T (2009) Groundwater recharge, flow and discharge in a large crystalline watershed. PhD thesis. Queen's University, Kingston, Ontario, Canada.

Gleeson T, Manning AH (2008) Regional groundwater flow in mountainous terrain: three-dimensional simulations of topographic and hydrogeologic controls. Water Resour. Res. 44(10): W10403. DOI: 10.1029/2008wr006848.

Globensky Y (1987) Géologie des Basses-Terres du Saint-Laurent *[Geology of the St. Lawrence Lowlands]*. Provincial Quebec Ministry of Natural Resources. Report MM 85-02.

Glynn PD, Plummer LN (2005) Geochemistry and the understanding of ground-water systems. Hydrogeol J. 13(1): 263-287. DOI: 10.1007/s10040-004-0429-y.

Goderniaux P, Davy P, Bresciani E et al. (2013) Partitioning a regional groundwater flow system into shallow local and deep regional flow compartments. Water Resour Res. 49(4): 2274-2286. DOI: 10.1002/wrcr.20186.

Gouvernement du Québec (2013a) Politique de protection des sols et de réhabilitation des terrains contaminés - Annexe 2: Les critères génériques pour les sols et pour les eaux souterraines, updated 1st May of 2013. [Soil protection and contaminated sites rehabilitation policy - Appendix 2: Generic criteria for soils and groundwater]. Available from http://www.mddep.gouv.qc.ca/sol/terrains/politique/annexe_2_grille_eaux.htm. Last access on 12/02/2014.

Gouvernement du Québec (2013b) Règlement sur la Qualité de l'Eau Potable (RQEP) (L.R.Q., c. Q-2, r. 40), updated 1st May of 2013. [Regulation respecting to the quality of drinking water]. Available from http://www2.publicationsduquebec.gouv.qc.ca/dynamicSearch/telecharge.php?type=2&file=//Q_2/Q2R40.htm. Last access on 11/03/2014.

Güler C, Thyne G, McCray J et al. (2002) Evaluation of graphical and multivariate statistical methods for classification of water chemistry data. Hydrogeol J. 10(4): 455-474. DOI: 10.1007/s10040-002-0196-6.

Guo H, Wang Y (2004) Hydrogeochemical processes in shallow quaternary aquifers from the northern part of the Datong Basin, China. Appl Geochem. 19(1): 19-27.

Han L-F, Plummer LN (2013) Revision of Fontes & Garnier's model for the initial 14C content of dissolved inorganic carbon used in groundwater dating. Chem Geol. 351(0): 105-114. DOI: http://dx.doi.org/10.1016/j.chemgeo.2013.05.011.

Han L-F, Plummer LN, Aggarwal P (2012) A graphical method to evaluate predominant geochemical processes occurring in groundwater systems for radiocarbon dating. Chem Geol. 318–319(0): 88-112. DOI: http://dx.doi.org/10.1016/j.chemgeo.2012.05.004.

Health Canada (2014) Guidelines for Canadian drinking water quality - Summary table. Available from http://www.hc-sc.gc.ca/ewh-semt/pubs/water-eau/2012-sum_guide-res_recom/index-eng.php. Last access on 12/02/2014.

Heaton THE (1984) Rates and sources of4 He accumulation in groundwater. Hydrol Sci J. 29(1): 29-47.

Heaton THE, Vogel JC (1981) “Excess air” in groundwater. J Hydrol. 50(0): 201-216. DOI: http://dx.doi.org/10.1016/0022-1694(81)90070-6.

Hem JD (1972) Chemical factors that influence availability of iron and manganese in aqueous systems. Geol Soc Am Bull. 83(2): 443-&. DOI: 10.1130/0016-7606(1972)83[443:cftita]2.0.co;2.

Hem JD (1985) Study and Interpretation of the Chemical Characteristics of Natural Water. 3rd. edn. Department of the Interior, U.S. Geological Survey. 263 pp.

Herczeg AL, Leaney FW (2011) Review: Environmental tracers in arid-zone hydrology. Hydrogeol J. 19(1): 17-29. DOI: 10.1007/s10040-010-0652-7.

Hounslow AW (1995) Water Quality Data: Analysis and Interpretation. Lewis Publisher. Boca Raton, Florida, USA.

Hunter FMI, Hartley LJ, Hoch A et al. (2008) Calibration of regional palaeohydrogeology and sensitivity analysis using hydrochemistry data in site investigations. Appl Geochem. 23(7): 1982-2003.

IAEA/WMO (2011) Global Network of Isotopes in Precipitation. The GNIP Database. Accessible at: http://www.iaea.org/water. Last access on 06/09/2011.

Illman WA (2004) Interpretation of pressure recovery data from packer inflation. Water Resour Res. 40(9). DOI: 10.1029/2004wr003310.

Ingerson E, Pearson F (1964) Estimation of age and rate of motion of groundwater by the 14C-method. In: T. Koyama, Y. Miyake and K. Sugawara, Eds. Recent Researches in the Fields of Atmosphere, Hydrosphere and Nuclear Geochemistry. Editorial Committee for Sugawara Volume, distributed by Maruzen, Tokyo: 263-283.

Jacks G, Bhattacharya P, Chaudhary V et al. (2005) Controls on the genesis of some high-fluoride groundwaters in India. Appl Geochem. 20(2): 221-228. DOI: http://dx.doi.org/10.1016/j.apgeochem.2004.07.002.

Jin L, Ogrinc N, Hamilton SK et al. (2009) Inorganic carbon isotope systematics in soil profiles undergoing silicate and carbonate weathering (Southern Michigan, USA). Chem Geol. 264(1–4): 139-153. DOI: http://dx.doi.org/10.1016/j.chemgeo.2009.03.002.

Kipfer R, Aeschbach-Hertig W, Peeters F et al. (2002) Noble gases in lakes and ground waters. Rev Mineral & Geoch. 47(1): 615-700. DOI: 10.2138/rmg.2002.47.14.

Krupka KM, Serne RJ (2002) Geochemical factors affecting the behavior of antimony, cobalt, europium, technetium, and uranium in vadose sediments. Pacific Northwest National Laboratory operated by Battelle for the United States Deparment of Energy. Richland, Washington.

Laaksoharju M, Gascoyne M, Gurban I (2008a) Understanding groundwater chemistry using mixing models. Appl Geochem. 23(7): 1921-1940. DOI: http://dx.doi.org/10.1016/j.apgeochem.2008.02.018.

Laaksoharju M, Smellie J, Tullborg E-L et al. (2008b) Hydrogeochemical evaluation and modelling performed within the Swedish site investigation programme. Appl Geochem. 23(7): 1761-1795.

Langmuir D (1997) Aqueous Environmental Geochemistry. Prentice Hall. Upper Saddle River, New Jersey, USA.

Lapierre C, Leroueil S, Locat J (1990) Mercury intrusion and permeability of Louiseville clay. Can Geotech J. 27(6): 761-773.

Larocque M, Gagné S, Tremblay L et al. (2013) Projet de connaissances des eaux souterraines du bassin versant de la rivière Bécancour et de la MRC de Bécancour - Rapport synthèse [Groundwater resources project in the watershed of Bécancour River and RCM of Bécancour - Final report]. Report submitted to the provincial Quebec Ministry of Environment, Wildlife and Parks. 62 pp.

Leblanc Y, Légaré G, Lacasse A et al. (2013) Caractérisation hydrogéologique du sud-ouest de la Mauricie [Hydrogeologic characterization of south-west Mauricie]. Report submitted to the provincial Quebec Ministry of Environment, Wildlife and Parks within the Québec Groundwater Characterization Program. Département des Sciences de l'Environnement, Université du Québec à Trois-Rivières. 134 pp.

Lehmann BE, Davis SN, Fabryka-Martin JT (1993) Atmospheric and subsurface sources of stable and radioactive nuclides used for groundwater dating. Water Resour Res. 29(7): 2027-2040. DOI: 10.1029/93wr00543.

Lemieux JM, Fiset P, Molson JW et al. (2014) Évaluation de la qualité de l'eau souterraine et de surface dans la MRC des Collines-de-l'Outaouais dans le cadre du programme H2O des Collines. Département de géologie et de génie géologique, Université Laval. 189 pp.

Lemieux JM, Sudicky EA, Peltier WR et al. (2008) Simulating the impact of glaciations on continental groundwater flow systems: 2. Model application to the Wisconsinian glaciation over the Canadian landscape. J Geophys Res: Earth Surf. 113(F3): F03018. DOI: 10.1029/2007jf000929.

Leroueil S, Diene M, Tavenas F et al. (1988) Direct determination of permeability of clay under embankment. J of Geotech Eng. 114(6): 645-657. DOI: doi:10.1061/(ASCE)0733-9410(1988)114:6(645).

Leroueil S, Hamouche K, Ravenasi F et al. (2003) Geotechnical characterization and properties of a sensitive clay from Quebec. In: T. S. Tan, K. Phoon, D. Hight and S. Leroueil, Eds. Characterization and Engineering Properties of Natural Soils. A.A. Belkema, The Netherlands: 363-394.

Lichtner PC, Kelkar S, Robinson B (2002) New form of dispersion tensor for axisymmetric porous media with implementation in particle tracking. Water Resour Res. 38(8): 21-21-21-16. DOI: 10.1029/2000wr000100.

Mahara Y (1995) Noble gases dissolved in groundwater in a volcanic aquifer: Helium isotopes in the Kumamoto Plain. Environ Geol. 25(4): 215-224. DOI: 10.1007/bf00766749.

Mamyrin BA, Tolstikhin IN (1984) Helium isotopes in nature. In: W. S. Fyfe, Ed. Developments in Geochemistry. Elsevier, New York.

Manning AH, Caine JS (2007) Groundwater noble gas, age, and temperature signatures in an Alpine watershed: Valuable tools in conceptual model development. Water Resour. Res. 43(4): W04404. DOI: 10.1029/2006wr005349.

Mao X, Prommer H, Barry DA et al. (2006) Three-dimensional model for multi-component reactive transport with variable density groundwater flow. Environ Model & Softw. 21(5): 615-628. DOI: http://dx.doi.org/10.1016/j.envsoft.2004.11.008.

Maréchal J-C (1998) Les circulations d'eau dans les massifs cristallins alpins et leurs relations avec les ouvrages souterrains [Flow patterns in alpine cristalline massifs and their intereactions with underground facilities]. PhD thesis. Département de Génie Civil, EPFL, Lausanne, Switzerland. DOI: 10.5075/epfl-thesis-1769.

Marques MES, Leroueil S, Soares de Almeida MdS (2004) Viscous behaviour of St-Roch-de-l'Achigan clay, Quebec. Can Geotech J. 41(1): 25-38.

Mayer A, Sültenfuß J, Travi Y et al. (2013) A multi-tracer study of groundwater origin and transit-time in the aquifers of the Venice region (Italy). Appl Geochem. DOI: http://dx.doi.org/10.1016/j.apgeochem.2013.10.009.

Mayer KU, Frind EO, Blowes DW (2002) Multicomponent reactive transport modeling in variably saturated porous media using a generalized formulation for kinetically controlled reactions. Water Resour Res. 38(9): 1174. DOI: 10.1029/2001wr000862.

MDDEFP (2008) Programme d'acquisition de connaissances sur les eaux souterraines *[Regional groundwater characterization program]*. From http://www.mddefp.gouv.qc.ca/eau/souterraines/programmes/acquisition-connaissance.htm (in French). Last access on 14/01/2014.

MDDEFP (2012) Système d'information hydrogéologique *[Hydrogeological Information System].* Accessible at: http://www.mddelcc.gouv.qc.ca/eau/souterraines/sih/. Last access on 24/11/2014.

Molinero J, Raposo JR, Galíndez JM et al. (2008) Coupled hydrogeological and reactive transport modelling of the Simpevarp area (Sweden). Appl Geochem. 23(7): 1957-1981.

Molson J, Aubertin M, Bussière B (2007) Simulating transport and geochemical evolution of acid mine drainage through discretely fractured porous media, Proc., 60th Annual CGS and 8th Joint IAH-CNC Groundwater Specialty Conference, Ottawa.

Molson JW, Frind EO (2014) User guide version 3.0 for Flonet/TR2 - A two-dimensional simulator for groundwater flownets, contaminant transport and residence time. Université Laval & University of Waterloo. 55 pp.

Moncur M (2010) Uranium anomalies in shallow groundwater near Bonnyville, Alberta. Alberta Innovates - Technology Futures. Calgary, AB. 0778599523.

Montcoudiol N, Molson JW, Lemieux JM (2015) Hydrogeochemical characterization of groundwater in the Outaouais Region (Québec, Canada) – A regional scale study. Hydrogeol J. 23(2): 377-396. DOI: 10.1007/s10040-014-1190-5.

Montcoudiol N, Molson JW, Lemieux JM (in prep.) A numerical groundwater flow and geochemical evolution model near Shawville in the Outaouais Region, Québec, Canada: validation of a conceptual hydrogeological model.

Montcoudiol N, Molson JW, Lemieux JM et al. (accepted) A conceptual model for groundwater flow and geochemical evolution in the southern Outaouais region, Québec, Canada. Appl Geochem.

Mook W (1976) The dissolution-exchange model for dating groundwater with 14 C. In: Interpretation of Environmental Isotope and Hydrochemical Data in Groundwater Hydrology.

Mook WG, Ed. (2000) Environmental Isotopes in the Hydrological Cycle: Principles and Applications. Volume 4: Groundwater Saturated and Unsaturated Zones. Paris, IHP-V. Technical documents in hydrology. No. 39, Vol IV. UNESCO.

Normani S, Sykes J, Yin Y (2009) Regional-scale paleoclimate influences on a proposed Deep Geologic Repository in Canada for low and intermediate level waste, Proceedings of the 3rd CANUS Rock Mechanics Symposium, M. Diederichs and G. Grassell Eds, Toronto, Canada.

O'Shaughnessy V, Garga VK (1994) The hydrogeological and contaminant-transport properties of fractured Champlain Sea clay in Eastern Ontario. Part 1. Hydrogeological properties. Can Geotech J. 31(6): 885-901. DOI: 10.1139/t94-104.

Ophori DU (1999) Constraining permeabilities in a large-scale groundwater system through model calibration. J Hydrol. 224(1–2): 1-20. DOI: http://dx.doi.org/10.1016/S0022-1694(99)00083-9.

Ophori DU (2004) A simulation of large-scale groundwater flow and travel time in a fractured rock environment for waste disposal purposes. Hydrol Process. 18(9): 1579-1593. DOI: 10.1002/hyp.1407.

Ophori DU, Brown A, Chan T et al. (1996) Revised model of regional groundwater flow in the Whiteshell Research Area. Atomic Energy of Canada Ltd., Pinawa, MB (Canada). Whiteshell Labs.

Ozsvath DL (2009) Fluoride and environmental health: a review. Rev Environ Sci Biotechnol. 8(1): 59-79. DOI: 10.1007/s11157-008-9136-9.

Panno SV, Hackley KC, Hwang HH et al. (2006) Characterization and identification of Na-Cl sources in ground water. Ground Water. 44(2): 176-187. DOI: 10.1111/j.1745-6584.2005.00127.x.

Parent M, Occhietti S (1988) Late Wisconsinan deglaciation and Champlain Sea invasion in the St. Lawrence Valley, Québec. Géogr Phys et Quat. 42(3): 215-246.

Parisi S, Paternoster M, Kohfahl C et al. (2011) Groundwater recharge areas of a volcanic aquifer system inferred from hydraulic, hydrogeochemical and stable isotope data: Mount Vulture, southern Italy. Hydrogeol J. 19(1): 133-153. DOI: 10.1007/s10040-010-0619-8.

Parkhurst DL, Appelo CAJ (1999) User's guide to PHREEQC (version 2) - a computer program for speciation, batch-reaction, one-dimensional transport, and inverse geochemical calculations. U.S. Geological Survey. Water-Resources Investigations Report 99-4259. 326 pp.

Pearson FJ, White DE (1967) Carbon 14 ages and flow rates of water in Carrizo Sand, Atascosa County, Texas. Water Resour Res. 3(1): 251-261. DOI: 10.1029/WR003i001p00251.

Peeters F, Beyerle U, Aeschbach-Hertig W et al. (2002) Improving noble gas based paleoclimate reconstruction and groundwater dating using $^{20}Ne/^{22}Ne$ ratios. Geochim et Cosmochim Acta. 67(4): 587-600. DOI: 10.1016/s0016-7037(02)00969-9.

Plummer LN, Bexfield LM, Anderholm SK et al. (2004) Hydrochemical tracers in the middle Rio Grande Basin, USA: 1. conceptualization of groundwater flow. Hydrogeol J. 12(4): 359-388.

Plummer LN, Prestemon EC, Parkhurst DL (1991) An interactive code (NETPATH) for modeling net geochemical reactions along a flow path. Department of the Interior, US Geological Survey. 231 pp.

Poage MA, Chamberlain CP (2001) Empirical Relationships Between Elevation and the Stable Isotope Composition of Precipitation and Surface Waters: Considerations for Studies of Paleoelevation Change. Am J of Sci. 301(1): 1-15. DOI: 10.2475/ajs.301.1.1.

Quigley RM, Gwyn QHJ, White OL et al. (1983) Leda clay from deep boreholes at Hawkesbury, Ontario. Part I: Geology and geotechnique. Can Geotech J. 20(2): 288-298. DOI: 10.1139/t83-032.

Rajmohan N, Elango L (2004) Identification and evolution of hydrogeochemical processes in the groundwater environment in an area of the Palar and Cheyyar River basins, Southern India. Environ Geol. 46(1): 47-61. DOI: 10.1007/s00254-004-1012-5.

Rankka K, Andersson-Sköld Y, Hultén C et al. (2004) Quick clay in Sweden. Statens Geotekniska Institut (Swedish Geotechnical Institute), Linköping, Sweden.

Rao NS (2009) Fluoride in groundwater, Varaha River basin, Visakhapatnam District, Andhra Pradesh, India. Environ Monit Assess. 152(1-4): 47-60. DOI: 10.1007/s10661-008-0295-5.

Robertson WD, Cherry JA (1989) Tritium as an indicator of recharge and dispersion in a groundwater system in central Ontario. Water Resour Res. 25(6): 1097-1109. DOI: 10.1029/WR025i006p01097.

Salas J, Ayora C (2004) Groundwater chemistry of the Okélobondo uraninite deposit area (Oklo, Gabon): two-dimensional reactive transport modelling. J of Contam Hydrol. 69(1–2): 115-137. DOI: http://dx.doi.org/10.1016/S0169-7722(03)00140-2.

Sanford W (2011) Calibration of models using groundwater age. Hydrogeol J. 19(1): 13-16. DOI: 10.1007/s10040-010-0637-6.

Sanford WE, Aeschbach-Hertig W, Herczeg AL (2011) Preface: Insights from environmental tracers in groundwater systems. Hydrogeol J. 19(1): 1-3. DOI: 10.1007/s10040-010-0687-9.

Sanford WE, Plummer LN, McAda DP et al. (2004) Hydrochemical tracers in the middle Rio Grande Basin, USA: 2. calibration of a groundwater-flow model. Hydrogeol J. 12(4): 389-407.

SAS Institute Inc. (2009) SAS/STAT 9.2 user's guide. 2nd edn.

Schroeder PR, Ammon DC (1994) The hydrologic evaluation of landfill performance (HELP) model: User's guide for version 3. Risk Reduction Engineering Laboratory, Office of Research and Development, US Environmental Protection Agency.

Shapiro SD, Rowe G, Schlosser P et al. (1998) Tritium–helium 3 dating under complex conditions in hydraulically stressed areas of a buried-valley aquifer. Water Resour Res. 34(5): 1165-1180. DOI: 10.1029/97wr03322.

Smedley PL, Edmunds WM (2002) Redox patterns and trace-element behavior in the East Midlands Triassic sandstone aquifer, U.K. Ground Water. 40(1): 44-58. DOI: 10.1111/j.1745-6584.2002.tb02490.x.

Solomon DK, Sudicky EA (1991) Tritium and helium 3 isotope ratios for direct estimation of spatial variations in groundwater recharge. Water Resour. Res. 27(9): 2309-2319.

Sonkamble S, Sahya A, Mondal NC et al. (2012) Appraisal and evolution of hydrochemical processes from proximity basalt and granite areas of Deccan Volcanic Province (DVP) in India. J Hydrol. 438–439(0): 181-193. DOI: http://dx.doi.org/10.1016/j.jhydrol.2012.03.022.

Sracek O, Hirata R (2002) Geochemical and stable isotopic evolution of the Guarani aquifer system in the State of São Paulo, Brazil. Hydrogeol J. 10(6): 643-655.

Sterckx A (2013) Étude des facteurs influençant le rendement des puits d'alimentation de particuliers qui exploitent le roc fracturé en Outaouais, Québec, Canada [Study of the factors impacting on the productivity of individual wells in fractured bedrock from the Outaouais Region, Québec, Canada]. Master thesis. Département de Géologie et Génie Géologique, Université Laval, Québec, Canada.

Stotler RL, Frape SK, El Mugammar HT et al. (2011) Geochemical heterogeneity in a small, stratigraphically complex moraine aquifer system (Ontario, Canada): interpretation of flow and recharge using multiple geochemical parameters. Hydrogeol J. 19(1): 101-115. DOI: 10.1007/s10040-010-0628-7.

Stute M, Sonntag C, Deák J et al. (1992) Helium in deep circulating groundwater in the Great Hungarian Plain: Flow dynamics and crustal and mantle helium fluxes. Geochim et Cosmochim Acta. 56(5): 2051-2067. DOI: http://dx.doi.org/10.1016/0016-7037(92)90329-H.

Sudicky EA, Frind EO (1981) Carbon 14 dating of groundwater in confined aquifers: implications of aquitard diffusion. Water Resour Res. 17(4): 1060-1064. DOI: 10.1029/WR017i004p01060.

Sültenfuβ J, Purtschert R, Führböter J (2011) Age structure and recharge conditions of a coastal aquifer (northern Germany) investigated with ^{39}Ar, ^{14}C, ^{3}H, He isotopes and Ne. Hydrogeol J. 19(1): 221-236.

Sun T, Hall CM, Castro MC (2010) Statistical properties of groundwater noble gas paleoclimate models: are they robust and unbiased estimators? Geochem, Geophys, Geosyst. 11(2): Q02002. DOI: 10.1029/2009gc002717.

Sykes JF, Normani SD, Jensen MR et al. (2009) Regional-scale groundwater flow in a Canadian Shield setting. Can Geotech J. 46(7): 813-827. DOI: 10.1139/t09-017.

Talbot Poulin M-C, Comeau G, Tremblay Y et al. (2013) Projet d'acquisition de connaissances sur les eaux souterraines du territoire de la Communauté Métropolitaine de Québec, rapport final [Groundwater characterisation program in Québec City, final report]. Département de géologie et de génie géologique, Université Laval. 172 pp.

Tamers MA (1975) Validity of radiocarbon dates on ground water. Geophys Surv. 2(2): 217-239. DOI: 10.1007/bf01447909.

Tavenas F, Jean P, Leblond P et al. (1983) The permeability of natural soft clays. Part II: Permeability characteristics. Can Geotech J. 20(4): 645-660. DOI: 10.1139/t83-073.

Tecplot Inc. (2014) Tecplot 360 EX 2014, User's Manual. Tecplot Inc. Bellevue, WA, USA.

Teller JT (1990) Volume and routing of late-glacial runoff from the southern Laurentide Ice Sheet. Quat Res. 34(1): 12-23. DOI: http://dx.doi.org/10.1016/0033-5894(90)90069-W.

Terasmae J (1961) Notes on late-Quaternary climatic changes in Canada. Ann of the N.Y. Acad of Sci. 95(1): 658-675. DOI: 10.1111/j.1749-6632.1961.tb50065.x.

Tolstikhin IN, Kamensky I (1969) Determination of groundwater age by the T-^{3}He method. Geochem Int. 6: 810-811.

Torrance JK (1979) Post-depositional changes in the pore-water chemistry of the sensitive marine clays of the Ottawa area, eastern Canada. Eng Geol. 14(2–3): 135-147. DOI: http://dx.doi.org/10.1016/0013-7952(79)90081-4.

Torrance JK (1988) Mineralogy, pore-water chemistry, and geotechnical behaviour of Champlain Sea and related sediments. In: N. R. Gadd, Ed. The Late Quaternary Development of the Champlain Sea Basin. Geological Association of Canada, St John's, Newfoundland, Canada. 35: 259-275.

Tóth J (1963) A theoretical analysis of groundwater flow in small drainage basins. J Geophys Res. 68(16): 4795-4812.

Tóth J (1999) Groundwater as a geologic agent: an overview of the causes, processes, and manifestations. Hydrogeol J. 7(1): 1-14. DOI: 10.1007/s100400050176.

Vengosh A, Pankratov I (1998) Chloride/bromide and chloride/fluoride ratios of domestic sewage effluents and associated contaminated ground water. Ground Water. 36(5): 815-824. DOI: 10.1111/j.1745-6584.1998.tb02200.x.

Visser A, Broers HP, Bierkens MFP (2007) Dating degassed groundwater with 3H/3He. Water Resour Res. 43(10): W10434. DOI: 10.1029/2006wr005847.

Vogel J (1970) Carbon-14 dating of groundwater. Isot Hydrol. 1970: 225-239.

Walraevens K, Cardenal-Escarcena J, Van Camp M (2007) Reaction transport modelling of a freshening aquifer (Tertiary Ledo-Paniselian Aquifer, Flanders-Belgium). Appl Geochem. 22(2): 289-305.

Walraevens K, Van Camp M, Lermytte J et al. (2001) Pleistocene and Holocene groundwaters in the freshening Ledo-Paniselian aquifer in Flanders, Belgium. Geological Society, London, Special Publications. 189(1): 49-70. DOI: 10.1144/gsl.sp.2001.189.01.05.

Walter AL, Frind EO, Blowes DW et al. (1994) Modeling of multicomponent reactive transport in groundwater: 2. Metal mobility in aquifers impacted by acidic mine tailings discharge. Water Resour Res. 30(11): 3149-3158. DOI: 10.1029/94wr00954.

Weiss RF (1968) Piggyback sampler for dissolved gas studies on sealed water samples. Deep Sea Res and Oceanogr Abstr. 15(6): 695-699. DOI: http://dx.doi.org/10.1016/0011-7471(68)90082-X.

Woo NC, Choi MJ, Lee KS (2002) Assessment of groundwater quality and contamination from uranium-bearing black shale in Goesan–Boeun Areas, Korea. Environ Geochem and Health. 24(3): 264-273. DOI: 10.1023/a:1016010626263.

Zouari K, Trabelsi R, Chkir N (2011) Using geochemical indicators to investigate groundwater mixing and residence time in the aquifer system of Djeffara of Medenine (southeastern Tunisia). Hydrogeol J. 19(1): 209-219. DOI: 10.1007/s10040-010-0673-2.

Zuber A, Rozanski K, Kania J et al. (2011) On some methodological problems in the use of environmental tracers to estimate hydrogeologic parameters and to calibrate flow and transport models. Hydrogeol J. 19(1): 53-69. DOI: 10.1007/s10040-010-0655-4.

Zuber A, Weise SM, Motyka J et al. (2004) Age and flow pattern of groundwater in a Jurassic limestone aquifer and related Tertiary sands derived from combined isotope, noble gas and chemical data. J Hydrol. 286(1-4): 87-112. DOI: 10.1016/j.jhydrol.2003.09.004.

Annexe 1 – Cartes supplémentaires issues du rapport du projet PACES

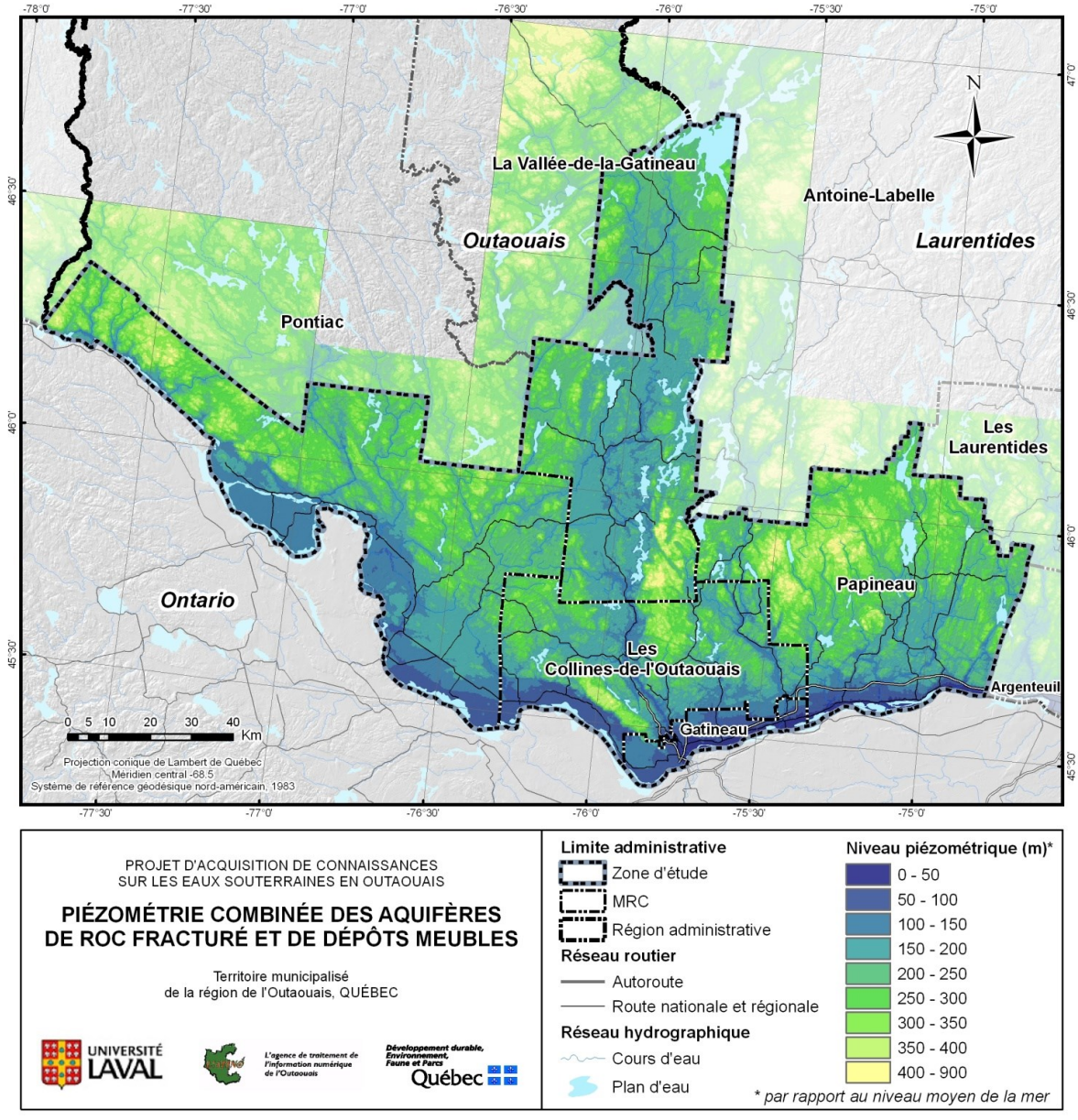

Fig. A1 Carte piézométrique combinée des aquifères de roc fracturé et de dépôts meubles (d'après Comeau et al. (2013), méthodologie de construction de la carte disponible dans ce même rapport)

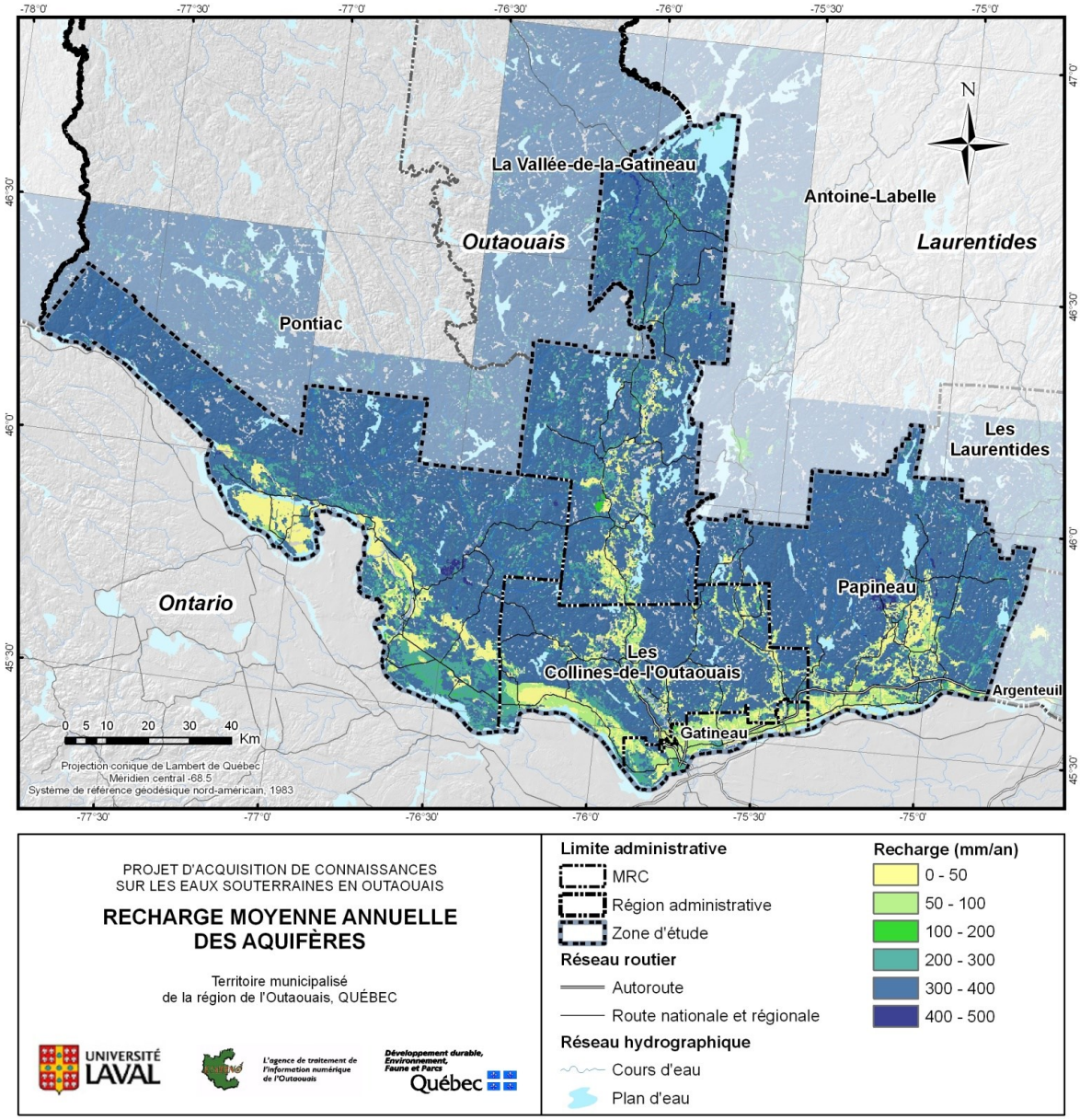

Fig. A2 Distribution spatiale de la recharge moyenne annuelle des aquifères (d'après Comeau et al. (2013))

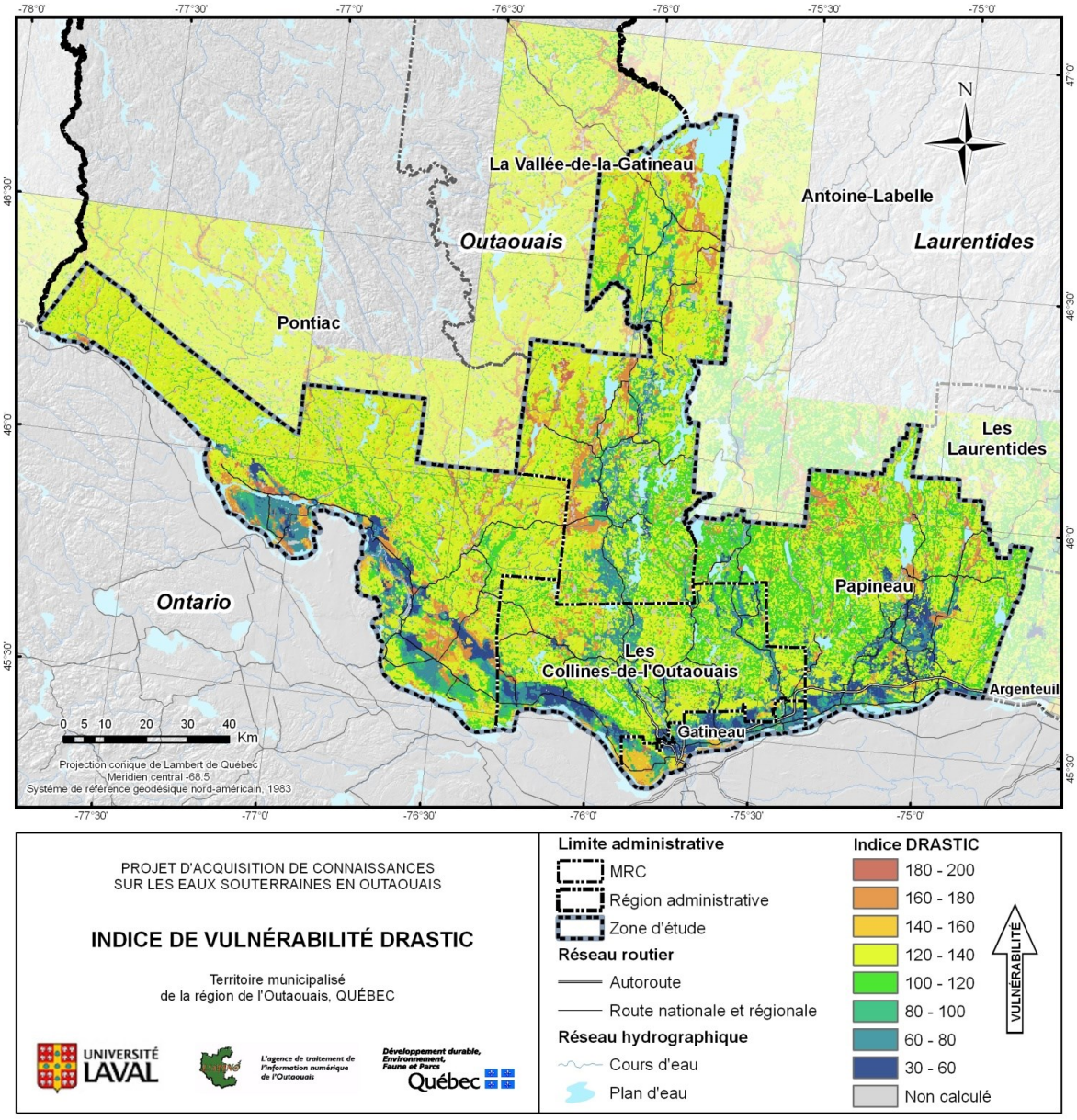

Fig. A3 Carte de distribution de la vulnérabilité des aquifères telle que estimée par la méthode DRASTIC (d'après Comeau et al. (2013))

Annexe 2 – Résultats des analyses des échantillons d'eau souterraine

[a] Type d'aquifère

Aquifères dans les dépôts du Quaternaire : sédiments fluvio-glaciaires (F-G), deltaïques, alluvions, indéfini (G)

Aquifères dans le roc : Bouclier Canadien (syénite, gneiss, paragneiss, marbre, granite, diorite) et roches sédimentaires des Basses Terres du St Laurent (carbonates)

[b] Confinement : confiné (C), semi-confiné (SC) et libre (L)

[c] Prof. : profondeur en mètre

[d] Temp. : température

[e] C.S. : conductivité spécifique à 25°C

[f] O.D. : oxygène dissous

[g] Eh : potentiel d'oxydo-réduction relatif à l'électrode standard d'hydrogène

[h] E.N. : électro-neutralité (balance ionique) de l'échantillon

A1 : Caractéristiques des puits échantillonnés et paramètres physico-chimiques

Echantillon	Aquifère[a]	Confinement[b]	Prof.[c] m	Temp.[d] °C	pH -	C.S.[e] µS/cm	O.D.[f] mg/l	Eh[g] mV	E.N.[h] %	Facies	HCA
OUT000419	F-G	SC	29.6	10	7.25	46	6.93	383	1.0	Ca-HCO3	C1
OUT003848	F-G	C	49.3	11.6	8.2	89	2.53	282.6	-1.6	Ca-HCO3	C3
OUT004005	Gneiss	SC	69	14.6	7.86	387	0.29	37.3	-0.8	Ca-HCO3	C4
OUT004007	Marbre	C	138.7	9.5	7.93	182	0.46	254.9	-0.1	Na-HCO3	C6
OUT004013	F-G	C	36.1	8.7	7.97	108	8.28	232.8	-1.9	Ca-HCO3	C3
OUT004020	Gneiss	C	81.4	8.8	8.77	193	0.1	63.8	1.4	Na-HCO3	C6
OUT004087	Deltaïque	L	8.5	8.2	7.49	123	4.47	473.3	-0.5	Ca-HCO3	C3
OUT016466	F-G	C	72.6	9	9.66	705	0.08	-66	-2.8	Na-HCO3	C6
OUT018365	Marbre	SC	97.5	8.6	8.99	69	6.36	76	-0.4	Ca-HCO3	C2
OUT018375	Marbre	C	152.5	9	9.11	940	0.11	-87.1	4.8	Na-Cl	C6
OUT018376	Marbre	L	74.7	9.3	7.64	349	0.1	-143.3	-2.9	Ca-SO4	C3
OUT018387	F-G	L	29	8.9	8.09	261	0.31	66.8	2.4	Ca-HCO3	C4
OUT018393	Marbre	L	117.4	9	8.47	232	1.6	32.3	13.1		
OUT018395	Marbre	L	44.2	8.5	7.4	286	7.27	334.6	1.5	Ca-HCO3	C3
OUT018401	Gneiss	C	14	9.2	8.6	170	0.16	-50.1	1.2	Ca-HCO3	C2
OUT018407	Syénite	SC	93.0	8.5	8.15	180	7.87	300.4	-0.3	Ca-HCO3	C3
OUT018662	Carbonates	C	114.3	11.5	9.35	598	0.06	-120	0.6	Na-HCO3	C6
OUT018746	Syénite	C	91.5	10	8.28	1360	0.16	78.1	-10.8		
OUT018832	Gneiss	L	82.3	9.1	7.81	254	5.84	161	1.4	Ca-HCO3	C3
OUT018910	Gneiss	SC	91.5	9.2	7.27	237	1.37	356.3	7.8	Ca-HCO3	C4
OUT018925	Carbonates.	L	54.9	11.9	7.34	601	5.88	125.3	2.4	Ca-HCO3	C7
OUT019120	Marbre	C	62.5	10.6	7.52	261	2.43	323.6	-2.9	Ca-HCO3	C4
OUT019124	F-G	C	89.9	10.1	8.65	585	0.13	-84.9	-4.1	Na-Cl	C7
OUT019143	Gneiss	L	38.1	10.5	8.47	158	0.11	-77.2	-0.2	Ca-HCO3	C2
OUT019147	Paragneiss	SC	74.7	9.1	7.32	377	11.07	338.1	2.8	Ca-HCO3	C3
OUT019181	Syénite	L	25.9	10.7	6.77	810	4.93	93.3	0.2	Ca-Cl	C7
OUT019200	Gneiss	L	68.6	10.7	7.61	192	8.62	208.1	1.9	Ca-HCO3	C2
OUT019283	Gneiss	L	74.7	10.4	8.69	205	0.67	13	2.3	Ca-HCO3	C2
OUT019459	Deltaïque	L	44.8	9.7	8.96	319	0.38	-87.7	0.4	Na-HCO3	C6
OUT019536	Carbonates	L	86	9.7	9.32	312	0.16	622.1	-0.3	Ca-Cl	C6
OUT019695	F-G	C	58	8.9	8.38	303	0.17	-26.8	8.1	Ca-HCO3	C4
OUT019761	Gneiss	C	75.9	9.2	8.65	1130	0.11	-116.4	-5.4	Na-Cl	C7
OUT019864	Carbonates	L	39.3	9.8	7.63	920	2.05	-21.7	-2.0	Ca-HCO3	C7
OUT019914	Syénite	L	68.3	9.7	6.4	359	2.4	260.4	-1.7	Ca-HCO3	C4
OUT020035	Marbre	SC	117.4	9.5	7.77	274	1.69	237.2	-1.6	Ca-HCO3	C3
OUT020065	Marbre	C	54.9	9.8	7.56	278	6.39	293.9	-0.6	Ca-HCO3	C3
OUT020086	Gneiss	L	81	8.5	8.15	63	0.24	82	2.1	Ca-HCO3	C2
OUT020091	Gneiss	L	93.0	9.7	6.43	120	4.38	448.7	-1.6	Ca-Mixte	C4
OUT020318	F-G	C	77.7	9.2	8.43	189	0.2	72.9	-1.9	Ca-HCO3	C2

Echantillon	Aquifère[a]	Confinement[b]	Prof.[c] m	Temp.[d] °C	pH -	C.S.[e] µS/cm	O.D.[f] mg/l	Eh[g] mV	E.N.[h] %	Facies	HCA
OUT020341	Carbonates	L	61	10.2	7.49	543	1.31	196.7	5.5	Ca-HCO3	C7
OUT020412	F-G	L	34.1	8.4	8.82	47	0.25	12.2	-0.5	Ca-HCO3	C2
OUT020440	F-G	L	29.9	7.8	6.51	60	10.03	309.4	-2.4	Ca-HCO3	C1
OUT020566	Carbonates	C	76.2	9.7	7.39	222	0.37	309.3	2.6	Ca-HCO3	C6
OUT020694	Gneiss	C	53	10.4	8.29	372	0.18	-51	0.0	Na-HCO3	C6
OUT020717	Syénite	L	91.2	9.7	6.88	268	2.72	323.5	-3.3	Ca-HCO3	C3
OUT020768	Syénite	L	75.9	10.2	7.26	268	7.23	190.9	-0.8	Ca-HCO3	C4
OUT021157	Gneiss	L	91.5	9.4	5.98	71	11.01	418.7	-5.7	Ca-Cl	C1
OUT021327	Gneiss	SC	61.9	8.7	8.89	131	0.1	14.5	1.5	Na-HCO3	C2
OUT021530	Carbonates	SC	91.2	10.1	7.45	607	1.99	156	24.7		
OUT021917	F-G	C	74.7	12.5	8.24	1140	0.08	8	1.1	Na-Cl	C7
OUT022127	Gneiss	L	91.5	8.3	7.76	109	6.61	446.6	-0.6	Ca-HCO3	C2
OUT022187	Marbre	L	91.5	9.1	8.51	498	0.2	-80	-0.6	Na-HCO3	C6
OUT022252	Marbre	SC	104.6	10.3	6.8	178	0.08	97.6	-17.7		
OUT022258	Granite	L	73.8	8.4	6.78	166	10.96	320	-1.4	Ca-HCO3	C1
OUT022274	Marbre	L	131.1	9.7	8.43	3450	0.14	-146.3	4.3	Na-SO4	C7
OUT022292	Paragneiss	C	54.9	9.1	9.28	890	0.1	-156	-2.4	Na-HCO3	C6
OUT022510	Carbonates	C	33.2	10.1	8.24	3230	2.77	119.9	2.7	Na-Cl	C7
OUT022560	Carbonates	L	152	10	7.56	437	1.66	192	14.9		
OUT022620	Marbre	SC	120.1	9	7.58	238	3.48	716.8	29.7		
OUT022829	Syénite	L	70.1	9.2	7.16	657	3.52	308.7	2.2	Na-HCO3	C7
OUT022963	Marbre	L	76.2	8.1	8.49	180	0.21	-115	1.4	Ca-HCO3	C3
OUT022995	Marbre	C	36.6	8.7	7.57	169	0.34	140	-3.5	Ca-HCO3	C2
OUT023044	F-G	C	41.2	13.6	8.78	85	0.07	25.5	-3.6	Ca-HCO3	C6
OUT023067	F-G	C	42.1	10.7	8.33	82.2	0.14	86.1	1.8	Ca-HCO3	C2
OUT023092	Marbre	L	103.7	9.4	7.9	108	0.91	30.8	-1.2	Ca-HCO3	C2
OUT023108	Paragneiss	L	103.7	11.3	7.38	88	0.12	161.1	0.8	Ca-HCO3	C2
OUT023157	Gneiss	C	92.7	9.8	7.59	261	6.58	194.6	1.5	Ca-HCO3	C3
OUT023259	Marbre	L	75.9	11.1	7.85	289	0.17	54.5	-0.1	Ca-HCO3	C2
OUT023496	Syénite	L	109.8	7.9	8.37	46.6	2.5	175.1	1.0	Ca-HCO3	C2
OUT023553	Syénite	L	94.5	12.1	7.85	163	0.52	-60	-0.6	Ca-HCO3	C2
OUT023574	Gneiss	C	58	9.6	8.52	404	0.11	29.2	-6.2	Na-HCO3	C6
OUT023612	Diorite	C	70.2	9.3	8.48	142	0.22	437.6	3.0	Ca-HCO3	C2
OUT023623	Gneiss	C	94.5	9	8.73	532	0.34	-172.4	0.6	Na-HCO3	C6
OUT025998	Syénite	SC	0	12.9	7.89	99	0.45	5.7	2.9	Ca-HCO3	C2
OUT026101	Gneiss	C	38	11.2	7.38	441	3.22	228	-4.9	Na-Cl	C7
OUT026102	Syénite	C	0	8.3	7.72	374	1.33	146.8	4.8	Ca-HCO3	C3
OUT026103	Carbonates	L	88.4	9.4	7.55	403	0.3	257.7	-1.6	Ca-HCO3	C4
OUT026104	Carbonates	C	122	10.9	8.01	1970	0.1	-63.6	-6.9	Na-Cl	C7
OUT026105	Paragneiss	C	0	10.7	7.83	424	0.69	-32	1.0	Na-HCO3	C6
OUT026106	Gneiss	C	0	10.4	7.46	800	0.15	194.9	-2.9	Mixte-Cl	C7

Echantillon	Aquifère[a]	Confinement[b]	Prof.[c] m	Temp.[d] °C	pH -	C.S.[e] µS/cm	O.D.[f] mg/l	Eh[g] mV	E.N.[h] %	Facies	HCA
OUT026107	Paragneiss	C	0	10.1	9.22	295	0.2	-34.6	0.2	Na-HCO3	C6
OUT026108	F-G	C	9.1	10.1	7.88	503	0.54	-62.7	8.8	Ca-HCO3	C4
OUT026109	G	L	4.3	10	7.32	314	5.1	474.1	19.1		
OUT026110	Marbre	L	21.3	7.7	7.16	122	10.63	122	2.4	Ca-HCO3	C3
OUT026112	G	L	0	10.8	6.71	94	7.38	242.2	-1.8	Ca-SO4	C1
OUT026115	G	SC	25.9	8.8	8.6	283	0.08	-170.2	1.1	Ca-HCO3	C6
OUT026116	Deltaïque	L	0	9.4	8.17	289	3.49	123.5	-3.8	Ca-HCO3	C3
OUT026117	F-G	L	6.71	8.8	7.39	52	5.54	234.9	-4.6	Ca-HCO3	C1
OUT026118	Marbre	SC	67.1	8.7	7.28	371	0.87	162.6	0.6	Ca-HCO3	C4
OUT026119	Marbre	SC	61.0	12.5	8.64	249	3.29	79.5	-0.2	Ca-HCO3	C3
OUT026120	Marbre	C	0	9	7.53	566	0.94	282.1	-1.8	Ca-HCO3	C3
OUT026121	Marbre	C	70.1	9	8.3	203	0.14	35.4	-0.8	Ca-HCO3	C4
OUT026122	Gneiss	SC	109.7	10.3	7.15	155	0.15	233.9	-1.8	Ca-HCO3	C4
OUT026123	Syénite	SC	91.1	9	7.27	306	0.4	238.7	-2.3	Ca-HCO3	C4
OUT026124	Syénite	L	0	9.4	7.15	1180	1.99	285.8	-4.0	Ca-Cl	C7
OUT026125	Alluvions	L	0	9.8	6.8	193	8.64	20.4	-3.3	Ca-Cl	C1
OUT026126	Paragneiss	L	99.1	8.5	7.93	183	0.86	312.6	-0.6	Ca-HCO3	C2
OUT026127	Carbonates	C	105.2	8.5	8.9	287	0.17	152.3	-2.5	Na-HCO3	C6
OUT026128	Paragneiss	C	0	9.5	8.49	414	0.2	-126.9	0.0	Na-HCO3	C6
OUT026129	F-G	C	0	8.1	7.98	450	0.18	111.5	3.3	Ca-HCO3	C4
OUT026130	Paragneiss	C	0	11.3	8.29	274	0.37	420	2.9	Ca-HCO3	C2
OUT026131	Paragneiss	C	100.6	9.7	8.59	452	0.23	-31.4	0.0	Na-HCO3	C6
OUT026132	F-G	L	34	7.7	8.06	70	0.24	112.4	0.1	Ca-HCO3	C2
OUT026135	Alluvions	L	0	9.9	6.44	83	1.21	143.1	-2.9	Ca-HCO3	C1
CONV-COL	Gneiss	SC	42.1	10.8	7.48	423	3.08	289.3	-1.7	Ca-HCO3	C4
CONV-GAT	Carbonates	SC	36.0	-	-	0		240	7.0	Ca-HCO3	C7
CONV-PAP1	F-G	C	65.5	9.3	8.44	201	3.49	113	12.3		
CONV-VAL1	FG	SC	22.9	10.5	8.41	81	6.82	128.4	-0.4	Ca-HCO3	C3
CPT-GAT1	F-G	C	19	9.4	7.31	314	3.41	100.9	1.5	Mg-HCO3	C5
CPT-PON03	Deltaïque	L	35	8.5	8.63	111	8.81	303.2	4.7	Ca-HCO3	C2
CPT-VAL1	Deltaïque	L	35	8.3	8.33	83	2.98	57.5	2.0	Ca-HCO3	C2
CPT-VAL2	Deltaïque	L	35	8.4	6.67	23	8.84	198.3	-2.4	Ca-HCO3	C1
OUT020439	Syénite	C	92.1	11.5	8.18	179	0.39	-0.6	-2.0	Na-HCO3	C6
OUT021341	Marbre	L	77.7	9.6	8.09	324	4.23	80.6	-0.4	Na-HCO3	C6
OUT021369	Gneiss	C	85.4	8.9	8.55	87	1.92	48.1	-0.8	Ca-HCO3	C2
OUT021959	Marbre	L	38.1	9.4	6.92	760	1.61	160	15.1		
OUT022124	Gneiss	L	79.3	9.3	9.63	159	1.04	-72.4	21.1		
OUT023118	F-G	L	40.3	11.1	9.11	140	1.31	169.1	4.5	Ca-HCO3	C2
OUT036351	Alluvions	L	22	10.4	7.87	288	0.73	97.1	0.5	Ca-HCO3	C6
OUT036352	Gneiss	L	68.6	9.3	7.51	91	5.38	251.8	1.4	Ca-HCO3	C2
OUT036353	F-G	L	0	9.5	8	373	0.6	45.3	2.9	Ca-HCO3	C4

Echantillon	Aquifère[a]	Confinement[b]	Prof.[c] m	Temp.[d] °C	pH -	C.S.[e] µS/cm	O.D.[f] mg/l	Eh[g] mV	E.N.[h] %	Facies	HCA
OUT036354	Carbonates	C	24	10.1	8.53	181	1.38	15.2	0.4	Na-HCO3	C2
OUT036355	Paragneiss	C	47.5	10.2	7.65	444	2.45	25.7	1.4	Ca-HCO3	C4
OUT036356	Marbre	C	41.3	11	8.72	1420	2.78	36.1	0.2	Na-Cl	C7
OUT036357	Gneiss	NP	54	9.2	7.03	186	4.2	101.1	-5.9	Ca-HCO3	C3
OUT036358	F-G	L	38	8.6	8.43	287	10.27	216	3.3	Ca-HCO3	C3
OUT036359	Syénite	C	0	11	8.89	1650	1.38	108.1	-0.4	Na-Cl	C7
OUT036360	Marbre	C	54.9	9.9	9.1	211	0.11	-225	1.3	Na-HCO3	C6
OUT036361	Marbre	SC	0	8.1	7.07	66	9.67	272.6	10.8		
OUT036362	F-G	L	8.5	8.8	7	38	9.62	91.8	5.2	Ca-HCO3	C1
OUT036363	F-G	C	77.4	10.1	8.87	304	5.77	77.5	15.6		
OUT036364	F-G	C	4.6	15.1	6.26	46	5.55	200.5	8.0	Na-HCO3	C1
OUT036365	Syénite	SC	62.5	8.4	8.36	69	3.03	79.9	4.4	Ca-HCO3	C2
OUT036370	Marbre	SC	94.1	12	8.26	149	0.82	78.6	-0.1	Ca-HCO3	C2
OUT036371	Deltaïque	L	4.6	16.7	6.34	160	2.1	310	-0.7	Ca-mixte	C1
OUT036373	F-G	C	6	27.9	6.98	83	0	240	-2.5	Ca-HCO3	C2
OUT036376	Gneiss	C	91.4	10.5	8.46	820	0.97	38	-1.5	Na-HCO3	C7
PACES-CONV-PON	Paragneiss	L	42.1	9.8	8.55	112	1.96	191.5	-0.9	Ca-HCO3	C2
PUITS-SANDBAY	Paragneiss	C	90	12.1	7.84	391	0.65	-69	3.2	Mixte-HCO3	C6

Tableau A2 : Résultats d'analyses pour les paramètres chimiques 1/4

Echantillon	Ca mg/l	Mg mg/l	Na mg/l	K mg/l	Cl- mg/l	SO4 mg/l	Alc. totale mg/l CaCO3	Fe mg/l	Mn mg/l	Br- mg/l	Sr mg/l	F- mg/l	Ba mg/l
OUT000419	20	2.7	4	1.5	3.9	8.9	54	<0.1	0.0084	<0.1	0.14	<0.1	0.016
OUT003848	29	4.7	7.4	2.2	12	21	75	<0.1	0.00055	<0.1	0.12	<0.1	0.011
OUT004005	54	13	31	3.7	60	19	160	<0.1	0.042	<0.1	0.48	0.2	0.25
OUT004007	35	11	67	7.2	22	64	190	<0.1	0.073	0.1	0.66	0.5	0.1
OUT004013	47	5.2	10	2.1	19	19	120	<0.1	<0.0004	<0.1	0.3	0.1	0.018
OUT004020	18	7.2	28	2.2	29	13	79	<0.1	0.0034	0.1	0.12	0.4	0.02
OUT004087	37	3.3	19	2.1	38	12	78	<0.1	0.0035	<0.1	0.14	<0.1	0.044
OUT016466	5.3	5.2	150	7.9	110	14	220	0.3	0.028	0.5	0.17	1.2	0.015
OUT018365	13	4.3	3	1.3	0.96	13	42	<0.1	<0.0004	<0.1	0.098	0.2	0.017
OUT018375	31	18	280	6.9	400	78	54	0.24	0.31	1	0.54	0.2	0.049
OUT018376	83	18	11	2.9	3	190	130	2.3	0.17	<0.1	1	0.2	0.028
OUT018387	79	13	3.1	4.7	12	24	210	0.41	0.14	<0.1	0.35	0.1	0.15
OUT018393	65	11	11	1.1	5.4	14	160	<0.1	0.005	<0.1	4.8	0.4	0.077
OUT018395	86	12	2.8	1.6	5.5	12	240	<0.1	<0.0004	<0.1	0.12	0.1	0.066
OUT018401	38	9.9	7.9	3.8	1.1	11	140	<0.1	0.048	<0.1	0.39	0.5	0.065
OUT018407	48	3.6	4	1.7	9.6	15	110	<0.1	<0.0004	<0.1	0.34	<0.1	0.022
OUT018662	7.7	5.2	210	7.2	27	37	420	<0.1	0.011	0.1	0.24	1.5	0.072
OUT018746	<0.3	0.05	380	4.7	470	120	240	<0.1	0.00056	3	0.011	2.2	<0.002
OUT018832	45	21	7.9	1.5	16	25	160	<0.1	<0.0004	<0.1	0.8	0.2	0.12
OUT018910	66	5.2	4.4	1.9	4.8	29	140	<0.1	0.0056	<0.1	8.8	0.3	0.18
OUT018925	91	23	64	5.7	82	67	260	<0.1	0.0058	0.2	2	0.2	0.053
OUT019120	78	27	67	4.7	130	28	270	<0.1	0.004	<0.1	0.25	0.2	0.093
OUT019124	25	43	700	20	1000	110	410	0.14	0.017	4	0.77	2.7	0.056
OUT019143	33	4.1	2.5	1.2	1.1	4.6	100	<0.1	0.049	<0.1	0.11	0.2	0.0093
OUT019147	87	6.3	5.1	1.7	2.8	15	210	<0.1	<0.0004	<0.1	0.17	0.1	0.026
OUT019181	160	26	130	3.4	350	80	210	0.54	0.45	<0.5	1.4	0.3	0.71
OUT019200	68	3.3	3.8	3	0.73	14	170	<0.1	<0.0004	<0.1	0.23	0.1	0.011
OUT019283	25	6.1	15	1.8	3.9	11	100	<0.1	0.013	<0.1	0.46	0.2	0.008
OUT019459	17	5.2	59	3.9	38	30	110	<0.1	0.0064	0.2	0.64	0.5	0.17
OUT019536	39	9.4	12	8.2	68	15	61	<0.1	0.01	<0.1	0.57	0.7	0.043
OUT019695	52	14	21	3.4	32	35	120	0.31	0.059	<0.1	0.29	0.4	0.04
OUT019761	22	14	230	6.9	290	110	170	<0.1	0.0099	0.5	3.2	1.1	0.058
OUT019864	120	27	89	4.6	150	120	310	<0.1	0.036	<0.5	10	0.2	0.019
OUT019914	63	17	14	1.2	50	36	160	0.26	0.21	<0.1	0.39	0.2	0.36
OUT020035	62	17	11	1.9	2.3	21	230	<0.1	0.0019	<0.1	0.43	0.3	0.027
OUT020065	64	27	4.1	1.7	5.6	15	260	<0.1	<0.0004	<0.1	0.12	<0.1	0.052
OUT020086	33	2.2	4.2	0.53	0.54	17	79	<0.1	0.02	<0.1	0.8	0.2	0.065
OUT020091	58	12	22	4	48	49	80	<0.1	0.043	<0.1	0.62	0.1	0.017
OUT020318	42	6.6	2.4	3.2	2.1	32	110	<0.1	0.0099	<0.1	0.18	0.2	0.065

Echantillon	Ca mg/l	Mg mg/l	Na mg/l	K mg/l	Cl- mg/l	SO4 mg/l	Alc. totale mg/l CaCO3	Fe mg/l	Mn mg/l	Br- mg/l	Sr mg/l	F- mg/l	Ba mg/l
OUT020341	95	35	49	8.8	51	81	310	<0.1	0.007	0.1	20	0.3	0.047
OUT020412	21	2.9	1.5	1.7	1.1	22	46	<0.1	0.098	<0.1	0.078	<0.1	0.064
OUT020440	4.6	1.1	2.5	1	0.99	6.8	15	<0.1	<0.0004	<0.1	0.032	<0.1	0.0029
OUT020566	60	23	28	6.8	15	17	260	0.66	0.32	<0.1	0.92	0.4	0.15
OUT020694	22	17	89	9.1	8.8	16	300	<0.1	0.019	<0.1	2.1	1.3	0.24
OUT020717	55	6.6	4	0.94	5.7	24	150	<0.1	0.00083	<0.1	0.25	0.2	0.016
OUT020768	57	9.8	5.8	1.3	24	16	140	<0.1	<0.0004	0.2	0.31	0.3	0.75
OUT021157	20	3.2	5.7	1.3	25	8.2	27	<0.1	0.015	<0.1	0.17	0.1	0.035
OUT021327	13	2.8	18	1	1.6	8.5	70	<0.1	0.018	<0.1	0.2	0.4	0.0022
OUT021530	77	22	49	8.3	54	63	100	<0.1	0.009	<0.5	3.3	0.2	0.04
OUT021917	42	28	270	13	420	31	180	0.38	0.036	1	0.61	0.8	0.1
OUT022127	52	1.3	2	0.63	1.8	19	120	<0.1	0.00056	<0.1	1.3	<0.1	0.0069
OUT022187	23	8.5	87	6	39	59	170	<0.1	<0.0004	0.1	1.4	1.1	0.045
OUT022252	23	1.9	1.2	1	0.55	14	79	<0.1	0.0023	<0.1	0.18	1.8	0.0043
OUT022258	21	4.4	5.3	0.87	23	12	40	<0.1	<0.0004	0.1	0.13	0.1	0.011
OUT022274	290	57	620	12	670	970	180	<0.1	0.056	4	7.6	0.6	0.0081
OUT022292	1.9	1.6	250	7.1	45	18	500	<0.1	0.0047	0.2	0.13	3.6	0.024
OUT022510	29	50	860	26	1100	71	440	0.25	0.015	5	1.8	1.4	0.095
OUT022560	120	35	22	3.5	51	68	250	<0.1	0.013	<0.1	31	0.2	0.13
OUT022620	74	9.8	3.8	1.5	0.7	6.3	120	<0.1	<0.0004	<0.1	0.52	<0.1	0.047
OUT022829	42	48	130	9.3	58	92	380	<0.1	0.00065	0.1	0.14	0.1	0.069
OUT022963	43	5.3	14	2.4	9.7	32	110	<0.1	0.038	<0.1	0.21	0.5	<0.002
OUT022995	49	6.3	7.6	2.5	2.2	7.1	170	0.56	0.091	<0.1	0.64	0.5	0.084
OUT023044	33	5.3	7.9	3.8	38	12	62	<0.1	0.036	<0.1	0.25	0.2	0.02
OUT023067	24	5.5	8.6	3.1	1.1	13	85	<0.1	0.041	<0.1	0.22	0.5	0.01
OUT023092	33	7.2	9.5	1.1	1.2	16	120	<0.1	0.0084	<0.1	1.3	0.2	0.15
OUT023108	30	6.6	9.7	7.2	2.1	21	110	3.8	0.2	<0.1	0.18	0.9	0.088
OUT023157	34	13	11	2.3	11	16	100	<0.1	0.0043	<0.1	0.16	0.5	0.011
OUT023259	56	9.7	5.2	2.2	1.3	31	160	<0.1	0.024	<0.1	0.79	0.4	0.032
OUT023496	20	4.5	6.1	1.6	8	9.6	60	<0.1	0.00053	<0.1	0.16	0.2	0.007
OUT023553	33	4.9	13	2.6	0.7	35	96	<0.1	0.0073	<0.1	0.53	0.9	0.084
OUT023574	10	3.5	100	4.7	49	63	160	<0.1	0.0075	0.3	0.96	1.5	0.068
OUT023612	26	3.7	5.5	2	0.82	14	73	<0.1	0.0087	<0.1	0.09	0.2	0.0077
OUT023623	44	11	81	3.5	60	55	190	<0.1	0.025	0.2	2.3	0.9	0.026
OUT025998	37	3.5	4.1	2.1	5	14	94	2.5	0.25	<0.1	0.21	0.1	0.015
OUT026101	100	5.3	220	6.6	380	66	230	<0.1	0.0054	<0.5	0.93	<0.1	0.03
OUT026102	61	19	16	4.2	5.6	26	210	<0.1	0.0045	<0.1	0.34	0.4	0.04
OUT026103	72	10	20	1.7	13	36	220	<0.1	0.0033	<0.1	1.2	0.3	0.097
OUT026104	89	33	460	4.1	670	490	120	0.24	0.006	3	11	1.9	0.012
OUT026105	56	17	69	7.6	21	91	240	<0.1	0.0057	<0.1	4.6	1.2	0.055
OUT026106	84	36	110	7.7	250	49	240	<0.1	0.06	<0.5	3.9	1.3	0.21

Echantillon	Ca mg/l	Mg mg/l	Na mg/l	K mg/l	Cl- mg/l	SO4 mg/l	Alc. totale mg/l CaCO3	Fe mg/l	Mn mg/l	Br- mg/l	Sr mg/l	F- mg/l	Ba mg/l
OUT026107	3.3	1.2	100	3.3	16	37	170	<0.1	0.0029	<0.1	0.3	1.2	0.03
OUT026108	120	15	52	2.6	58	96	220	0.64	0.31	<0.1	0.89	0.1	0.18
OUT026109	81	22	18	3.3	11	13	190	<0.1	<0.0004	<0.1	0.28	0.1	0.043
OUT026110	32	8.5	5.7	1.7	8.2	11	98	<0.1	<0.0004	<0.1	0.1	0.1	0.038
OUT026112	26	5.3	8.2	2.9	14	42	21	<0.1	0.00086	<0.1	0.18	<0.1	0.016
OUT026115	52	17	9.5	10	73	14	110	<0.1	0.022	<0.1	0.66	0.4	0.047
OUT026116	54	10	14	3.3	66	27	94	<0.1	<0.0004	<0.1	0.46	0.1	0.051
OUT026117	9.8	2.9	1.2	1.2	0.75	6	37	<0.1	0.0011	<0.1	0.042	<0.1	0.013
OUT026118	70	10	41	3.9	74	83	140	14	0.34	<0.1	0.22	0.2	0.058
OUT026119	77	5.2	12	1.8	7.1	59	170	<0.1	0.0043	<0.1	2.1	1	0.033
OUT026120	70	4.9	4.6	1.3	15	12	180	<0.1	0.0024	<0.1	0.57	0.1	0.015
OUT026121	50	17	4.5	2.3	25	15	160	0.14	0.035	<0.1	0.14	0.1	0.076
OUT026122	45	7.1	8.4	1.5	11	11	140	<0.1	0.071	<0.1	2.4	1.4	0.46
OUT026123	94	9.6	3	2.1	44	33	200	<0.1	0.34	0.1	0.97	0.6	0.2
OUT026124	180	33	150	7	450	48	310	<0.1	0.026	0.2	1.1	0.1	0.068
OUT026125	22	6.6	7.6	2.5	30	13	36	<0.1	0.00066	0.1	0.19	<0.1	0.012
OUT026126	26	1.6	16	2.5	1.5	29	72	<0.1	0.0013	<0.1	0.35	2.4	0.049
OUT026127	8.8	3.1	54	3.7	5	25	130	<0.1	0.0071	<0.1	0.26	0.9	0.033
OUT026128	33	10	71	6.8	13	37	230	0.19	0.099	<0.1	0.98	0.5	0.1
OUT026129	65	18	15	3.7	27	36	180	0.36	0.15	<0.1	0.22	0.5	0.22
OUT026130	34	19	8.6	7.1	1.1	26	150	0.15	0.011	<0.1	0.69	0.9	0.078
OUT026131	15	9.8	88	8.7	39	40	180	<0.1	0.011	0.2	0.83	1.8	0.063
OUT026132	35	3.4	1.9	1.9	1.9	18	87	0.47	0.11	<0.1	0.13	<0.1	0.033
OUT026135	12	1.6	8.7	1	15	7.6	30	1	0.26	<0.1	0.076	<0.1	0.017
CONV-COL	98	2.4	39	1.2	94	29	190	<0.1	0.033	<0.5	1.1	0.1	0.078
CONV-GAT	160	54	83	6.7	180	120	370	<0.1	0.049	<0.5	47	0.6	0.061
CONV-PAP1	26	6.5	79	3.9	46	13	130	<0.1	0.017	<0.5	0.14	0.5	0.06
CONV-VAL1	34	5.7	3.2	2.5	8.4	22	82	<0.1	0.0058	<0.1	0.11	<0.1	0.055
CPT-GAT1	75	56	16	16	5.3	0.25	470	11	0.63	<0.5	0.56	0.3	0.16
CPT-PON03	24	6	3.2	1.5	2.8	6.2	69	<0.1	0.00055	<0.5	0.071	<0.1	0.05
CPT-VAL1	37	7.1	1.9	1.9	0.39	12	110	<0.1	0.04	<0.1	0.09	0.1	0.024
CPT-VAL2	6.2	1.4	3.1	1	1.6	8.1	14	<0.1	0.0022	<0.1	0.074	<0.1	0.0095
OUT020439	15	2.1	37	2.6	6.9	19	100	<0.1	0.11	<0.5	0.45	2.3	0.062
OUT021341	41	12	55	2.5	12	10	250	0.11	0.3	<0.5	1.8	0.6	0.46
OUT021369	19	0.71	20	1.4	0.6	17	76	<0.1	0.013	<0.5	0.54	1.2	0.019
OUT021959	0.37	0.05	240	0.22	100	110	130	<0.1	0.00063	<0.5	<0.002	0.1	<0.002
OUT022124	0.42	0.05	87	0.76	11	76	27	<0.1	<0.0004	<0.5	<0.002	1.1	<0.002
OUT023118	36	4.8	3.4	1.8	0.7	23	83	<0.1	0.014	<0.5	0.16	0.4	0.053
OUT036351	47	20	35	7.1	18	8.8	250	0.35	0.024	<0.5	3.6	0.7	0.45
OUT036352	25	1.4	2.9	1.2	0.5	15	56	<0.1	<0.0004	<0.5	0.14	0.3	0.0038
OUT036353	74	19	11	3.8	39	48	170	0.31	0.099	<0.5	0.2	0.2	0.19

Echantillon	Ca mg/l	Mg mg/l	Na mg/l	K mg/l	Cl- mg/l	SO4 mg/l	Alc. totale mg/l CaCO3	Fe mg/l	Mn mg/l	Br- mg/l	Sr mg/l	F- mg/l	Ba mg/l
OUT036354	18	8	28	7.1	1	16	130	0.18	0.0083	<0.5	2.4	0.5	0.086
OUT036355	85	25	22	4.5	34	59	240	<0.1	0.0088	<0.5	2.8	0.3	0.2
OUT036356	6.7	11	460	14	350	130	440	<0.1	0.0045	1.3	0.45	2.5	0.061
OUT036357	33	4.7	6.7	1.8	17	30	72	<0.1	0.018	<0.5	0.11	0.4	0.0084
OUT036358	68	16	3.8	2.9	8	24	180	<0.1	<0.0004	<0.5	0.12	0.2	0.11
OUT036359	65	44	370	14	700	25	170	<0.1	0.019	2.6	9.6	0.9	1
OUT036360	10	5.2	82	6	19	17	180	<0.1	0.0072	<0.5	0.35	0.8	0.04
OUT036361	29	3.5	3.6	3.9	1	5.4	69	<0.1	0.00043	<0.5	0.35	0.1	0.086
OUT036362	14	5.4	7.4	1.4	3.6	4.2	57	<0.1	0.00066	<0.5	0.081	0.1	0.012
OUT036363	25	5.3	140	4.5	81	30	140	<0.1	0.0095	<0.5	0.44	1	0.034
OUT036364	8.7	2.3	11	1.6	3	8.3	34	<0.1	0.0021	<0.5	0.077	<0.1	0.019
OUT036365	29	4	4.4	0.99	0.8	7.5	82	0.36	0.063	<0.5	0.15	0.3	0.022
OUT036370	23	6.4	11	3	0.9	18	91	<0.1	0.016	<0.5	0.34	0.4	0.041
OUT036371	33	3.8	9.2	1.5	27	15	40	<0.1	0.021	<0.5	0.1	0.2	0.019
OUT036373	14	4.4	4.8	2.1	0.6	7.5	53	<0.1	0.014	<0.5	0.086	0.2	0.023
OUT036376	13	9	230	8	140	35	360	<0.1	0.0074	0.5	0.73	1.9	0.11
PACES-CONV-PON	23	7.5	3.8	3	6	25	66	<0.1	0.013	<0.5	0.36	0.3	0.11
PUITS-SANDBAY	73	32	65	13	15	67	350	<0.1	0.27	<0.5	0.38	0.5	0.076

Tableau A3 : Résultats d'analyses pour les paramètres chimiques 2/4

Echantillon	S. totaux mg/l H2S	Si mg/l	NO3+NO2 mg/l N	NH4 mg/l N	P-inorg mg/l P	Al mg/l	Li mg/l	Ag mg/l	As mg/l	Be mg/l	Bi mg/l
OUT000419	<0.02	4.9	0.44	0.03	<0.03	0.0037	<0.01	<0.0001	<0.001	<0.0005	<0.00025
OUT003848	<0.02	6.7	0.16	0.04	<0.03	0.0074	<0.01	<0.0001	<0.001	<0.0005	<0.00025
OUT004005	<0.02	5.8	0.04	0.03	<0.03	<0.001	<0.01	<0.0001	<0.001	<0.0005	0.0029
OUT004007	<0.02	6.9	0.05	0.14	<0.03	0.0048	<0.01	<0.0001	<0.001	<0.0005	<0.00025
OUT004013	<0.02	7.1	0.8	0.04	<0.03	0.0024	<0.01	<0.0001	<0.001	<0.0005	<0.00025
OUT004020	<0.02	5.3	<0.02	0.1	<0.03	0.0052	<0.01	<0.0001	<0.001	<0.0005	<0.00025
OUT004087	<0.02	4.2	2.1	0.02	<0.03	0.024	<0.01	<0.0001	<0.001	<0.0005	<0.00025
OUT016466	0.05	3.8	0.02	0.46	0.2	<0.001	<0.01	<0.0001	<0.001	<0.0005	<0.00025
OUT018365	<0.02	6.7	0.44	0.03	<0.03	0.0038	<0.01	<0.0001	<0.001	<0.0005	<0.00025
OUT018375	<0.02	1.1	0.1	0.26	<0.03	0.001	<0.01	<0.0001	<0.001	<0.0005	<0.00025
OUT018376	<0.02	9.6	<0.02	0.09	<0.03	0.001	<0.01	0.00018	<0.001	<0.0005	<0.00025
OUT018387	<0.02	6.7	<0.02	0.04	<0.03	0.001	<0.01	<0.0001	<0.001	<0.0005	<0.00025
OUT018393	<0.02	8.3	<0.02	<0.02	<0.03	<0.001	<0.01	0.00015	<0.001	<0.0005	<0.00025
OUT018395	<0.02	5.6	1.1	<0.02	<0.03	<0.001	<0.01	<0.0001	<0.001	<0.0005	<0.00025
OUT018401	<0.02	8	<0.02	0.08	<0.03	0.001	<0.01	<0.0001	<0.001	<0.0005	<0.00025
OUT018407	<0.02	7.7	2.1	<0.02	<0.03	0.011	<0.01	0.00016	<0.001	<0.0005	<0.00025
OUT018662	0.55	8.2	<0.02	0.98	2.1	<0.001	<0.01	0.00012	<0.001	<0.0005	<0.00025
OUT018746	<0.02	6.9	0.4	0.33	0.05	<0.001	0.014	<0.0001	<0.001	<0.0005	<0.00025
OUT018832	<0.02	9.2	0.97	<0.02	<0.03	<0.001	<0.01	<0.0001	<0.001	<0.0005	<0.00025
OUT018910	<0.02	5.7	0.09	0.02	<0.03	0.0018	0.01	<0.0001	<0.001	<0.0005	<0.00025
OUT018925	<0.02	3.9	0.8	0.13	<0.03	0.0024	0.024	<0.0001	<0.001	<0.0005	<0.00025
OUT019120	<0.02	7	0.5	<0.02	<0.03	0.0094	<0.01	0.00023	<0.001	<0.0005	<0.00025
OUT019124	0.14	6.6	0.2	1.6	1.3	0.0027	<0.01	<0.0001	<0.001	<0.0005	<0.00025
OUT019143	0.04	7.9	<0.02	0.12	<0.03	<0.001	<0.01	<0.0001	<0.001	<0.0005	<0.00025
OUT019147	<0.02	7.3	3.6	0.03	<0.03	0.0017	<0.01	<0.0001	<0.001	<0.0005	<0.00025
OUT019181	<0.02	4	1.2	0.05	<0.03	<0.001	<0.01	0.00015	<0.001	<0.0005	0.00031
OUT019200	<0.02	7.2	0.7	0.05	<0.03	0.001	<0.01	<0.0001	<0.001	<0.0005	<0.00025
OUT019283	<0.02	4.9	<0.02	0.06	<0.03	<0.001	<0.01	<0.0001	<0.001	<0.0005	<0.00025
OUT019459	0.05	6.1	<0.02	0.16	0.04	0.003	<0.01	<0.0001	<0.001	<0.0005	<0.00025
OUT019536	0.32	5.8	<0.02	0.13	<0.03	0.0094	<0.01	<0.0001	<0.001	<0.0005	<0.00025
OUT019695	<0.02	9.5	<0.02	0.1	<0.03	0.0017	<0.01	<0.0001	<0.001	<0.0005	<0.00025
OUT019761	0.08	6.5	0.1	0.2	<0.03	<0.001	0.014	<0.0001	<0.001	<0.0005	<0.00025
OUT019864	<0.02	5.2	0.05	0.13	<0.03	<0.001	0.019	<0.0001	<0.001	<0.0005	<0.00025
OUT019914	<0.02	4.1	0.12	<0.02	<0.03	0.0018	<0.01	<0.0001	<0.001	<0.0005	<0.00025
OUT020035	<0.02	10	1.1	<0.02	<0.03	0.0032	<0.01	<0.0001	<0.001	<0.0005	<0.00025
OUT020065	<0.02	6.7	0.56	<0.02	<0.03	<0.001	<0.01	0.00014	<0.001	<0.0005	<0.00025
OUT020086	<0.02	3.9	<0.02	0.08	<0.03	0.0055	<0.01	<0.0001	<0.001	<0.0005	<0.00025
OUT020091	<0.02	6.5	16	0.04	<0.03	0.0046	<0.01	<0.0001	<0.001	<0.0005	<0.00025
OUT020318	<0.02	5.8	0.03	0.03	<0.03	<0.001	<0.01	<0.0001	<0.001	<0.0005	<0.00025

Echantillon	S. totaux mg/l H2S	Si mg/l	NO3+NO2 mg/l N	NH4 mg/l N	P-inorg mg/l P	Al mg/l	Li mg/l	Ag mg/l	As mg/l	Be mg/l	Bi mg/l
OUT020341	<0.02	5.6	<0.02	0.4	<0.03	1.6	0.017	0.00026	<0.001	<0.0005	<0.00025
OUT020412	0.02	5.9	<0.02	0.05	<0.03	0.0044	<0.01	<0.0001	<0.001	<0.0005	<0.00025
OUT020440	<0.02	5.6	0.1	0.06	<0.03	0.0028	<0.01	<0.0001	<0.001	<0.0005	<0.00025
OUT020566	<0.02	9	0.04	0.09	<0.03	0.0077	<0.01	<0.0001	<0.001	<0.0005	<0.00025
OUT020694	0.05	8.6	<0.02	0.41	0.23	<0.001	<0.01	<0.0001	<0.001	<0.0005	<0.00025
OUT020717	<0.02	6.3	0.85	<0.02	<0.03	<0.001	<0.01	<0.0001	<0.001	<0.0005	<0.00025
OUT020768	<0.02	2.5	2.6	0.08	<0.03	<0.001	<0.01	<0.0001	<0.001	<0.0005	<0.00025
OUT021157	<0.02	4.6	4.4	0.04	<0.03	0.019	<0.01	<0.0001	<0.001	<0.0005	<0.00025
OUT021327	<0.02	<0.1	<0.02	0.02	<0.03	0.006	<0.01	0.00019	<0.001	<0.0005	<0.00025
OUT021530	<0.02	5.7	0.5	0.11	<0.03	<0.001	0.022	<0.0001	<0.001	<0.0005	<0.00025
OUT021917	<0.02	8.6	0.1	0.6	<0.03	<0.001	<0.01	<0.0001	<0.001	<0.0005	<0.00025
OUT022127	<0.02	3.2	0.31	<0.02	<0.03	0.0058	<0.01	<0.0001	<0.001	<0.0005	<0.00025
OUT022187	<0.02	7.7	0.07	0.14	<0.03	0.32	<0.01	<0.0001	<0.001	<0.0005	<0.00025
OUT022252	<0.02	6.4	0.06	0.05	<0.03	0.001	<0.01	<0.0001	<0.001	<0.0005	<0.00025
OUT022258	<0.02	7.3	0.13	0.05	<0.03	0.0032	<0.01	<0.0001	<0.001	<0.0005	<0.00025
OUT022274	<0.02	8.5	0.05	0.44	<0.03	<0.01	<0.01	<0.0001	<0.001	<0.0005	<0.00025
OUT022292	0.06	7.7	<0.02	0.27	0.3	0.015	<0.01	<0.0001	<0.001	<0.0005	<0.00025
OUT022510	<0.02	7.8	0.2	1.6	0.07	0.0017	0.017	<0.0001	<0.001	<0.0005	<0.00025
OUT022560	<0.02	9.5	0.02	0.02	<0.03	<0.001	0.013	<0.0001	<0.001	<0.0005	<0.00025
OUT022620	<0.02	8.2	<0.02	<0.02	<0.03	<0.001	<0.01	<0.0001	<0.001	<0.0005	<0.00025
OUT022829	<0.02	3.3	3.8	0.04	<0.03	<0.001	<0.01	0.0001	<0.001	<0.0005	<0.00025
OUT022963	<0.02	8.5	<0.02	0.02	<0.03	0.001	<0.01	<0.0001	<0.001	<0.0005	<0.00025
OUT022995	<0.02	9.4	<0.02	0.03	<0.03	0.014	<0.01	<0.0001	<0.001	<0.0005	<0.00025
OUT023044	<0.02	5.5	2.1	0.07	<0.03	0.0055	<0.01	<0.0001	<0.001	<0.0005	<0.00025
OUT023067	<0.02	8.1	0.09	0.09	<0.03	0.0011	<0.01	0.00024	<0.001	<0.0005	<0.00025
OUT023092	<0.02	3.7	<0.02	0.03	<0.03	0.0075	<0.01	<0.0001	<0.001	<0.0005	<0.00025
OUT023108	<0.02	7.3	<0.02	0.08	<0.03	0.0024	<0.01	<0.0001	<0.001	<0.0005	<0.00025
OUT023157	0.015	12	7.5	0.06	<0.03	<0.001	<0.01	<0.0001	<0.001	<0.0005	<0.00025
OUT023259	<0.02	6.3	0.04	<0.02	<0.03	<0.001	<0.01	<0.0001	<0.001	<0.0005	<0.00025
OUT023496	<0.02	4.8	0.16	<0.02	<0.03	0.0029	<0.01	0.00014	<0.001	<0.0005	<0.00025
OUT023553	<0.02	6.4	0.15	0.02	<0.03	<0.001	<0.01	0.00012	<0.001	<0.0005	<0.00025
OUT023574	<0.02	5.7	0.03	0.07	<0.03	<0.001	<0.01	<0.0001	<0.001	<0.0005	<0.00025
OUT023612	<0.02	6.7	<0.02	0.05	<0.03	0.0019	<0.01	<0.0001	<0.001	<0.0005	<0.00025
OUT023623	<0.02	6.1	0.11	0.03	<0.03	0.016	0.011	<0.0001	<0.001	<0.0005	<0.00025
OUT025998	<0.02	7.9	0.08	0.06	<0.03	<0.001	<0.01	0.00015	<0.001	<0.0005	<0.00025
OUT026101	<0.02	4.7	1	0.03	<0.03	0.0062	<0.01	<0.0001	<0.001	<0.0005	<0.00025
OUT026102	<0.02	7.6	0.07	0.03	<0.03	0.0029	0.01	<0.0001	<0.001	<0.0005	<0.00025
OUT026103	<0.02	4.3	0.05	<0.02	<0.03	<0.001	<0.01	<0.0001	<0.001	<0.0005	<0.00025
OUT026104	<0.02	4	0.2	0.13	<0.03	<0.001	0.26	<0.0001	<0.001	<0.0005	<0.00025
OUT026105	<0.02	8.1	0.05	0.03	<0.03	<0.001	<0.01	0.00014	<0.001	<0.0005	<0.00025
OUT026106	<0.02	7.6	0.05	0.06	<0.03	<0.001	0.01	0.00026	<0.001	<0.0005	<0.00025

Echantillon	S. totaux mg/l H2S	Si mg/l	NO3+NO2 mg/l N	NH4 mg/l N	P-inorg mg/l P	Al mg/l	Li mg/l	Ag mg/l	As mg/l	Be mg/l	Bi mg/l
OUT026107	<0.02	6.1	<0.02	0.12	<0.03	<0.001	<0.01	0.00011	<0.001	<0.0005	<0.00025
OUT026108	<0.02	5.7	0.02	0.1	<0.03	<0.001	<0.01	<0.0001	<0.001	<0.0005	<0.00025
OUT026109	<0.02	10	2.6	<0.02	<0.03	0.001	<0.01	<0.0001	<0.001	<0.0005	<0.00025
OUT026110	<0.02	6	0.61	0.02	<0.03	0.001	<0.01	<0.0001	<0.001	<0.0005	<0.00025
OUT026112	<0.02	6.7	7.8	0.02	<0.03	0.0047	<0.01	<0.0001	<0.001	<0.0005	<0.00025
OUT026115	<0.02	6.8	0.03	0.07	<0.03	0.03	<0.01	<0.0001	<0.001	<0.0005	<0.00025
OUT026116	<0.02	7.5	3.5	<0.02	<0.03	<0.001	<0.01	<0.0001	<0.001	<0.0005	<0.00025
OUT026117	<0.02	5.4	0.03	<0.02	<0.03	0.0013	<0.01	<0.0001	<0.001	<0.0005	<0.00025
OUT026118	0.05	8.9	<0.02	0.1	<0.03	0.0064	<0.01	0.00022	<0.001	<0.0005	<0.00025
OUT026119	<0.02	7.2	0.33	<0.02	<0.03	0.0045	<0.01	0.00015	<0.001	<0.0005	<0.00025
OUT026120	<0.02	5.6	0.2	<0.02	<0.03	<0.001	<0.01	0.00021	<0.001	<0.0005	<0.00025
OUT026121	<0.02	8.1	<0.02	<0.02	<0.03	<0.001	<0.01	0.00012	<0.001	<0.0005	<0.00025
OUT026122	<0.02	4.5	<0.02	<0.02	<0.03	0.0061	0.01	0.00014	<0.001	<0.0005	<0.00025
OUT026123	<0.02	7.6	0.02	<0.02	<0.03	0.002	0.012	0.00019	<0.001	<0.0005	<0.00025
OUT026124	<0.02	11	0.8	<0.02	<0.03	0.011	0.023	0.00039	<0.001	<0.0005	<0.00025
OUT026125	<0.02	11	4.8	<0.02	<0.03	0.48	<0.01	<0.0001	<0.001	<0.0005	<0.00025
OUT026126	<0.02	5.1	0.17	<0.02	<0.03	0.0053	<0.01	<0.0001	<0.001	<0.0005	<0.00025
OUT026127	<0.02	5.2	<0.02	0.07	<0.03	0.0051	<0.01	<0.0001	<0.001	<0.0005	<0.00025
OUT026128	<0.02	6.8	<0.02	0.2	<0.03	0.0034	<0.01	<0.0001	<0.001	<0.0005	<0.00025
OUT026129	<0.02	9.3	<0.02	3.2	<0.03	0.0031	<0.01	<0.0001	<0.001	<0.0005	<0.00025
OUT026130	<0.02	11	<0.02	0.15	<0.03	0.0053	<0.01	<0.0001	<0.001	<0.0005	<0.00025
OUT026131	<0.02	6.3	<0.02	0.15	<0.03	0.0027	<0.01	<0.0001	0.0013	<0.0005	<0.00025
OUT026132	<0.02	6.3	<0.02	0.02	<0.03	<0.001	<0.01	<0.0001	<0.001	<0.0005	<0.00025
OUT026135	<0.02	5.4	0.8	0.21	<0.03	0.02	<0.01	<0.0001	<0.001	<0.0005	<0.00025
CONV-COL	<0.02	6	0.2	<0.02	<0.03	<0.01	<0.01	<0.0001	<0.001	<0.0005	<0.00025
CONV-GAT	<0.02	10	0.3	<0.02	<0.03	<0.01	0.052	<0.0001	<0.001	<0.0005	<0.00025
CONV-PAP1	<0.02	6.6	0.05	0.19	0.08	<0.01	<0.01	<0.0001	0.0016	<0.0005	<0.00025
CONV-VAL1	<0.02	7.4	0.79	0.05	<0.03	<0.01	<0.01	<0.0001	<0.001	<0.0005	<0.00025
CPT-GAT1	<0.02	22	0.05	6.4	0.4	<0.01	0.014	0.00062	<0.001	<0.0005	<0.00025
CPT-PON03	<0.02	5.7	1.6	<0.02	<0.03	<0.01	<0.01	<0.0001	<0.001	<0.0005	<0.00025
CPT-VAL1	<0.02	7.1	<0.02	0.07	<0.03	<0.01	<0.01	<0.0001	<0.001	<0.0005	<0.00025
CPT-VAL2	<0.02	7.4	1.7	0.04	<0.03	<0.01	<0.01	<0.0001	<0.001	<0.0005	<0.00025
OUT020439	0.04	6.3	<0.1	1.1	<0.03	<0.01	<0.01	<0.0001	<0.001	<0.0005	<0.00025
OUT021341	<0.02	8.9	<0.1	0.14	<0.03	<0.01	<0.01	<0.0001	<0.001	<0.0005	<0.00025
OUT021369	<0.02	4.2	<0.1	<0.02	0.11	<0.01	<0.01	<0.0001	<0.001	<0.0005	<0.00025
OUT021959	<0.02	6.4	0.1	<0.02	<0.03	<0.01	<0.01	<0.0001	<0.001	<0.0005	<0.00025
OUT022124	<0.02	7.9	<0.1	0.04	<0.03	<0.01	<0.01	<0.0001	<0.001	<0.0005	<0.00025
OUT023118	<0.02	8.8	<0.1	0.07	<0.03	<0.01	<0.01	<0.0001	<0.001	<0.0005	<0.00025
OUT036351	<0.02	7.7	<0.1	0.18	<0.03	<0.01	<0.01	<0.0001	<0.001	<0.0005	<0.00025
OUT036352	<0.02	3.8	0.3	<0.02	<0.03	<0.01	<0.01	<0.0001	<0.001	<0.0005	<0.00025
OUT036353	<0.02	7.6	<0.1	0.11	<0.03	<0.01	<0.01	<0.0001	<0.001	<0.0005	<0.00025

Echantillon	S. totaux mg/l H2S	Si mg/l	NO3+NO2 mg/l N	NH4 mg/l N	P-inorg mg/l P	Al mg/l	Li mg/l	Ag mg/l	As mg/l	Be mg/l	Bi mg/l
OUT036354	0.05	6.6	<0.1	0.34	0.06	<0.01	<0.01	<0.0001	<0.001	<0.0005	<0.00025
OUT036355	<0.02	6.6	3.2	<0.02	<0.03	<0.01	0.014	<0.0001	<0.001	<0.0005	<0.00025
OUT036356	<0.02	7.8	<0.1	0.45	0.18	<0.01	<0.01	<0.0001	<0.001	<0.0005	<0.00025
OUT036357	<0.02	7.4	1.5	0.02	<0.03	<0.01	<0.01	<0.0001	<0.001	<0.0005	<0.00025
OUT036358	<0.02	6.4	4.2	<0.02	<0.03	<0.01	<0.01	<0.0001	<0.001	<0.0005	<0.00025
OUT036359	<0.02	7.7	0.1	1.2	<0.03	<0.01	<0.01	<0.0001	<0.001	<0.0005	<0.00025
OUT036360	<0.02	6.6	<0.1	0.07	<0.03	<0.01	<0.01	<0.0001	<0.001	<0.0005	<0.00025
OUT036361	<0.02	6	1.2	0.04	<0.03	<0.01	<0.01	<0.0001	<0.001	<0.0005	<0.00025
OUT036362	<0.02	5.2	0.3	0.04	<0.03	0.012	<0.01	<0.0001	<0.001	<0.0005	<0.00025
OUT036363	<0.02	6.5	<0.1	0.39	0.06	<0.01	<0.01	<0.0001	<0.001	<0.0005	<0.00025
OUT036364	<0.02	7.2	0.5	0.04	<0.03	<0.01	<0.01	<0.0001	<0.001	<0.0005	<0.00025
OUT036365	<0.02	6.2	<0.1	0.04	<0.03	<0.01	<0.01	<0.0001	<0.001	<0.0005	<0.00025
OUT036370	<0.02	8.6	<0.1	0.03	<0.03	<0.01	<0.01	<0.0001	<0.001	<0.0005	<0.00025
OUT036371	<0.02	4.5	7.7	0.1	0.14	0.025	<0.01	<0.0001	<0.001	<0.0005	<0.00025
OUT036373	<0.02	13	2.1	<0.02	<0.03	<0.01	<0.01	<0.0001	<0.001	<0.0005	<0.00025
OUT036376	0.09	7.8	<0.1	0.43	0.86	<0.01	<0.01	<0.0001	<0.001	<0.0005	<0.00025
PACES-CONV-PON	<0.02	5.4	0.4	<0.02	<0.03	<0.01	<0.01	<0.0001	<0.001	<0.0005	<0.00025
PUITS-SANDBAY	<0.02	10	0.3	0.2	0.06	<0.01	<0.01	<0.0001	<0.001	<0.0005	<0.00025

Tableau A4 : Résultats d'analyses pour les paramètres chimiques 3/4

Echantillon	Cd mg/l	Co mg/l	Cr mg/l	Cu mg/l	Mo mg/l	Ni mg/l	Pb mg/l	Sb mg/l	Se mg/l	Sn mg/l	Ti mg/l	U mg/l
OUT000419	<0.0002	<0.0005	<0.0005	0.00077	<0.0005	<0.001	0.00024	<0.001	<0.001	<0.001	<0.001	<0.001
OUT003848	<0.0002	<0.0005	0.00087	0.0023	0.0014	0.0032	0.00023	<0.001	<0.001	<0.001	<0.001	0.0025
OUT004005	0.00026	<0.0005	0.0018	0.0055	0.00058	0.0065	0.0027	<0.001	<0.001	0.0011	<0.001	<0.001
OUT004007	<0.0002	<0.0005	0.00058	0.00061	0.0013	<0.001	<0.0001	<0.001	<0.001	<0.001	<0.001	<0.001
OUT004013	<0.0002	<0.0005	0.00072	<0.0005	0.00054	<0.001	<0.0001	<0.001	<0.001	<0.001	<0.001	0.0017
OUT004020	<0.0002	<0.0005	0.00064	<0.0005	0.00073	<0.001	<0.0001	<0.001	<0.001	<0.001	<0.001	<0.001
OUT004087	<0.0002	0.00052	0.00095	0.0028	<0.0005	0.005	0.0015	<0.001	<0.001	<0.001	<0.001	<0.001
OUT016466	<0.0002	<0.0005	<0.0005	<0.0005	0.0016	<0.001	<0.0001	<0.001	<0.001	<0.001	0.0025	<0.001
OUT018365	<0.0002	<0.0005	0.0023	<0.0005	0.00091	<0.001	<0.0001	<0.001	<0.001	<0.001	<0.001	<0.001
OUT018375	<0.0002	<0.0005	<0.0005	<0.0005	0.0027	<0.001	<0.0001	<0.001	<0.001	<0.001	<0.001	<0.001
OUT018376	<0.0002	<0.0005	0.00056	<0.0005	0.0013	<0.001	<0.0001	<0.001	<0.001	<0.001	<0.001	<0.001
OUT018387	<0.0002	<0.0005	<0.0005	<0.0005	0.0019	<0.001	<0.0001	<0.001	<0.001	<0.001	<0.001	0.0011
OUT018393	<0.0002	<0.0005	0.00062	0.0096	0.0035	<0.001	<0.0001	<0.001	<0.001	<0.001	<0.001	0.0032
OUT018395	<0.0002	<0.0005	0.00081	<0.0005	0.0013	<0.001	<0.0001	<0.001	<0.001	<0.001	<0.001	0.0013
OUT018401	<0.0002	<0.0005	<0.0005	<0.0005	0.0034	<0.001	<0.0001	<0.001	<0.001	<0.001	<0.001	0.003
OUT018407	<0.0002	<0.0005	0.0029	<0.0005	0.015	<0.001	<0.0001	<0.001	<0.001	<0.001	<0.001	0.0013
OUT018662	<0.0002	<0.0005	0.0017	0.0006	0.0012	<0.001	<0.0001	<0.001	<0.001	<0.001	<0.001	<0.001
OUT018746	<0.0002	<0.0005	<0.0005	0.0006	0.0023	<0.001	0.00032	<0.001	<0.001	<0.001	<0.001	0.0015
OUT018832	<0.0002	<0.0005	<0.0005	0.0022	0.00052	<0.001	0.0004	<0.001	<0.001	<0.001	<0.001	<0.001
OUT018910	<0.0002	<0.0005	<0.0005	0.011	0.003	<0.001	0.00029	<0.001	<0.001	<0.001	<0.001	0.0087
OUT018925	<0.0002	<0.0005	<0.0005	0.0025	<0.0005	<0.001	<0.0001	<0.001	<0.001	<0.001	<0.001	<0.001
OUT019120	<0.0002	<0.0005	<0.0005	<0.0005	0.0026	<0.001	0.0002	<0.001	0.0014	<0.001	<0.001	<0.001
OUT019124	<0.0002	<0.0005	0.0011	0.00083	0.0043	<0.001	0.00014	<0.001	<0.001	<0.001	<0.001	<0.001
OUT019143	<0.0002	<0.0005	<0.0005	<0.0005	0.00054	0.0015	<0.0001	<0.001	<0.001	<0.001	<0.001	<0.001
OUT019147	<0.0002	<0.0005	<0.0005	0.0045	<0.0005	<0.001	0.00054	<0.001	<0.001	<0.001	<0.001	<0.001
OUT019181	<0.0002	<0.0005	<0.0005	0.028	0.003	0.0016	0.00022	<0.001	<0.001	<0.001	<0.001	0.0014
OUT019200	<0.0002	<0.0005	<0.0005	0.0086	0.00075	<0.001	0.00016	<0.001	<0.001	<0.001	<0.001	0.0062
OUT019283	<0.0002	<0.0005	<0.0005	<0.0005	<0.0005	<0.001	<0.0001	<0.001	<0.001	<0.001	<0.001	0.002
OUT019459	<0.0002	<0.0005	<0.0005	<0.0005	0.0014	<0.001	<0.0001	<0.001	<0.001	<0.001	<0.001	<0.001
OUT019536	<0.0002	<0.0005	<0.0005	<0.0005	0.00081	<0.001	0.00023	<0.001	<0.001	<0.001	<0.001	<0.001
OUT019695	<0.0002	<0.0005	<0.0005	<0.0005	0.00076	<0.001	<0.0001	<0.001	<0.001	<0.001	<0.001	<0.001
OUT019761	<0.0002	<0.0005	<0.0005	0.0015	0.0019	0.0039	0.00024	<0.001	<0.001	<0.001	<0.001	0.0013
OUT019864	<0.0002	<0.0005	<0.0005	0.00066	<0.0005	0.0026	0.00015	<0.001	<0.001	<0.001	<0.001	<0.001
OUT019914	<0.0002	0.00055	<0.0005	0.012	0.001	0.0055	0.00072	<0.001	<0.001	<0.001	0.0018	0.046
OUT020035	<0.0002	<0.0005	0.0021	0.013	0.0014	<0.001	<0.0001	<0.001	<0.001	<0.001	<0.001	0.0026
OUT020065	<0.0002	<0.0005	0.00083	0.017	0.0023	<0.001	<0.0001	<0.001	<0.001	<0.001	<0.001	<0.001
OUT020086	<0.0002	<0.0005	<0.0005	<0.0005	<0.0005	<0.001	<0.0001	<0.001	<0.001	<0.001	<0.001	<0.001
OUT020091	<0.0002	0.00059	0.001	0.017	<0.0005	0.0034	0.00081	<0.001	<0.001	<0.001	<0.001	<0.001
OUT020318	<0.0002	<0.0005	<0.0005	<0.0005	0.0011	<0.001	<0.0001	<0.001	<0.001	<0.001	<0.001	<0.001

Echantillon	Cd mg/l	Co mg/l	Cr mg/l	Cu mg/l	Mo mg/l	Ni mg/l	Pb mg/l	Sb mg/l	Se mg/l	Sn mg/l	Ti mg/l	U mg/l
OUT020341	<0.0002	<0.0005	<0.0005	0.0078	0.0028	0.018	0.00052	<0.001	<0.001	<0.001	<0.001	<0.001
OUT020412	<0.0002	<0.0005	<0.0005	<0.0005	0.001	<0.001	<0.0001	<0.001	<0.001	<0.001	<0.001	<0.001
OUT020440	<0.0002	<0.0005	<0.0005	0.0011	<0.0005	<0.001	<0.0001	<0.001	<0.001	<0.001	<0.001	<0.001
OUT020566	<0.0002	<0.0005	<0.0005	<0.0005	0.0012	<0.001	<0.0001	<0.001	<0.001	<0.001	<0.001	0.0012
OUT020694	<0.0002	<0.0005	<0.0005	<0.0005	0.001	<0.001	<0.0001	<0.001	<0.001	<0.001	<0.001	<0.001
OUT020717	<0.0002	<0.0005	<0.0005	0.0015	<0.0005	0.0032	0.00026	<0.001	<0.001	<0.001	<0.001	0.0039
OUT020768	<0.0002	<0.0005	<0.0005	0.0031	<0.0005	<0.001	0.00014	<0.001	<0.001	<0.001	<0.001	0.0019
OUT021157	<0.0002	<0.0005	0.001	0.049	<0.0005	<0.001	0.0023	<0.001	<0.001	<0.001	<0.001	<0.001
OUT021327	<0.0002	<0.0005	<0.0005	<0.0005	0.0021	<0.001	0.00014	<0.001	<0.001	0.0011	<0.001	<0.001
OUT021530	<0.0002	<0.0005	<0.0005	0.0019	0.0017	0.0019	<0.0001	<0.001	<0.001	<0.001	<0.001	<0.001
OUT021917	<0.0002	<0.0005	<0.0005	<0.0005	0.003	<0.001	<0.0001	<0.001	<0.001	<0.001	<0.001	<0.001
OUT022127	<0.0002	<0.0005	<0.0005	0.0012	<0.0005	0.0041	0.00013	<0.001	<0.001	<0.001	<0.001	<0.001
OUT022187	<0.0002	<0.0005	<0.0005	<0.0005	0.0071	<0.001	<0.0001	<0.001	<0.001	<0.001	<0.001	0.0026
OUT022252	<0.0002	<0.0005	<0.0005	<0.0005	<0.0005	<0.001	<0.0001	<0.001	<0.001	<0.001	<0.001	0.0015
OUT022258	<0.0002	<0.0005	<0.0005	0.0059	<0.0005	<0.001	0.00052	<0.001	<0.001	<0.001	<0.001	<0.001
OUT022274	<0.0002	<0.0005	<0.0005	<0.0005	0.0025	<0.001	<0.0001	<0.001	<0.001	<0.001	<0.001	<0.001
OUT022292	<0.0002	<0.0005	<0.0005	<0.0005	0.0089	<0.001	<0.0001	<0.001	<0.001	<0.001	<0.001	0.0027
OUT022510	<0.0002	<0.0005	<0.0005	<0.0005	0.0013	<0.001	<0.0001	<0.001	<0.001	<0.001	<0.001	0.0025
OUT022560	<0.0002	<0.0005	0.001	<0.0005	<0.0005	<0.001	<0.0001	<0.001	<0.001	<0.001	<0.001	<0.001
OUT022620	<0.0002	<0.0005	0.0024	<0.0005	<0.0005	<0.001	0.00019	<0.001	<0.001	<0.001	<0.001	<0.001
OUT022829	<0.0002	<0.0005	<0.0005	0.013	<0.0005	<0.001	0.00023	<0.001	<0.001	<0.001	<0.001	0.0019
OUT022963	<0.0002	<0.0005	0.0012	<0.0005	0.00084	0.0035	<0.0001	<0.001	<0.001	<0.001	<0.001	0.0092
OUT022995	<0.0002	<0.0005	0.00052	<0.0005	0.0019	<0.001	<0.0001	0.001	<0.001	<0.001	<0.001	0.0095
OUT023044	<0.0002	<0.0005	0.00081	<0.0005	0.0019	0.0039	0.00015	<0.001	<0.001	<0.001	<0.001	<0.001
OUT023067	<0.0002	<0.0005	<0.0005	<0.0005	0.0014	<0.001	0.00011	<0.001	<0.001	<0.001	<0.001	<0.001
OUT023092	<0.0002	<0.0005	0.0012	<0.0005	<0.0005	0.0016	0.00033	<0.001	<0.001	<0.001	<0.001	0.002
OUT023108	<0.0002	<0.0005	0.00075	<0.0005	0.0039	<0.001	<0.0001	<0.001	<0.001	<0.001	<0.001	<0.001
OUT023157	<0.0002	<0.0005	<0.0005	0.0091	0.25	<0.001	0.00045	<0.001	<0.001	<0.001	<0.001	0.025
OUT023259	<0.0002	<0.0005	<0.0005	<0.0005	0.00069	0.0064	0.00029	<0.001	<0.001	<0.001	<0.001	0.0014
OUT023496	<0.0002	<0.0005	<0.0005	<0.0005	<0.0005	<0.001	<0.0001	<0.001	<0.001	<0.001	<0.001	<0.001
OUT023553	<0.0002	<0.0005	<0.0005	0.0082	0.00055	0.0023	0.00067	<0.001	<0.001	<0.001	<0.001	0.037
OUT023574	0.0036	<0.0005	<0.0005	<0.0005	<0.0005	0.0015	0.00015	<0.001	<0.001	<0.001	<0.001	<0.001
OUT023612	<0.0002	<0.0005	<0.0005	<0.0005	0.0017	<0.001	<0.0001	<0.001	<0.001	<0.001	<0.001	0.0021
OUT023623	<0.0002	<0.0005	0.00065	<0.0005	0.0036	<0.001	<0.0001	<0.001	<0.001	<0.001	<0.001	0.022
OUT025998	<0.0002	<0.0005	<0.0005	<0.0005	0.0013	<0.001	<0.0001	<0.001	<0.001	<0.001	<0.001	<0.001
OUT026101	<0.0002	<0.0005	<0.0005	0.017	<0.0005	0.0017	0.00065	<0.001	<0.001	<0.001	<0.001	<0.001
OUT026102	<0.0002	<0.0005	<0.0005	<0.0005	0.002	<0.001	<0.0001	<0.001	<0.001	<0.001	<0.001	0.0019
OUT026103	<0.0002	<0.0005	<0.0005	0.0011	0.0006	0.0015	<0.0001	<0.001	<0.001	<0.001	<0.001	<0.001
OUT026104	<0.0002	<0.0005	<0.0005	<0.0005	0.00093	<0.001	0.00015	<0.001	<0.001	<0.001	<0.001	<0.001
OUT026105	<0.0002	<0.0005	<0.0005	0.0027	0.0017	<0.001	0.00033	<0.001	<0.001	<0.001	<0.001	<0.001
OUT026106	<0.0002	<0.0005	<0.0005	0.0064	<0.0005	<0.001	0.00049	<0.001	<0.001	<0.001	<0.001	0.0013

Echantillon	Cd mg/l	Co mg/l	Cr mg/l	Cu mg/l	Mo mg/l	Ni mg/l	Pb mg/l	Sb mg/l	Se mg/l	Sn mg/l	Ti mg/l	U mg/l
OUT026107	<0.0002	<0.0005	<0.0005	<0.0005	<0.0005	<0.001	<0.0001	<0.001	<0.001	<0.001	<0.001	<0.001
OUT026108	<0.0002	0.00062	0.021	<0.0005	<0.0005	0.0065	<0.0001	<0.001	<0.001	<0.001	<0.001	<0.001
OUT026109	<0.0002	<0.0005	0.0014	0.0047	0.0014	<0.001	0.00019	<0.001	<0.001	<0.001	<0.001	<0.001
OUT026110	<0.0002	<0.0005	<0.0005	0.0012	<0.0005	<0.001	0.00025	<0.001	<0.001	<0.001	<0.001	<0.001
OUT026112	<0.0002	<0.0005	0.0014	0.0025	<0.0005	0.0012	0.00034	<0.001	<0.001	<0.001	<0.001	<0.001
OUT026115	<0.0002	<0.0005	0.001	<0.0005	0.0008	<0.001	<0.0001	<0.001	<0.001	<0.001	<0.001	<0.001
OUT026116	<0.0002	<0.0005	0.0046	<0.0005	0.00099	<0.001	0.00028	<0.001	<0.001	<0.001	<0.001	<0.001
OUT026117	<0.0002	<0.0005	0.0012	0.033	<0.0005	<0.001	<0.0001	<0.001	<0.001	<0.001	<0.001	<0.001
OUT026118	<0.0002	<0.0005	<0.0005	<0.0005	0.0034	<0.001	<0.0001	<0.001	<0.001	<0.001	<0.001	<0.001
OUT026119	<0.0002	<0.0005	0.00057	0.023	0.0026	0.0047	0.00017	<0.001	<0.001	<0.001	<0.001	0.016
OUT026120	<0.0002	<0.0005	<0.0005	0.013	0.0023	<0.001	<0.0001	<0.001	<0.001	<0.001	<0.001	<0.001
OUT026121	<0.0002	<0.0005	<0.0005	<0.0005	0.0023	<0.001	<0.0001	<0.001	<0.001	<0.001	<0.001	0.001
OUT026122	<0.0002	<0.0005	<0.0005	<0.0005	0.0016	<0.001	0.00023	<0.001	<0.001	<0.001	<0.001	0.021
OUT026123	<0.0002	<0.0005	<0.0005	<0.0005	0.0017	<0.001	<0.0001	<0.001	<0.001	<0.001	<0.001	0.0097
OUT026124	<0.0002	<0.0005	<0.0005	0.013	0.0076	0.0014	0.00085	<0.001	0.0066	<0.001	<0.001	0.0017
OUT026125	<0.0002	<0.0005	<0.0005	<0.0005	<0.0005	0.0017	0.00023	<0.001	<0.001	<0.001	<0.001	<0.001
OUT026126	<0.0002	<0.0005	<0.0005	<0.0005	0.0045	<0.001	0.00011	<0.001	<0.001	<0.001	<0.001	0.0084
OUT026127	<0.0002	<0.0005	<0.0005	<0.0005	<0.0005	<0.001	0.00039	<0.001	<0.001	<0.001	<0.001	<0.001
OUT026128	<0.0002	<0.0005	<0.0005	<0.0005	<0.0005	<0.001	<0.0001	<0.001	<0.001	<0.001	<0.001	0.0014
OUT026129	<0.0002	<0.0005	<0.0005	<0.0005	0.0026	<0.001	<0.0001	<0.001	<0.001	<0.001	<0.001	<0.001
OUT026130	<0.0002	<0.0005	<0.0005	<0.0005	0.0031	<0.001	0.00016	<0.001	<0.001	<0.001	<0.001	0.0045
OUT026131	<0.0002	<0.0005	<0.0005	<0.0005	0.0043	<0.001	<0.0001	<0.001	<0.001	<0.001	<0.001	0.0059
OUT026132	<0.0002	<0.0005	<0.0005	<0.0005	0.00052	0.0021	<0.0001	<0.001	<0.001	<0.001	<0.001	<0.001
OUT026135	<0.0002	0.0013	0.0016	<0.0005	0.00069	<0.001	0.00049	<0.001	<0.001	<0.001	<0.001	<0.001
CONV-COL	<0.0002	<0.0005	<0.0005	<0.0005	0.00056	0.0012	0.00081	<0.001	<0.001	<0.001	<0.01	<0.001
CONV-GAT	<0.0002	0.0016	<0.0005	<0.0005	<0.0005	0.002	<0.0001	<0.001	<0.001	<0.001	<0.01	<0.001
CONV-PAP1	<0.0002	<0.0005	<0.0005	<0.0005	0.0028	0.0025	<0.0001	<0.001	<0.001	<0.001	<0.01	<0.001
CONV-VAL1	<0.0002	<0.0005	0.0013	<0.0005	0.00095	<0.001	<0.0001	<0.001	<0.001	<0.001	<0.01	<0.001
CPT-GAT1	<0.0002	<0.0005	0.00093	<0.0005	<0.0005	<0.001	<0.0001	<0.001	<0.001	<0.001	<0.01	<0.001
CPT-PON03	<0.0002	<0.0005	<0.0005	<0.0005	0.00071	0.0029	0.00016	<0.001	<0.001	<0.001	<0.01	<0.001
CPT-VAL1	<0.0002	<0.0005	0.00059	<0.0005	0.0023	<0.001	<0.0001	<0.001	<0.001	<0.001	<0.01	<0.001
CPT-VAL2	<0.0002	<0.0005	0.0012	<0.0005	<0.0005	<0.001	<0.0001	<0.001	<0.001	<0.001	<0.01	<0.001
OUT020439	<0.0002	<0.0005	0.00025	<0.0005	0.0024	<0.001	<0.0001	<0.001	<0.001	<0.001	<0.01	0.025
OUT021341	<0.0002	<0.0005	0.00025	0.0015	<0.0005	<0.001	<0.0001	<0.001	<0.001	<0.001	<0.01	<0.001
OUT021369	<0.0002	<0.0005	<0.0005	0.00057	0.0027	<0.001	<0.0001	<0.001	<0.001	<0.001	<0.01	0.0047
OUT021959	<0.0002	<0.0005	<0.0005	0.00086	<0.0005	0.004	0.00011	<0.001	<0.001	<0.001	<0.01	<0.001
OUT022124	<0.0002	<0.0005	<0.0005	<0.0005	0.00095	<0.001	<0.0001	<0.001	<0.001	<0.001	<0.01	<0.001
OUT023118	<0.0002	<0.0005	<0.0005	<0.0005	0.0035	<0.001	0.00025	<0.001	<0.001	<0.001	<0.01	<0.001
OUT036351	<0.0002	<0.0005	<0.0005	0.0007	<0.0005	0.0011	<0.0001	<0.001	<0.001	<0.001	<0.01	<0.001
OUT036352	<0.0002	<0.0005	<0.0005	0.015	0.0048	<0.001	0.00036	<0.001	<0.001	<0.001	<0.01	0.0034
OUT036353	<0.0002	<0.0005	<0.0005	0.001	0.0031	0.0011	0.00015	<0.001	<0.001	<0.001	<0.01	0.0059

Echantillon	Cd mg/l	Co mg/l	Cr mg/l	Cu mg/l	Mo mg/l	Ni mg/l	Pb mg/l	Sb mg/l	Se mg/l	Sn mg/l	Ti mg/l	U mg/l
OUT036354	<0.0002	<0.0005	<0.0005	0.00063	0.00091	<0.001	<0.0001	<0.001	<0.001	<0.001	<0.01	<0.001
OUT036355	<0.0002	<0.0005	<0.0005	0.0019	0.0038	<0.001	<0.0001	<0.001	<0.001	<0.001	<0.01	0.13
OUT036356	<0.0002	<0.0005	<0.0005	0.00076	0.0097	0.003	<0.0001	<0.001	<0.001	<0.001	<0.01	0.0026
OUT036357	<0.0002	<0.0005	<0.0005	0.0038	0.0033	0.002	0.00015	<0.001	<0.001	<0.001	<0.01	0.0079
OUT036358	<0.0002	<0.0005	<0.0005	<0.0005	0.0019	0.0018	0.00024	<0.001	<0.001	<0.001	<0.01	0.0039
OUT036359	<0.0002	<0.0005	<0.0005	<0.0005	0.0018	<0.001	0.00017	<0.001	<0.001	<0.001	<0.01	<0.001
OUT036360	<0.0002	<0.0005	<0.0005	<0.0005	0.0019	<0.001	0.00015	<0.001	<0.001	<0.001	<0.01	0.0042
OUT036361	<0.0002	<0.0005	0.00069	0.03	<0.0005	<0.001	0.00044	<0.001	<0.001	<0.001	<0.01	<0.001
OUT036362	<0.0002	<0.0005	0.00063	<0.0005	<0.0005	<0.001	<0.0001	<0.001	<0.001	<0.001	<0.01	<0.001
OUT036363	<0.0002	<0.0005	<0.0005	<0.0005	0.0022	<0.001	<0.0001	<0.001	<0.001	<0.001	<0.01	<0.001
OUT036364	<0.0002	<0.0005	0.00094	0.0026	<0.0005	<0.001	0.00021	<0.001	<0.001	<0.001	<0.01	<0.001
OUT036365	<0.0002	<0.0005	<0.0005	<0.0005	0.0055	<0.001	<0.0001	<0.001	<0.001	<0.001	<0.01	<0.001
OUT036370	<0.0002	<0.0005	<0.0005	<0.0005	0.0035	<0.001	0.00026	<0.001	<0.001	<0.001	<0.01	<0.001
OUT036371	<0.0002	0.00063	<0.0005	<0.0005	<0.0005	0.0037	0.00036	<0.001	<0.001	<0.001	<0.01	<0.001
OUT036373	<0.0002	<0.0005	0.00066	0.027	<0.0005	0.0011	0.00017	<0.001	<0.001	<0.001	<0.01	<0.001
OUT036376	<0.0002	<0.0005	<0.0005	<0.0005	0.0041	<0.001	<0.0001	<0.001	<0.001	<0.001	<0.01	<0.001
PACES-CONV-PON	<0.0002	<0.0005	<0.0005	0.0017	0.0038	0.0011	<0.0001	<0.001	<0.001	<0.001	<0.01	0.004
PUITS-SANDBAY	<0.0002	<0.0005	<0.0005	0.0017	0.0023	0.0021	0.00016	<0.001	<0.001	<0.001	<0.01	0.0036

Tableau A5 : Résultats d'analyses pour les paramètres chimiques 4/4

Echantillon	V mg/l	Zn mg/l	Dureté totale mg/l CaCO3	TDS mg/l	HCO3 mg/l	CO3 mg/l	log PCO2 atm	SI		
								Calcite	Dolomite	Anorthite
OUT000419	<0.002	<0.005	61	117	65.7	0.054	-2.28	-1.21	-3.18	-5.24
OUT003848	<0.002	0.0084	92	181	90.1	0.657	-3.12	0.02	-0.59	-4.25
OUT004005	<0.002	0.12	188	388	193.8	0.646	-2.48	0.27	0.13	-6.60
OUT004007	<0.002	<0.005	133	452	229.9	0.900	-2.43	0.13	-0.12	-4.53
OUT004013	<0.002	<0.005	139	263	145.1	0.623	-2.66	0.14	-0.58	-4.90
OUT004020	<0.002	0.028	75	203	91.3	2.473	-3.66	0.33	0.37	-4.91
OUT004087	<0.002	0.038	106	215	94.8	0.135	-2.35	-0.62	-2.20	-3.44
OUT016466	<0.002	<0.005	35	528	187.9	39.506	-4.25	0.82	1.78	-8.22
OUT018365	<0.002	0.0057	50	99	46.9	2.109	-4.16	0.16	-0.07	-5.09
OUT018375	<0.002	<0.005	152	879	58.8	3.482	-4.25	0.55	0.98	-7.69
OUT018376	<0.002	0.063	281	487	157.9	0.317	-2.31	0.00	-0.56	-5.29
OUT018387	<0.002	0.005	251	405	253.2	1.433	-2.55	0.68	0.68	-5.54
OUT018393	<0.002	0.008			189.9	2.577	-3.06	0.87	1.07	-6.03
OUT018395	<0.002	0.006	264	424	292.0	0.337	-1.79	0.09	-0.58	-6.27
OUT018401	<0.002	<0.005	136	256	164.6	3.014	-3.24	0.73	0.99	-5.68
OUT018407	<0.002	0.0064	135	232	132.4	0.860	-2.87	0.29	-0.45	-3.48
OUT018662	0.0047	<0.005	41	779	423.5	43.605	-3.63	0.99	2.00	-7.42
OUT018746	<0.002	<0.005			287.5	2.520	-2.71	-1.89	-4.12	-9.01
OUT018832	<0.002	<0.005	199	331	193.9	0.576	-2.38	0.07	-0.09	-6.09
OUT018910	<0.002	0.0077	186	294	170.4	0.146	-1.89	-0.35	-1.70	-5.30
OUT018925	<0.002	0.013	322	658	316.4	0.318	-1.74	0.09	-0.26	-5.37
OUT019120	<0.002	0.016	306	678	328.2	0.500	-1.89	0.21	0.09	-3.68
OUT019124	0.0034	<0.005	239	2402	479.9	9.860	-2.90	0.81	1.99	-5.49
OUT019143	<0.002	<0.005	99	184	118.7	1.611	-3.26	0.45	0.13	-6.36
OUT019147	<0.002	0.021	243	389	255.6	0.246	-1.77	-0.02	-1.08	-5.00
OUT019181	<0.002	0.0097	507	1014	255.9	0.069	-1.26	-0.40	-1.45	-7.39
OUT019200	<0.002	<0.005	183	315	206.5	0.387	-2.16	0.11	-0.95	-5.57
OUT019283	<0.002	<0.005	88	193	116.6	2.627	-3.49	0.53	0.58	-6.91
OUT019459	<0.002	0.0064	64	295	123.6	5.185	-3.73	0.60	0.82	-5.39
OUT019536	<0.002	<0.005	136	232	62.2	5.980	-4.43	0.99	1.49	-4.15
OUT019695	<0.002	0.0069	187	322	143.1	1.579	-3.09	0.55	0.64	-4.94
OUT019761	<0.002	0.0075	113	890	199.0	4.088	-3.23	0.50	0.91	-6.85
OUT019864	<0.002	<0.005	411	899	376.5	0.739	-1.94	0.50	0.47	-6.32
OUT019914	<0.002	0.026	227	385	195.1	0.023	-0.97	-1.20	-2.85	-8.59
OUT020035	0.0029	0.0089	225	416	278.9	0.755	-2.19	0.32	0.19	-4.30
OUT020065	<0.002	0.0058	271	448	316.0	0.528	-1.93	0.17	0.09	-6.28
OUT020086	<0.002	0.011	91	162	95.1	0.618	-3.01	0.01	-1.06	-4.81
OUT020091	<0.002	0.006	194	304	97.5	0.012	-1.30	-1.50	-3.56	-6.38
OUT020318	<0.002	<0.005	132	233	130.8	1.620	-3.17	0.51	0.32	-6.51

Echantillon	V mg/l	Zn mg/l	Dureté totale mg/l CaCO3	TDS mg/l	HCO3 mg/l	CO3 mg/l	log PCO2 atm	SI		
								Calcite	Dolomite	Anorthite
OUT020341	<0.002	0.0092	381	709	376.9	0.536	-1.82	0.27	0.24	0.66
OUT020412	<0.002	<0.005	64	117	52.8	1.605	-3.94	0.23	-0.30	-4.85
OUT020440	<0.002	<0.005	16	47	18.3	0.003	-2.06	-3.14	-6.81	-7.21
OUT020566	<0.002	<0.005	245	486	316.3	0.357	-1.76	-0.03	-0.36	-3.70
OUT020694	<0.002	0.011	125	543	359.3	3.222	-2.61	0.49	1.00	-6.54
OUT020717	<0.002	<0.005	165	293	182.8	0.064	-1.48	-0.77	-2.35	-6.79
OUT020768	<0.002	0.0088	183	290	170.4	0.143	-1.89	-0.40	-1.45	-7.21
OUT021157	<0.002	0.0064	63	106	32.9	0.001	-1.30	-2.80	-6.28	-8.90
OUT021327	<0.002	0.0069	44	127	79.6	2.841	-3.83	0.28	0.00	-8.95
OUT021530	<0.002	0.0074			121.6	0.158	-2.24	-0.28	-0.99	-6.37
OUT021917	<0.002	<0.005	220	1040	216.0	1.726	-2.82	0.46	0.91	-6.41
OUT022127	<0.002	<0.005	135	230	145.5	0.385	-2.44	-0.02	-1.56	-4.76
OUT022187	<0.002	<0.005	92	443	201.2	2.995	-3.07	0.44	0.56	-0.99
OUT022252	<0.002	0.0064			96.3	0.028	-1.67	-1.44	-3.85	-9.92
OUT022258	<0.002	0.012	71	131	48.7	0.014	-1.92	-1.83	-4.24	-5.49
OUT022274	<0.002	<0.005	959	2854	214.1	2.651	-3.06	1.17	1.77	-3.75
OUT022292	0.0022	<0.005	11	903	517.5	45.353	-3.43	0.39	0.86	-5.01
OUT022510	<0.002	<0.005	278	2685	528.0	4.220	-2.44	0.52	1.41	-5.66
OUT022560	<0.002	<0.005			303.8	0.507	-1.96	0.37	0.33	-5.77
OUT022620	<0.002	<0.005			145.8	0.255	-2.27	-0.05	-0.89	-5.97
OUT022829	<0.002	0.013	302	849	462.8	0.308	-1.37	-0.33	-0.49	-7.22
OUT022963	<0.002	0.0096	129	257	130.4	1.853	-3.22	0.55	0.29	-5.54
OUT022995	<0.002	<0.005	148	302	206.6	0.353	-2.10	-0.09	-0.97	-3.12
OUT023044	<0.002	<0.005	104	185	71.6	1.984	-3.83	0.57	0.53	-4.73
OUT023067	<0.002	<0.005	83	175	101.6	0.999	-3.18	0.12	-0.27	-5.79
OUT023092	<0.002	<0.005	112	222	145.3	0.531	-2.59	-0.06	-0.67	-4.63
OUT023108	<0.002	0.0071	102	226	133.8	0.148	-2.12	-0.63	-1.77	-5.21
OUT023157	0.0045	0.0055	138	235	121.5	0.217	-2.36	-0.43	-1.17	-5.99
OUT023259	<0.002	0.0099	180	313	193.8	0.631	-2.44	0.24	-0.14	-6.39
OUT023496	<0.002	<0.005	68	132	71.6	0.772	-3.34	-0.10	-0.77	-5.37
OUT023553	<0.002	0.013	103	220	116.3	0.379	-2.66	-0.17	-1.00	-6.60
OUT023574	<0.002	<0.005	39	435	189.2	2.882	-3.10	0.10	-0.14	-7.22
OUT023612	<0.002	<0.005	80	154	86.6	1.203	-3.39	0.21	-0.31	-5.40
OUT023623	<0.002	<0.005	155	494	220.6	5.449	-3.26	0.97	1.45	-3.53
OUT025998	<0.002	<0.005	107	197	113.8	0.406	-2.72	-0.07	-0.99	-6.38
OUT026101	<0.002	0.019	272	1068	279.8	0.309	-1.83	0.07	-0.99	-4.36
OUT026102	<0.002	0.0051	231	404	254.8	0.615	-2.17	0.20	-0.01	-4.60
OUT026103	<0.002	<0.005	221	430	267.4	0.436	-1.99	0.14	-0.47	-6.60
OUT026104	<0.002	0.0078	358	1900	144.9	0.682	-2.77	0.22	0.15	-6.85
OUT026105	<0.002	0.01	210	571	290.8	0.904	-2.25	0.32	0.27	-6.23
OUT026106	<0.002	<0.005	358	845	291.9	0.387	-1.89	0.10	-0.05	-6.20

Echantillon	V mg/l	Zn mg/l	Dureté totale mg/l CaCO3	TDS mg/l	HCO3 mg/l	CO3 mg/l	log PCO2 atm	SI		
								Calcite	Dolomite	Anorthite
OUT026107	<0.002	<0.005	13	367	179.4	13.698	-3.82	0.28	0.27	-7.77
OUT026108	<0.002	0.007	361	623	266.4	0.929	-2.34	0.63	0.49	-6.20
OUT026109	<0.002	<0.005			231.2	0.222	-1.83	-0.10	-0.64	-5.25
OUT026110	<0.002	0.024	115	199	119.3	0.079	-1.91	-0.91	-2.33	-6.01
OUT026112	<0.002	<0.005	87	138	25.6	0.006	-2.16	-2.07	-4.70	-5.16
OUT026115	<0.002	<0.005	200	322	129.3	2.368	-3.36	0.73	1.07	-2.75
OUT026116	<0.002	0.072	176	304	113.1	0.769	-2.98	0.28	-0.06	-6.20
OUT026117	<0.002	0.0099	36	78	45.0	0.051	-2.57	-1.54	-3.52	-6.29
OUT026118	<0.002	0.019	216	472	170.4	0.149	-1.91	-0.38	-1.51	-3.81
OUT026119	<0.002	0.014	214	381	199.2	3.999	-3.25	1.14	1.29	-4.33
OUT026120	<0.002	0.013	195	339	218.8	0.341	-2.04	0.04	-0.97	-6.34
OUT026121	<0.002	<0.005	195	324	191.5	1.758	-2.88	0.59	0.83	-6.16
OUT026122	<0.002	0.015	142	264	170.5	0.111	-1.77	-0.61	-1.92	-5.52
OUT026123	<0.002	<0.005	274	446	243.5	0.209	-1.74	-0.08	-1.05	-4.89
OUT026124	<0.002	0.0091	585	1269	377.5	0.245	-1.47	0.16	-0.30	-2.91
OUT026125	0.0022	0.017	82	149	43.9	0.013	-2.04	-1.86	-4.12	-0.59
OUT026126	<0.002	<0.005	72	175	87.1	0.341	-2.83	-0.35	-1.83	-4.72
OUT026127	<0.002	0.0075	35	264	147.6	5.391	-3.57	0.34	0.33	-5.28
OUT026128	<0.002	0.0063	124	462	272.6	3.875	-2.92	0.74	1.07	-4.88
OUT026129	<0.002	<0.005	236	403	217.6	0.956	-2.50	0.41	0.35	-4.33
OUT026130	<0.002	0.022	163	301	179.6	1.611	-2.92	0.43	0.76	-4.08
OUT026131	<0.002	0.0075	78	430	211.8	3.790	-3.13	0.40	0.73	-5.50
OUT026132	<0.002	0.0091	101	181	105.0	0.554	-2.87	-0.03	-0.99	-6.43
OUT026135	<0.002	0.0096	37	94	36.6	0.005	-1.72	-2.49	-5.73	-5.25
CONV-COL	<0.002	0.056	255	508	231.0	0.321	-2.00	0.15	-1.18	-4.24
CONV-GAT	<0.002	0.9	622	1076	451.2		-1.36	0.25	0.39	-4.20
CONV-PAP1	<0.002	<0.005			154.5	1.958	-3.11	0.37	0.25	-4.63
CONV-VAL1	0.0031	0.0098	108	190	97.6	1.154	-3.28	0.31	-0.03	-4.41
CPT-GAT1	<0.002	0.012	418	788	572.0	0.537	-1.44	0.18	0.35	-3.26
CPT-PON03	<0.002	0.0055	85	138	80.9	1.588	-3.56	0.29	0.07	-4.71
CPT-VAL1	<0.002	0.0061	122	208	131.5	1.293	-3.05	0.36	0.09	-4.34
CPT-VAL2	<0.002	<0.005	21	54	17.1	0.004	-2.26	-2.88	-6.31	-5.71
OUT020439	<0.002	0.0053	46	217	120.2	0.837	-2.97	-0.16	-1.03	-4.93
OUT021341	<0.002	<0.005	152	455	301.4	1.706	-2.47	0.49	0.57	-4.19
OUT021369	<0.002	<0.005	50	159	89.7	1.464	-3.44	0.16	-1.01	-5.09
OUT021959	<0.002	0.033			158.4	0.061	-1.58	-3.04	-6.85	-6.84
OUT022124	<0.002	0.063			23.5	4.617	-5.14	-1.08	-2.97	-6.51
OUT023118	<0.002	0.0025	110	184	90.3	5.352	-4.05	0.97	1.21	-4.35
OUT036351	<0.002	<0.005	200	456	302.8	1.032	-2.26	0.34	0.45	-4.29
OUT036352	<0.002	0.0074	68	122	68.1	0.101	-2.52	-0.86	-2.87	-5.06
OUT036353	<0.002	0.018	263	417	205.4	0.945	-2.56	0.47	0.47	-4.09

Echantillon	V mg/l	Zn mg/l	Dureté totale mg/l CaCO3	TDS mg/l	HCO3 mg/l	CO3 mg/l	log PCO2 atm	SI		
								Calcite	Dolomite	Anorthite
OUT036354	<0.002	<0.005	78	248	153.7	2.395	-3.20	0.33	0.44	-4.79
OUT036355	<0.002	0.0077	315	536	291.4	0.599	-2.06	0.32	0.24	-4.21
OUT036356	<0.002	0.027	62	1512	511.4	12.346	-2.92	0.41	1.19	-5.37
OUT036357	<0.002	0.0057	102	197	87.7	0.043	-1.93	-1.14	-3.03	-4.78
OUT036358	<0.002	0.0052	236	353	214.1	2.651	-2.96	0.88	1.23	-4.24
OUT036359	<0.002	0.0095	343	1435	193.3	6.901	-3.55	1.14	2.26	-4.38
OUT036360	<0.002	<0.005	46	361	196.4	11.371	-3.67	0.69	1.24	-5.17
OUT036361	<0.002	0.011			84.0	0.045	-1.98	-1.17	-3.17	-4.70
OUT036362	<0.002	0.015	57	117	69.4	0.032	-1.99	-1.61	-3.54	-4.42
OUT036363	<0.002	<0.005			159.6	5.444	-3.55	0.76	0.98	-4.77
OUT036364	<0.002	<0.005	31	92	41.5	0.003	-1.53	-2.67	-5.70	-6.79
OUT036365	<0.002	<0.005	89	159	97.9	1.032	-3.21	0.18	-0.41	-4.54
OUT036370	<0.002	0.0098	84	191	109.1	0.913	-3.10	0.07	-0.25	-4.48
OUT036371	<0.002	0.064	98	148	48.8	0.005	-1.56	-1.96	-4.63	-5.66
OUT036373	<0.002	0.073	53	126	64.6	0.028	-2.14	-1.38	-2.88	-4.82
OUT036376	<0.002	0.0053	70	885	427.5	5.671	-2.71	0.45	0.88	-4.93
PACES-CONV-PON	<0.002	0.011	88	159	77.9	1.271	-3.51	0.18	-0.01	-4.83
PUITS-SANDBAY	0.0039	0.036	314	712	424.1	1.349	-2.55	1.00	1.76	-3.91

Annexe 3 – Matériel électronique supplémentaire de l'article soumis à Hydrogeology Journal (Chapitre 1)

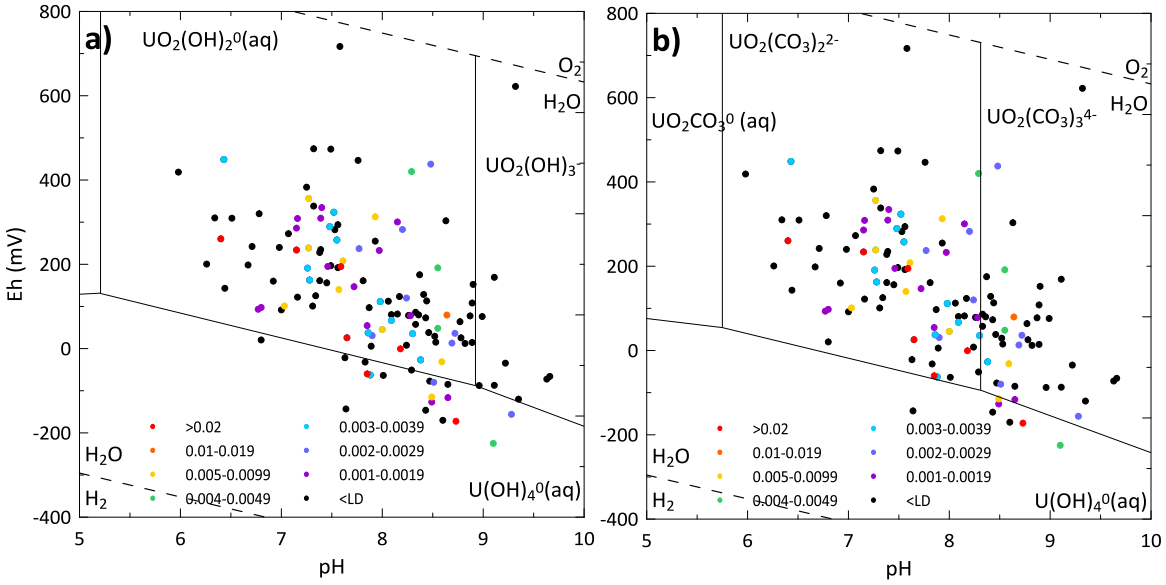

Fig. A4 Eh-pH diagrams showing the hydrolysis of U(VI) and U(IV): a) in absence of ligands, b) in presence of other ligands (modified from Krupka & Serne (2002)). The range of concentrations is expressed as $mg.l^{-1}$.

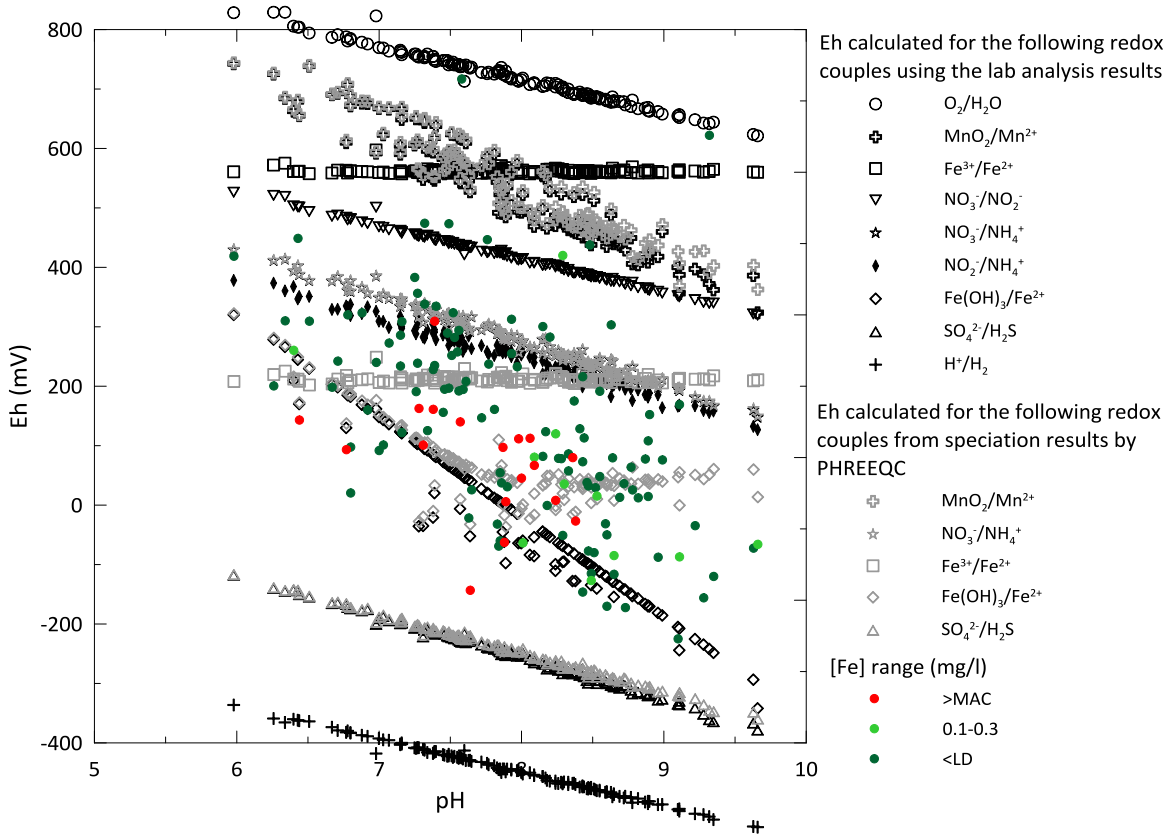

Fig. A5 Eh-pH diagram for the samples according to their concentration in total dissolved iron. For each sample, theoretical Eh values were calculated for different redox couples based on hypothesis on lab analysis results and using the speciation results from PHREEQC (Parkhurst & Appelo 1999)

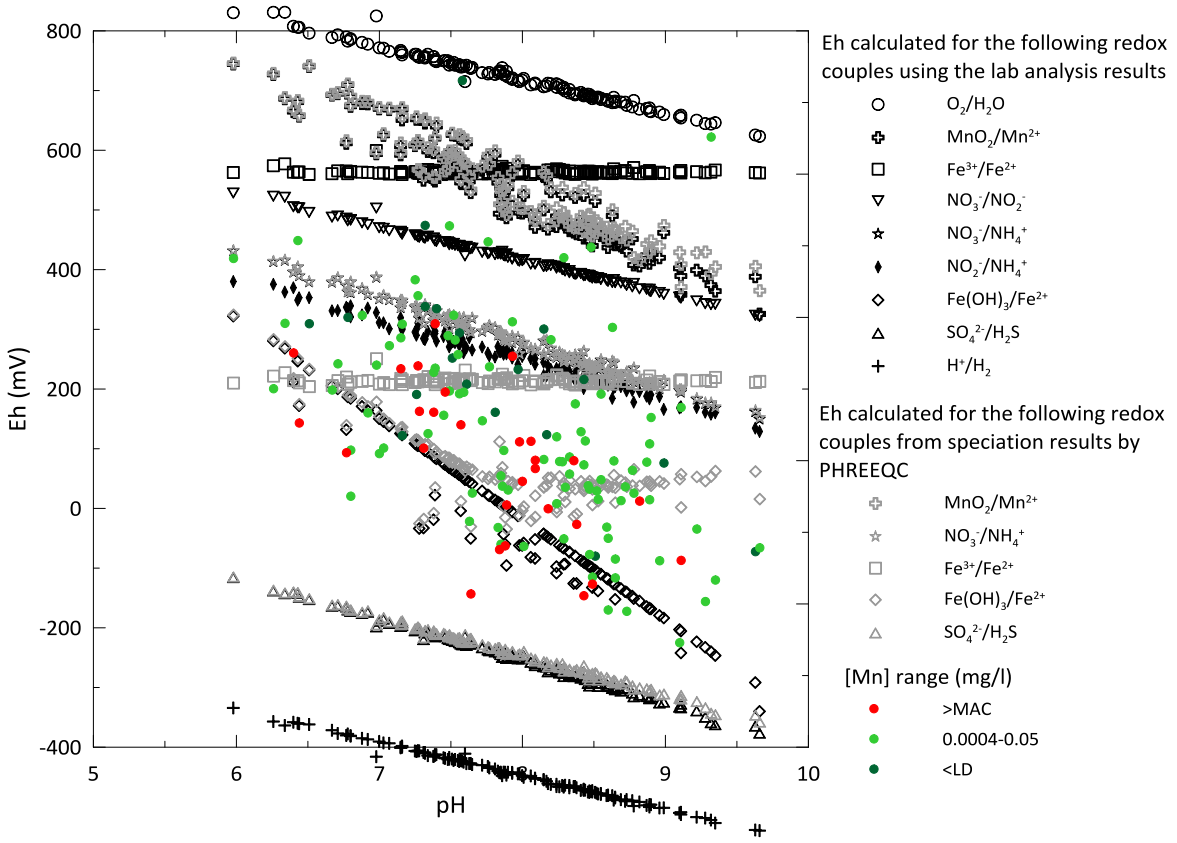

Fig. A6 Eh-pH diagram for the samples according to their concentration in total dissolved manganese. For each sample, theoretical Eh values were calculated for different redox couples based on hypothesis on lab analysis results and using the speciation results from PHREEQC (Parkhurst & Appelo 1999)

Annexe 4 – Figures supplémentaires du Chapitre 2

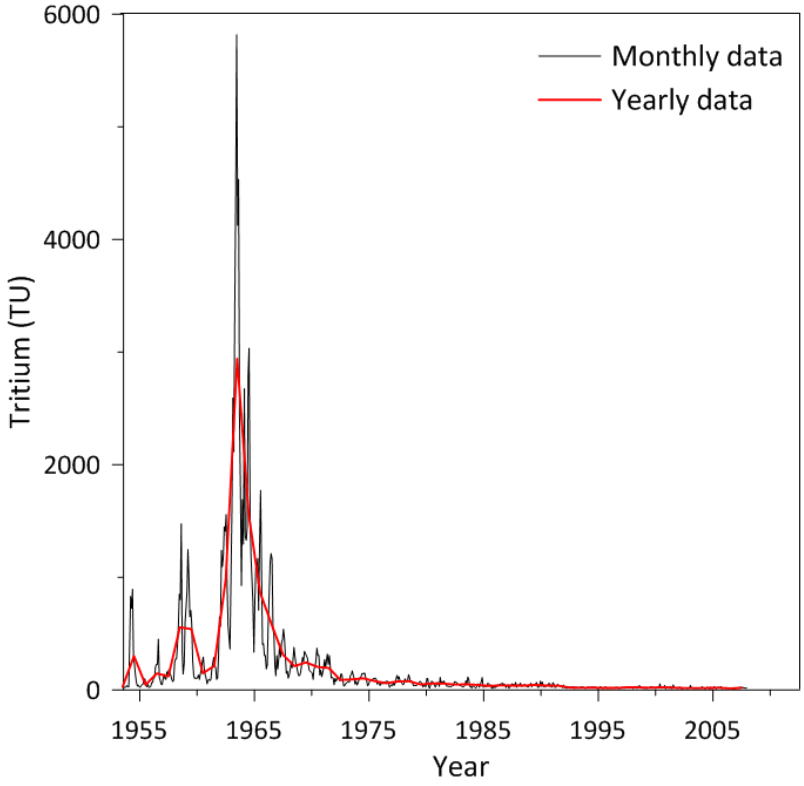

Fig. A7 Monthly and yearly tritium recharge input curves based on data from the Ottawa meteorological station (IAEA/WMO 2011)

Table A1 Concentrations in noble gases

Sample ID	VHe cm^3 STP.g^{-1}	VNe cm^3 STP.g^{-1}	VAr cm^3 STP.g^{-1}	VKr cm^3 TP.g^{-1}	VXe cm^3 TP.g^{-1}
OUT036357a	$1.151x10^{-6}$	$2.049x10^{-7}$	$4.471x10^{-4}$	$1.041x10^{-7}$	$1.499x10^{-8}$
OUT036357b	$1.971x10^{-6}$	$2.336x10^{-7}$	$4.425x10^{-4}$	$1.106x10^{-7}$	$1.572x10^{-8}$
CONV-PON/27-31.5m	$1.352x10^{-6}$	$2.302x10^{-7}$	$4.302x10^{-4}$	$1.121x10^{-7}$	$1.635x10^{-8}$
OUT036356	$1.624x10^{-7}$	$2.055x10^{-7}$	$4.826x10^{-4}$	$9.762x10^{-8}$	$1.384x10^{-8}$
OUT021341a	$1.982x10^{-6}$	$1.963x10^{-7}$	$4.820x10^{-4}$	$1.045x10^{-7}$	$1.539x10^{-8}$
OUT021341b	$3.577x10^{-6}$	$2.317x10^{-7}$	$4.675x10^{-4}$	$1.007x10^{-7}$	$1.431x10^{-8}$
Error ±1σ (%)	1.5	1.3	1.3	1.5	2.2
Equilibrium with atmosphere	[a]4.760x10-8	a2.123x10-7	a4.359x10-4	a1.057x10-7	a1.581x10-8

[a]At 5°C (Peeters et al. 2002)

Table A2 Isotopic ratios for Ne and Ar

Sample ID	Ne^{20}/Ne^{22}	Error ±1σ	Ne^{21}/Ne^{22}	Error ±1σ	Ar^{38}/Ar^{36}	Error ±1σ	Ar^{40}/Ar^{36}	Error ±1σ
OUT036357a	9.881	$5.49x10^{-2}$	$2.942x10^{-2}$	$2.47x10^{-4}$	0.1872	$5.07x10^{-4}$	290.5	1.96
OUT036357b	9.881	$4.41x10^{-2}$	$2.885x10^{-2}$	$1.80x10^{-4}$	0.1873	$5.91x10^{-4}$	296.7	1.08
CONV-PON/27-31.5m	9.888	$6.79x10^{-2}$	$2.939x10^{-2}$	$2.54x10^{-4}$	0.1880	$6.25x10^{-4}$	295.8	2.09
OUT036356	9.883	$5.45x10^{-2}$	$2.905x10^{-2}$	$2.13x10^{-4}$	0.1889	$6.40x10^{-4}$	294.2	1.67
OUT021341a	9.820	$6.47x10^{-2}$	$2.926x10^{-2}$	$3.13x10^{-4}$	0.1879	$7.10x10^{-4}$	297.0	9.70
OUT021341b	9.898	$5.93x10^{-2}$	$2.881x10^{-2}$	$2.26x10^{-4}$	0.1862	$4.43x10^{-4}$	291.6	2.21
Equilibrium with atmosphere	[a]9.7804						[a]295.9	

[a]At 5°C (Peeters et al. 2002)

Table A3 Isotopic ratios for Kr

Sample ID	Kr^{80}/Kr^{84}	Error ±1σ	Kr^{82}/Kr^{84}	Error ±1σ	Kr^{83}/Kr^{84}	Error ±1σ	Kr^{86}/Kr^{84}	Error ±1σ
OUT036357a	$3.960x10^{-2}$	$3.51x10^{-4}$	0.2008	$8.81x10^{-4}$	0.2032	$1.33x10^{-3}$	0.3075	$1.41x10^{-3}$
OUT036357b	$3.996x10^{-2}$	$2.82x10^{-4}$	0.2025	$1.14x10^{-3}$	0.2010	$1.49x10^{-3}$	0.3072	$1.43x10^{-3}$
CONV-PON/27-31.5m	$3.980x10^{-2}$	$3.18x10^{-4}$	0.2030	$1.40x10^{-3}$	0.1991	$1.34x10^{-3}$	0.3075	$1.52x10^{-3}$
OUT036356	$4.003x10^{-2}$	$3.54x10^{-4}$	0.2039	$1.53x10^{-3}$	0.2022	$1.45x10^{-3}$	0.3045	$1.91x10^{-3}$
OUT021341a	$3.978x10^{-2}$	$3.83x10^{-4}$	0.2042	$1.51x10^{-3}$	0.2016	$1.43x10^{-3}$	0.3066	$1.25x10^{-3}$
OUT021341b	$3.961x10^{-2}$	$3.33x10^{-4}$	0.2015	$9.20x10^{-4}$	0.2013	$1.56x10^{-3}$	0.3073	$1.28x10^{-3}$

Table A4 Isotopic ratios for Xe

Sample ID	Xe^{128}/Xe^{130}	Error ±1σ	Xe^{129}/Xe^{130}	Error ±1σ	Xe^{131}/Xe^{130}	Error ±1σ	Xe^{132}/Xe^{130}	Error ±1σ	Xe^{134}/Xe^{130}	Error ±1σ	Xe^{136}/Xe^{130}	Error ±1σ
OUT036357a	0.4707	$3.65x10^{-3}$	6.488	$4.24x10^{-2}$	5.208	$3.25x10^{-2}$	6.583	$4.03x10^{-2}$	2.571	$1.64x10^{-2}$	2.172	$1.55x10^{-2}$
OUT036357b	0.4795	$3.39x10^{-3}$	6.518	$3.34x10^{-2}$	5.244	$2.64x10^{-2}$	6.619	$3.33x10^{-2}$	2.580	$1.32x10^{-2}$	2.191	$1.31x10^{-2}$
CONV-PON/27-31.5m	0.4688	$3.43x10^{-3}$	6.442	$4.01x10^{-2}$	5.176	$2.86x10^{-2}$	6.575	$3.78x10^{-2}$	2.558	$1.67x10^{-2}$	2.186	$1.40x10^{-2}$
OUT036356	0.4701	$3.04x10^{-3}$	6.392	$3.78x10^{-2}$	5.187	$3.26x10^{-2}$	6.573	$3.93x10^{-2}$	2.546	$1.60x10^{-2}$	2.166	$1.46x10^{-2}$
OUT021341a	0.4688	$4.16x10^{-3}$	6.459	$3.41x10^{-2}$	5.210	$2.92x10^{-2}$	6.550	$3.13x10^{-2}$	2.543	$1.42x10^{-2}$	2.167	$1.36x10^{-2}$
OUT021341b	0.4781	$3.03x10^{-3}$	6.514	$3.90x10^{-2}$	5.211	$3.01x10^{-2}$	6.620	$3.79x10^{-2}$	2.561	$1.54x10^{-2}$	2.180	$1.71x10^{-2}$

Annexe 5 – Figures supplémentaires du Chapitre 3

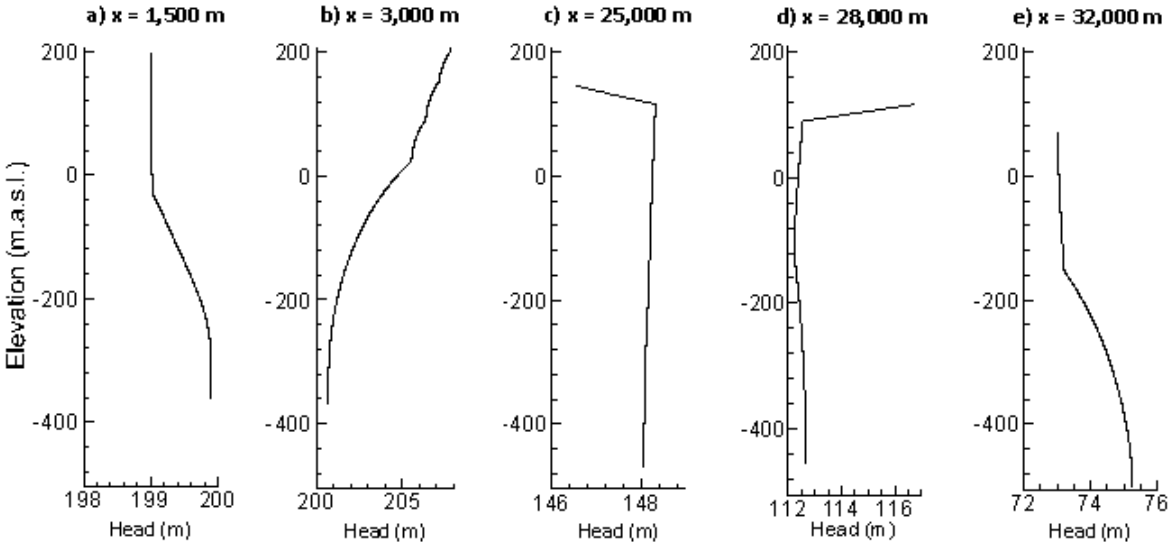

Fig. A8 Head profiles along the 2D cross-section in different hydrogeological situations: a) discharge zone under Lake Johnson, b) recharge zone, c) artesian conditions and d) non-artesian conditions in the confined aquifer and e) discharge zone under the Ottawa River

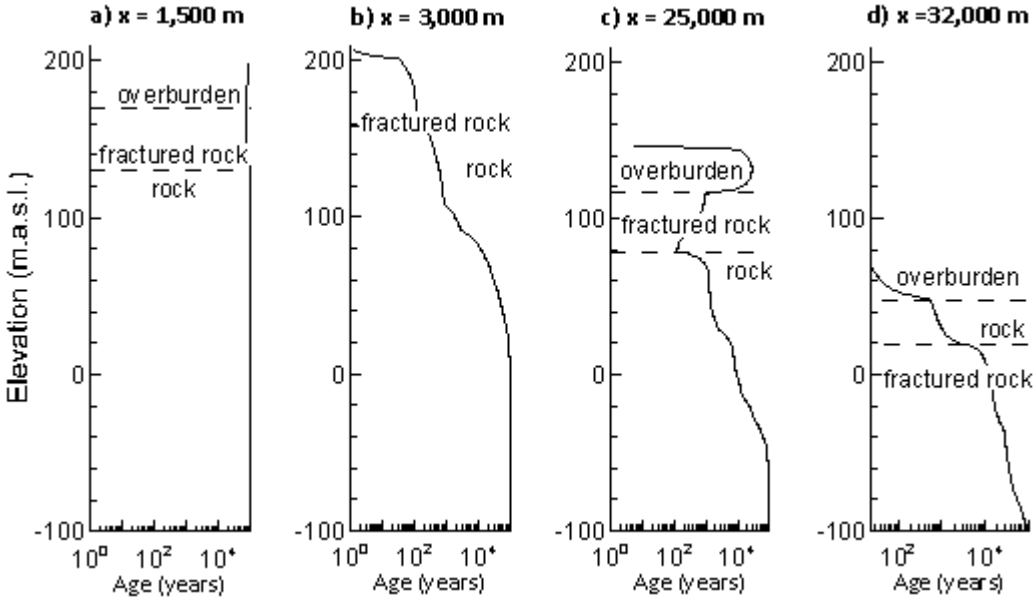

Fig. A9 Age profiles along the 2D cross-section in different hydrogeological situations: a) discharge zone under Lake Johnson, b) recharge zone, c) in the confined aquifer and d) discharge zone under the Ottawa River